ACKNOWLEDGEMENTS

First and foremost I express my deep sense of gratitude to my supervisor Dr. Satrajit Adhikari for his inspiring guidance. It has been an honor and a privilege to work under his kind and invaluable supervision. His constant encouragement has build confidence in me in persuing the research work. I shall remain indebted to him in all my future endeavor in the field of research.

I am extremely grateful to my lab mate Mr. Biplab Sarkar, for not only his tireless help during the entire period of my Ph.D program but also for the valuable discussions that has helped me in learning many things in the field. It has been a great pleasure to work with him.

I am also highly grateful to Mr. Manabendra Sarma of IIT Bombay, who has helped me through his valuable suggestions time to time and also by providing necessary informations in the field as and when I was in need of it.

I gratefully acknowledge the help I gained from the Doctoral committee members Dr. Manabendra Ray, Dr. Arun Chattopadhyay and Dr. S. B. Santra through their constructive criticism and suggestions.

I am also indebted to Prof. Abu Taleb Khan for his generous support and encouragement towards my research work.

I am glad to record my thanks to Miss R. S. Swathi and Mr. Sarin A. Deshpande, for their helping hand while solving some of the problems in the course of my research.

My sincere gratitude is due for the Department of Chemistry, IIT Guwahati, for providing me the requisite facilities and also the opportunity to work in such a wonderful place.

I express my thanks and gratitude to the staff members, Department of Chemistry,

IIT Guwahati, for their support and cooperation throughout the period of my research work.

No word can express my indebtedness to my mother; it is her blessings and support that has made me what I am today. I deeply remember the affectionate blessings of my departed father who would have been the happiest person by seeing this project in a completed shape.

Last but not the least, I express my profound gratitude to my wife Mallika, for her constant support and encouragement that had helped me a lot to make this project a success.

(Panchanan Puzari)

TH-421_02612202

TABLE OF CONTENTS

TH-421_02612202

TH-421_02612202

TH-421_02612202

भारतीय प्रौद्योगिकी संस्थान गुवाहाटी • Indian Institute of Technology Guwahati •

TH-421_02612202

LIST OF TABLES

TH-421_02612202

TH-421_02612202

TH-421_02612202

TH-421_02612202

LIST OF FIGURES

TH-421_02612202

TH-421_02612202

TH-421_02612202

TH-421_02612202

TH-421_02612202

TH-421_02612202

CHAPTER I

INTRODUCTION

1.1 Overview of methods

The development of advanced beam and laser experiments has made available a large amount of experimental data and thereby, provide information on chemical reactivity and energy transfer processes at the molecular level. In many cases the interpretation of these data is straightforward but in many others, the complexity of the experiments and the chemical processes demands the support and interpretation from reliable dynamical calculations. Moreover, information on many dynamical processes at the "state resolved" level is needed for simulating bulk phenomena. This kind of information is often not obtainable experimentally, hence, dynamical calculations are even more important in those cases. Traditional approach of dynamical calculations are based on the use of Born-Oppenheimer (BO) separation of the nuclear and electronic motion. The approach consists three parts: (1) Born-Oppenheimer separation; (2) Construction of the potential energy surface; and (3) Dynamical calculations. However many chemical and physico-chemical processes involve so strong coupling between nuclear and electronic degrees of freedom that this separation is neither the most convenient nor correct way of proceeding. Nevertheless if the BO separation is introduced at all, the next step is to construct suitable potential energy surfaces (one or more) for the nuclear dynamics. If more than one surface is involved, nonadiabatic coupling terms needed, in principle, can be evaluated by using *ab initio* electronic structure calculations. Due to the complexity of the many-electron problem and the fact that a large part of the nuclear configuration space has to be covered, such calculations are not yet performed routinely. On the other hand, most potential energy

TH-421_02612202

surfaces are calculated semi-empirically by using *ab initio* calculation. The next required step is the construction of analytical potential-energy-surface expressions. At this stage, it is necessary to include information from sources such as spectroscopy, experimentally or theoretically determined long-range interactions, measurements of transport properties and barrier heights. The construction of analytical potential energy surface is a discipline of its own and no standard methodology is available at present [1, 2]. Once the potential surface is being constructed, one can perform the dynamical calculations. When we remove the center of mass motion and assume that the total angular momentum and its projection on a space-fixed axis are conserved, the exact solution of the nuclear motion is reduced to $3N - 5$ dimensional problem, where N is the number of particles. At this stage, it is also necessary to introduce approximations for $N > 3$ to 4. However, since the nuclear masses are much larger than the mass of the electrons, it is possible, without significant errors, to introduce an approximate description of all, or at least part, of the nuclear motion. Though one obvious choice is to use classical dynamics, quantum-classical (semi-classical) techniques are in many cases more appropriate. The reason for this is that the nuclear motion is subject to various quantum phenomena such as tunneling, zero-point vibrational energy, nonadiabatic electronic processes, interference and resonances. Methods which mix quantum and classical mechanics offer enough flexibility to treat the significant portion of reaction dynamics rigorously leaving the rest approximately. For dissociative and reaction coordinates it is convenient to introduce discrete representation of the wave function namely grid methodology.

Some methods of dynamical calculation do not require complete knowledge of potential energy surface such as the reaction path approach and the variational and quantum transition state methods. From the computational point of view, some of the methods need much less information than, say, state- and energy-resolved differential cross sections. For example, the transition state theory calculates rate constants

TH-421_02612202

as a function of temperature or the reaction path approach evaluates state-resolved rates. These methods require less information on the potential energy surface, that is information around the transition state and along the reaction path. When very little information is available on the interaction potential, one can estimate reaction cross sections using statistical or phase space methods.

Another class of interesting problem is how the environment influences reactivity, whether the influence is from a solvent, an external field, a "rigid" part of the reacting molecules or catalytic effects from metals or active sites on proteins. In order to investigate such processes we need to obtain information about the change of molecular properties when the molecular system is interacting either with solvent molecules, surfaces, or electromagnetic fields. The purpose of introducing density operator and reduced density operator is to handle such complex problem. Such methodology helps us to focus more on the system of interest with simplified description of the (chemically) less interesting degrees of freedom.

The molecular processes covering from simple energy transfer processes in the gas phase, to solvent effects on reactions in liquids, and from small to large molecular systems within the field of molecular dynamics requires the introduction of many different methods starting from exact quantum mechanical descriptions of small system to approximate statistical methods for large systems. The outline of some of these methods are given in Table 1.1.

Table 1.1: Overview of Methods and Descriptions in Molecular Dynamics

Description	Dynamics	Potential
Classical	Trajectories	Full
Semiclassical	Trajectories, Gaussian wavepackets, coupled equations	Full
Quantum	Coupled equations, coupled wavepackets	Full
Reaction path	Wavepackets, trajectories	Restricted
Phase space/statistical	Counting of states	Restricted
Transition state	Counting of states, reactive flux	Restricted

TH-421_02612202

1.2 Classical dynamics

The dynamics of chemical reactions can often be well approximated by classical mechanics. It has special importance for heavy atom dynamics because (1) for heavy atoms, quantum effects such as tunneling, large vibrational energy spacing, contributions from resonances, zero point energy and so on, are of little importance and, (2) the solution of the classical equations of motion usually poses no numerical problem even for a large number of atoms. The approach consists three steps: (1) Initially specific rotational-vibrational quantum numbers are determined for the asymptotic molecular states on a given potential energy surface; (2) A classical trajectory is calculated and analyzed asymptotically in order to determine whether the trajectory is reactive or inelastic/elastic; (3) The information about final coordinates and momenta may be used to find the classical quantities (actions) corresponding to the vibrational and rotational quantum numbers whereby, state-to-state probabilities and rates are in principle obtainable from classical dynamics.

1.2.1 Classical equation of motion

Let us consider a system consisting of three atoms A, B and C. The atom A approaches the diatomic molecule BC (Fig. 1.1) and the following coordinates and momenta are used to describe the motion of A with respect to the center of mass of BC:

$$(X\ Y\ Z\ P_X\ P_Y\ P_Z) \tag{1.2.1}$$

where the coordinate and momenta of the diatomic molecule are

$$(x\ y\ z\ p_x\ p_y\ p_z) \tag{1.2.2}$$

The kinetic energy for the motion of A relative to the center of mass of BC is:

$$E_{kin} = \frac{1}{2\mu}(P_X^2 + P_Y^2 + P_Z^2) = \frac{P_R^2}{2\mu} + \frac{L^2}{2\mu R^2} \tag{1.2.3}$$

TH-421_02612202

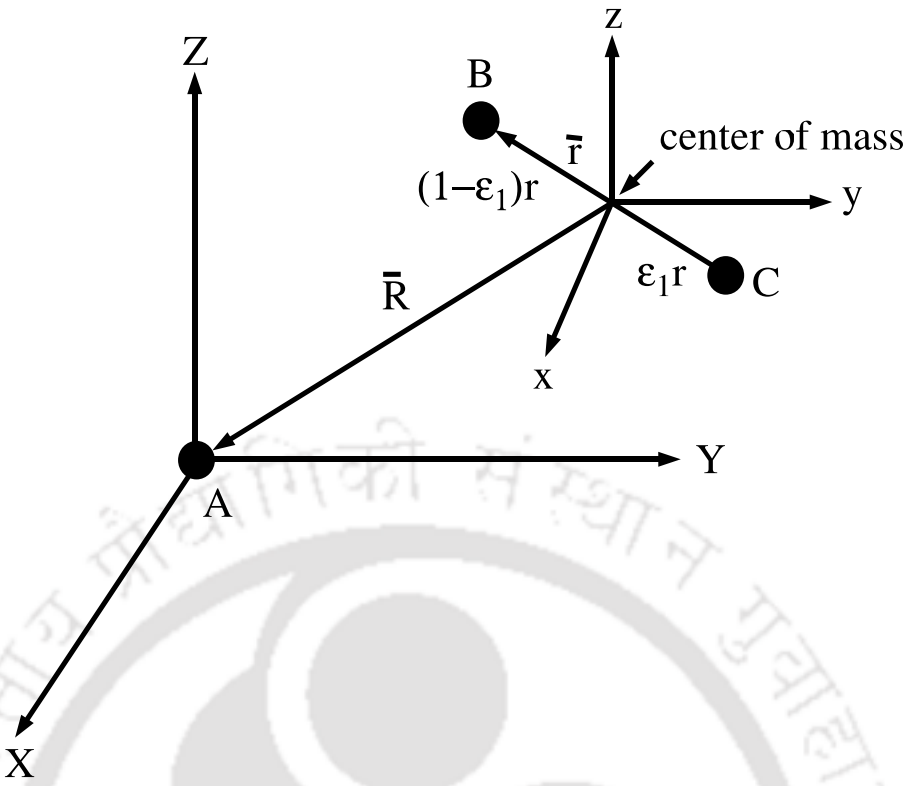

Figure 1.1: Coordinates used for a classical treatment of A + BC collisions; $\epsilon_1 = m_B/(m_B + m_C)$.

where L is the orbital angular momentum, and P_R the momentum for the motion along the R-axis (the R-axis being that connecting A and BC), and μ is the reduced mass

$$\mu = \frac{m_A(m_B + m_C)}{(m_A + m_B + m_C)} \tag{1.2.4}$$

For the motion of the diatomic molecule we have

$$E_{int} = \frac{1}{2m}(p_x^2 + p_y^2 + p_z^2) + \nu(r) = \frac{p_r^2}{2m} + \frac{j^2}{2mr^2} + \nu(r) \tag{1.2.5}$$

where j the rotational angular momentum, $\nu(r)$ the intramolecular potential, and m is the reduced mass of the diatomic molecule, $m = m_B m_C/(m_B + m_C)$.

If a reaction occurs it is convenient to describe the system using the $\mathbf{r'R'}$ coordinates shown in Fig. 1.2. They may however, be easily expressed in terms of the

TH-421_02612202

original initial coordinates $\mathbf{r}$, $\mathbf{R}$:

$$\mathbf{r}' = (x', y', z') = -(X + \epsilon_1 x, Y + \epsilon_1 y, Z + \epsilon_1 z) \quad (1.2.6)$$

$$\mathbf{R}' = (X', Y', Z') \quad (1.2.7)$$

$$X' = -X\epsilon_2 + x(1 - \epsilon_2\epsilon_1) \quad (1.2.8)$$

$$Y' = -Y\epsilon_2 + y(1 - \epsilon_2\epsilon_1) \quad (1.2.9)$$

$$Z' = -Z\epsilon_2 + z(1 - \epsilon_2\epsilon_1) \quad (1.2.10)$$

where $\epsilon_1 = m_B/(m_B + m_C)$ and $\epsilon_2 = m_A/(m_A + m_C)$. Once the system is initialized in any channel, say, channel 1 (A + BC), the equations of motion are solved using the Hamiltonian

$$H = \frac{1}{2\mu}(P_X^2 + P_Y^2 + P_Z^2) + \frac{1}{2m}(p_x^2 + p_y^2 + p_z^2) + V(R_{AB}, R_{BC}, R_{AC}). \quad (1.2.11)$$

which leads to the following equations of motion

$$\dot{X} = \frac{P_X}{\mu} \quad (1.2.12)$$

$$\dot{P}_X = -\frac{\partial V}{\partial X} \quad (1.2.13)$$

$$\dot{x} = \frac{p_x}{m} \quad (1.2.14)$$

$$\dot{p}_x = -\frac{\partial V}{\partial x} \quad (1.2.15)$$

along with the corresponding equation for the y/Y- and z/Z-components.

After the collision, the magnitudes of the three distances R_{AB}, R_{BC}, and R_{AC} determine the channel to which the trajectory contributes

$$\text{Channel 1:} \quad R_{AB} \text{ and } R_{AC} \text{ large} \quad (1.2.16)$$

$$\text{Channel 2:} \quad R_{AB} \text{ and } R_{BC} \text{ large} \quad (1.2.17)$$

$$\text{Channel 3:} \quad R_{AC} \text{ and } R_{BC} \text{ large} \quad (1.2.18)$$

The coordinates for channel 2 are indicated above and the corresponding momenta

TH-421_02612202

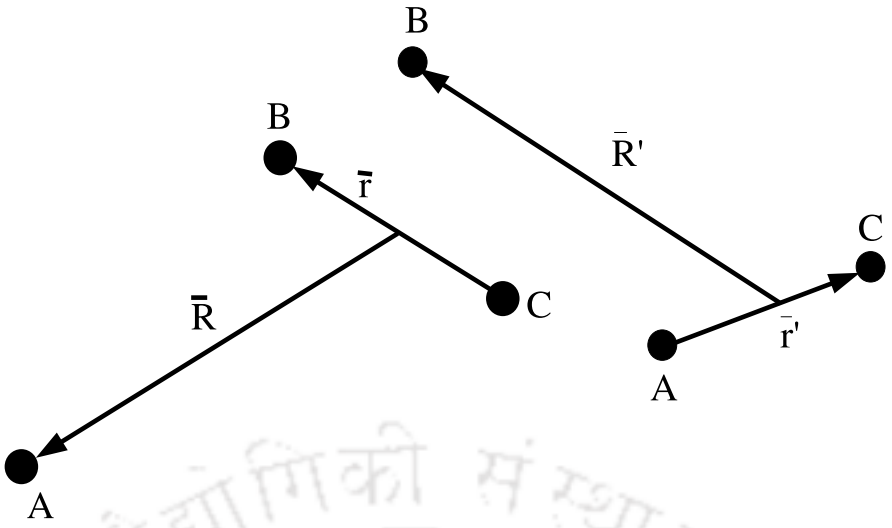

Figure 1.2: Change in the relative position vectors for a chemical reaction.

are

$$\frac{p_{x'}}{m'} = \dot{x}' = -\dot{X} - \epsilon_1 \dot{x} \tag{1.2.19}$$

$$\frac{P_{X'}}{\mu'} = \dot{X}' = -\dot{X}\epsilon_2 + \dot{x}(1 - \epsilon_2\epsilon_1) \tag{1.2.20}$$

or

$$p_{x'} = -\frac{m'}{\mu} P_X - \epsilon_1 \frac{m'}{m} p_x \tag{1.2.21}$$

$$P_{X'} = -\frac{\mu'}{\mu} P_X \epsilon_2 + \frac{\mu'}{m} p_x (1 - \epsilon_2\epsilon_1) \tag{1.2.22}$$

along with corresponding equations for the y/Y- and z/Z-components. The reduced channel masses $m' = m_A m_C/(m_A + m_C)$ and $\mu' = m_B(m_A + m_C)/(m_A + m_B + m_C)$. Similar equations can be obtained for channel 3.

1.3 Semiclassical theories

The solution of the classical equations of motion does not give rise to problems even for many-particle system but we know as well that quantum effects such as tunneling and interference, among others can not be neglected in a number of situations. It is therefore natural attempt to account these effects at least approximately while

TH-421_02612202

retaining the computational advantage of classical propagation schemes. Several such quantum-classical or semiclassical schemes have been proposed. In this section we shall discuss theories which are based on a semiclassical evaluation of the quantum propagators.

1.3.1 Feynman path integrals

The Feynman path integral formulation is a natural starting point for the introduction of the semiclassical limit. The approach involves the introduction of a quantity S which has a definition resembling that of an action integral [3]. Considering a particle with mass m moving along the x-axis under a one dimensional potential $V(x,t)$, the quantity S is defined by

$$S(x_2t_2;x_1t_1) = \int_{t_1}^{t_2} L(\dot{x},x,t)dt \tag{1.3.1}$$

where $\dot{x} = dx/dt$ and L is Lagrangian,

$$L = \frac{m}{2}\dot{x}^2 - V(x,t) \tag{1.3.2}$$

Its connection with quantum mechanics is made through the equation

$$\psi(x_2,t_2) = \int_{-\infty}^{\infty} K(x_2,t_2;x_1,t_1)\psi(x_1,t_1)dx_1 \tag{1.3.3}$$

where $K(x_2,t_2;x_1,t_1)$ is the propagator indicating the amplitude for a particle going from the position x_1 at time t_1 to x_2 at t_2. The amplitude for a final position, namely $\psi(x_2,t_2)$ can be obtained by summing or integrating over all such "transition" amplitudes multiplied with the amplitude for a given initial position. We now postulate that the propagator can be written as an integral over all "paths" leading from (x_1,t_1) to (x_2,t_2) each weighted by a phase factor

$$\exp\left[\frac{i}{\hbar}S(x_2,t_2;x_1,t_1)\right] \tag{1.3.4}$$

Thus one postulates that

$$\psi(x_2,t_2) = \frac{1}{N}\int_{-\infty}^{\infty} \exp\left(\frac{i}{\hbar}S(x_2,t_2;x_1,t_1)\right)\psi(x_1,t_1)dx_1 \tag{1.3.5}$$

TH-421_02612202

where N is a normalization factor at $t_2 = t_1 + \triangle t$. The above expression is being justified by considering a small time increment $t_2 = t_1 + \triangle t$ and thereby, to arrive time dependent Schroedinger equation. Thus the left hand side of Eq. (1.3.5) is expanded as

$$\psi(x,t) + \triangle t \frac{\partial \psi(x,t)}{\partial t} \tag{1.3.6}$$

where x_2 has been replaced by x, and t_1 by t. The action given by Eq. (1.3.1) can be approximated as

$$\frac{m}{2}\frac{(x-x_1)^2}{\triangle t} - \triangle t V(\bar{x},t) \tag{1.3.7}$$

where $\bar{x}$ is an average distance, $\bar{x} = \frac{1}{2}(x + x_1)$. Now we introducing the variable $\eta = x_1 - x$, and expand in η and $\triangle t$ and get

$$\begin{aligned} \psi(x,t) + \triangle t \frac{\partial \psi}{\partial t} &= \int_{-\infty}^{\infty} d\eta \frac{1}{N} \exp\left(\frac{im\eta^2}{2\hbar \triangle t}\right)\left(1 - \frac{i\triangle t}{\hbar} V(x,t)\right) \\ &\cdot\left(\psi(x,t) + \eta \frac{\partial \psi}{\partial x} + \frac{1}{2}\eta^2 \frac{\partial^2 \psi}{\partial x^2}\right) \end{aligned} \tag{1.3.8}$$

where the normalization condition

$$\frac{1}{N}\int_{-\infty}^{\infty} d\eta \exp\left(\frac{im\eta^2}{2\hbar\triangle t}\right) = 1 \tag{1.3.9}$$

with

$$N = \sqrt{\frac{2\pi\hbar\triangle t}{im}} \tag{1.3.10}$$

When we equate terms of order $\triangle t$ and perform the integrals over the variable η, we obtain the time dependent Schroedinger equation

$$i\hbar\frac{\partial \psi}{\partial t} = -\frac{\hbar^2}{2m}\frac{\partial^2 \psi}{\partial x^2} + V(x,t)\psi \tag{1.3.11}$$

This result can now be generalized to a finite time interval−simply by repetition−such that the propagator becomes

$$K(x_2,t_2;x_1,t_1) = \lim_{\triangle t \to 0} \frac{1}{N^{(n-1)}} \int\int .... \int \exp\left(\frac{1}{\hbar} S(x_2 t_2; x_1 t_1)\right) dy_1 dy_2 .....dy_{n-1} \tag{1.3.12}$$

TH-421_02612202

The integration is performed over the $n-1$ time segments between the end point x_1 and x_2, i.e., y_i is integrated from $-\infty$ to ∞ for $i = 1, \ldots, n-1$. In some cases this integration can be carried out analytically−namely if the force is at most linear in the coordinate x, and in the general case for quadratic Hamiltonian.

1.3.2 Short-time propagator

In order to apply the Feynman path concept in actual numerical calculations it is convenient to introduce the short time propagator by incorporating various approximations in the limit of a small $\triangle t$. One such approximation is Trotter formula [4]

$$K(x_2, t_1 + \triangle t; x_1, t) = \frac{1}{N} \exp\left[\frac{im(x_2 - x_1)^2}{2\hbar\triangle t} - \frac{i\triangle t}{\hbar}\frac{1}{2}\big(V(x_2) + V(x_1)\big)\right] \quad (1.3.13)$$

By considering the short time propagator for Harmonic oscillator one gets (to order $\triangle t$) an exponent

$$\frac{im(x_2 - x_1)^2}{2\hbar\triangle t} - \frac{1}{6}\frac{i\triangle t m\omega^2}{\hbar}(x_2^2 + x_1^2 + x_1 x_2) \quad (1.3.14)$$

While comparing the exponent with the Trotter formula we find that the first term is identical but the latter is being replaced by

$$-\frac{1}{4}\frac{i\triangle t m\omega^2}{\hbar}(x_2^2 + x_1^2) \quad (1.3.15)$$

where for the Harmonic oscillator $V(x) = \frac{1}{2}m\omega^2 x^2$.

Makri and Miller has demonstrated that the proper short time propagator for small but finite $\triangle t$ is

$$K(x_2, t_1 + \triangle t; x_1, t) = \frac{1}{N} \exp\left(\frac{im(x_2 - x_1)^2}{2\hbar\triangle t} - \frac{i\triangle t\langle V\rangle}{\hbar}\right) \quad (1.3.16)$$

where

$$\langle V\rangle = \frac{1}{\triangle x}\int_{x_1}^{x_2} dx V(x) \quad (1.3.17)$$

For higher order terms of order $\triangle t^3$ detail description is available elsewhere [5, 6]. It can easily be demonstrated that expression in Eq. (1.3.16) for the Harmonic oscillator gives the correct $\triangle t$ terms.

TH-421_02612202

1.4 Evaluation of kinetic and potential energy operators and Wave packet propagation on space grid

The efficient evaluation of the effect of kinetic energy operators on a wavefunction helps to propagate the wavefunction on a space grid with time. In the grid representation, the wavefunction is expressed in a discrete manner where the potential is diagonal. The coupling between the wavefunctions at various grid-points appears through the kinetic energy term and the potential energy operator is just a multiplication with the wavefunction at the grid-point. The Fast Fourier Transformation (FFT) and Discrete Variable Representation (DVR) methods are the usual way of evaluating the kinetic energy terms. On the other hand, the time propagation of the wavefuntion can be performed in different ways, namely, Chebyshev or the Lanczos time propagation method.

1.4.1 Fourier Transform Method

The FFT method is based on the Fourier transform of the wave function

$$\psi(x_j) = \sqrt{\frac{1}{N}} \sum_{k=-N/2}^{N/2-1} c_k \exp\Big(\frac{-i2\pi kj}{N}\Big) \tag{1.4.1}$$

where $j = 0, 1, \ldots, N-1$, N the number of grid points, $x_j = j\triangle x + 0.5\triangle x$ and $\triangle x = (x_{max} - x_{min})/N$. The FFT method is termed fast due to the fact that it is an N logN process in the number of operations leading to less computing time [7].

The kinetic energy terms in Fourier space are evaluated by differentiating Eq. (1.4.1)

$$\frac{\partial^n \psi(x)}{\partial x^n} = \sqrt{\frac{1}{N}} \sum_k c_k \Big(-\frac{i2\pi k}{N\triangle x}\Big)^n \exp\Big(\frac{-i2\pi kj}{N}\Big) \tag{1.4.2}$$

The operators $\partial/\partial x$ working on the wavefunction can be evaluated by introducing the Fourier coefficients

$$d_k = (\omega_k)^n c_k \tag{1.4.3}$$

TH-421_02612202

with the frequency

$$\omega_k = -\frac{i2\pi k}{N\triangle x} \tag{1.4.4}$$

and then performing the reverse transform FFT^{-1} with these coefficients. A complex FFT routine gives a certain order of the frequencies, starting with zero and ending with $-1/N\triangle x$ as output, i.e., we have [7],

$$\omega_j = -\frac{i2\pi}{N\triangle x} j \quad \text{for } j < \frac{N}{2} \tag{1.4.5}$$

$$\omega_j = -\frac{i2\pi}{N\triangle x}(j-N) \quad \text{for } j \geq \frac{N}{2} \tag{1.4.6}$$

where j and k are related by $j = k + N/2$.

1.4.2 DVR method

If specific boundary conditions need to be fulfilled it is sometimes advantageous to use the discrete variable representation (DVR) method, which however is of order N^2 in the number of operations.

In the DVR method the wavefunction is represented at a discrete set of points, x_m. The function in between the grid points can be evaluated by using a suitable interpolation,

$$f(x) = \sum_{j=1}^{N} l_j(x) f(x_j) + E(x) \tag{1.4.7}$$

where $l_j(x)$ is the interpolation polynomial and $E(x)$ is the error. One example of the interpolation function $l_j(x)$ is the Lagrange polynomial,

$$l_j(x) = \frac{P_N(x)}{(x - x_j)p'_N(x_j)} \tag{1.4.8}$$

with

$$P_N(x) = \prod_{i=1}^{N}(x - x_i) \tag{1.4.9}$$

TH-421_02612202

and P'_N the derivative of P_N. The Lagrange polynomial possesses the property

$$l_j(x_k) = \delta_{jk} \tag{1.4.10}$$

This representation of the function $f(x)$ helps to obtain the derivatives

$$\frac{\partial^k f(x)}{\partial x^k} = \sum_{j=1}^{N} \frac{\partial^k}{\partial x^k} l_j(x) f(x_j) + \frac{\partial^k E(x)}{\partial x^k} \tag{1.4.11}$$

Instead of using the Lagrange function as an interpolation function, it is more convenient to use a basis set to construct functions with the above property. Thus a set of primitive basis functions can be chosen in such a way that specific boundary conditions are fulfilled. As for example we consider the particle in box (PIB) basis functions

$$\psi_n(x) = \sqrt{\frac{2}{\pi}} \sin(nx) \tag{1.4.12}$$

where $0 \leq x \leq \pi$. This basis functions are zero at the end points. Hence the grid points are the zeros of $\psi_{N+1}(x)$

$$x_k = \frac{k\pi}{N+1} \tag{1.4.13}$$

where $k = 1, \ldots, N$. Let an arbitrary wavefunction $f(x,t)$ be expanded in terms of interpolation polynomial

$$f(x,t) = \sum_n c_n(t) l_n(x) \tag{1.4.14}$$

The expansion coefficients, $c_n(t)$ can be evaluated as

$$c_n(t) = \omega_n \int_0^{\pi} dx f(x,t) l_n(x), \tag{1.4.15}$$

with ω_n is a normalization constant and

$$l_n(x) = \frac{2}{N} \sum_{k=1}^{N} \sin(kx) \sin(kx_n) \tag{1.4.16}$$

TH-421_02612202

Finally, $l_n(x)$ is determined by performing the summation over k

$$\begin{aligned} l_n(x) &= \frac{1}{N}\Bigg\{ \cos\Big[\frac{N+1}{2}(x-x_n)\Big] \sin\Big[\frac{N}{2}(x-x_n)\Big] \mathrm{cosec}\Big(\frac{x-x_n}{2}\Big) \\ &- \cos\Big[\frac{N+1}{2}(x+x_n)\Big] \sin\Big[\frac{N}{2}(x+x_n)\Big] \mathrm{cosec}\Big(\frac{x+x_n}{2}\Big)\Bigg\} \end{aligned} \tag{1.4.17}$$

From this expression we can conclude that the basis functions have the following δ function property: $l_n(x_k) \sim \delta_{nk}$. For other values of x the function oscillates near zero. It is important to note that the basis function $l_n(x)$ constitute an orthogonal but not necessarily normalized basis set, namely,

$$\int_0^\pi dx l_n(x) l_m(x) \sim \frac{\pi}{2N}\delta_{nm} \tag{1.4.18}$$

As the function $l_n(x)$ have the δ function property therefore the integral from Eq. (1.4.13) is evaluated as

$$c_n(t) = f(x_n, t)\omega_n \tag{1.4.19}$$

Thus the representation of the wavefunction (Eq. (1.4.12)) becomes

$$f(x,t) = \sum_n \omega_n f(x_n, t) l_n(x) \tag{1.4.20}$$

and the derivatives of the wavefunction are now easy to evaluate,

$$\frac{\partial^k f(x,t)}{\partial x^k} = \sum_n \omega_n f(x_n, t) \frac{\partial^k}{\partial x^k} l_n(x) \tag{1.4.21}$$

where the basis functions $l_n(x)$, as shown above, are constructed from an orthonormal basis set $\psi_n(x), (n = 1, \ldots, N)$

$$l_n(x) = \sum_i \psi_i^*(x_n)\psi_i(x) \tag{1.4.22}$$

and thereby, the derivatives are

$$\frac{\partial^k}{\partial x^k} l_n(x) = \sum_i \psi_i^*(x_n) \frac{\partial^k \psi_i(x)}{\partial x^k} \tag{1.4.23}$$

TH-421_02612202

The evaluation of the derivative at each of the N grid points requires N operations and therefore, the DVR method is an N^2 method. One advantage of DVR method is that the grid points do not have to be evenly spaced but can be placed in the regions where the wavefunction is located. The number of grid points can be reduced by removing points corresponding to the high-energy components by the sequential adiabatic reduction technique developed by Light and coworkers [8, 9]. This removal of the high-energy components of the spectrum is also important for the time propagation, since the time step of the propagators is roughly proportional to $\hbar/E_{max}$.

1.4.3 Time propagation

There can be different paths for time propagation. The simplest one is the second order difference (SOD) scheme as shown below

$$\phi(x_n, t+\Delta t) = \phi(x_n, t-\Delta t) + \frac{2\Delta t}{i\hbar}\widehat{H}(x_n, t)\phi(x_n, t) \tag{1.4.24}$$

where $\hat{H}$ denotes the Hamiltonian operator for the system. The error in the SOD method is of order $\triangle t^3$. Though the SOD method is simple to apply, it requires much smaller time step lengths in order to achieve comparable stability with respect to the other methods.

A popular as well as stable approach is the split operator method,

$$\begin{aligned}\phi(x_n, t+\Delta t) &= \exp\left(\frac{-i\Delta t\hat{H}}{\hbar}\right)\phi(x_n, t) \\ &= \exp\left(\frac{i\hbar\nabla^2\Delta t}{4m}\right)\exp\left(\frac{-iV\Delta t}{\hbar}\right)\exp\left(\frac{i\hbar\nabla^2\Delta t}{4m}\right)\phi(x_n, t)\end{aligned} \tag{1.4.25}$$

The splitting of the kinetic energy operator makes the algorithm a third order method in $\triangle t$, and the exponentiation keeps the operator unitary. The operation with the exponential operators on the wavefunction is evaluated by using an FFT or a DVR method. While using (Eq. 1.4.1) FFT method, one obtains,

$$\exp\left(\frac{i\hbar\nabla^2\Delta t}{2m}\right)\phi(x_j) = \frac{1}{\sqrt{N}}\sum_k c_k \exp\left[\frac{i\hbar\Delta t}{2m}\left(-\frac{i2\pi k}{N\Delta x}\right)^2\right]\exp\left(\frac{-i2\pi kj}{N}\right) \tag{1.4.26}$$

TH-421_02612202

Thus the result of operating with the exponential operator on the wavefunction is found by performing a Fourier transform to obtain the c_k coefficients and a back transformation with

$$d_k = c_k \exp\left(\frac{-i\hbar\Delta t}{2m}\frac{4\pi^2 k^2}{N^2\Delta x^2}\right) \tag{1.4.27}$$

The split operator method appears to use two FFTs per time step, but considering two consecutive time step we obtain

$$\begin{aligned}\phi(x_n, t+\Delta t) &= \exp\left(\frac{i\hbar\nabla^2\Delta t}{4m}\right)\exp\left(\frac{-iV\Delta t}{\hbar}\right)\exp\left(\frac{i\hbar\nabla^2\Delta t}{2m}\right) \\ &\quad \exp\left(\frac{-iV\Delta t}{\hbar}\right)\exp\left(\frac{i\hbar\nabla^2\Delta t}{4m}\right)\phi(x_n, t-\Delta t)\end{aligned} \tag{1.4.28}$$

etc. Hence only one FFT evaluation per time step is needed. However, it is also possible to split the potential instead of kinetic energy term,

$$\exp\left(\frac{-i0.5V\Delta t}{\hbar}\right)\exp\left(\frac{i\hbar\nabla^2\Delta t}{2m}\right)\exp\left(\frac{-i0.5V\Delta t}{\hbar}\right) \tag{1.4.29}$$

and therby to use. Since the potential is diagonal on the grid, this may be convenient if the Hamiltonian is time-dependent. The method is not restricted to the above simple kinetic energy operator, though complicated operator require more splittings.

The Chebyshev polynomial based method is capable of taking large time step (for time-independent Hamiltonian) by using the following relation [10]

$$\exp\left(\frac{-i\hat{H}\Delta t}{\hbar}\right) = 2\sum_{k=1}^{\infty} i^k J_k(Z)\cos(k\phi) + J_0(z) \tag{1.4.30}$$

where J_n is a Bessel function and

$$iz\cos\phi = -\frac{i\hat{H}\Delta t}{\hbar} \tag{1.4.31}$$

When we introduce $x = \cos\phi$ and the recursion relations

$$i^k T_k = 2x i^k T_{k-1} - i^k T_{k-2} \tag{1.4.32}$$

TH-421_02612202

where $T_0 = 1$, $T_1 = \cos\phi$ and $T_k = \cos(k\phi)$ are the Chebyshev polynomials, we obtain

$$S_k(y) = 2yS_{k-1}(y) + S_{k-2}(y) \tag{1.4.33}$$

with $y = ix$ and $S_k = i^k T_k$. Thus we get

$$zy = -\frac{i\hat{H}\Delta t}{\hbar} \tag{1.4.34}$$

Since x must be smaller than unity ($x = \cos\phi$) the energy (the Hamiltonian) has to be rescaled in order to achieve the convergence of the method. Thus, one should introduce

$$x = -\frac{\hat{H}}{E_{max}} \tag{1.4.35}$$

$$z = \frac{\Delta t E_{max}}{\hbar} \tag{1.4.36}$$

and obtain

$$\exp\Big(-\frac{i\hat{H}\Delta t}{\hbar}\Big)\phi = \phi + 2\left(\sum_{n=1}^{\infty} J_n(z)\tilde{\phi_n} - \sum_{n=1}^{\infty} J_{2n}(z)\phi\right) \tag{1.4.37}$$

where $\tilde{\phi_n}$ is calculated from the recursion formula

$$\tilde{\phi_n} = 2y\tilde{\phi}_{n-1} + \tilde{\phi}_{n-2} \tag{1.4.38}$$

by using $\tilde{\phi_n} = S_n\phi$, and

$$J_0(z) = 1 - 2\sum_{k=1} J_{2k}(z) \tag{1.4.39}$$

Thus the above scheme is initiated by evaluating $\tilde{\phi_0} = \phi$ (the initial wave function) and $\tilde{\phi_1} = -i\hat{H}\phi/E_{max}$ with the relation $y = -i\hat{H}/E_{max}$.

The Chebyshev method is convenient to use if the Hamiltonian is time - independent [11]. Time interval Δt is taken to be large enough to cover the complete dynamics of the system where the convergence criterion is $J_k(z) << 0$. The value

TH-421_02612202

of k for which the series may be truncated is being estimated from the asymptotic formula

$$J_k(z) \sim \frac{1}{\sqrt{2\pi k}}(\frac{ez}{2k})^k. \tag{1.4.40}$$

The Lanczos reduction technique is yet another method for time propagation. When the Hamiltonian is time-dependent, either because external fields are are included or because part of the system is treated within the classical mechanical approximation, it is more convenient to use the Lanczos reduction technique [12]. In this method, the time dependent Schrödinger equation (TDSE) is written in matrix form as

$$i\hbar\dot{\phi} = \mathbf{H}\phi \tag{1.4.41}$$

where ϕ is a vector of length N, containing the value of the wavefunction at the N grid points, and $\mathbf{H}$ is an $N \times N$ matrix. Then a transformation matrix transforms the grid representation of the wavefunction to a tridiagonal form and the matrix is defined by

$$\mathbf{T} = [\phi_0, \phi_1, \ldots, \phi_{L-1}] \tag{1.4.42}$$

where $L << N$ is the number of Lanczos recursions. The elements of $\mathbf{T}$ are called the recursion (Krylov) vectors and are obtained as

$$\mathbf{H}\phi_0 = \alpha_0\phi_0 + \beta_1\phi_1 \tag{1.4.43}$$

$$\mathbf{H}\phi_k = \beta_k\phi_{k-1} + \alpha_k\phi_k + \beta_{k+1}\phi_{k+1} \tag{1.4.44}$$

where ϕ_0 is the initial wavefunction. Thus the Hamiltonian operates on the initial wavefunction ϕ_0 and creates the nearest dynamical environment around ϕ_0. If the step length was zero, the initial wavefunction would be an eigenfunction, i.e., $\beta_1 = 0$. Equations (1.4.41) and (1.4.42) along with the orthonormality conditions

$$\langle\phi_n|\phi_m\rangle = \delta_{nm} \tag{1.4.45}$$

TH-421_02612202

define the recursion coefficients α_k and β_k. Hence, the transformed tridiagonal matrix is given by

$$\tilde{\mathbf{H}} = \mathbf{T}^{\dagger}\mathbf{H}\mathbf{T} = \begin{pmatrix} \alpha_0 & \beta_1 & 0 & \dots & 0 & 0 \\ \beta_1 & \alpha_1 & \beta_2 & \dots & 0 & 0 \\ 0 & \beta_2 & \alpha_2 & \dots & 0 & 0 \\ . & . & . & & . & . \\ . & . & . & . & . & . \\ . & . & . & & . & . \\ 0 & 0 & 0 & \dots & \alpha_{L-2} & \beta_{L-1} \\ 0 & 0 & 0 & \dots & \beta_{L-1} & \alpha_{L-1} \end{pmatrix} \tag{1.4.46}$$

The tridiagonal matrix is of order $L \times L$ and can easily be diagonalized. Thus the propagated wavefunction is obtained through

$$\phi(t + \Delta t) = \mathbf{T}\mathbf{S} \exp\left(-\frac{i}{\hbar}\mathbf{D}\Delta t\right) \mathbf{S}^{\dagger}\mathbf{T}^{\dagger}\phi(t) \tag{1.4.47}$$

where $\mathbf{D}$ is diagonal $(L \times L)$ matrix containing the eigenvalues of the tridiagonal matrix; $\mathbf{T}$ is an $(N \times L)$ matrix with the L recursion vectors of length N (the number of grid points); and $\mathbf{S}$ is an $(L \times L)$ matrix containing the eigen vectors of the tridiagonal matrix. The number of Lanczos recursions depends upon the length of the time step and the magnitude of the Hamiltonian. The rapid convergence of the recursion demands a Hamiltonian bounded to a region $H_{min} \leq H \leq H_{max}$ at each grid point. Thus if the potential goes to infinity in certain regions it is simply replaced by a maximum value V_{max} in these regions. The value of V_{max} depends, of course, on the actual problem under consideration and the final result should be independent of its choice. For a given input vector, Lanczos method will create the nearest dynamical environment around the input state. The method requires one FFT evaluation per iteration and is very stable, i.e., can be used for long time propagations.

TH-421_02612202

1.5 Gaussian Wave Packet based methods

1.5.1 The classical path equations

In the classical path equations [13] the degrees of freedom of a system are separated into classical and quantum subsets. The classical degrees of freedom are solved with an effective potential where the quantum degrees have been averaged over. The classical path equations can be obtained from the first principles by introducing two approximations: (1) A separability assumption, i.e., a wavefunction of two degrees of freedom is written as a product type function $\psi(r,t)\Phi(R,t)$ where the r and R coordinates represent the quantum and the " classical" degrees of freedom, respectively. (2) The second approximation has to do with the form of $\Phi(R,t)$. It is taken to be a Gaussian wave packet (GWP).

The Hamiltonian for a system with two degrees of freedom, r and R, is given by

$$H = \hat{H}_0(r,\hat{p_r}) - \frac{\hbar^2}{2\mu}\frac{\partial^2}{\partial R^2} + V(r,R) \tag{1.5.1}$$

and the form of the trial function

$$\psi(R,r,t) = \phi(r,t)\exp\left\{\frac{i}{\hbar}\Big[\gamma(t) + P_R(t)(R-R(t)) + A(t)(R-R(t))^2\Big]\right\} \tag{1.5.2}$$

If we insert the Hamiltonian and the trial function in the TDSE and equate equal powers of $(R-R(t))^k$ with $k = 0$, 1, and 2, we obtain the following set of equation

$$\dot{R}(t) = \frac{P_R(t)}{\mu} \tag{1.5.3}$$

$$\dot{P}_R = -\frac{\partial}{\partial R}\langle\phi|V(r,R)|\phi\rangle\Big|_{R=R(t)} \tag{1.5.4}$$

$$\dot{A} = -\frac{2}{\mu}A^2 - \frac{1}{2}\frac{\partial^2}{\partial R^2}\langle\phi|V(r,R)|\phi\rangle\Big|_{R=R(t)} \tag{1.5.5}$$

$$\dot{\gamma} = \frac{i\hbar A}{\mu} + \frac{P_R^2}{\mu} \tag{1.5.6}$$

where the brackets indicate integration over r. For the quantum part of the system we obtain the following equation of motion

$$i\hbar\frac{\partial\phi}{\partial t} = \Big[\hat{H}_0 + V(r,R(t)) + F(t)\Big] \tag{1.5.7}$$

TH-421_02612202

where the phase factor $F(t)$ is

$$F(t) = \dot{\gamma} - \frac{P_R(t)^2}{2\mu} - \frac{i\hbar A(t)}{\mu} = \frac{P_R(t)^2}{2\mu} \tag{1.5.8}$$

Thus we see that the classical path equations perform the simultaneous integration of the "classical" equations of motion (Eqs. (1.5.3) and (1.5.4)) and the time-dependent Schrodinger equation (Eq. (1.5.7)). The equations are coupled self-consistently through the effective potential.

1.5.2 Corrections to the classical path equations: Hermite corrections

There can be two corrections to the Classical path equations. One is the self-consistent field (SCF) approach to correct the Gaussian form of the Wave packet [14]. One such correction is the multitrajectory approach [15], where the interaction between the two subsystems, namely the quantum and the classical, demands more GWP's as the coupling increases. However, these equations of motion for the GWP's can be troublesome to work with in practical calculations. The GWP's form a nonorthogonal basis set and the solution of the equations of motion involves the inversion of nearly singular matrices.

Another correction is the attempt to correct the separability approximation, namely, if the degrees of freedom are strongly coupled, we can not expect to get an accurate description with the simple product form of the wave function. This kind of correction is termed as the MCSCF (multiconfiguration self-consistent field) approach. If the coupling between the R and r degrees of freedom is weak we expect the separability approximation to be valid. Since GWP is the correct form of the asymptotic (the initial) wavefunction leading to the classical limit in a natural fashion, the corrected theory has the classical path theory as the limit. A convenient way to achieve this correction is based on the use of Hermite polynomial with GWP [15]. The Hermite correction is also known as the quantum correction to the classical path equation.

TH-421_02612202

The quantum correction to the classical path equation is based upon the introduction of time-dependent basis function which in the limit gives the classical path equation. This basis set is introduced only in those degrees of freedom which are expected to behave classically. The method corrects both in the SCF and MCSCF direction, and is therefore ideal for the correction of the classical path equations. It also contains the options for an easy determination of the correlation between the classical and the quantum degree(s) of freedom and thereby, to determine whether the primitive classical path theory is expected to work or not.

1.5.3 The Hermite correction method

The product type wavefunction is expressed as

$$\Psi(r, R, t) = \sum_{nk} a_{nk}(t)\phi_n(r)\Phi_k(R, t) \tag{1.5.9}$$

The total Hamiltonian contains the following terms:

$$H(r, R) = \hat{H}_0 + T_R + V(r, R) \tag{1.5.10}$$

where the function $\phi_n(r)$ are chosen to be the eigenfunction of H_0,

$$H_0\phi_n(r) = E_n\phi_n(r) \tag{1.5.11}$$

and T_R is the kinetic energy for the R-motion and $V(r, R)$ the potential which couples the the two degrees of freedom. At $t = t_0$, the system is represented by the wavefunction

$$\Psi(r, R, t_0) = \phi_l(r)\Phi_{GWP}(R, t_0) \tag{1.5.12}$$

where $\Phi_{GWP}(R, t_0)$ is a Gaussian wave packet

$$\Phi_{GWP}(R, t_0) = \exp\left\{\frac{i}{\hbar}[\gamma(t_0) + P_0(R - R(t_0)) + A(t_0)(R - R(t_0))^2]\right\} \tag{1.5.13}$$

TH-421_02612202

centered around $R_0 = R(t_0)$ in coordinate and P_0 in momentum space. The initial condition of the parameters can be taken to be

$$R_0 \quad \text{large}, \tag{1.5.14}$$

$$P_0 \quad \text{arbitrary}, \tag{1.5.15}$$

$$ReA(t_0) = 0, \tag{1.5.16}$$

$$ImA(t_0) \quad \text{arbitrary}, \tag{1.5.17}$$

$$Re\gamma(t_0) = 0, \quad \text{and} \tag{1.5.18}$$

$$Im\gamma(t_0) = -\frac{\hbar}{4} ln(2ImA(t_0)/\pi\hbar) \tag{1.5.19}$$

where the last equation follows from normalization. The initial value of the width parameter $ImA(t_0)$ and P_0 are arbitrary in the sense that the final solution is independent of where in momentum space we place the wave packet and also of its width. In practical calculation there will be a dependence on those parameters due to numerical inaccuracies but the wave packet can represent a finite energy range around the center momentum accurately.

Let the function $\Phi_k(R,t)$ at any time t is

$$\Phi_k(R,t) = \pi^{\frac{1}{4}} \exp\left\{\frac{i}{\hbar}\left(\gamma(t) + P(t)[R - R(t)] + ReA(t)[R - R(t)]^2\right)\right\} \xi_k(x) \tag{1.5.20}$$

where

$$x = \sqrt{\frac{2ImA(t)}{\hbar}}[R - R(t)] \tag{1.5.21}$$

and

$$\xi_k(x) = \frac{1}{\sqrt{k!2^k\sqrt{\pi}}} \exp\left(\frac{-x^2}{2}\right) H_k(x) \tag{1.5.22}$$

are the Harmonic oscillator wave functions. The basis function has two important properties. First they form an orthonormal basis, i.e.,

$$\int dR \Phi_k^*(R,t)\phi_n(R,t) = \delta_{kn} \tag{1.5.23}$$

TH-421_02612202

and second the ground state is the Gaussian wave packet given by Eq. (1.5.13). It is important to note that the normalization condition not only holds at t_0 but at all time t.

If we include only one basis function and replace a_{n0} with a_n we obtain

$$\Psi(r,R,t) = \sum_n a_n(t)\phi_n(r)\phi_0(R,t) \tag{1.5.24}$$

When this expansion is inserted in the TDSE, the classical path equations appears as

$$\begin{aligned}
i\hbar\dot{a_n}(t) &= E_n a_n(t) + \sum_m V_{nm}(R(t))a_m(t), && (1.5.25)\\
\dot{P}(t) &= -\sum_{nm} a_n^*(t)a_m(t)\frac{\partial V_{nm}(R)}{\partial R}\Big|_{R=R(t)}, && (1.5.26)\\
\dot{R} &= \frac{P(t)}{\mu}, && (1.5.27)\\
\dot{A}(t) &= -\frac{2}{\mu}A(t)^2 - \frac{1}{2}\sum_{nm} a_n^*(t)a_m(t)\frac{\partial^2 V_{nm}}{\partial R^2}\Big|_{R=R(t)}, && (1.5.28)\\
\dot{\gamma}(t) &= \frac{P(t)^2}{\mu} + \frac{i\hbar A(t)}{\mu}, && (1.5.29)
\end{aligned}$$

where the matrix element V_{nm} is defined by

$$V_{nm}(R) = \langle\phi_n|V(R,r)|\phi_m\rangle \tag{1.5.30}$$

At this junction, we can formulate rigorous classical path equations of motion within the MCSCF framework by using the following equations

$$\begin{aligned}
\frac{d}{dt}R(t) &= \frac{P(t)}{\mu} && (1.5.31)\\
\frac{d}{dt}ImA(t) &= -\frac{4}{\mu}ReA(t)ImA(t) && (1.5.32)\\
\frac{d}{dt}Im\gamma(t) &= \frac{\hbar}{\mu}ReA(t) && (1.5.33)
\end{aligned}$$

The first equation introduce the classical path picture (the center of the wave packet follows a classical equation of motion) and the two other equations ensures that the

TH-421_02612202

basis set is normalized at all time t. If we insert the Eq. (1.5.9) in the TDSE and use Eqs. (1.5.26) - (1.5.28), the coupled equations for the expansion coefficients a_{ml} are as below,

$$\begin{aligned} i\hbar\dot{a}_{ml} &= E_m a_{ml} + \sum_{nk} a_{nk} V_{mn}^{lk}(t) + a_{ml}\left(2l\frac{\hbar ImA(t)}{\mu} + \frac{P(t)^2}{2\mu} - \frac{\hbar(l-\frac{1}{2})}{4ImA(t)}V''_{eff}\right) \\ &- \frac{1}{2}V'_{eff}\sqrt{\hbar/ImA(t)}\left(\sqrt{l}a_{m,l-1} + \sqrt{l+1}a_{m,l+1}\right) \\ &- \frac{1}{8}\frac{\hbar}{ImA(t)}V''_{eff}\left[\sqrt{l(l-1)}a_{m,l-2} + \sqrt{(l+1)(l+2)}a_{m,l+2}\right] \end{aligned} \quad (1.5.34)$$

where

$$V_{mn}^{lk}(t) = \int dR \Phi_l^*(R,t) V_{mn}(R) \Phi_k(R,t) \quad (1.5.35)$$

but V'_{eff} and V''_{eff} are not specified yet. These quantities enter into the equations of motion for $P(t)$ and $ReA(t)$,

$$\dot{P}(t) = -V'_{eff} \quad (1.5.36)$$

$$\frac{d}{dt}ReA(t) = -\frac{2}{\mu}(ReA(t)^2 - ImA(t)^2) - \frac{1}{2}V''_{eff} \quad (1.5.37)$$

Comparing Eqs. (1.5.21) and (1.5.23) we can write

$$V'_{eff} = \sum_{ml;nk} a_{ml}^*(t)a_{nk}(t) \int dR \times \Phi_l^*(R,t)\frac{d}{dR}V_{nm}(R)|_{R=R(t)}\Phi_k(R,t) \quad (1.5.38)$$

$$V''_{eff} = \sum_{ml;nk} a_{ml}^*(t)a_{nk}(t) \int dR \times \Phi_l^*(R,t)\frac{d}{dR}^2 V_{nm}(R)|_{R=R(t)}\Phi_k(R,t) \quad (1.5.39)$$

However it is possible to derive rigorous expressions by using the Dirac - Frenkel variational principle by minimizing the following integral

$$\int drdR\left(-i\hbar\frac{\partial\Psi(r,R,t)^*}{\partial t} - H\Psi(r,R,t)^*\right) \times \left(i\hbar\frac{\partial}{\partial t}\Psi(r,R,t) - H\Psi(r,R,t)\right) \quad (1.5.40)$$

The equations of motion are obtained by differentiation with respect to $\dot{P}$ and $\frac{d}{dt}ReA(t)$

TH-421_02612202

and after some manipulations(!) we finally get

$$V'_{eff} = \frac{\begin{vmatrix} Q_1 & S^{(3)} - X_{12} \\ Q_2 & S^{(4)} - X_{22} \end{vmatrix}}{\begin{vmatrix} S^{(2)} - X_{11} & S^{(3)} - X_{12} \\ S^{(3)} - X_{21} & S^{(4)} - X_{22} \end{vmatrix}} \tag{1.5.41}$$

and

$$\frac{1}{2}V''_{eff} = \frac{\begin{vmatrix} S^{(2)} - X_{11} & Q_1 \\ S^{(3)} - X_{21} & Q_2 \end{vmatrix}}{\begin{vmatrix} S^{(2)} - X_{11} & S^{(3)} - X_{12} \\ S^{(3)} - X_{21} & S^{(4)} - X_{22} \end{vmatrix}} \tag{1.5.42}$$

where

$$Q_1 = \sum_{nk;ml} a^*_{nk} a_{ml} \left(V^{(1)}_{ml;nk} - \sum_p S^{(1)}_{kp} V^{(0)}_{np;ml} \right) \tag{1.5.43}$$

$$Q_2 = \sum_{nk;ml} a^*_{nk} a_{ml} \left(V^{(2)}_{ml;nk} - \sum_p S^{(2)}_{kp} V^{(0)}_{np;ml} \right) \tag{1.5.44}$$

$$X_{ij} = \sum_{nk;np} \sum_l a^*_{nk} a_{np} S^{(i)}_{kl} S^{(j)}_{lp} \tag{1.5.45}$$

$$V^{(j)}_{ml;nk} = \int dR \Phi^*_l(R,t) V_{mn}(R) (R - R(t))^j \Phi_k(R,t) \tag{1.5.46}$$

$$S^{(j)}_{lk} = \int dR \Phi^*_l(R,t) (R - R(t))^j \Phi_k(R,t) \tag{1.5.47}$$

$$S^{(j)} = \sum_n \sum_{lk} a^*_{nk} a_{nl} S^{(j)}_{kl} \tag{1.5.48}$$

One can introduce the projection operator $Q = I - P$, where I is the identity operator and

$$P = \sum_{m=0}^{N} |\Phi_m\rangle\langle\Phi_m| \tag{1.5.49}$$

and N is the highest Hermite polynomial used in the expansion. Thus we can express

TH-421_02612202

the quantities involved in calculating the potential derivatives as

$$Q_i = \sum_{mnkl} a^*_{nk} a_{ml} \langle \Phi_k | \triangle R^i Q V_{mn}(R) | \Phi_l \rangle \quad (1.5.50)$$

$$S^{(i+j)} - X_{ij} = \sum_{nkl} a^*_{nk} a_{nl} \langle \Phi_k | \triangle R^i Q \triangle R^j | \Phi_l \rangle \quad (1.5.51)$$

Though in the limit $P \rightarrow I$ we have $Q \rightarrow 0$, i.e., both numerator and denominator approaches zero, still a meaningful ratio can be obtained.

1.5.4 Time-dependent discrete variable representation method (TDDVR)

Based on the classical path theory, Adhikari and Billing have used the time - dependent Gauss - Hermite (G-H) basis functions as the primitive one to construct time - dependent DVR basis and formulated the novel time - dependent discrete variable representation (TDDVR) method [16, 17]. In the first version of TDDVR [16], all the parameters in the GWP were considered time dependent but found that the non-linear equation of motion for the width parameters (ImA, ReA) leads to extreme values in many cases. In the subsequent formulation [17], it was attempted to overcome this problem by introducing a special choice, i.e., the fixed width approach $[ReA(t) = 0, V''_{eff} = 4ImA(t)^2/\mu]$, and derived an approximate quantum-classical equation of motion. In this article the potential has been expanded around the trajectory $(s - s(t))$, and thereby, the comparison of first order terms gives $\dot{p_{s_c}}(t) = -V'_{eff}$ and the second order provides $4ImA(t)^2/\mu = V''_{eff}$. When the quantities, $\dot{p_{s_c}}(t)$ and $4ImA(t)^2/\mu$, were re-substituted by V'_{eff} and V''_{eff}, respectively in the quantum equation of motion, an effective potential such as $[V(s) - V(s(t)) - V'_{eff}(s - s(t)) - 1/2V''_{eff}(s - s(t))^2]$ dictates the dynamics around the trajectory. This version of fixed width approach was based on an approximation that the second order term is diagonal and subsequently was introduced as the reference potential. It can be shown that in DVR representation the matrix elements over the first order term, $(s - s(t))$, are diagonal but the second order terms are not. Moreover, this formulation is valid only when the second derivative of the potential is non zero. On the other hand, the

TH-421_02612202

present version of fixed width approach is general and does not introduce any approximation. Indeed, the derivation has the scope to formulate the rigorous expression for V'_{eff} and V''_{eff} with the help of the Dirac-Frenckel variational principle. It is possible to apply TDDVR to any kind of potential with the help of the force not really known from Newtonian mechanics.

TH-421_02612202

CHAPTER II

THEORETICAL ASPECTS OF TDDVR METHOD

2.1 Introduction

Physical processes on the molecular scale are inherently quantum [18] in nature but rigorous quantum mechanical treatment of large molecular systems is impractical. Processes like electronic transitions, tunneling and zero-point motion are inherently quantum mechanical effects and must be treated as such. When we attempt to incorporate these quantum effects, calculations even for the motion on a single potential energy curve/surface, require enormous computational effort. Traditional QM approaches are impractical even for three or four particle systems, especially when the atoms are heavy, the energy is high and multiple PESs are involved. Formulation of quantum molecular dynamical approach for large systems is a growing area of current interest. In this context, one can distinguish two dynamical regimes namely, quasi-classical and deep quantum. In the case of quasi-classical regime, classical mechanical methods with some mild corrections for simple quantum features are good enough whereas classical mechanics fails even qualitatively to explain features in the deep quantum regime. Quantum correction to classical mechanics is one of the avenues to develop first principles based quantum-classical approaches with the motivation: The method can distinguish both quasi-classical and deep quantum regimes of a system and treat quasi-classical regime classically with some mild quantum corrections and the quantum regime rigorously. Moreover, traditional time-dependent approaches

TH-421_02612202

use stationary grid-points/basis set to represent a wavefunction and waste many grid-points/basis functions to specify empty space. Methods with time-dependent basis functions or moving grid-points may have the scope to achieve convergence significantly fast.

One of the commonest ways to pursue such approaches is the use of Gaussian wave packet (GWP) [19] and its' extension Gauss - Hermite (G-H) basis set [20–27]. It is possible to parametrize the solution of time - dependent Schroedinger equation (TDSE) by expanding the wavefunction in terms of G-H basis functions. Time - dependent parameters of GWP appear naturally in the "classical" equation of motion with more generalized force, not really known from ordinary Newtonian mechanics. Several attempts to develop methods using time - dependent basis set have been made but in all the cases main focus has been on how accurately as well as efficiently the following two tasks can be performed: (a) Equations of motion for the "classical" parameters of G-H basis have to be solved at each time step to propagate the time-dependent basis; (b) Evaluation of the matrix elements of the Hamiltonian/effective Hamiltonian has to be performed at each time step. Kucar and Meyer [25], Hsu and Coker [26], and Billing [27] proposed different approaches to determine variationally optimized equations of motion for the parameters but all these approaches some way or the other, encounter computational bottleneck while evaluating the matrix elements over potential or effective potential. Even if these matrix elements are calculated numerically or analytically (by expressing the potential as a infinite sum of exponential, Gaussian or powers of the coordinate), we have found [28–30] that the efficiency remains poor. We have also noticed that bulk of the CPU time goes for evaluating matrix elements (compared to propagation time) even though the kinetic energy term is local in G-H basis. Moreover, differential equations for propagating the "classical" parameters are rather stiff in all these approaches, thereby affecting the quantum equations of motion too, and increasing the computation time significantly.

TH-421_02612202

In the discrete variable representation (DVR) [31–35], the wavefunction is presented as a quadrature over the basis of points ($\{x\}_N$) with approximate amplitudes at these grid-points. It gives the possibility of formulating novel time-dependent DVR methods [16, 17, 36] for which only time-propagation is needed. Time - dependent discrete variable representation (TDDVR) method [16, 17, 36] is a very convenient formulation with the following attributes: (a) TDDVR is appealing from the computational point of view; (b) It paves the blending of classical and quantum concepts with a new twist. Since G-H basis functions are used as the primitive basis, TDDVR has the advantages arising from DVR representation as well as time - dependent basis. In this formulation: (a) An optimized set of asymmetrically dense grid-points are generated from the eigenfunctions of harmonic oscillator around the center of initial wavepacket, GWP; (b) The movements of unevenly spaced grid-points are dictated by the "classical" dynamics of the time - dependent parameters of GWP and this reduces the requirement of number of grid-points for each mode drastically; (c) Both kinetic and potential energy operators are local. The evaluation of KE matrices is once for the entire propagation whereas potential energy is diagonal, need to be calculated at each time step; (d) Couplings among grid-points appear through KE matrices of different modes. The contribution of various modes on the time - dependent amplitude of a grid-point of any mode can be evaluated independently on different CPUs; (e) The requirement of physical memory is negligibly small since the algorithm does not need the entire string of amplitudes of wavefunction at a time; (f) Quantum - classical equations indicate the reason for the stiffness of differential equations and allow one to predict the possibility to eliminate such problems.

In the first attempt, TDDVR [16] was formulated considering all the parameters in the GWP as time - dependent variables and found, in many cases, width parameters (ImA, ReA) accumulate extreme values due to nonlinear classical equation

TH-421_02612202

of motion, finally affecting the quantum propagation also. In a subsequent article [17], we tried to overcome the problem by introducing a fixed width approach [$ReA(t) = 0, V''_{eff} = 4ImA(t)^2/m$] and derived an *approximate* quantum - classical equation of motion (TDDVR). *Even though ImA was treated as a time-dependent variable, solutions of the resulting TDDVR [17] equations were effectively independent of the time dependence of ImA.* In the same article [17], we expanded the potential around the trajectory ($(s-s(t))$), compared the second-order term ($(s-s(t))^2$), in the Schrodinger equation, and equated $4ImA(t)^2/\mu$ with the double derivative of the potential (V''_{eff}) [Eq. (B5) in Appendix B]. Similarly, from the first order terms, we get $\dot{p_{s_c}}(t) = -V'_{eff}$ [Eq. (B3) in Appendix B]. When these terms, $\dot{p_{s_c}}(t)$ and $4ImA(t)^2/\mu$, were re-substituted by V'_{eff} and V''_{eff}, respectively, in the quantum equation of motion, an effective potential $[V(s) - V(s(t)) - V'_{eff}(s - s(t)) - 1/2V''_{eff}(s - s(t))^2]$ around the trajectory was obtained. Finally, the second term in Eq. (24) of Ref. [17], which forms a full matrix, was an obvious outcome (Appendix B). *Let us now take note of the following: (1) The first-order term gives an effective potential but the assumption that the second-order term is diagonal and its subsequent introduction as the reference potential are approximations. Matrix elements over the first-order term, $(s - s(t))$, are diagonal but the same does not apply to the second order term, $(s - s(t))^2$. (2) One can pursue this fixed width approach, i.e., $V''_{eff} = 4ImA(t)^2/\mu$ (even though it approximates the quantum equations of motion) only when the second derivative of the potential is defined and is nonzero. (3) The time dependence of p_{s_c} and ImA in both the methods [16, 17] was approximately obtained by using the force $[V'_{eff} = (d/ds)V(s)|_{s=s(t)}]$ and $[V''_{eff} = (d^2/ds^2)V(s)|_{s=s(t)}]$ known from classical mechanics. Of course, one can attempt to derive the rigorous expression of V'_{eff} and V''_{eff} from the Dirac-Frenkel variational principle [37, 38], but it is possible only when $(s - s_c(t))^k, k \geq 2$ terms are not approximated as diagonal. While deriving this expression of $\dot{p_{s_c}}$, we see that the denominator of Eq. (D6) in Appendix D will be*

TH-421_02612202

trivially zero if $(s - s_c(t))^2$ *term is considered diagonal in DVR.*

We reformulate TDDVR method [36, 39–45] for multi - dimensional multi-surface system where the formulation is based on the following assumptions: (a) The total wavefunction is expressed as linear combination of product type TDDVR basis functions of different modes with time - dependent coefficients; (b) The TDDVR basis set is formed by multiplying DVR basis with plane wave; (c) Eigenfunctions of harmonic oscillator are chosen as the primitive basis to construct DVR basis set; (d) The plane wave is constituted with "classical" trajectory and its' momentum. When the total wavefunction is inserted into the TDSE, we obtain the parametrized quantum equation of motion for time - dependent coefficients and "classical" equation of motion for the central trajectory and its' momentum. Since the width parameters are associated with on- and off-diagonal matrix elements of quantum equation of motion, any non-linear classical propagation of widths [16] not only increases inaccuracy in the quantum equation of motion but also brings the stiffness in the classical equation of motion. Thus, an alternative version of fixed width approach [17] with time - independent width parameters [36, 39–45] is the obvious choice. On the other hand, since central trajectory and its' momentum appear only with on-diagonal elements of quantum equation of motion, their time-dependence does not affect the final solution of SE. In this formulation, we are able to bypass all the approximations made earlier and obtain rigorous quantum equation of motion. Moreover, this approach has enough scope to formulate variationally optimized "classical" equation of motion starting from first principles and can achieve quantum correction to "classical" trajectory or "classical" feedback to quantum dynamics in a self-consistent manner. The theory can be applied near the classical limit with few grid-points on a particular mode or in the quantum limit with sufficient grid-points. Nevertheless, it is important to note that one grid-point corresponds to classical limit.

In the TDDVR [16, 17, 36, 39–45] /DVR [31–35] approaches, evaluation of kinetic

TH-421_02612202

energy operator (KEO) is an N^2 but single step process whereas in FFT [46], this cost scales as $C * N \log N$ with typical computational overhead, $C \approx \frac{N}{\log N}$ and needs to be calculated at each time step. Multi-dimensional DVR/TDDVR involves sparse matrix $(N \sum_i N_i)$ multiplication and gains the speed effectively on a vector machine. Since DVR/TDDVR grid-points are unevenly spaced but located around the wavefunction, convergence reaches with smaller number of grid-points compared to FFT. DVR and FFT based algorithms require considerable number of grid-points for absorbing potential but TDDVR approaches do not need such potential (Appendix A). Finally, moving grid-points (TDDVR) reduce computational cost remarkably with respect to fixed grid-points (DVR). We may mention here that nested interaction representation (IR) approach [47, 48] is another formulation which introduces moving grid-point and propagates the wavefunctions $(\psi_I(t))$ via FFT-Lanczos routine. Though TDDVR and PR-adapted nested IR approaches are developed through different routes, their working equations have similarities. The interaction Hamiltonian (H_I) (Appendix A of ref. [47]) have similar terms like the first three terms of the Hamiltonian matrix (Eq. (18)). At the same time, the evaluation of $H_I\psi_I$ in the PR-adapted nested IR could be computationally costly. Thus, considering the following expansion,

$$H_I\psi_I = \sum_{n=0}^{N} a_n(\mathbf{R} + \frac{\mathbf{P}t}{m})^n\psi_I, \tag{2.1.1}$$

any general term $(\mathbf{R} + \frac{\mathbf{P}t}{m})^n\psi_I$ can be evaluated by sequential operation of $(\mathbf{R} + \frac{\mathbf{P}t}{m})$ on ψ_I. The $\mathbf{R}$ operation is local in coordinate space but $\mathbf{P}$ operation is non-local. For complicated potentials, polynomial expansion could reach high powers (n) and the method could become computationally very demanding. We may mention that the nested IR was formulated in the interaction/Heisenberg representations while TDDVR is in the Schroedinger representation, although the latter can be derived in the interaction/Heisenberg representations, also. Time-dependent DVR formulated by Makri *et. al.* [49] introduces DVR representation before the evaluation of KEO from primitive basis. The present TDDVR approach where DVR representation is

TH-421_02612202

introduced after the kinetic energy operators have acted on the basis functions is local and it is very simple to evaluate the remaining kinetic energy couplings. In this respect, TDDVR is similar to the distributed approximating function (DAF) approach [50, 51] which is again different from TDDVR in the sense that TDDVR grid-points propagate according to the "classical" dynamics of the system.

2.2 Formulation of the TDDVR method for one - dimensional multi - curve systems

The general form of the matrix equation for any one-dimensional multi-curve system in the diabatic representation can be expressed as,

$$i\hbar\frac{\partial}{\partial t}\Xi(s,t) = [\hat{\mathbf{T}}_s + \hat{\mathbf{V}}(s)]\Xi(s,t), \tag{2.2.1}$$

where

$$\hat{\mathbf{T}}_s \equiv \hat{T}_s \begin{pmatrix} 1 & 0 & \cdot & \cdot & 0 \\ 0 & 1 & \cdot & \cdot & 0 \\ \cdot & \cdot & \cdot & \cdot & \cdot \\ \cdot & \cdot & \cdot & \cdot & \cdot \\ 0 & 0 & \cdot & \cdot & 1 \end{pmatrix}, \quad \hat{\mathbf{V}}(s) \equiv \begin{pmatrix} \hat{V}_{11}(s) & \hat{V}_{12}(s) & \cdot & \cdot & \hat{V}_{1k}(s) \\ \hat{V}_{21}(s) & \hat{V}_{22}(s) & \cdot & \cdot & \hat{V}_{2k}(s) \\ \cdot & \cdot & \cdot & \cdot & \cdot \\ \cdot & \cdot & \cdot & \cdot & \cdot \\ \hat{V}_{k1}(s) & \hat{V}_{k2}(s) & \cdot & \cdot & \hat{V}_{kk}(s) \end{pmatrix}, \tag{2.2.2}$$

and

$$\Xi(s,t) \equiv \begin{pmatrix} \Psi_1(s,t) \\ \Psi_2(s,t) \\ \cdot \\ \cdot \\ \Psi_k(s,t) \end{pmatrix} \tag{2.2.3}$$

with $\int ds\Xi^{\dagger}(s,t)\Xi(s,t)= 1$ at all time t.

The kinetic energy operator, $\hat{T}_s = -\frac{\hbar^2}{2\mu}\frac{\partial^2}{\partial s^2}$, and the diagonal elements of the matrix in Eq. (2.2.2) represent potential energy operators for different curves while

TH-421_02612202

off-diagonal elements define the coupling among them. The lth element of the wavefunction matrix in Eq. (2.2.3) is the wavefunction for the lth curve and we can expand the time-dependent wavefunction ($\Psi_l(s,t)$) as follows:

$$\Psi_l(s,t) = \sum_i c_{il}(t)\psi_i(s,t), \tag{2.2.4}$$

where $\psi_i(s,t)$ is the time-dependent DVR basis function which can again be expanded in terms of a primitive (Gauss-Hermite) basis set to represent the coordinate, s, as a function of time, t,

$$\psi_i(s,t) = \Phi(s,t)\sum_{n=0}^{N}\xi_n^{\star}(x_i)\xi_n(x) = \sum_{n=0}^{N}\xi_n^{\star}(x_i)\Phi_n'(s,t) \tag{2.2.5}$$

with

$$\Phi(s,t) = \pi^{1/4}\exp\Big(\frac{i}{\hbar}\big\{\gamma + p_{s_c}(t)[s-s_c(t)] + ReA[s-s_c(t)]^2\big\}\Big), \tag{2.2.6}$$

$$\xi_n(x) = \frac{1}{\sqrt{n!2^n\sqrt{\pi}}}\exp\Big(-\frac{x^2}{2}\Big)H_n(x), \tag{2.2.7}$$

$$\xi_n(x_i) = \frac{1}{\sqrt{n!2^n\sqrt{\pi}}}\exp\Big(-\frac{x_i^2}{2}\Big)H_n(x_i) \tag{2.2.8}$$

and

$$x = \sqrt{\frac{2ImA}{\hbar}}(s-s_c(t)), \tag{2.2.9}$$

$$x_i = \sqrt{\frac{2ImA}{\hbar}}(s_i(t)-s_c(t)). \tag{2.2.10}$$

Among the parameters in GWP (Eqs. (2.2.6) - (2.2.10)) we choose the centre of the wavepacket (s_c) and its momenta (p_{s_c}) as time-dependent variable whereas γ and width (A) as time-independent with their real parts ($Re\gamma = ReA = 0$) equal to zero.

The index, i, in Eqs. (2.2.4) and (2.2.5) counts the DVR basis functions where N is the maximum number of Hermite basis functions included in Eq. (2.2.5) to expand a particular DVR basis. A DVR grid-point, s_i, will be determined by Eq. (2.2.10) using the root, x_i, of N th Hermite polynomial, $H_N(x)$ [17]. Though the roots ($x_i s$)

TH-421_02612202

of the polynomial are fixed, the position of the DVR grid-points (s_is) will change as a function of time due to the time-dependent variables, $s_c(t)$,

$$s_i(t) = s_c(t) + \sqrt{\frac{\hbar}{2ImA}} x_i \tag{2.2.11}$$

The Hermite basis functions, $\Phi'_n(s,t)$, as introduced in Eq. (2.2.5) have the following two important properties. Firstly, they form an orthonormal basis, i.e.,

$$\int ds \Phi^{\star\prime}_m(s,t)\Phi'_n(s,t) = \delta_{mn} \tag{2.2.12}$$

which is ensured by

$$Im\gamma = -\frac{\hbar}{4}\log(\frac{2ImA}{\pi\hbar}) \tag{2.2.13}$$

and secondly, the ground state of the Hermite basis is the Gaussian Wave Packet.

The DVR basis functions, $\psi_i s$, in Eq. (2.2.4) constitute an orthogonal but not normalized set,

$$\int ds \psi^{\star}_i(s,t)\psi_j(s,t) = \frac{\delta_{ij}}{A_{ij}}, \tag{2.2.14}$$

where A is the normalization factor.

We substitute Eqs. (2.2.2) and (2.2.3) in the time-dependent Schroedinger equation (Eq. (2.2.1)) and due to the special choice of the form of the TDDVR basis functions as defined in Eq. (2.2.5), the classical path picture appears naturally along with the TDDVR matrix equation.

The compact form of the quantum evolution equation for the motion on the kth curve is given in matrix form as follows:

$$i\hbar \mathbf{A}\dot{\mathbf{C}}_\mathbf{k} = \mathbf{H}^\mathbf{t}_\mathbf{kk}\mathbf{C}_\mathbf{k} + \mathbf{A}\sum_{\mathbf{l}\neq\mathbf{k}} \mathbf{V}_\mathbf{kl}\mathbf{C}_\mathbf{l} \tag{2.2.15}$$

Equation (2.2.15) can be reorganized into a more convenient form by a similarity transformation,

$$i\hbar \dot{\mathbf{D}}_\mathbf{k}(\mathbf{t}) = \mathbf{A}^{-1/2}\mathbf{H}^\mathbf{t}_\mathbf{kk}\mathbf{A}^{-1/2}\mathbf{D}_\mathbf{k} + \sum_{\mathbf{l}\neq\mathbf{k}} \mathbf{V}_\mathbf{kl}\mathbf{D}_\mathbf{l} \tag{2.2.16}$$

TH-421_02612202

where $\mathbf{D_k} = \mathbf{A^{1/2}C_k}$ and the explicit expression of an element of the time-dependent DVR Hamiltonian matrix, $\mathbf{H^t}$ (Appendix B) is,

$$\begin{aligned}
\{H_{kk}\}^t_{i,j} &= \Big[\frac{1}{2} \times \dot{p}_{s_c}(t) \times \sqrt{\frac{\hbar}{ImA}} \times X_{i,j} + \frac{\mu \dot{s}_c^2(t)}{2} \times A_{i,j} \\
&+ \frac{\hbar ImA}{\mu} \times Y_{i,j} - \frac{\hbar ImA}{2\mu} \times Z_{i,j} + V_{kk}(s_i) \times A_{i,j}\Big], \qquad (2.2.17)
\end{aligned}$$

$$\text{where} \quad A_{i,j} = \sum_{k=0}^{N} \xi_k^\star(x_j)\xi_k(x_i), \qquad (2.2.18)$$

$$X_{i,j} = \sum_{k=0}^{N-1} \xi_{k+1}^\star(x_j)\sqrt{k+1}\xi_k(x_i) + \sum_{k=1}^{N} \xi_{k-1}^\star(x_j)\sqrt{k}\xi_k(x_i), \qquad (2.2.19)$$

$$Y_{i,j} = \sum_{k=0}^{N} \xi_k^\star(x_j)2k\xi_k(x_i), \qquad (2.2.20)$$

$$\begin{aligned}
Z_{i,j} &= \sum_{k=0}^{N-2} \xi_{k+2}^\star(x_j)\sqrt{(k+1)(k+2)}\xi_k(x_i) + \sum_{k=2}^{N} \xi_{k-2}^\star(x_j)\sqrt{k(k-1)}\xi_k(x_i) \\
&+ \sum_{k=0}^{N} \xi_k^\star(x_j)(2k+1)\xi_k(x_i). \qquad (2.2.21)
\end{aligned}$$

Examination of the component matrices ($\mathbf{A}$, $\mathbf{X}$, $\mathbf{Y}$, $\mathbf{Z}$) that make up the time-dependent DVR Hamiltonian matrix ($\mathbf{H^t}$) bring out several computationally important features of the method. Thus, we note that $\mathbf{A}$, $\mathbf{X}$, $\mathbf{Y}$ and $\mathbf{Z}$ matrices (Tables 2.1-2.4) are time-independent and need to be evaluated once for all. As $\mathbf{A}$ and $\mathbf{X}$ matrices are diagonal and multiplied with "classical" variables $\dot{s}_c(t)$ and $\dot{p}_{s_c}(t)$ respectively, quantum equation of motion is free from any non-linearity due to "classical" motion, i.e., "classical" mechanics can only affect the convergence of the quantum dynamics. Again, as coupling among the grid-points appears through the full matrices $\mathbf{Y}$ and $\mathbf{Z}$ and plays major role in quantum dynamics, we wish them to be free from any non-linearity due to "classical" propagation. The choice of ImA as a time-independent variable ensures this. We may further note, that although both the $\mathbf{Y}$ and $\mathbf{Z}$ matrices are diagonally dominant, the average value of the off-diagonal elements of $\mathbf{Z}$ matrix is much larger than those of the $\mathbf{Y}$ matrix. Hence the $\mathbf{Z}$ matrix can not facilitate convergence of the solution of quantum equation of motion like $\mathbf{Y}$ if

TH-421_02612202

ImA is considered as time-dependent. On the other hand, in order to formulate a rigorous equation of motion, one needs to include **Z** matrix and therefore automatically treat ImA as a time-independent variable, if smooth convergence is to be achieved.

Table 2.1: DVR matrix elements $A_{i,j}$ for $N = 8$

i/j	1	2	3	4	5	6	7	8
1	3.7018	0.0000	0.0000	0.0000	0.0000	0.0000	0.0000	0.0000
2	0.0000	4.5781	0.0000	0.0000	0.0000	0.0000	0.0000	0.0000
3	0.0000	0.0000	5.0046	0.0000	0.0000	0.0000	0.0000	0.0000
4	0.0000	0.0000	0.0000	5.1901	0.0000	0.0000	0.0000	0.0000
5	0.0000	0.0000	0.0000	0.0000	5.1901	0.0000	0.0000	0.0000
6	0.0000	0.0000	0.0000	0.0000	0.0000	5.0046	0.0000	0.0000
7	0.0000	0.0000	0.0000	0.0000	0.0000	0.0000	4.5781	0.0000
8	0.0000	0.0000	0.0000	0.0000	0.0000	0.0000	0.0000	3.7018

Table 2.2: DVR matrix elements $X_{i,j}$ for $N = 8$

i/j	1	2	3	4	5	6	7	8
1	−15.3425	0.0000	0.0000	0.0000	0.0000	0.0000	0.0000	0.0000
2	0.0000	−12.8302	0.0000	0.0000	0.0000	0.0000	0.0000	0.0000
3	0.0000	0.0000	−8.1902	0.0000	0.0000	0.0000	0.0000	0.0000
4	0.0000	0.0000	0.0000	−2.7979	0.0000	0.0000	0.0000	0.0000
5	0.0000	0.0000	0.0000	0.0000	2.7979	0.0000	0.0000	0.0000
6	0.0000	0.0000	0.0000	0.0000	0.0000	8.1902	0.0000	0.0000
7	0.0000	0.0000	0.0000	0.0000	0.0000	0.0000	12.8302	0.0000
8	0.0000	0.0000	0.0000	0.0000	0.0000	0.0000	0.0000	15.3425

Table 2.3: DVR matrix elements $Y_{i,j}$ for $N = 8$

i/j	1	2	3	4	5	6	7	8
1	38.4712	−9.1426	2.7371	−1.3487	0.7992	−0.5151	0.3412	−0.2155
2	−9.1426	33.3502	−14.0838	3.8060	−1.7462	0.9716	−0.5829	0.3412
3	2.7371	−14.0838	27.8228	−16.9269	4.3070	−1.8686	0.9716	−0.5151
4	−1.3487	3.8060	−16.9269	24.7236	−17.8598	4.3070	−1.7462	0.7992
5	0.7992	−1.7462	4.3070	−17.8598	24.7236	−16.9269	3.8060	−1.3487
6	−0.5151	0.9716	−1.8686	4.3070	−16.9269	27.8228	−14.0838	2.7371
7	0.3412	−0.5829	0.9716	−1.7462	3.8060	−14.0838	33.3502	−9.1426
8	−0.2155	0.3412	−0.5151	0.7992	−1.3487	2.7371	−9.1426	38.4712

TH-421_02612202

Table 2.4: DVR matrix elements $Z_{i,j}$ for $N = 8$

i/j	1	2	3	4	5	6	7	8
1	67.2897	−4.1167	4.3042	−4.3833	4.3833	−4.3042	4.1167	−3.7018
2	−4.1167	40.5347	−4.7866	4.8745	−4.8745	4.7866	−4.5781	4.1167
3	4.3042	−4.7866	18.4080	−5.0965	5.0965	−5.0046	4.7866	−4.3042
4	−4.3833	4.8745	−5.0965	6.6985	−5.1901	5.0965	−4.8745	4.3833
5	4.3833	−4.8745	5.0965	−5.1901	6.6985	−5.0965	4.8745	−4.3833
6	−4.3042	4.7866	−5.0046	5.0965	−5.0965	18.4080	−4.7866	4.3042
7	4.1167	−4.5781	4.7866	−4.8745	4.8745	−4.7866	40.5347	−4.1167
8	−3.7018	4.1167	−4.3042	4.3833	−4.3833	4.3042	−4.1167	67.2897

Similarly the classical path equations can be written as

$$\dot{s}_c(t) = \frac{p_{s_c}(t)}{\mu} \tag{2.2.22}$$

$$\dot{p}_{s_c}(t) = -\Big\langle \Xi(s,t)\Big|\frac{d\hat{V}(s)}{ds}\Big|_{s=s_c(t)}\Big|\Xi(s,t)\Big\rangle \tag{2.2.23}$$

where the classical force is evaluated by substituting the matrices, $\Xi(s,t)$ and $\hat{V}(s)$ (Eqs. (2.2.2) and (2.2.3) respectively). Using Dirac-Frenkel variational principle [37], we have arrived at a rigorous expression of $\dot{p}_{s_c}$ for non-adiabatic processes by minimizing the following integral (Appendix D),

$$\begin{aligned} I &= \int ds\Big(-i\hbar\frac{\partial\Xi^\star(s,t)}{\partial t} - H(p_s,s)\Xi^\star(s,t)\Big) \\ &\times \Big(i\hbar\frac{\partial\Xi(s,t)}{\partial t} - H(p_s,s)\Xi(s,t)\Big), \end{aligned} \tag{2.2.24}$$

with respect to $\dot{p}_{s_c}$. At this point, it is important to note that compared to earlier versions [16, 17], only the present form of TDDVR [36] has the scope for the variational derivation of the evolution equation for p_{s_c}. The compact form of $\dot{p}_{s_c}$ in Eq. (D6) (Appendix D) can further be simplified when we replace $S^{(1)}_{ij}$ by $S^{(1)}_{ij}\delta_{ij}$ as first order term $(s - s_c(t))$ is diagonal in DVR (Table 2.2), leading to

$$\begin{aligned} \dot{p}_{s_c}(t) &= \sum_k\sum_{ij} c^\star_{ik}(t)c_{jk}(t)\Big\{\frac{2ImA^2}{\mu}\Big[S^{(2)}_{ij}\frac{S^{(1)\star}_{ii}}{A_{ii}} - S^{(3)}_{ij}\Big] - \frac{\hbar ImA}{\mu}\Big[R_{ij}\frac{S^{(1)\star}_{ii}}{A_{ii}} - T^\star_{ij}\Big]\Big\} \\ &\Big/ \Big[\sum_k\sum_i c^\star_{ik}(t)c_{ik}(t)\frac{S^{(1)\star}_{ii}S^{(1)}_{ii}}{A_{ii}} - \sum_k\sum_{ij} c^\star_{ik}(t)c_{jk}(t)S^{\star(2)}_{ij}\Big] \end{aligned} \tag{2.2.25}$$

TH-421_02612202

2.3 Formulation of the TDDVR method for multi - dimensional multi - surface systems

The general form of the matrix equation for any multi-dimensional multi-surface system in the diabatic representation can be expressed as,

$$i\hbar\frac{\partial}{\partial t}\Xi(\{s^k\},t) = [\hat{\mathbf{T}}_{\{s^k\}} + \hat{\mathbf{V}}(\{s^k\})]\Xi(\{s^k\},t), \tag{2.3.1}$$

where

$$\hat{\mathbf{T}}_{\{s^k\}} \equiv \hat{T}_{\{s^k\}} \begin{pmatrix} 1 & 0 & \cdot & \cdot & 0 \\ 0 & 1 & \cdot & \cdot & 0 \\ \cdot & \cdot & \cdot & \cdot & \cdot \\ \cdot & \cdot & \cdot & \cdot & \cdot \\ 0 & 0 & \cdot & \cdot & 1 \end{pmatrix}, \tag{2.3.2}$$

$$\hat{\mathbf{V}}(\{s^k\}) \equiv \begin{pmatrix} \hat{V}_{11}(\{s^k\}) & \hat{V}_{12}(\{s^k\}) & \cdot & \cdot & \hat{V}_{1M}(\{s^k\}) \\ \hat{V}_{21}(\{s^k\}) & \hat{V}_{22}(\{s^k\}) & \cdot & \cdot & \hat{V}_{2M}(\{s^k\}) \\ \cdot & \cdot & \cdot & \cdot & \cdot \\ \hat{V}_{l1}(\{s^k\}) & \hat{V}_{l2}(\{s^k\}) & \cdot & \cdot & \hat{V}_{lM}(\{s^k\}) \\ \cdot & \cdot & \cdot & \cdot & \cdot \\ \hat{V}_{M1}(\{s^k\}) & \hat{V}_{M2}(\{s^k\}) & \cdot & \cdot & \hat{V}_{MM}(\{s^k\}) \end{pmatrix}, \tag{2.3.3}$$

and

$$\Xi(\{s^k\},t) \equiv \begin{pmatrix} \Psi_1(\{s^k\},t) \\ \Psi_2(\{s^k\},t) \\ \cdot \\ \Psi_l(\{s^k\},t) \\ \cdot \\ \Psi_M(\{s^k\},t) \end{pmatrix} \tag{2.3.4}$$

with $\int \Xi^{\dagger}(\{s^k\},t)\Xi(\{s^k\},t)\prod_{k=1}^{p} ds^k = 1$ at any time t.

TH-421_02612202

The kinetic energy operator, $\hat{T}_{\{s^k\}} = -\frac{\hbar^2}{2\mu}\Big[\frac{\partial^2}{\partial {s^k}^2} + \frac{\partial^2}{\partial {s^k}^2} + \cdots + \frac{\partial^2}{\partial {s^k}^2}\Big]$, and the diagonal elements of the matrix in Eq. (2.3.3) represent potential energy operators for different surfaces where off-diagonal elements define the coupling among them. The lth element of the wavefunction matrix in Eq. (2.3.4) is the wavefunction for the lth surface and we can expand the time-dependent wavefunction ($\Psi_l(\{s^k\}, t)$) as below,

$$\Psi_l(\{s^k\}, t) = \sum_{i_1 i_2 \ldots i_p} c_{i_1 i_2 \ldots i_p, l}(t) \prod_{k=1}^{p} \psi_{i_k}(s^k, t), \tag{2.3.5}$$

where $\psi_{i_k}(s^k, t)$ is the TDDVR basis function for the kth mode which can again be expanded in terms of DVR basis multiplied by plane wave to represent the coordinate, s^k, as a function of time, t,

$$\begin{aligned}
\psi_{i_k}(s^k, t) &= \phi(s^k, t) \sum_{n=0}^{N_k} \xi_n^\star(x_{i_k}^k) \xi_n(x^k) && (2.3.6)\\
&= \sum_{n=0}^{N_k} \xi_n^\star(x_{i_k}^k) \Phi_n(s^k, t) && (2.3.7)\\
\phi(s^k, t) &= \pi^{1/4} \exp\Big(\frac{i}{\hbar}\big\{p_{s_c^k}(t)[s^k - s_c^k(t)]\big\}\Big), && (2.3.8)
\end{aligned}$$

with harmonic oscillator eigenfunctions as the primitive ones to construct the DVR basis,

$$\xi_n(x^k) = \Big(\frac{2ImA^k}{\pi\hbar}\Big)^{1/4} \frac{1}{\sqrt{n! 2^n \sqrt{\pi}}} \exp\Big\{-\frac{(x^k)^2}{2}\Big\} H_n(x^k) \tag{2.3.9}$$

and

$$\begin{aligned}
x^k &= \sqrt{\frac{2ImA^k}{\hbar}}(s^k - s_c^k(t)), && (2.3.10)\\
x_{i_k}^k &= \sqrt{\frac{2ImA^k}{\hbar}}(s_{i_k}^k(t) - s_c^k(t)). && (2.3.11)
\end{aligned}$$

Alternatively, we can say $\{\Phi_n(s^k, t)\}$ form the G-H basis set. Among the parameters in the G-H basis (Eqs. (2.3.5) - (2.3.11)) we choose the center of the wavepacket ($\{s_c^k\}$) and its' momentum ($\{p_{s_c^k}\}$) as time-dependent variables, imaginary part of

TH-421_02612202

the width ($\{ImA^k\}$) as time-independent parameter and real part of $\{\gamma^k\}$ and width ($\{ReA^k\}$) are zero for all the time.

The index, i_k, in Eqs. (2.3.5) and (2.3.6) counts the DVR basis functions for the kth mode where N_k is the maximum number of Hermite basis functions included in Eq. (2.3.6) to expand a particular DVR basis for the same mode, p and M are the maximum number of modes and surfaces, respectively involved in a system. A DVR grid-point, $s^k_{i_k}$, will be determined by Eq. (2.3.11) using the root, $x^k_{i_k}$, of $N_k th$ Hermite polynomial, $H_{N_k}(x^k)$ [17] Though the roots ($x^k_{i_k}$s) of the polynomial are fixed values, the position of the DVR grid-points ($s^k_{i_k}$s) will change as a function of time due to the time-dependent variables, $s^k_c(t)$,

$$s^k_{i_k}(t) = s^k_c(t) + \sqrt{\frac{\hbar}{2ImA^k}} x^k_{i_k} \tag{2.3.12}$$

The Gauss-Hermite basis, $\Phi_n(s^k, t)$, for the kth mode as introduced in Eq. (2.3.7) have the following two important properties. Firstly, they form an orthonormal basis,

$$\int ds^k \Phi^\star_m(s^k, t)\Phi_n(s^k, t) = \delta^k_{mn} \tag{2.3.13}$$

and secondly, the ground state of the G-H basis is the Gaussian Wave Packet.

The DVR basis functions, ψ_{i_k}s, in Eq. (2.3.6) for the kth mode constitute an orthogonal but not normalized set,

$$\int ds_k \psi^\star_{i_k}(s^k, t)\psi_{i'_k}(s^k, t) = \delta_{i_k i'_k} A^k_{i_k i'_k}, \tag{2.3.14}$$

where A^k is the normalization factor.

We substitute Eqs. (2.3.2) - (2.3.5) in the time-dependent Schroedinger equation (Eq. (2.3.1)) and due to the special choice of the form of the TDDVR basis functions as defined in Eq. (2.3.6), the classical path picture appears naturally along with the DVR matrix equation. The general form of differential equation for any surface, l, (

TH-421_02612202

$l, l' \in \{1, M\}$) turns out to be,

$$
\begin{aligned}
& i\hbar \sum_{i_1 i_2 \ldots i_p} \dot{c}_{i_1 i_2 \ldots i_p, l}(t) \prod_{k=1}^{p} \Big\{ \sum_{n=0}^{N_k} \xi_n^\star(x_{i_k}^k) \Phi_n(s^k, t) \Big\} \\
+ \; & i\hbar \sum_k \sum_{i_1 i_2 \ldots i_p} c_{i_1 i_2 \ldots i_p, l}(t) \Big\{ \sum_{n=0}^{N_k} \xi_n^\star(x_{i_k}^k) \frac{\partial}{\partial t} \Phi_n(s^k, t) \Big\} \prod_{k' \neq k}^{p} \Big\{ \sum_{n=0}^{N_{k'}} \xi_n^\star(x_{i_{k'}}^{k'}) \Phi_n(s^{k'}, t) \Big\} \\
= \; & \sum_k \sum_{i_1 i_2 \ldots i_p} c_{i_1 i_2 \ldots i_p, l}(t) \Big\{ \sum_{n=0}^{N_k} \xi_n^\star(x_{i_k}^k) \hat{T}_{s^k} \Phi_n(s^k, t) \Big\} \prod_{k' \neq k}^{p} \Big\{ \sum_{n=0}^{N_{k'}} \xi_n^\star(x_{i_{k'}}^{k'}) \Phi_n(s^{k'}, t) \Big\} \\
+ \; & \sum_{i_1 i_2 \ldots i_p} c_{i_1 i_2 \ldots i_p, l}(t) V_{ll}(\{s_{i_k}^k\}) \prod_{k=1}^{p} \Big\{ \sum_{n=0}^{N_k} \xi_n^\star(x_i^k) \Phi_n(x^k) \Big\} \\
+ \; & \sum_{l' \neq l} \sum_{i_1 i_2 \ldots i_p} c_{i_1 i_2 \ldots i_p, l'}(t) V_{ll'}(\{s_{i_k}^k\}) \prod_{k=1}^{p} \Big\{ \sum_{n=0}^{N_k} \xi_n^\star(x_i^k) \Phi_n(x^k) \Big\} \qquad (2.3.15)
\end{aligned}
$$

When we evaluate the terms of $\frac{\partial}{\partial t}\Phi_n(s^k, t)$ and $\hat{T}_{s^k}\Phi_n(s^k, t)$ for the kth mode and substitute back in Eq. (2.3.15), some of these terms cancel each other. Collecting the remaining terms, along with simple manipulation we arrive at the evolution equation for quantum motion on the lth surface in a compact matrix form,

$$
i\hbar \mathbf{A}\dot{\mathbf{C}}_\mathbf{l} \;=\; \mathbf{H}_\mathbf{ll}^\mathbf{t}\mathbf{C}_\mathbf{l} + \mathbf{A}\sum_{\mathbf{l'}\neq\mathbf{l}} \mathbf{V}_\mathbf{ll'}\mathbf{C}_\mathbf{l'} \qquad (2.3.16)
$$

which can be reorganized into a more convenient form by a similarity transformation,

$$
i\hbar\dot{\mathbf{D}}_\mathbf{l}(\mathbf{t}) = \mathbf{A}^{-\mathbf{1/2}}\mathbf{H}_\mathbf{ll}^\mathbf{t}\mathbf{A}^{-\mathbf{1/2}}\mathbf{D}_\mathbf{l} + \sum_{\mathbf{l'}\neq\mathbf{l}} \mathbf{V}_\mathbf{ll'}\mathbf{D}_\mathbf{l'} \qquad (2.3.17)
$$

where $\mathbf{D}_\mathbf{l} = \mathbf{A}^{\mathbf{1/2}}\mathbf{C}_\mathbf{l}$.

The explicit expression of an element of the TDDVR coefficients, $d_{i_1 i_2 \ldots i_p, l}$ is,

$$
\begin{aligned}
i\hbar\dot{d}_{i_1 i_2 \ldots i_p, l} \;=\; & \frac{1}{2}\Big\{ \sum_k \dot{p}_{s_c^k} \sqrt{\frac{\hbar}{ImA^k}} \bar{X}_{i_k i_k}^k \Big\} d_{i_1 i_2 \ldots i_p, l} + \Big\{ \sum_k \frac{\mu(\dot{s}_c^k)^2}{2} \Big\} d_{i_1 i_2 \ldots i_p, l} \\
+ \; & V_{ll}(i_1 i_2 \ldots i_p) d_{i_1 i_2 \ldots i_p, l} + \sum_{l' \neq l} V_{ll'}(i_1 i_1 \ldots i_p) d_{i_1 i_2 \ldots i_p, l'} \\
+ \; & \sum_k \Big\{ \frac{\hbar ImA^k}{2\mu} \sum_{i'_1 i'_2 \ldots i'_p} \{ 2\bar{Y}_{i_k i'_k}^k - \bar{Z}_{i_k i'_k}^k \} d_{i'_1 i'_2 \ldots i'_p, l} \prod_{k' \neq k}^{p} \delta_{i_{k'} i'_{k'}} \Big\} \qquad (2.3.18)
\end{aligned}
$$

TH-421_02612202

where

$$\bar{X}^k_{i_k,i'_k} = \frac{X^k_{i_k,i'_k}}{\sqrt{A^k_{i_k,i_k}A^k_{i'_k,i'_k}}},\ \bar{Y}^k_{i_k,i'_k} = \frac{Y^k_{i_k,i'_k}}{\sqrt{A^k_{i_k,i_k}A^k_{i'_k,i'_k}}},\ \text{and}\ \bar{Z}^k_{i_k,i'_k} = \frac{Z^k_{i_k,i'_k}}{\sqrt{A^k_{i_k,i_k}A^k_{i'_k,i'_k}}} \quad (2.3.19)$$

$$d_{i_1 i_2 \ldots i_p,l} = c_{i_1 i_2 \ldots i_p,l} \prod_{k=1}^{p} (A^k_{i_k,i_k})^{\frac{1}{2}}, \quad (2.3.20)$$

$$A^k_{i_k,i'_k} = \sum_{n=0}^{N^k} \xi^\star_n(x^k_{i_k})\xi_n(x^k_{i'_k}), \quad (2.3.21)$$

$$X^k_{i_k,i'_k} = \sum_{n=0}^{N^k-1} \xi^\star_{n+1}(x^k_{i_k})\sqrt{n+1}\xi_n(x^k_{i'_k}) + \sum_{n=1}^{N^k} \xi^\star_{n-1}(x^k_{i_k})\sqrt{n}\xi_n(x^k_{i'_k}), \quad (2.3.22)$$

$$Y^k_{i_k,i'_k} = \sum_{n=0}^{N^k} \xi^\star_n(x^k_{i_k})2n\xi_n(x^k_{i'_k}), \quad (2.3.23)$$

$$Z^k_{i_k,i'_k} = \sum_{n=0}^{N^k-2} \xi^\star_{n+2}(x^k_{i_k})\sqrt{(n+1)(n+2)}\xi_n(x^k_{i'_k}) + \sum_{n=2}^{N^k} \xi^\star_{n-2}(x^k_{i_k})\sqrt{n(n-1)}\xi_n(x^k_{i'_k}) + \sum_{n=0}^{N^k} \xi^\star_n(x^k_{i_k})(2n+1)\xi_n(x^k_{i'_k}) \quad (2.3.24)$$

Component matrices ($\{\mathbf{A^k}\}$, $\{\mathbf{X^k}\}$, $\{\mathbf{Y^k}\}$, $\{\mathbf{Z^k}\}$) of the TDDVR Hamiltonian matrix Eq. (2.3.18) can infer very important significance on the quantum-classical nature of this approach. $\{\mathbf{A^k}\}$, $\{\mathbf{X^k}\}$, $\{\mathbf{Y^k}\}$ and $\{\mathbf{Z^k}\}$ matrices (Tables 2.1 - 2.4) are time-independent and need to be evaluated once for all. As $\{\mathbf{X^k}\}$ matrices are diagonal and multiplied with the "classical" variables $\{\dot{p}_{s^k_c}(t)\}$ respectively, the quantum equations of motion is free from any non-linearity due to "classical" motion, i.e., "classical" mechanics can only affect the convergence of the quantum dynamics. Again, as couplings among the grid-points come through the full matrices $\{\mathbf{Y^k}\}$ and $\{\mathbf{Z^k}\}$ and dominantly shape the quantum dynamics, we wish them to be free from any non-linearity due to "classical" propagation by choosing $\{ImA^k\}$ as the time-independent variable. Moreover, both the matrices $\{\mathbf{Y^k}\}$ and $\{\mathbf{Z^k}\}$ are diagonally dominant, but the average value of the off-diagonal elements of $\{\mathbf{Z^k}\}$ matrix is much larger than these of the $\{\mathbf{Y^k}\}$ matrix. Hence the $\{\mathbf{Z^k}\}$ matrix unlike $\{\mathbf{Y^k}\}$ can not facilitate the

TH-421_02612202

converged solution of quantum equations of motion if $\{ImA^k\}$ is considered as time-dependent. On the other hand, in order to formulate a rigorous equation of motion, one needs to include $\{\mathbf{Z^k}\}$ matrix and also treat $\{ImA^k\}$ as a time-independent variable. Last but not the least, Eq. (2.3.18) clearly indicates that $\{\mathbf{Y^k}\}$ and $\{\mathbf{Z^k}\}$ matrices couple grid-points or basis function of the kth mode only, hence numerical handling of differential equation for each mode can be done by parallel computation, reducing computational cost and making large dimensional calculations possible.

Similarly, the classical path equations for the kth mode can be written as

$$\dot{s^k_c}(t) = \frac{p_{s^k_c}(t)}{\mu} \tag{2.3.25}$$

$$\dot{p}_{s^k_c}(t) = -\Big\langle \Xi(\{s^k\},t)\Big|\frac{d\hat{V}(\{s^k\})}{ds^k}\Big|_{s^k=s^k_c(t)}\Big|\Xi(\{s^k\},t)\Big\rangle \tag{2.3.26}$$

where the classical force is evaluated by substituting the matrices, $\Xi(\{s^k\},t)$ and $\hat{V}(\{s^k\})$ (Eqs. (2.3.3) and (2.3.4)), respectively.

Using Dirac-Frenkel variational principle [37], we now arrive at a rigorous expression of $\dot{p}_{s^k_c}$ for multi-dimensional multi-surface systems by minimizing the following integral,

$$\begin{aligned} I &= \int \Big(-i\hbar\frac{\partial\Xi^\star(\{s^k\},t)}{\partial t} - H(\{p^k_s\},\{s^k\})\Xi^\star(\{s^k\},t)\Big) \\ &\times \Big(i\hbar\frac{\partial\Xi(\{s^k\},t)}{\partial t} - H(\{p^k_s\},\{s^k\})\Xi(\{s^k\},t)\Big)\prod_{k=1}^{p} ds^k, \end{aligned} \tag{2.3.27}$$

with respect to $\{\dot{p}_{s^k_c}\}$. When this derivation (!!!) is done, $\{\dot{p}_{s^k_c}\}$ takes the following

TH-421_02612202

form,

$$
\begin{aligned}
\dot{p}_{s_c^k}(t) &= \Big[\frac{2(ImA^k)^2}{\mu}\Big\{\sum_l\sum_{i_ki'_k} c^\star_{i_1i_2..i_k..i_p,l}(t)\frac{\sum_{i''_k} c_{i_1i_2..i''_k..i_p,l}(t)S^{(2)}_{i''_ki'_k}}{A_{i'_ki'_k}}S^{\star(1)}_{i_ki'_k} \\
&+ \sum_l\sum_{i_ki'_k}\frac{\sum_{i''} c^\star_{i_1i_2..i''_k..i_p,l}(t)S^{\star(2)}_{i''_ki_k}}{A_{i_ki_k}}c_{i_1i_2..i'_k..i_p,l}(t)S^{\star(1)}_{i_ki'_k} \\
&- 2\sum_l\sum_{i_ki'_k} c^\star_{i_1i_2..i_k..i_p,l}(t)c_{i_1i_2..i'_k..i_p,l}(t)S^{\star(3)}_{i_ki'_k}\Big\} \\
&- \frac{\hbar ImA^k}{\mu}\Big\{\sum_l\sum_{i_ki'_k} c^\star_{i_1i_2..i_k..i_p,l}(t)\frac{\sum_{i''_k} c_{i_1i_2..i''_k..i_p,l}(t)R_{i''_ki'_k}}{A_{i'_ki'_k}}S^{\star(1)}_{i_ki'_k} \\
&+ \sum_l\sum_{i_ki'_k}\frac{\sum_{i''_k} c^\star_{i_1i_2..i''_k..i_p,l}(t)R^\star_{i''_ki_k}}{A_{i_ki_k}}c_{i_1i_2..i'_k..i_p,l}(t)S^{\star(1)}_{i_ki'_k} \\
&- 2\sum_l\sum_{i_ki_{k'}} c^\star_{i_1i_2..i_k..i_p,l}(t)c_{i_1i_2..i'_k..i_p,l}(t)T^\star_{i_ki'_k}\Big\}\Big] \\
&\Big/ \Big[\sum_l\sum_{i_ki'_k} c^\star_{i_1i_2..i_k..i_p,l}(t)\frac{\sum_{i''_k} c_{i_1i_2..i''_k..i_p}(t)S^{(1)}_{i''_ki'_k}}{A_{i'_ki'_k}}S^{\star(1)}_{i_ki'_k} \\
&+ \sum_l\sum_{i_ki'_k}\frac{\sum_{i''_k} c^\star_{i_1i_2..i''_k..i_p,l}(t)S^{\star(1)}_{i''_ki_k}}{A_{i_ki_k}}c_{i_1i_2..i'_k..i_p,l}S^{\star(1)}_{i_ki'_k} \\
&- 2\sum_l\sum_{i_ki'_k} c^\star_{i_1i_2..i_k..i_p,l}(t)c_{i_1i_2..i'_k..i_p,l}(t)S^{\star(2)}_{i_ki'_k}\Big] \qquad (2.3.28)
\end{aligned}
$$

where

$$
\begin{aligned}
R_{i_ki'_k} &= \sum_p \xi^\star{}_p(x^k_{i_k})\xi_p(x^k_{i'_k})2p \\
S^{(n)}_{i_ki'_k} &= \sum_{pq}\xi^\star{}_p(x^k_{i_k})\xi_q(x^k_{i'_k})\int\Phi^\star{}_q(s^k,t)(s^k-s^k_c(t))^n\Phi_p(s^k,t)ds^k \\
T_{i_ki'_k} &= \sum_{pq}\xi_p(x^k_{i_k})\xi^\star{}_q(x^k_{i'_k})2p\int\Phi^\star{}_p(s^k,t)(s^k-s^k_c(t))\Phi_q(s^k,t)ds^k \qquad (2.3.29)
\end{aligned}
$$

TH-421_02612202

with

$$\begin{aligned}
\int \Phi^{\star}{}_p(s^k,t)(s^k-s_c^k(t))\Phi_q(s^k,t)ds^k &= \frac{1}{2}\sqrt{\frac{\hbar}{ImA^k}}\Big\{\sqrt{p+1}\delta_{p+1,q}+\sqrt{p}\delta_{p-1,q}\Big\} \\
\int \Phi^{\star}{}_p(s^k,t)(s^k-s_c^k(t))^2\Phi_q(s^k,t)ds^k &= \frac{\hbar}{4ImA^k}\Big\{\sqrt{(p+1)(p+2)}\delta_{p+2,q} \\
&+ (2p+1)\delta_{p,q}+\sqrt{p(p-1)}\delta_{p-2,q}\Big\} \\
\int \Phi^{\star}{}_p(s^k,t)(s^k-s_c^k(t))^3\Phi_q(s^k,t)ds^k &= \frac{1}{8}\Big(\frac{\hbar}{ImA^k}\Big)^{3/2}\Big\{\sqrt{(p+1)(p+2)(p+3)}\delta_{p+3,q} \\
&+ 3(p+1)\sqrt{p+1}\delta_{p+1,q}+3p\sqrt{p}\delta_{p-1,q} \\
&+ \sqrt{p(p-1)(p-2)}\delta_{p-3,q}\Big\} \qquad (2.3.30)
\end{aligned}$$

Matrices R, $S^{(n)}$, T and A involved in Eq. (2.3.28) are time-independent and can be calculated once for all the time while the time-dependence of $\dot{p}_{s_c^k}$ arises from the time-dependent coefficient $\{c_{i_1 i_2..i_k..i_p,l}(t)\}$. *At this point, it is important to note that* $\dot{p}_{s_c^k}, \quad k=1,\ldots,p$ *does not depend explicitly on the potential of the system unlike its form in ref [27].* The compact form of $\dot{p}_{s_c^k}$ in Eq. (2.3.28) can further be simplified when we replace $S^{(1)}_{i_k i'_k}$ by $S^{(1)}_{i_k i'_k}\delta_{i_k i'_k}$ as the first order term $(s^k-s_c^k(t))$ is diagonal in DVR (Table 2.2),

$$\begin{aligned}
\dot{p}_{s_c^k}(t) &= \sum_l \sum_{i_k i'_k} c^{\star}_{i_i i_2..i_k..i_p,l}(t)c_{i_1 i_2..i'_k..i_p,l}(t) \\
&\times \Big\{\frac{2(ImA^k)^2}{\mu}\Big[S^{(2)}_{i_k i'_k}\frac{S^{(1)\star}{}_{i_k i_k}}{A_{i_k i_k}}-S^{(3)}_{i_k i'_k}\Big]-\frac{\hbar ImA^k}{\mu}\Big[R_{i_k i'_k}\frac{S^{(1)\star}{}_{i_k i_k}}{A_{i_k i_k}}-T^{\star}_{i_k i'_k}\Big]\Big\} \\
&/ \Big[\sum_l\sum_{i_k} c^{\star}_{i_1 i_2..i_k..i_p,l}(t)c_{i_1 i_2..i_k..i_p,l}(t)\frac{S^{(1)\star}{}_{i_k i_k}S^{(1)}_{i_k i_k}}{A_{i_k i_k}} \\
&- \sum_i\sum_{i_k i'_k} c^{\star}_{i_1 i_2..i_k..i_p,l}(t)c_{i_1 i_2..i'_k..i_p,l}(t)S^{\star(2)}{}_{i_k i'_k}\Big] \qquad (2.3.31)
\end{aligned}$$

2.4 Summary of the TDDVR approach

The TDDVR introduces one central trajectory and a set of grid-points for each degree of freedom. The movement of these grid-points around the central trajectory is

TH-421_02612202

dictated by the classical mechanics and grid-points are associated with a distribution of "classical" momentum. The growth or decay of the amplitudes at these grid-points on each surface is shaped by quantum evolution. The movement of the grid-points as well as growth or decay of the amplitudes at these grid-points on a particular surface effectively wake this approach a multi-trajectory one and enable it to explain quantum features arising from the individual surface quantitatively. In principle, the method is exact with enough trajectories (grid-points) but in the other limit, with one grid-point, the method is reducible to the molecular dynamics approach which is very useful from the dynamical point of view. We can add even or odd number of grid-points for a given degree of freedom if the dynamical situation shows the requirement. Since the grid-points follow the dynamics of the system, depending on the situation TDDVR needs lesser number of grid-points for any mode compared to corresponding quantum (DVR/FFT) case. As the major advantages of TDDVR methods come from its' "classical" equation of motion and it is convenient to introduce classical mechanics either in Cartesian or in Jacobi coordinates, TDDVR approaches are formulated in these coordinate systems only. At the same time, one can reduce the number of degrees of freedom in special coordinate system like hyperspherical, where one can use TDDVR method combining with state expansion approaches.

It is important to note that, while implementing TDDVR on a multi-mode system, some of the degrees of freedom can be treated in the quantum limit, some other at near classical limit, and the rest with "classical" dynamics. At the classical limit the action (S) appearing in the Feynman path integral formulation can be used to define a trajectory by introducing a least action principle ($\delta S = 0$). The limit $\hbar \to 0$ corresponds to the TDDVR approach with one grid point, where contribution from paths away from the one defined by $\delta S = 0$ are small due to rapid oscillation of the path integrand. The quantum trajectory defined in Bohm trajectory is same with the TDDVR trajectory, when TDDVR is formulated with one basis function (one grid

TH-421_02612202

point). With a sufficient number of grid points, TDDVR introduces a more general quantum potential.

The approach is flexible enough to handle any form of complicity of the Hamiltonian. In the quantum regime, the dynamics of the centroid of the wavepacket obeys Ehrenfest theorem, which facilitates the movement of grid-points. At the classical limit, the lone grid and centroid of the wavepacket are the same point and it is propagated by "classical" dynamics only. TDDVR has appealing applicability for those large systems where quantum mechanical description is needed in a restricted region.

We found that the method obeys energy conservation, momentum conservation, microscopic reversibility and unitarity. Moreover, it is applicable to any number of coupled states and to any kind of electronic coupling. Any electronic representation is acceptable, although in some situation, diabatic representation may be advantageous to employ whereas in other cases adiabatic basis is needed.

The number of grid-points required to achieve convergence in DVR depends on the initial position of the wave-packet. If the initial wave-packet is located far away from the barrier, more grid-points are needed to cover the reactive side of the barrier. At the same time, once the convergence is achieved with certain number of grid-points (trajectories) in TDDVR approach, convergence is independent of the location of initial wave-packet. But in case of TDDVR, as the quantum propagation is approximated by "classical" equation of motion, some fluctuations appear in transition probabilities during the interaction period. We also found no matter how large number of grid-points are included in the TDDVR calculations,these fluctuations always remain.

TH-421_02612202

CHAPTER III

APPLICATION TO TUNNELING

3.1 Tunneling through an Eckart potential

3.1.1 Formulation of equation of motion

We have investigated the performance of the present method on simple tunneling problem through an Eckart barrier. The Eckart potential is given by

$$V(s) = V_0/\cosh^2(as), \tag{3.1.1}$$

where the barrier height, $V_0 = 100$ KJ/mol and the parameter $a = 2$ Å^{-1}. The mass (μ) of the system is 1 amu.

The compact form of the matrix equation and the classical path equations read as follows,

$$i\hbar\mathbf{A}\dot{\mathbf{C}} = \mathbf{H^t C} \tag{3.1.2}$$

$$\dot{s_c}(t) = \frac{p_{s_c}(t)}{\mu} \tag{3.1.3}$$

$$\dot{p}_{s_c}(t) = -\frac{dV(s)}{ds}\Big|_{s=s_c(t)} \tag{3.1.4}$$

We find the explicit expression of an element of the time - dependent DVR Hamiltonian matrix, $\mathbf{H^t}$ (Appendix B) and the normalization matrix, $\mathbf{A}$ are,

$$H^t_{i,j} = \Big[\frac{1}{2}\dot{p}_{s_c}(t)\sqrt{\frac{\hbar}{ImA}}X_{i,j} + \frac{\mu\dot{s}^2_c(t)}{2}A_{i,j} + \frac{\hbar ImA}{2\mu}\{2Y_{i,j} - Z_{i,j}\} + V(s_i)A_{i,j}\Big]; \tag{3.1.5}$$

where the rigorous expressions of $A_{i,j}$, $X_{i,j}$, $Y_{i,j}$ and $Z_{i,j}$ are shown in the previous chapter (see Eqs. (2.2.18) - (2.2.21)).

TH-421_02612202

Equation (3.1.2) can be rewritten into a more convenient form by a similarity transformation, i.e.,

$$i\hbar\dot{\mathbf{D}}(\mathbf{t}) = \mathbf{A^{-1/2}H^tA^{-1/2}D}, \tag{3.1.6}$$

where $\mathbf{D} = \mathbf{A}^{-1/2}\mathbf{C}$.

The initial amplitudes of the DVR wavefunction at the grid - points (s_is) are calculated from GWP ($\Phi(s_i, t_0)$) centred around s_c(t=0) = - 4 Å with it's momentum vector, $k_0 = 20\ \mathring{A}^{-1}$ and the imaginary part of the width, $ImA = 0.4$ amu/τ ($1\tau = 10^{-14}$ sec) as below,

$$\Phi(s_i, t_0) = \Big[\frac{2ImA}{\pi\hbar}\Big]^{1/4} \times \exp\Big[ik_0(s_i - s_0) - \frac{ImA}{\hbar}(s_i - s_0)^2\Big]. \tag{3.1.7}$$

In case of DVR, only Eq. (3.1.2) is solved to observe the dynamics and all the terms containing classical variable(s) in the Hamiltonian matrix (Eq. (3.1.5)) are dropped while propagation.

Similarly, the initial amplitudes of the TDDVR wavefunction at the grid - points (s_is) are obtained from GWP ($\Phi(s_i, t_0)$) with the same numerical value of the parameters used in DVR except zero momentum vector ($k_0 = 0$),

$$\Phi(s_i, t_0) = \Big[\frac{2ImA}{\pi\hbar}\Big]^{1/4} \times \exp\Big[-\frac{ImA}{\hbar}(s_i - s_0)^2\Big], \tag{3.1.8}$$

While TDDVR propagation (Eqs. (3.1.2) - (3.1.4) or Eq. (D6)) are solved simultaneously where p_{s_c} ($k_0 = 20\mathring{A}^{-1}$) enters as a classical variable through Eq. (3.2.3) and also through first two terms of the Hamiltonian matrix (Eq. (3.2.5)).

Using the properties of the DVR functions, we can write normalized amplitudes as

$$d_i(t = 0) = A_{i,i}^{-1/2}\Phi(x_i) \tag{3.1.9}$$

The transmission probability on the reactive side of the barrier can be determined by

TH-421_02612202

using the coefficient d_is,

$$\begin{aligned} P(t) &= \int_{s=0}^{\infty} ds|\Psi(s,t)|^2 \\ &= \sum_{i\geq i^\star} c_i^\star(t)c_i(t)\sum_{kk'}\xi_k^\star(x_i)\xi_{k'}(x_i)\int_{-\infty}^{\infty}\Phi_k'^\star(s',t)\Phi_{k'}'(s',t)ds' \\ &\approx \sum_{i\geq i^\star}^{N}|c_i(t)|^2A_{i,i} \\ &= \sum_{i\geq i^\star}^{N}|d_i(t)|^2, \end{aligned} \tag{3.1.10}$$

where $i^\star$ is defined by $s_{i^\star}(t) = s_c(t) + \sqrt{\frac{\hbar}{2ImA}}x_{i^\star} > 0$, i.e., the sum of the square of the amplitudes for the grid - points on the reactive side of the barrier gives the tunneling probability.

3.1.2 Results and discussion

Figure 3.1 shows the movement of the centre of wavepacket (s_c) and its momenta (p_{s_c}) as a function of time where in Fig. 3.2 we display the time - dependent grid - points (s_is) for N = 10 case. When we use 10 grid - points with the initial wavepacket

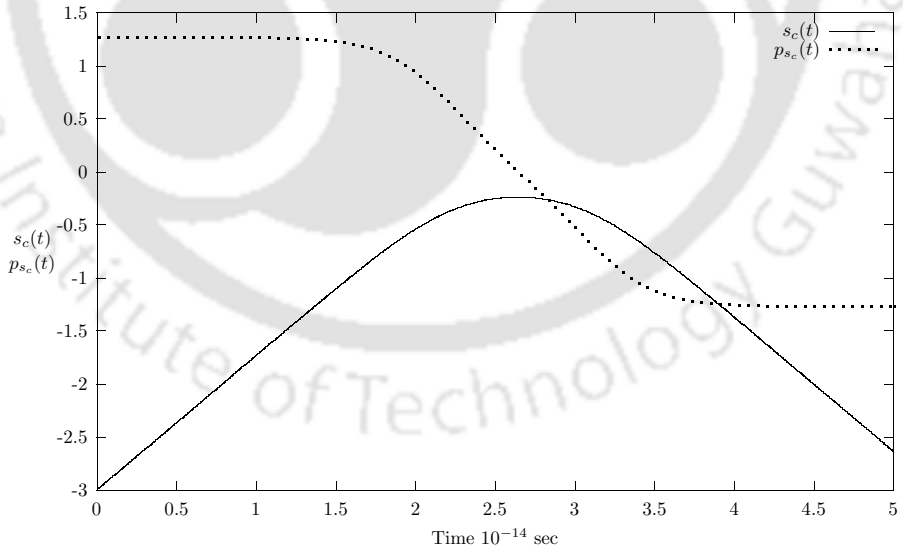

Figure 3.1: The trajectory, s_c and it's momenta, p_{s_c} as a function of time.

centred around -4 Å, three points ($i = 8, 9, 10$) move to the reactive side and back to

TH-421_02612202

the non - reactive side (Fig. 3.2) within the time - interval studied. *As this quantum - classical method allows the movement of grid - points, we get the same amount of tunneling even when the initial wavepacket is located at the farthest away from the barrier. On the other hand, when we freeze the classical motion in this TDDVR, it appears to be a full quantum method (DVR) and in order to get tunneling we need sufficient number of grid - points to cover the reactive side of the barrier.* To be

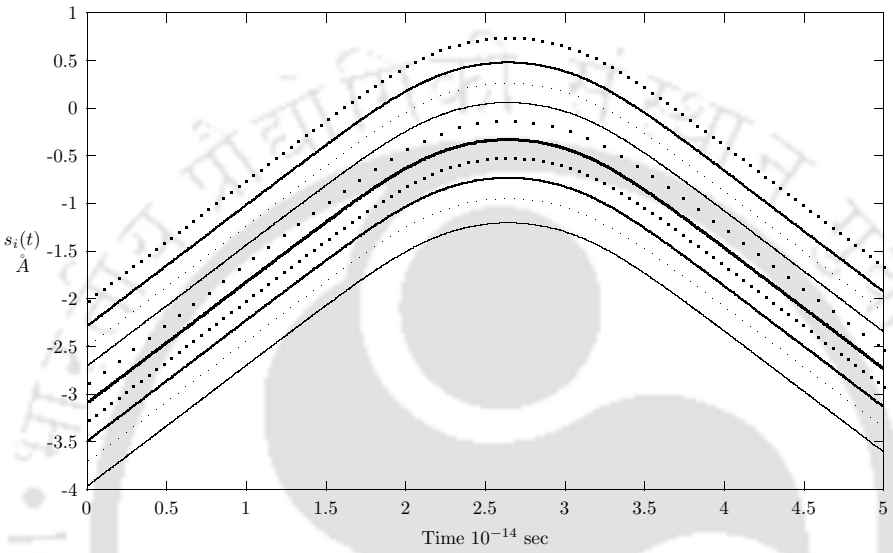

Figure 3.2: The grid - points (N=10) change their positions as a function of time.

specific, with the initial wavepacket centred around -4 Å, DVR need at least 150 grid - points to represent the other side of the barrier with few points and start showing up tunneling (which is far below than the converged result). Under the same situation, tunneling probability calculated by this TDDVR can reach almost the exact value with 100 grid - points but it decays fast because grid points come back to the non - reactive side. This problem can be avoided very easily by freezing the classical motion at the moment when tunneling probability reaches the converged value. If the interaction region of a system is spreaded over a longer region, one needs a lot of grid - points to perform accurate DVR/FFT calculation whereas TDDVR requires a moderate number of grid - points to obtain accurate results irrespective of the initial

TH-421_02612202

position of the wavepacket.

Figure 3.3 shows tunneling probability as a function of time with increasing number of grid - points (N). When more and more grid - points are added, not only the tunneling persists for longer time but also approaches the exact value, which is 0.1906 [52] at the energy ($k_0 = 20$ Å^{-1}) investigated. *We obtained a tunneling probability of 0.1906 well within 150 TDDVR grid - points but in order to keep the*

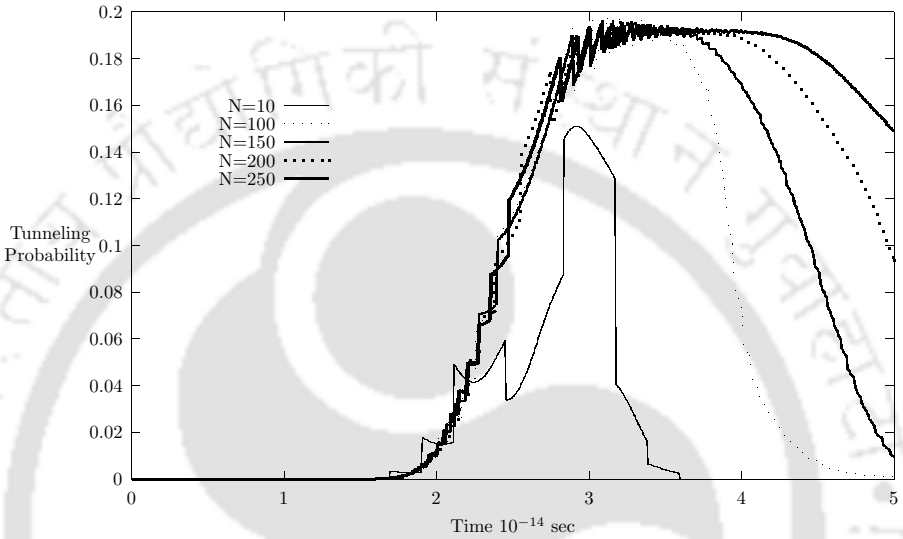

Figure 3.3: Tunneling probability ($P(t)$) calculated by TDDVR through the Eckart barrier with N = 10, 100, 150, 200, 250. Fluctuations are due to oscillations in the expansion coefficients.

converged profile unchanged for relatively longer period of time, we need to increase the number of grid - points (250). It means when we use a large grid, sufficient number of grid - points remain on the reactive side of the barrier for a long time and we obtain the desired profile. Instead of increasing grid points, one can freeze the classical motion at the time when the tunneling probability reaches the converged value with less number of grid - points (≤ 150) and can achieve the same profile.

In Fig. 3.4, we compare tunneling probabilities calculated by quantum - classical (TDDVR) and quantum (DVR) methods with 250 grid - points. Present calculation shows that fluctuations in tunneling probability as a function of time are much less

TH-421_02612202

compared to ref. [16, 17] and we believe this is because width (A) has been considered as a time - independent parameter.

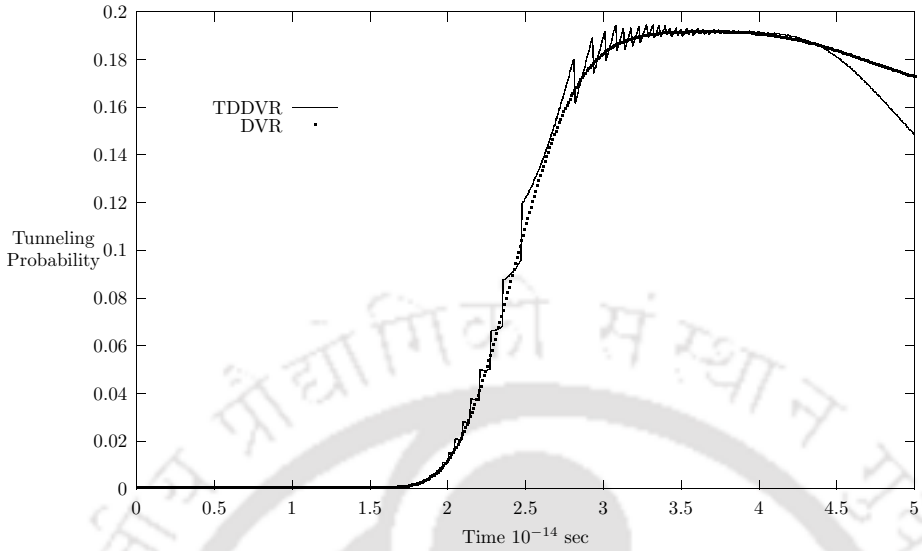

Figure 3.4: Quantum - classical (TDDVR) and quantum (DVR) results of tunneling probability ($P(t)$) as functions of time with N = 250.

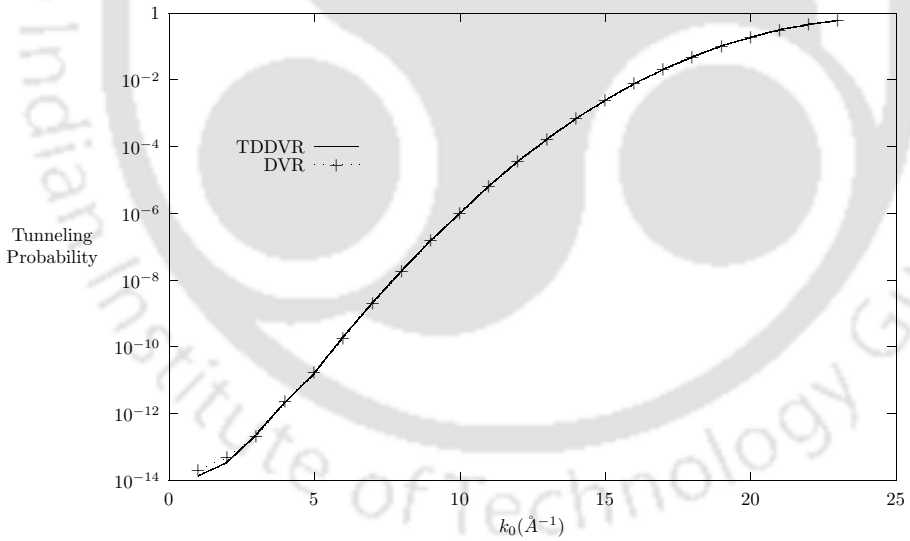

Figure 3.5: Quantum - classical (TDDVR) and quantum (DVR) results of tunneling probability ($P(t = 3.5\tau)$) as functions of $k_0(\text{Å}^{-1})$ with N = 250.

Finally, in Fig. 3.5, we have demonstrated tunneling probability at a particular

TH-421_02612202

time (3.5 τ) for different initial kinetic energies (k_0s) and obtained excellent agreement over the entire energy range with the corresponding quantum results. It is the most difficult task to achieve this much accuracy, particularly at low energy, from a quantum - classical method developed so far.

One can also vary the number of grid - points during propagation. If the wave packet reaches the end points of the grid, it is possible to add some more grid - points and this can be monitored by watching the magnitude of $|d_1|^2$ and $|d_N|^2$.

3.2 Tunneling through a symmetric double well potential

3.2.1 The Hamiltonian and the equation of motion

We explore the workability of our TDDVR method to a system investigated previously [30, 53, 54] and its Hamiltonian H is given by

$$\begin{aligned} H(s, p_s, \{P_k\}, \{Q_k\}) &= \frac{p_s^2}{2\mu} + V(s) \\ &+ \sum_k \left(\frac{P_k^2}{2m} + \frac{1}{2} m\omega_k^2 Q_k^2\right) + \sum_k Q_k f^k(s) \end{aligned} \tag{3.2.1}$$

where s is the reaction coordinate and Q_ks are the bath modes. The potential $V(s)$ is a symmetric double well where the tunneling probability and the time averaged tunneling rate from one of the wells to the other are calculated as a function of time. The time-dependent discrete variable representation method is formulated by using a coupled wavepacket approach, where the wavefunction is expanded as,

$$\Psi(s, \{Q_k\}, t) = \sum_i \sum_{l_1 l_2 \cdots l_k} C_{i l_1 l_2 \cdots l_k} \psi_i(s, t) \prod_k \phi_{l_k}(Q_k), \tag{3.2.2}$$

with $\phi_{k_l}(Q_k)$ is the harmonic oscillator basis function for the bath mode k and $\psi_i(s, t)$ is the time-dependent DVR basis function representing the reaction coordinate s. The time-dependent DVR basis functions are again expanded in terms of Gauss-Hermite

TH-421_02612202

basis set as follows:

$$\psi_i(s,t) = \Phi(s,t)\sum_{n=0}^{N}\xi_n^{\star}(x_i)\xi_n(x) = \sum_{n=0}^{N}\xi_n^{\star}(x_i)\Phi'_n(s,t), \tag{3.2.3}$$

where

$$\Phi(s,t) = \pi^{1/4}\exp\Big(\frac{i}{\hbar}\big\{\gamma + p_{s_c}(t)[s-s_c(t)] + ReA[s-s_c(t)]^2\big\}\Big), \tag{3.2.4}$$

$$\xi_n(x) = \frac{1}{\sqrt{n!2^n\sqrt{\pi}}}\exp(-x^2/2)H_n(x), \tag{3.2.5}$$

$$\xi_n(x_i) = \frac{1}{\sqrt{n!2^n\sqrt{\pi}}}\exp(-x_i^2/2)H_n(x_i) \tag{3.2.6}$$

and

$$x = \sqrt{\frac{2ImA}{\hbar}}(s-s_c(t)), \tag{3.2.7}$$

$$x_i = \sqrt{\frac{2ImA}{\hbar}}(s_i(t)-s_c(t)). \tag{3.2.8}$$

Parameters in GWP are defined in Eqs. (3.2.4) - (3.2.8). The centre of the wavepacket (s_c) and its momenta (p_{s_c}) are considered as time-dependent variables whereas γ and width (A) are considered time-independent with $Re\gamma = ReA = 0$.

The index, i, in Eqs. (3.2.2) and (3.2.3) counts the number of DVR basis functions and N is the maximum number of Gauss-Hermite basis functions included in Eq. (2.2.3) to expand a particular DVR basis function. It is important to note that a DVR grid-point, s_i, is determined by Eq. (3.2.8) using the root, x_i of the N *th* Hermite polynomial, $H_N(x)$ [17]. The compact form of the matrix equation and the classical path equations read as follows,

$$i\hbar\mathbf{A}\dot{\mathbf{C}} = \mathbf{H}^{\mathbf{t}}\mathbf{C} \tag{3.2.9}$$

$$\dot{p}_{s_c}(t) = -\frac{dV(s)}{ds}\Big|_{s=s_c(t)} \tag{3.2.10}$$

$$\dot{s_c}(t) = \frac{p_{s_c}(t)}{\mu} \tag{3.2.11}$$

where the explicit expression of an element of the time-dependent DVR Hamiltonian

TH-421_02612202

matrix, $\mathbf{H^t}$, is

$$\begin{aligned} H^t_{i,j,m_1,n_1,m_2,n_2,\ldots,m_k,n_l} &= \Big[\frac{1}{2}\dot{p}_{s_c}(t)\sqrt{\frac{\hbar}{ImA}}X_{i,j} + \frac{\mu\dot{s}_c^2(t)}{2}A_{i,j} + \frac{\hbar ImA}{2\mu}\big\{2Y_{i,j} - Z_{i,j}\big\} \\ &+ V(s_i)A_{i,j}\Big]\delta_{m_1,n_1}\delta_{m_2,n_2}\cdots\delta_{m_k,n_l} \\ &+ \Big[\Big\{\sum_{k'}\big(m_{k'}+\frac{1}{2}\big)\hbar\omega_{k'}\Big\}\delta_{m_1,n_1}\delta_{m_2,n_2}\cdots\delta_{m_k,n_l} \\ &+ \sum_{k'}\Big\{f^{k'}(s_i)\Big(\frac{\hbar}{2m\omega_{k'}}\Big)^{\frac{1}{2}}\Big(\sqrt{m_{k'}+1}\delta_{m_{k'}+1,n_{k'}} \\ &+ \sqrt{m_{k'}}\delta_{m_{k'}-1,n_{k'}}\Big)\prod_{k(l)\neq k'}\delta_{m_k,n_l}\Big\}\Big]A_{i,j}; \end{aligned} \tag{3.2.12}$$

In the above equation we see that in the DVR-basis, the potential for the reaction coordinate, s, is diagonal as usual.

Equation (3.2.9) can be reorganized into a more convenient form by a similarity transformation, i.e.,

$$i\hbar\dot{\mathbf{D}}(\mathbf{t}) = \mathbf{A^{-1/2}H^tA^{-1/2}D}, \tag{3.2.13}$$

where $\mathbf{D} = \mathbf{A}^{-1/2}\mathbf{C}$.

Using Dirac - Frenkel variational principle [37], it is possible to derive a rigorous expression for $\dot{p}_{s_c}$ by minimizing the following integral (Appendix D),

$$\begin{aligned} I &= \int\{dQ_k\}ds\Big(-i\hbar\frac{\partial\Psi^\star(s,\{Q_k\},t)}{\partial t} - H(p_s,s,\{P_k\},\{Q_k\})\Psi^\star(s,\{Q_k\},t)\Big) \\ &\times \Big(i\hbar\frac{\partial\Psi(s,\{Q_k\},t)}{\partial t} - H(p_s,s,\{P_k\},\{Q_k\})\Psi(s,\{Q_k\},t)\Big), \end{aligned} \tag{3.2.14}$$

with respect to $\dot{p}_{s_c}$. Incidentally, this is the first TDDVR formulation where we have been able to derive a compact form of $\dot{p}_{s_c}$. It is natural to expect that one can achieve correctly converged description of the observables with a minimum number of basis functions (DVR) and obtain quantum corrections to the classical variables if the rigorous expression of $\dot{p}_{s_c}$ is used. At the same time, as p_{s_c} is one of the phase variables in GWP, the convergence is guaranteed in the infinite limit of the basis

TH-421_02612202

functions even with the first order term as in Eq. (3.2.10). In this quantum - classical formulation, classical equations (Eqs. (3.2.10) - (3.2.11)) induce movement of grid - points in the direction where amplitudes grow to higher values.

3.2.2 Results and discussion

We have investigated the performance of the quantum - classical method proposed here on a system which is modeled by a double well potential with or without coupling to bath modes. A maximum of two bath modes has been considered. The potential along the reaction coordinate, s, and the linear coupling terms are given below,

$$V(s) = -\frac{1}{2}a_0 s^2 + \frac{1}{4}c_0 s^4 \tag{3.2.15}$$

$$f^k(s) = -c_k s \tag{3.2.16}$$

where $k = 1, 2$.

The initial amplitudes of the DVR wavefunction are calculated from a GWP centered around the minimum, s_0, in the left well of $V(s)$ where,

$$\Phi(s_i, t_0) = \Big[\frac{2ImA}{\pi\hbar}\Big]^{1/4} \times \exp\Big[-\frac{ImA}{\hbar}(s_i - s_0)^2\Big] \tag{3.2.17}$$

and

$$\left.\frac{\partial V(s)}{\partial s}\right|_{s=s_0} = 0, \quad s_0 = -\sqrt{2a_0/c_0} \tag{3.2.18}$$

and $ImA = m\omega/2, \quad p_{s_c}(t_0) = 0.$

Using the properties of the DVR functions, we can write

$$d_i(t=0) = A_{i,i}^{-1/2}\Phi(s_i) \tag{3.2.19}$$

The frequencies of the tunneling atom (hydrogen) and the two coupled bath modes are taken from ref. [53]. Potential parameters and frequencies are displayed in Table 3.1.

TH-421_02612202

Table 3.1: Potential parameters and frequencies. Distances are in Å and energy in units of $\hat{\epsilon} = 100$ KJ/mol.

Parameter	Value
a_0	4.1429 $\hat{\epsilon}$ Å^{-2}
c_0	16.357 $\hat{\epsilon}$ Å^{-4}
ω	1530 cm^{-1}
ω_1	2980 cm^{-1}
ω_2	765 cm^{-1}
μ	1.0 amu
m	1.0 amu
c_1	1.0 Å^{-1}
c_2	1.0 Å^{-1}

The differential Eqs. (3.2.9) - (3.2.11) have been solved numerically with a time step, 10^{-16} sec and classical force (CF) is included through Eq. (3.2.10). In the case of quantum force (QF), Eq. (D9) (Appendix D) is used instead of Eq. (3.2.10). The calculations are done mainly with CF unless the use of QF is specified. When we perform dynamical calculations with the particular initial states (k_1, k_2) of the heat bath, the tunneling probability on the reactive side of the barrier can be determined by using the time - dependent coefficient d_{i,k_1,k_2},

$$
\begin{aligned}
P_{tunn}(t) &= \int_{s=0}^{\infty} ds \int_{-\infty}^{\infty} dQ_1 \int_{-\infty}^{\infty} dQ_2 \Psi^{\star}(s, Q_1, Q_2, t)\Psi(s, Q_1, Q_2, t) \\
&= \sum_{i\geq i^{\star}} \sum_{k_1,k_2} \sum_{k_1',k_2'} c^{\star}_{i,k_1,k_2}(t) c_{i,k_1',k_2'}(t) \sum_{kk'} \xi^{\star}_{k}(x_i)\xi_{k'}(x_i) \int_{-\infty}^{\infty} \Phi'^{\star}_{k}(s',t)\Phi'_{k'}(s',t)ds' \\
&\times \int_{-\infty}^{\infty} \phi^{\star}_{k_1}(Q_1)\phi_{k_1'}(Q_1)dQ_1 \times \int_{-\infty}^{\infty} \phi^{\star}_{k_2}(Q_2)\phi_{k_2'}(Q_2)dQ_2 \\
&\approx \sum_{i\geq i^{\star}}^{N} \sum_{k_1,k_2} |c_{i,k_1,k_2}(t)|^2 A_{i,i} \\
&= \sum_{i\geq i^{\star}}^{N} \sum_{k_1,k_2} |d_{i,k_1,k_2}(t)|^2, \qquad (3.2.20)
\end{aligned}
$$

where $i^{\star}$ is defined by $s_{i^{\star}}(t) = s_c(t) + \sqrt{\frac{\hbar}{2ImA}} x_{i^{\star}} > 0$, i.e., the sum of the square of the amplitudes for the grid - points on the reactive side of the barrier gives the tunneling

TH-421_02612202

probability. The time - averaged tunneling rate is given by,

$$P^{av}_{tunn}(t) = \frac{1}{t}\int_0^t P(t')dt'. \tag{3.2.21}$$

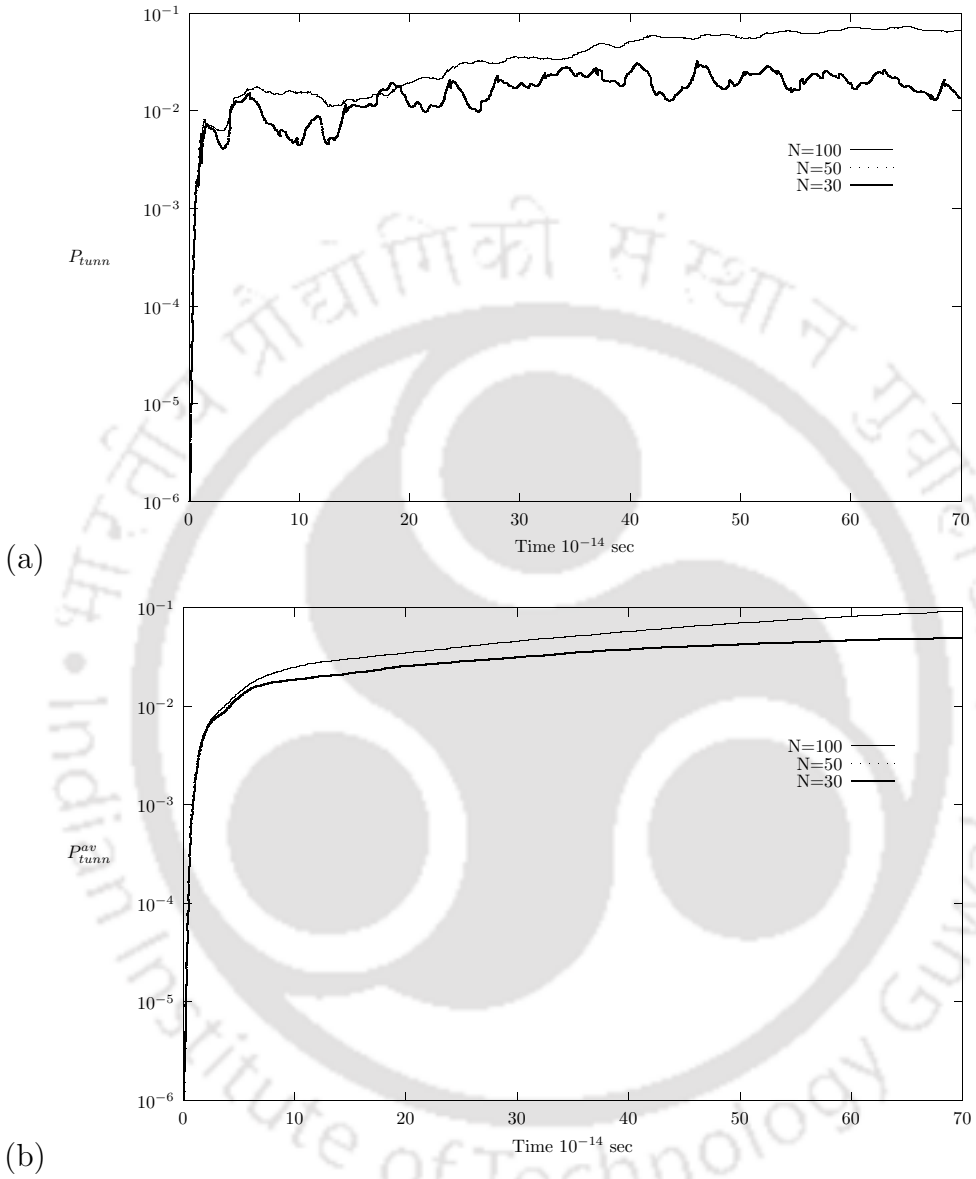

Figure 3.6: (a) Tunneling probability (P_{tunn}) as a function of time for $N = 30$, $N = 50$ and $N = 100$. The initial states of the bath oscillators are chosen as (0,0). (b) Time average tunneling rate (P^{av}_{tunn}) as a function of time for $N = 30$, $N = 50$ and $N = 100$. The initial states of the bath oscillators are chosen as (0,0).

Fig. 3.6 displays (a) the tunneling probability ($P_{tunn}(t)$) and (b) the time - averaged tunneling rate ($P^{av}_{tunn}(t)$) as functions of time for different grid - points (N) where

TH-421_02612202

the initial states of the bath oscillators are chosen as (0,0). When more and more grid - points are added, both $P_{tunn}(t)$ and $P^{av}_{tunn}(t)$ approach the converged values. The figures clearly indicates that 50 TDDVR basis is sufficient to achieve the convergence, i.e., the lines with 50 and 100 TDDVR basis are completely indistinguishable.

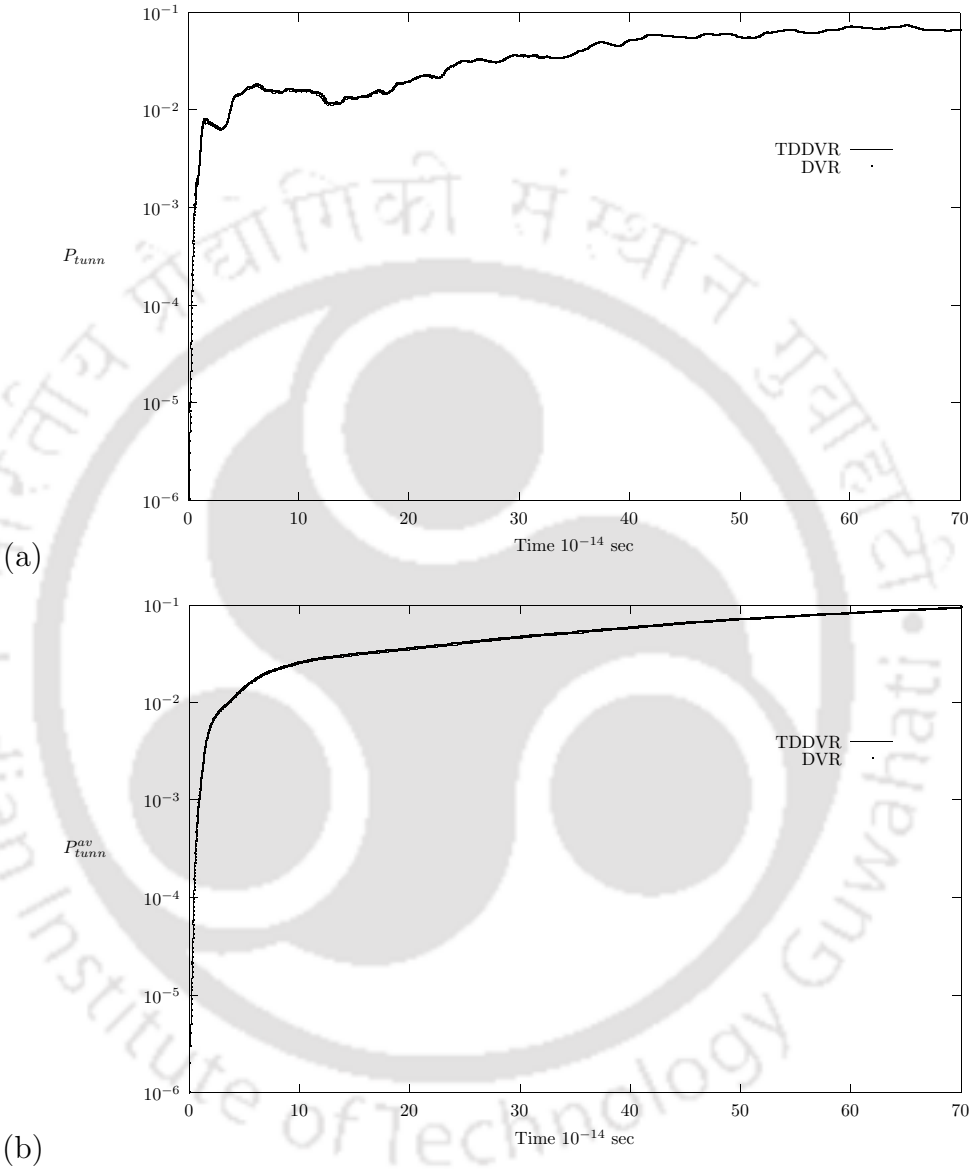

Figure 3.7: Comparison of quantum - classical (TDDVR) and quantum (DVR) results of the (a) tunneling probability (P_{tunn}) (b) time average tunneling rate (P^{av}_{tunn}) as a function of time with $N = 100$. The initial states of the bath oscillators are chosen as (0,0).

At this point, it is important to note that as this quantum - classical method allows

TH-421_02612202

the movement of grid - points, we get the same amount of tunneling even when the initial wavepacket is farthest away from the barrier. On the other hand, when we freeze the classical motion in the present formulation of TDDVR, it appears to be a full quantum method (DVR) and in order to get tunneling we need sufficient number of grid - points to cover the reactive side of the barrier. In the present problem,

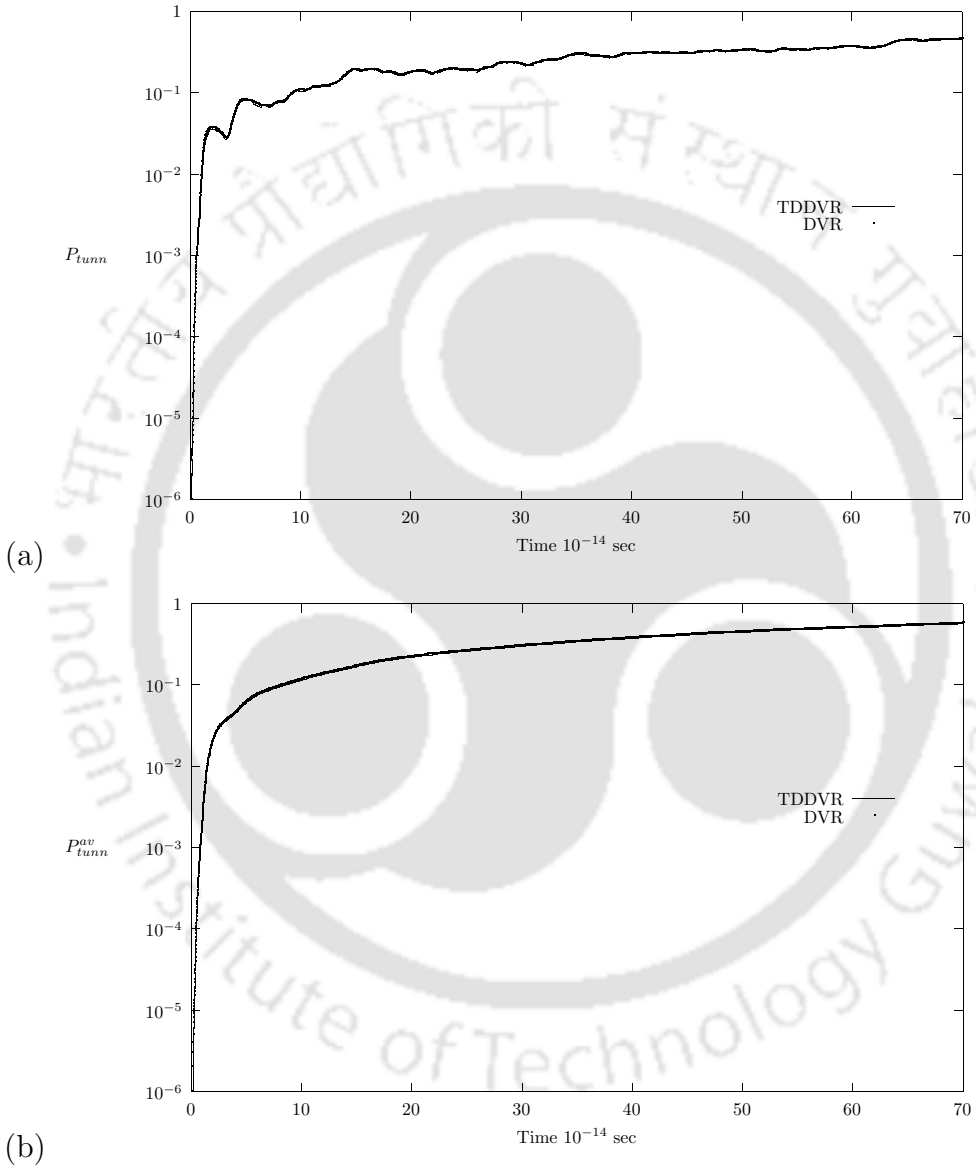

Figure 3.8: Comparison of quantum - classical (TDDVR) and quantum (DVR) results of the (a) tunneling probability (P_{tunn}) (b) time average tunneling rate (P^{av}_{tunn}) as a function of time with $N = 100$. The initial states of the bath oscillators are chosen as (0,2).

TH-421_02612202

both in quantum (DVR) and quantum - classical (TDDVR) calculations, we localized the initial wavefunction at the minimum of the left well of $V(s)$ and found, in case of DVR, more than 50 grid - points are needed to cover the other side of the barrier.

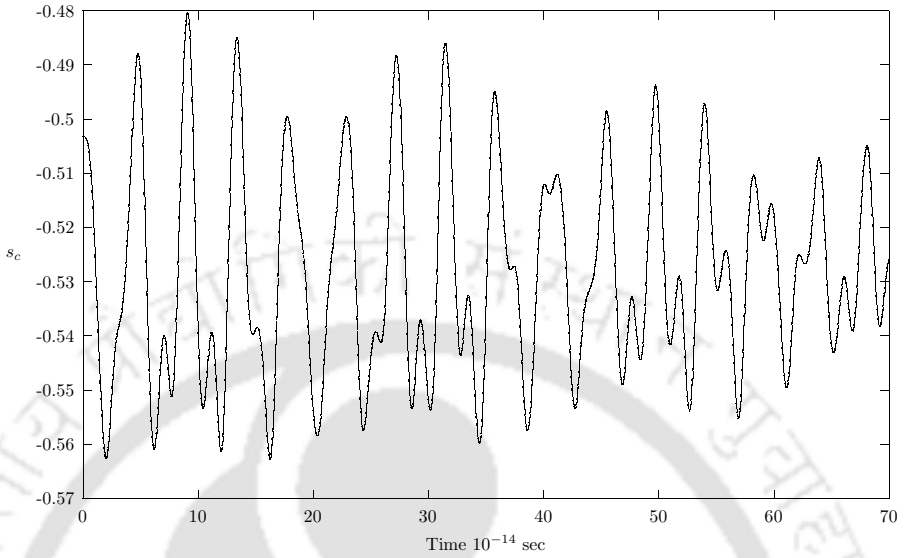

Figure 3.9: The center of the wavepacket, s_c, as a function of time. The initial states of the bath oscillators are chosen as (0,0) and $s_c\ (t = 0) = -\ 0.5$ Å.

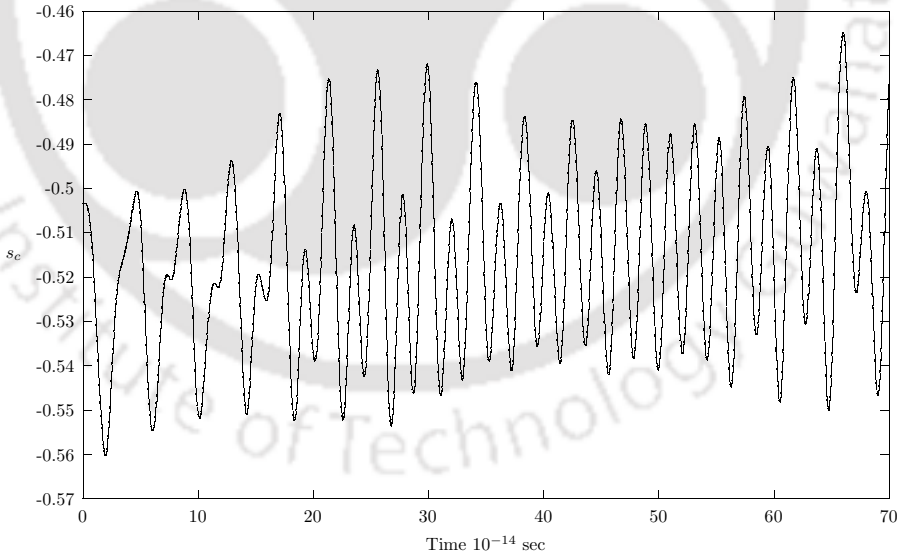

Figure 3.10: The center of the wavepacket, s_c, as a function of time. The initial states of the bath oscillators are chosen as (0,2) and $s_c\ (t = 0) = -\ 0.5$ Å.

Figs. 3.7 - 3.8 present (a) tunneling probability ($P_{tunn}(t)$) and (b) time - averaged

TH-421_02612202

tunneling rate ($P^{av}_{tunn}(t)$) as functions of time for two different cases corresponding to different initial states (0,0) and (0,2) of the heat bath, respectively. In all these cases, we have compared our quantum - classical results with the corresponding quantum ones and found excellent agreement between them. Moreover, it is important to note that earlier we had investigated the same system [16, 30] with different versions of quantum - classical method and calculated time - averaged tunneling rate ($P^{av}_{tunn}(t)$); but the present results have the best agreement with quantum ones, particularly at shorter times (0 to 10 τ, 1 $\tau = 10^{-14}$ sec).

We believe that the small oscillations in computed tunneling probabilities (Figs. 3.7(a) and 3.8(a)) are due to frequent collisional encounters of the wavepacket localized in the left well with the barrier. This explanation finds support when we monitor the center of the wavepacket, s_c as a function of time.

Figs. 3.9 and 3.10 show oscillations of s_c during the entire propagation time as we investigate the system for different initial states (0,0) and (0,2) of the heat bath, respectively. These trajectories clearly demonstrate a classical like feature of a pure quantum system.

In Table 3.2, we present the CPU time (sec) required to propagate the system localized in the minimum of the left well with zero initial momentum ($p_{s_c} = 0$) for different initial states (0,0) and (0,2) of the heat bath. In both the cases, we find quantum - classical (TDDVR) propagations are faster than corresponding quantum (DVR).

Table 3.2: CPU time (sec) to propagate the system up to 1 ps for different initial states of the heat bath.

Initial state	DVR	TDDVR(CF)
(0,0)	161505	63137
(0,2)	164819	62662

We have also investigated the dynamics of the reaction co-ordinate, s, without

TH-421_02612202

heat bath coupling for different initial kinetic energies (p_{s_c}) of the wavepacket. Figs. 3.11 display respectively the tunneling probability ($P_{tunn}(t)$) and the time - averaged tunneling rate ($P^{av}_{tunn}(t)$) as functions of time with the initial kinetic energy, $K_0 = 5$ Å^{-1} ($p_{s_c} = \hbar K_0$) and their comparison with DVR results.

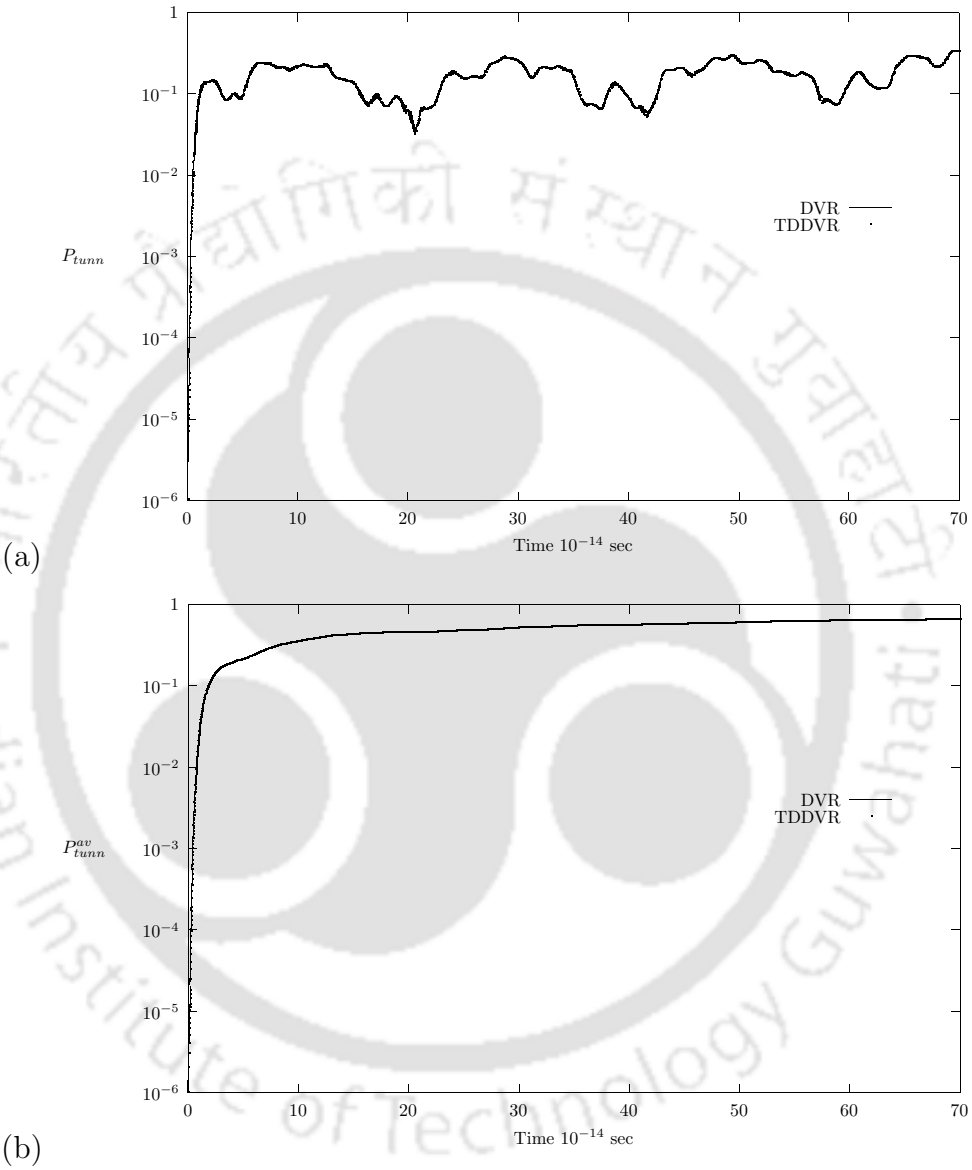

Figure 3.11: Comparison of quantum - classical (TDDVR) and quantum (DVR) results of the (a) tunneling probability (P_{tunn}) (b) time average tunneling rate (P^{av}_{tunn}) as a function of time with $N = 100$. The system is not coupled to a heat bath and the initial kinetic energy of wavepacket, $K_0 = 5$ Å^{-1}.

Fig. 3.12 shows the dynamics of the center of the wavepacket, s_c, as a function

TH-421_02612202

of time. *We notice a distinct difference between the trajectories when the wavepacket is coupled to a heat bath or is driven by an initial kinetic energy. If the system is coupled to a heat bath, trajectories oscillate with a mean value which is always away from the barrier. On the other hand, initial kinetic energy driven trajectory is always close to the barrier. Both the features are quite expected on the physical grounds.*

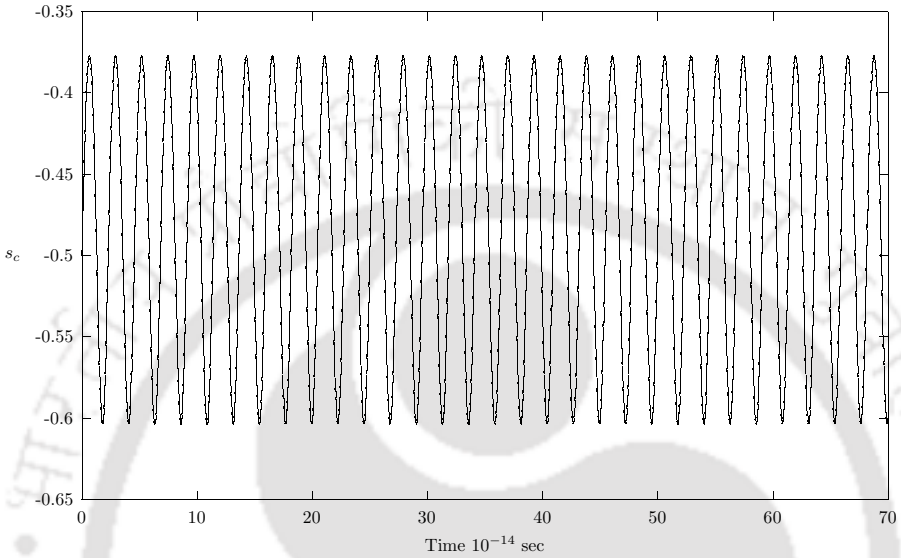

Figure 3.12: The center of the wavepacket, s_c, as a function of time for the quantum - classical calculations shown in Fig. 3.11 where $s_c(t = 0) = -0.5$ Å.

When the system is coupled to a heat bath, it spends most of the time interacting with bath modes and get little time to hit the barrier. On the other hand, an initial kinetic driven trajectory is forced to hit the barrier. This feature is further emphasized by the increase in both the tunneling probability and the time - averaged tunneling rate in comparison to when the system is coupled to bath modes.

Fig. 3.13 demonstrates the tunneling probability (P_{tunn}) at a particular time (1 ps) as functions of initial kinetic energies (K_0s). Excellent agreement with the corresponding quantum results verifies the accuracy and supremacy of the proposed quantum - classical method (TDDVR).

TH-421_02612202

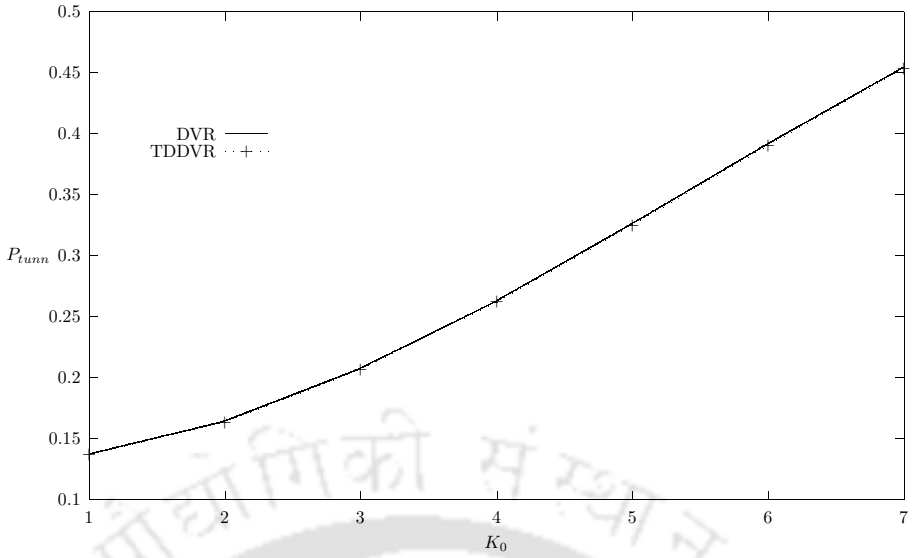

Figure 3.13: Comparison of quantum - classical (TDDVR) and quantum (DVR) results of the tunneling probability (P_{tunn}) at a particular time (1 ps) as a function of initial kinetic energy (K_0) of the wavepacket.

Table 3.3 presents CPU time (sec) to propagate the wavepacket localized in the minimum of the left well for different initial kinetic energies (K_0) and found TDDVR propagations to be faster than the corresponding DVR counterpart.

Table 3.3: CPU time (sec) to propagate the wavepacket up to 1 ps for different initial kinetic energy (p_{s_c}).

K_0	DVR	TDDVR(CF)
1	7940	3003
3	7733	3241
5	7956	3624
7	7727	3769
K_0	DVR	TDDVR(QF)
0	7547	6425

Finally, we have performed dynamical calculations using the rigorous expression of $\dot{p}_{s_c}$ (Eq. (D9) instead of Eq. (3.2.10)) where the system is not coupled to bath modes. Figures 3.14 show (a) the tunneling probability $[P_{tunn}(t)]$ and (b) time - averaged tunneling rate $[P^{av}_{tunn}(t)]$ as functions of time with zero initial kinetic energy $[p_{s_c}(t=0)=0]$ and excellent agreements with quantum results are obtained. Most

TH-421_02612202

interesting results are displayed in Fig. 3.15 where s_c s, obtained by using classical force (CF) (Eq. (3.2.10)) and quantum force (QF) (Eq. D9) respectively, are plotted as a function of time. When we localize initial wavepacket at the minimum of the left well ($s_c(t=0) = -\sqrt{2a_0/c_0}$), CF ($\frac{\partial V(s)}{\partial s}\big|_{s=s_c(t=0)}$) will be zero and the center of the wavepacket, $s_c(t)$, will remain at the same point for all the time. On the contrary,

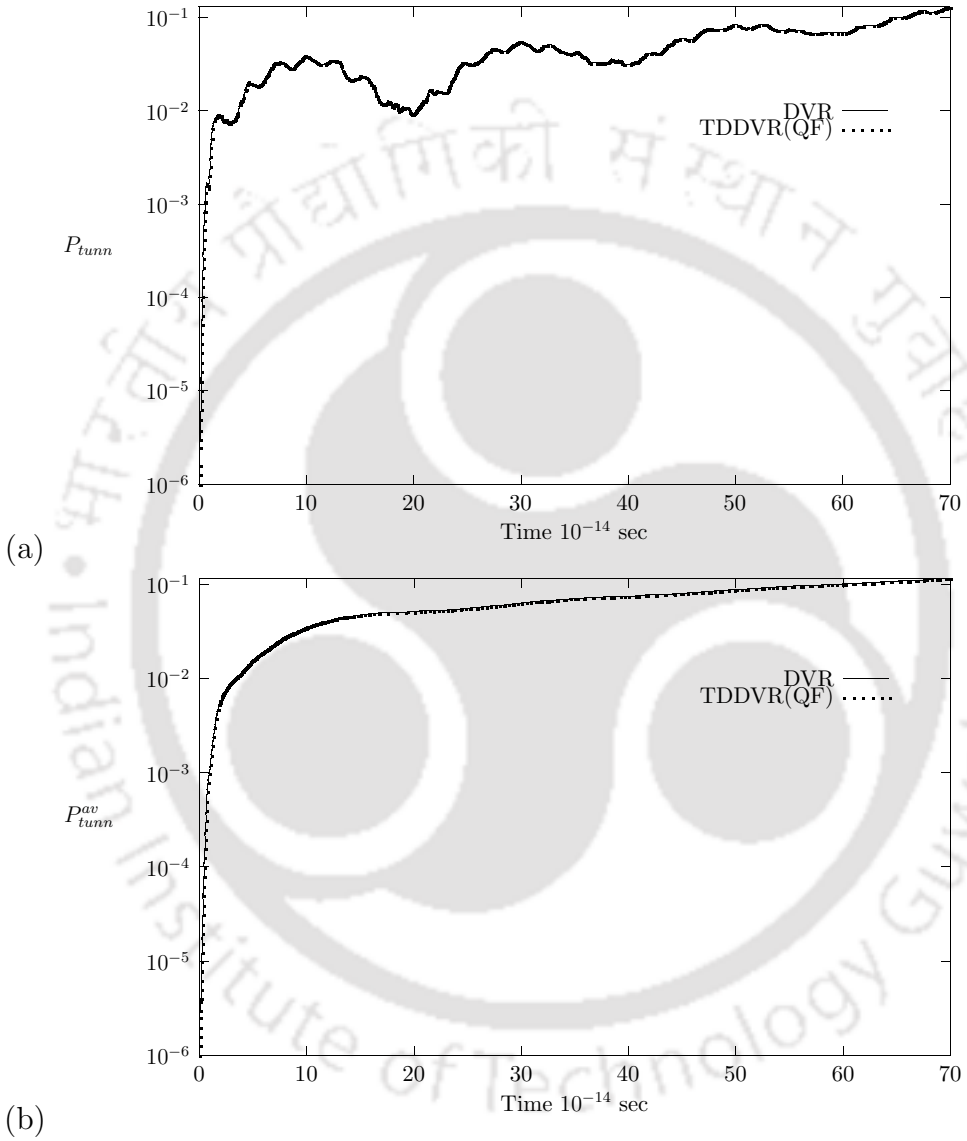

Figure 3.14: Comparison of quantum - classical (TDDVR(QF)) and quantum (DVR) results of the (a) tunneling probability (P_{tunn}) (b) time average tunneling rate (P^{av}_{tunn}) as a function of time with $N = 100$. The system is not coupled to a heat bath and the initial kinetic energy of wavepacket, p_{s_c}, is zero.

QF not only drives the movement of the center of the wavepacket, s_c, deep inside

TH-421_02612202

the barrier but also can possibly lead to a time - dependent effective potential and thereby, help to understand the mechanism of a tunneling process. CPU time taken to perform TDDVR(QF) calculation with zero initial kinetic energy is given in Table 3.3. Preliminarily, we see TDDVR(QF) (Eqs. (3.2.9), (D9) and (3.2.11)) is slower than TDDVR(CF) (Eqs. (3.2.9) - (3.2.11)) but slightly faster than the DVR.

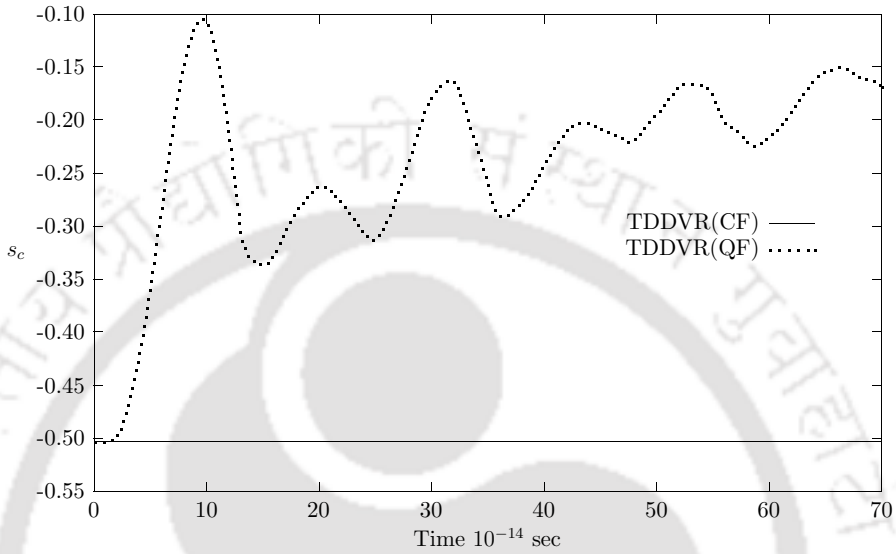

Figure 3.15: s_cs as a function of time for the quantum - classical calculation with CF and QF where, in both the cases, $s_c(t = 0)$=− 0.5 Å.

TH-421_02612202

TH-421_02612202

CHAPTER IV

APPLICATION TO NON-ADIABATIC TRANSITION

4.1 Introduction

There is considerable current interest [28, 55–80] in exploring quantitative techniques of molecular dynamics in the realm of electronically nonadiabatic processes [81–145]. We apply our method to the models [146] where typical non - adiabatic effects such as "trapping" and "Stueckelberg" oscillations are planted, to calculate transition probabilities, and thereby, compare with exact quantum results.

On the other hand, for the dynamics of reactive and non - reactive scattering processes in the presence of electronically non-adiabatic effects, [28, 64–76] we formulate our quantum - classical method for multi - dimensional multi - surface systems and apply it to the quasi - Jahn - Teller model where typical non - adiabatic effects are present. Here also we calculate transition probabilities and compare with traditional quantum results.

Moreover, we consider the single surface Extended Born - Oppenheimer (EBO) Hamiltonians for quasi - "JT scattering" model [70, 74] to calculate state - to - state transition probabilities. It is well known that calculated reactive transition probabilities undergo a very sharp change of symmetry from even → even to even → odd as the single surface Hamiltonian includes the non - adiabatic effects arising from excited state(s). We formulate the matrix equations of motion for both the EBO Hamiltonians by using DVR and TDDVR approaches and explore with a motivation whether TDDVR can follow this sharp change of transition probabilities with the

TH-421_02612202

change of effective KE of the Hamiltonian and quantitatively reproduce the DVR results.

4.2 The one dimensional models and TDDVR equations of motion

4.2.1 Simple avoided crossing

The first model is defined in the diabatic representation with the following interactions,

$$\begin{aligned} V_{11} &= A[1-\exp(-Bs)], \qquad s>0, \\ V_{11} &= -A[1-\exp(Bs)], \qquad s<0, \\ V_{22} &= -V_{11}(s), \\ V_{12} &= V_{21} = C\exp(-Ds^2) \end{aligned} \tag{4.2.1}$$

From quantum calculations, we expect slight tunneling on the ground adiabatic curve at momentum k < 4.5 a.u. and there is a trapping in the range 8 < k < 11 a.u. due to the well of the upper adiabatic curve apart from usual reflection and transmission on both the adiabatic curves.

4.2.2 Dual avoided crossing

The second model is much more challenging. It has two avoided crossings and can exhibit quantum interference effect (Stueckelberg oscillations). The interactions in the diabatic representation are

$$\begin{aligned} V_{11} &= 0, \\ V_{22} &= -A[1-\exp(-Bs^2)]+E_0, \\ V_{12} &= V_{21} = C\exp(-Ds^2). \end{aligned} \tag{4.2.2}$$

TH-421_02612202

4.2.3 Extended coupling with reflection

The third model is probably the most difficult to address by using classical mechanical based theory. Quantum calculations predict there will be substantial transmission on the ground as well as on the excited adiabatic state and very small reflection on the ground adiabatic state. The interaction in the adiabatic representation are

$$\begin{aligned} V_{11} &= A, \quad V_{22} = -A \\ V_{12} &= B\exp(Cs), \qquad s < 0, \\ V_{12} &= B[1-\exp(-Cs)], \qquad s > 0. \end{aligned} \tag{4.2.3}$$

The parameters used in the above models are given in Table 4.1.

Table 4.1: Potential parameters [146] and other useful data. 1 $\hat{\epsilon}$ = 100 KJ/mol and 1 $\tau = 10^{-14}$ s.

Parameter	Value	unit
μ	1.0893	amu
Im A_1(t=0)	0.5	amuτ^{-1}
Re A_1(t=0)	0.0	amuτ^{-1}
Re γ_1(t=0)	0.0	τ Å^{-2}amu^{-1}
Model I:		
A	0.2624	$\hat{\epsilon}$
B	3.0236	Å^{-1}
C	0.1312	$\hat{\epsilon}$
D	3.5711	Å^{-2}
Model II:		
A	2.6243	$\hat{\epsilon}$
B	0.9999	Å^{-2}
E_0	1.3121	$\hat{\epsilon}$
C	0.3936	$\hat{\epsilon}$
D	0.2143	Å^{-2}
Model III:		
A	0.0157	$\hat{\epsilon}$
B	2.6244	$\hat{\epsilon}$
C	1.7008	Å^{-1}

TH-421_02612202

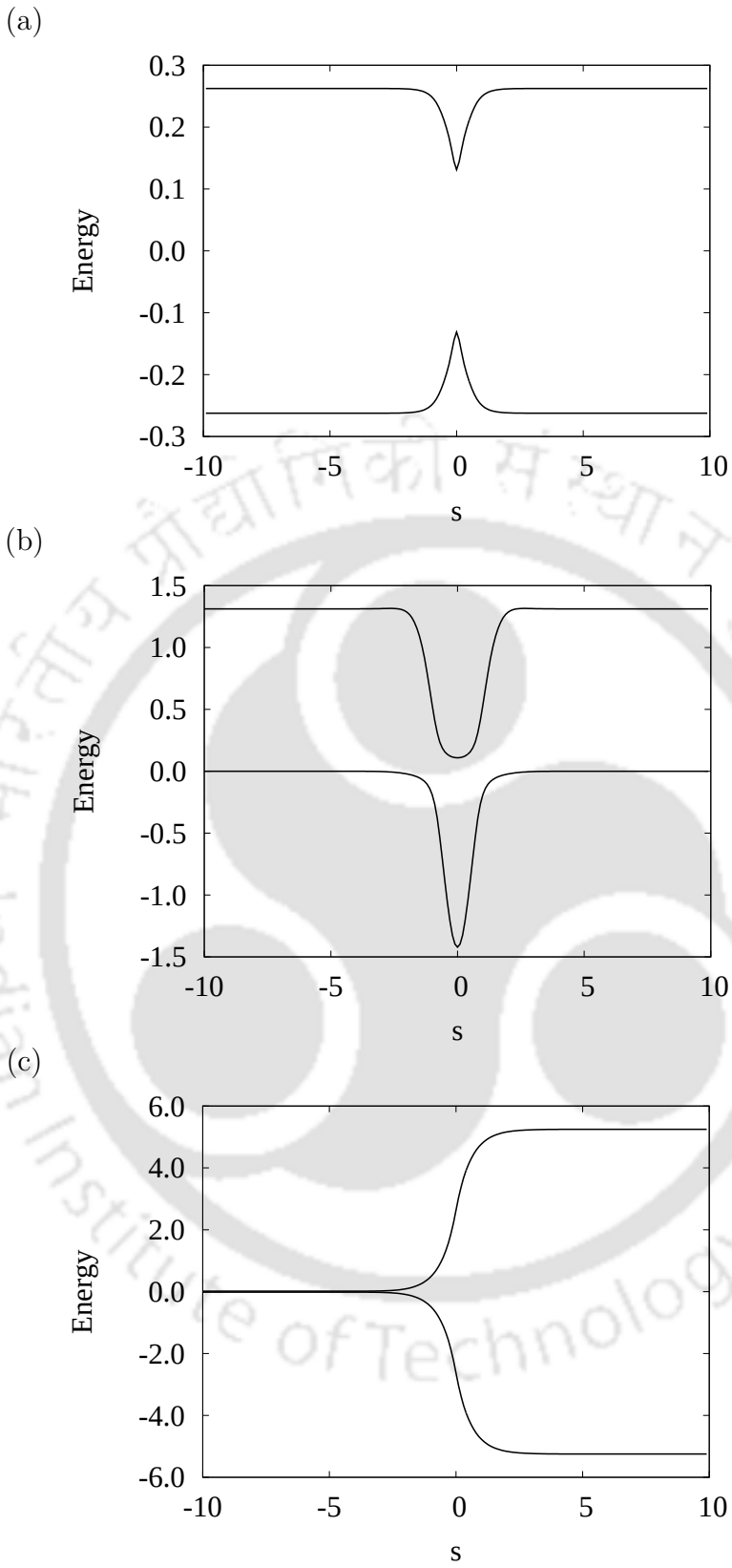

Figure 4.1: Adiabatic potential energy curve as a function of position s. (a) Simple avoided crossing, (b) Dual Avoided crossing and (c) Extended coupling with reflection.

TH-421_02612202

4.2.4 TDDVR equation of motion

The equation of the motion on the kth curve, in matrix form, is

$$i\hbar\mathbf{A}\dot{\mathbf{C}}_\mathbf{k} = \mathbf{H}^\mathbf{t}_\mathbf{kk}\mathbf{C}_\mathbf{k} + \mathbf{A}\sum_{\mathbf{l}\neq\mathbf{k}}\mathbf{V}_\mathbf{kl}\mathbf{C}_\mathbf{l} \tag{4.2.4}$$

with a similarity transformation, takes the form

$$i\hbar\dot{\mathbf{D}}_\mathbf{k}(\mathbf{t}) = \mathbf{A}^{-\mathbf{1/2}}\mathbf{H}^\mathbf{t}_\mathbf{kk}\mathbf{A}^{-\mathbf{1/2}}\mathbf{D}_\mathbf{k} + \sum_{\mathbf{l}\neq\mathbf{k}}\mathbf{V}_\mathbf{kl}\mathbf{D}_\mathbf{l} \tag{4.2.5}$$

where $\mathbf{D}_\mathbf{k} = \mathbf{A}^{\mathbf{1/2}}\mathbf{C}_\mathbf{k}$.

The explicit expression of an element of the time - dependent DVR Hamiltonian matrix, $\mathbf{H^t}$ (Appendix B) is,

$$\begin{aligned}\{H_{kk}\}^t_{i,j} &= \Big[\dot{p}_{s_c}(t)\times\frac{1}{2}\times\sqrt{\frac{\hbar}{ImA}}\times X_{i,j} + \frac{\mu\dot{s}_c^2(t)}{2}\times A_{i,j} \\ &+ \frac{\hbar ImA}{\mu}\times Y_{i,j} - \frac{\hbar ImA}{2\mu}\times Z_{i,j} + V_{kk}(s_i)\times A_{i,j}\Big],\end{aligned} \tag{4.2.6}$$

Similarly the classical path equations can be written as

$$\dot{s}_c(t) = \frac{p_{s_c}(t)}{\mu} \tag{4.2.7}$$

$$\dot{p}_{s_c}(t) = -\Big\langle\Xi(s,t)\Big|\frac{d\hat{V}(s)}{ds}\Big|_{s=s_c(t)}\Big|\Xi(s,t)\Big\rangle \tag{4.2.8}$$

where the classical force is evaluated by substituting the matrices, $\Xi(s,t)$ and $\hat{V}(s)$ (Eqs. (2.2.3) and (2.2.2) respectively). Using Dirac - Frenkel variational principle [37], we have arrived at a rigorous expression of $\dot{p}_{s_c}$ for non - adiabatic processes by minimizing the following integral (Appendix D),

$$\begin{aligned}I &= \int ds\Big(-i\hbar\frac{\partial\Xi^\star(s,t)}{\partial t} - H(p_s,s)\Xi^\star(s,t)\Big) \\ &\times \Big(i\hbar\frac{\partial\Xi(s,t)}{\partial t} - H(p_s,s)\Xi(s,t)\Big),\end{aligned} \tag{4.2.9}$$

with respect to $\dot{p}_{s_c}$. At this point, it is important to note that compared to earlier versions [16, 17] only the present form of TDDVR [36] has the scope for the variational

TH-421_02612202

derivation of the evolution equation for p_{s_c}. The compact form of $\dot{p}_{s_c}$ in Eq. (D6) (Appendix D) can further be simplified when we replace $S^{(1)}_{ij}$ by $S^{(1)}_{ij}\delta_{ij}$ as first order term $(s - s_c(t))$ is diagonal in DVR (Table 2.2), leading to

$$\dot{p}_{s_c}(t) = \sum_k \sum_{ij} c^\star_{ik}(t) c_{jk}(t) \Big\{ \frac{2ImA^2}{\mu} \Big[S^{(2)}_{ij} \frac{S^{(1)^\star}_{ii}}{A_{ii}} - S^{(3)}_{ij} \Big] - \frac{\hbar ImA}{\mu} \Big[R_{ij} \frac{S^{(1)^\star}_{ii}}{A_{ii}} - T^\star_{ij} \Big] \Big\}$$
$$\Big/ \Big[\sum_k \sum_i c^\star_{ik}(t) c_{ik}(t) \frac{S^{(1)^\star}_{ii} S^{(1)}_{ii}}{A_{ii}} - \sum_k \sum_{ij} c^\star_{ik}(t) c_{jk}(t) S^{\star(2)}_{ij} \Big] \qquad (4.2.10)$$

We have applied our quantum - classical method on the above three model problems [146] and in all the cases, we have also calculated accurate quantum mechanical (DVR/FFT) results for comparison. Each of these models is a two - state one - dimensional system. Considering the mass of these systems, we may anticipate significant quantum effect associated with their motion and classical mechanics has no hope of reproducing these results.

4.2.5 Initialization, propagation and projection

Quantum mechanical calculations have been carried out by using DVR method while in few cases FFT based technique was used. Quantum - classical results are obtained from the TDDVR approach proposed here.

The initial amplitudes of the DVR wavefunction at the grid - points (s_is) were calculated from GWP ($\Phi(s_i, t_0)$) centred around $s_c(t = 0) = -4$Å with it's momentum vector, k_0 and the imaginary part of the width, $ImA = 0.4$ amu/τ ($1\tau = 10^{-14}$ sec):

$$\Phi(s_i, t_0) = \Big[\frac{2ImA}{\pi\hbar} \Big]^{1/4} \times \exp \Big[ik_0(s_i - s_0) - \frac{ImA}{\hbar}(s_i - s_0)^2 \Big]. \qquad (4.2.11)$$

In case of DVR, only Eq. (4.2.5) was solved to see the dynamics and all the terms containing classical variable(s) in the Hamiltonian matrix (Eq. (4.2.6)) were dropped during propagation. At the same time, in FFT - Lanczos propagation we have used the initial amplitudes calculated from GWP in the presence of proper absorbing potential.

TH-421_02612202

Similarly, the initial amplitudes of the TDDVR wavefunction at the grid - points (s_is) were obtained from GWP ($\Phi(s_i, t_0)$) with the same numerical values of the parameters as used in DVR except that k_0 was chosen to be zero, leading to

$$\Phi(s_i, t_0) = \Big[\frac{2ImA}{\pi\hbar}\Big]^{1/4} \times \exp\Big[-\frac{ImA}{\hbar}(s_i - s_0)^2\Big]. \tag{4.2.12}$$

During the TDDVR propagation, Eqs. (4.2.5), (4.2.7) and (4.2.8) or Eq. (4.2.10) were solved simultaneously with p_{s_c} ($= \hbar k_0$) entering as a classical variable through Eq. (4.2.7) and also through the first two terms of the Hamiltonian matrix (Eq. (4.2.6)).

Using the properties of the DVR or TDDVR basis functions, we can write normalized amplitudes,

$$d_{i1}(t=0) = A_{i,i}^{-1/2}\Phi(x_i) \tag{4.2.13}$$

In all the quantum and quantum - classical calculations, wavepacket was prepared on the lowest adiabatic state ($d_{i1}^{ad} \equiv d_{i1}$) and diabatized ($\mathbf{D^{dia}} = \mathbf{TD^{ad}}$ where $\hat{\mathbf{V}}^{\mathbf{ad}}(\mathbf{s}) = \mathbf{T}^{\dagger}\hat{\mathbf{V}}^{\mathbf{dia}}(\mathbf{s})\mathbf{T}$) before propagation started. Equations of motion were integrated until the wavepacket or particle or both had completely left the interaction region.

The reflection or transmission probabilities on both the adiabatic curves can be calculated by using the time - dependent coefficient d_{ik}^{ad}s in the adiabatic representation,

$$\begin{aligned}
P(t) &= \int_{-\infty}^{\infty} ds \Xi^{ad\dagger}(s,t)\Xi^{ad}(s,t) = \sum_l \int_{-\infty}^{\infty} ds \Psi_l^{ad}(s,t)^{\star}\Psi_l^{ad}(s,t) = \sum_l P_l(t) = 1 \\
&= \sum_l \sum_i {c^{ad}}_{il}^{\star}(t) c_{il}^{ad}(t) \sum_{kk'} \xi_k^{\star}(x_i)\xi_{k'}(x_i) \int_{-\infty}^{\infty} \Phi_k'^{\star}(s',t)\Phi_{k'}'(s',t)ds' \\
&\approx \sum_{l=1}^{M}\sum_{i=1}^{N} |c_{il}^{ad}(t)|^2 A_{i,i} \\
&= \sum_{l=1}^{M}\sum_{i=1}^{N} |d_{il}^{ad}(t)|^2,
\end{aligned} \tag{4.2.14}$$

TH-421_02612202

where M is the number of curves involved in the calculations. Hence total probability of finding the system on a particular curve is,

$$P_l(t) = \sum_{i=1}^{N} |d_{il}^{ad}(t)|^2, \tag{4.2.15}$$

where transmission and reflection are defined as,

$$P_l^{tran}(t) = \sum_{i>i^\star} |d_{il}^{ad}(t)|^2, \tag{4.2.16}$$

$$P_l^{ref}(t) = \sum_{i<i^\star} |d_{il}^{ad}(t)|^2. \tag{4.2.17}$$

4.2.6 Results and Discussion

A. Simple avoided crossing

In Figs. 4.1(a) and 4.1(b), we present the convergence profile of transmission probability on the ground adiabatic state at momentum k_0 = 10 a.u. as functions of time with increasing number of grid - points (N). At this energy, sufficient transmission on the excited state also occurs (see Fig. 4.2(c)). Figure 4.1(a) indicates quantum results have reached the convergence at least with 200 DVR grid - points whereas quantum - classical calculations as shown in Fig. 4.1(b) have achieved the same level of accuracy even with less than 50 TDDVR grid - points.

This model is interesting as well as challenging for total energy below the asymptotic energy of the upper adiabatic potential energy curve (i.e. E $<$ 0.02 a.u. $\equiv$ k_0 = 9.0 a.u.). It is expected that the upper adiabatic curve is classically closed for the particle below this energy. At momentum $k_0 < 4.5$ a.u. classical particle can not cross the barrier of the lower adiabatic state and is reflected with cent percent probability. On the other hand, quantum mechanically neither the upper adiabatic curve is closed below the energy E $<$ 0.02 a.u. nor 100 % reflection on ground adiabatic state can occur below the momentum $k_0 < 4.5$.

Figures. 4.2(a) - (c) compare transmission and reflection probabilities calculated by the TDDVR recipe and traditional quantum mechanical method on both the curves

TH-421_02612202

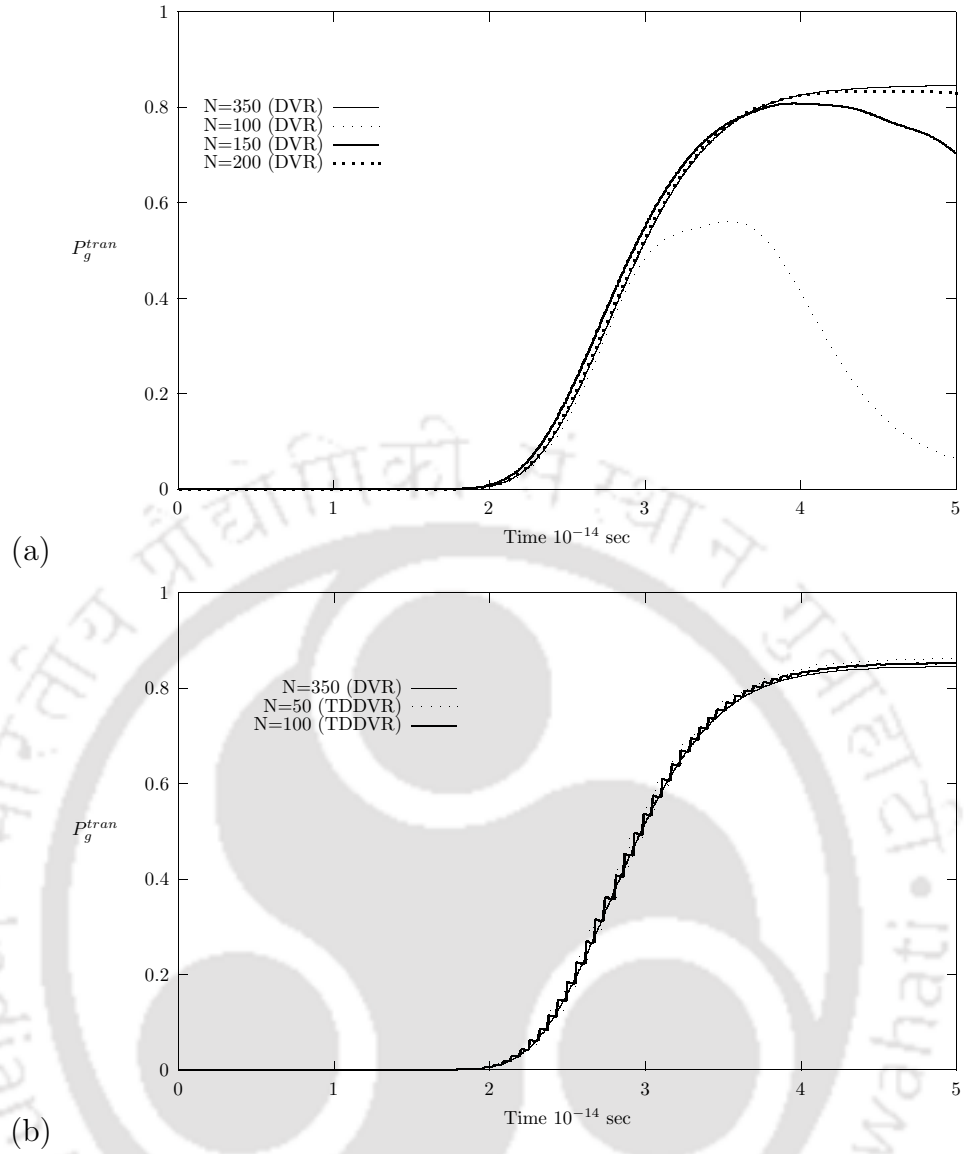

Figure 4.2: Simple avoided crossing model. Transmission probability on the ground adiabatic state as functions of time for (a) N=100, N=150, N=200 and N=350 (DVR) (b) N=50, N=100 (TDDVR), and N=350 (DVR).

and show excellent quantitative agreement between our TDDVR and quantum results for the entire energy range. Fig. 4.2(a) clearly indicates that the present quantum - classical method can quantitatively reproduce the transmission due to tunneling below $k_0 < 4.5$ and over barrier crossing above $k_0 > 4.5$. As the grid - points (s_i s) move around the central trajectory (s_c) and amplitudes of the grid - points changes with time, TDDVR essentially behave like a multi - trajectory approach and can mimic

TH-421_02612202

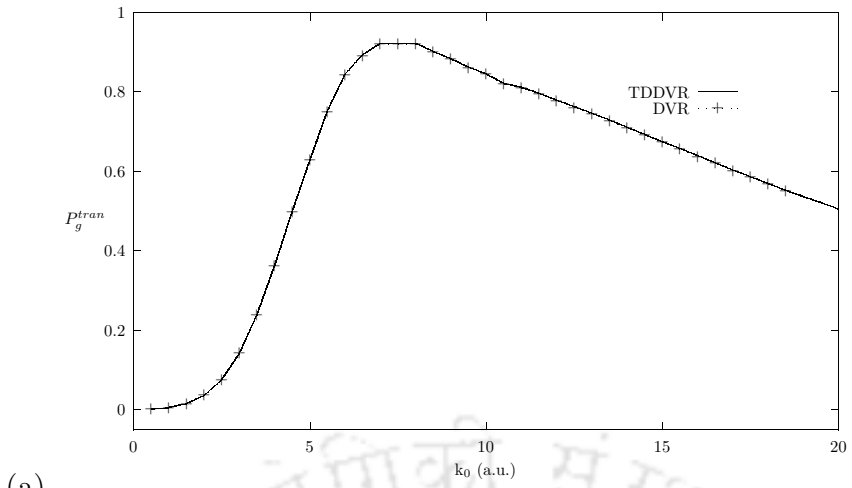

(a)

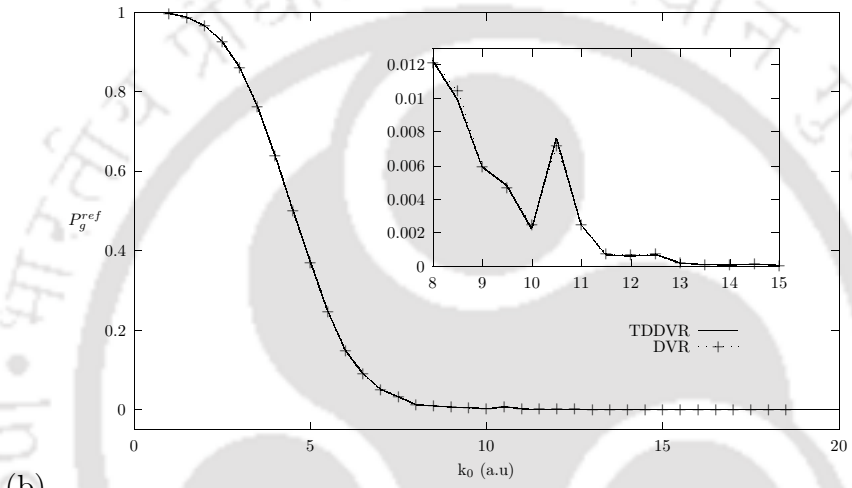

(b)

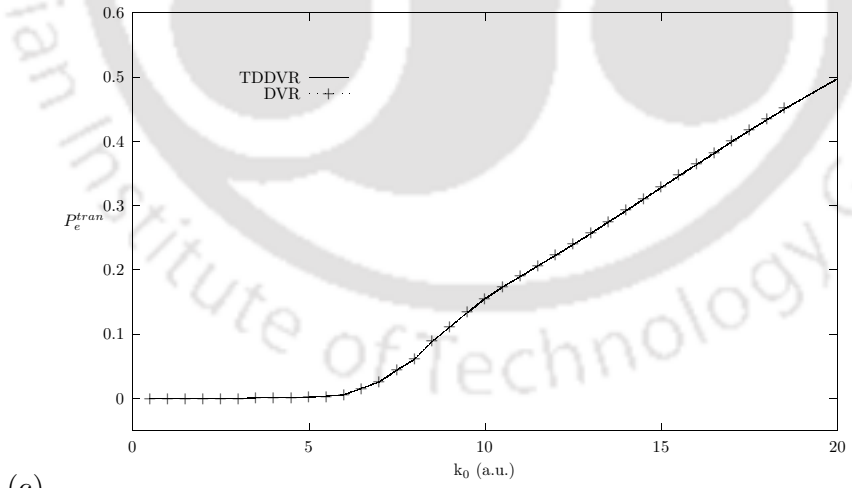

(c)

Figure 4.3: Simple avoided crossing model. Comparison of TDDVR and DVR results of (a) transmission probability on the ground adiabatic state, (b) reflection probability on the ground adiabatic state and (c) transmission probability on the excited adiabatic state as functions of initial kinetic energy ($\hbar k_0$). TDDVR and DVR calculations were performed with 50 and 350 grid - points respectively.

TH-421_02612202

the reflection due to trapping of the particle. Fig. 4.2(b) demonstrates reflection on the ground around $k_0 \approx 10.5$ a.u. due to temporary trapping of the particle in the well of the upper adiabatic state. Moreover, the transmission on upper state (Fig. 4.2(c)) increases gradually even below the asymptotic energy of upper adiabatic state ($E < 0.02$ a.u. $\equiv k_0 < 9$ a.u.) indicating that the present method as expected can access the upper state when it is classically closed.

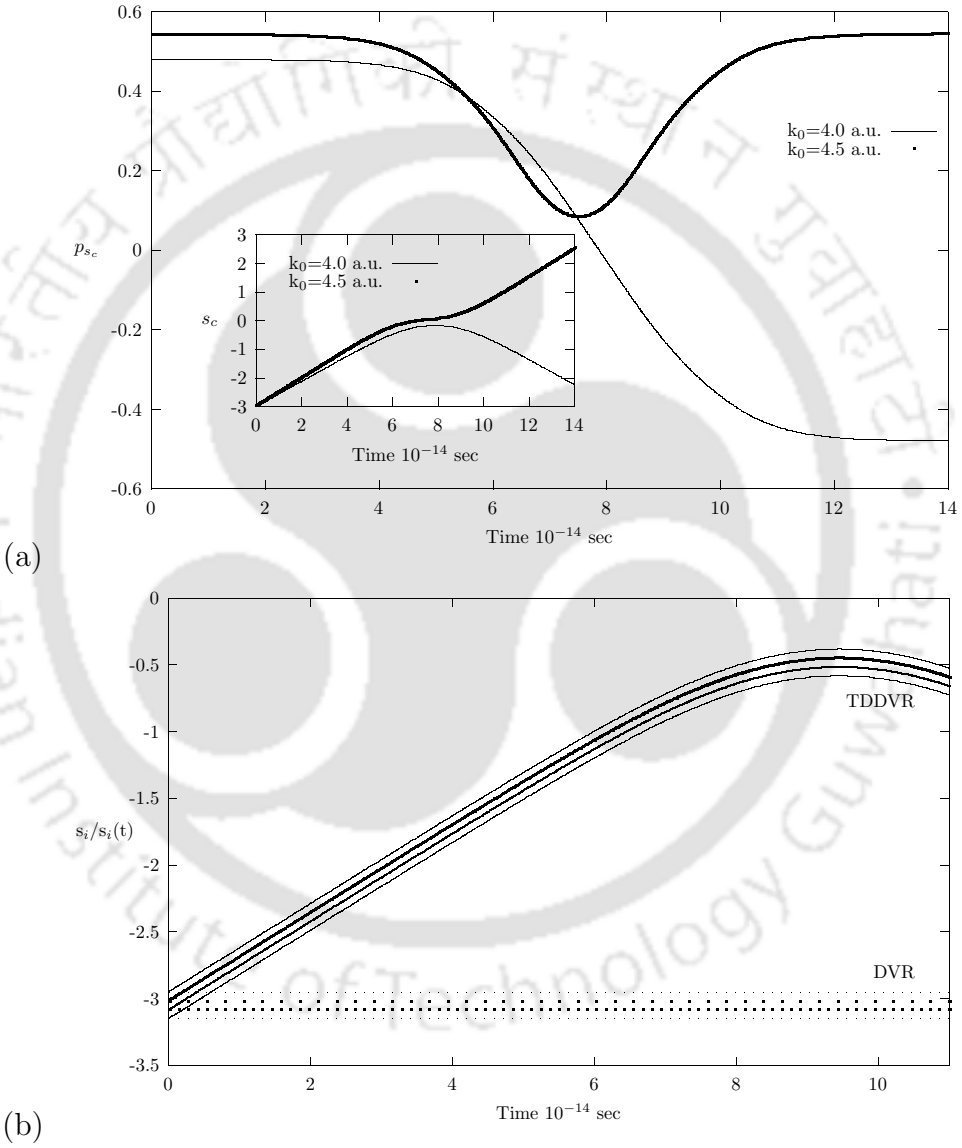

Figure 4.4: (a) Simple avoided crossing model. The center of the wavepacket, s_c, and it's momentum, p_{s_c} as functions of time, (b) Few DVR grid - points (s_i) and TDDVR grid - points ($s_i(t)$) as functions of time.

TH-421_02612202

Fig. 4.3(a) display "classical" momentum (p_{s_c}) as well as the central trajectory (s_c) as functions of time for two different initial momentum k_0 = 4.0 and 4.5 a.u.. At k_0 = 4.0 a.u. trajectory comes back to the negative s with a reverse "classical" momentum whereas at k_0 = 4.5 a.u. the trajectory passes over the barrier but it seems the particle is not moving between 6 - 9 τ which is again corroborated by sudden decrease of momentum within the same period of time. Fig. 4.3(b) exhibits the movement of few TDDVR grid - points (s_i(t)) around the central trajectory s_c(t) as functions of time (k_0 = 3 a.u.). As the grid - points move towards the reactive side (dictated by classical Eqs. (4.2.7) and (2.2.11)) and the amplitude of the wavefunction at those grid - points changes with time (quantum Eq. (4.2.5)), it becomes possible to cover the reactive side and achieve the required convergence with very small number of TDDVR grid - points.

B. Dual avoided crossing

Figs. 4.4(a) - (b) demonstrate the convergence profiles of ground state transmission probabilities at momentum k_0 = 24 a.u. as functions of time. As the interaction region of this model is spread over a long range, quantum calculations require a very large grid to cover the entire configuration space. Fig. 4.4(a) shows that the convergence is achieved at least with 350 DVR grid - points when the initial wavepacket is located around - 5$\mathring{A}$. On the other hand, as grid - points move in TDDVR, only 50 grid - points are sufficient to reach the convergence (Fig. 4.4(b)) with the same starting position of the initial wavepacket.

Figs. 4.5(a) - (c) exhibit excellent quantitative agreement between traditional quantal and present results at all energies, particularly it is impressive at energies below $\log_e$(E) < - 3 (a.u.). As the model has two avoided crossing, it shows strong Stueckelberg oscillations due to quantum interference effect. The present method can reproduce all these oscillations even at very low energies. At energies below $\log_e$(E) < - 3 (a.u.), asymptotically the excited adiabatic state is not classically accessible but

TH-421_02612202

at these energies or even much further below, the well of the excited adiabatic state can influence the ground state. When the flux is trapped in this well, the probability of reflection and quantum interference effects due to non - adiabatic transitions may compete with each other.

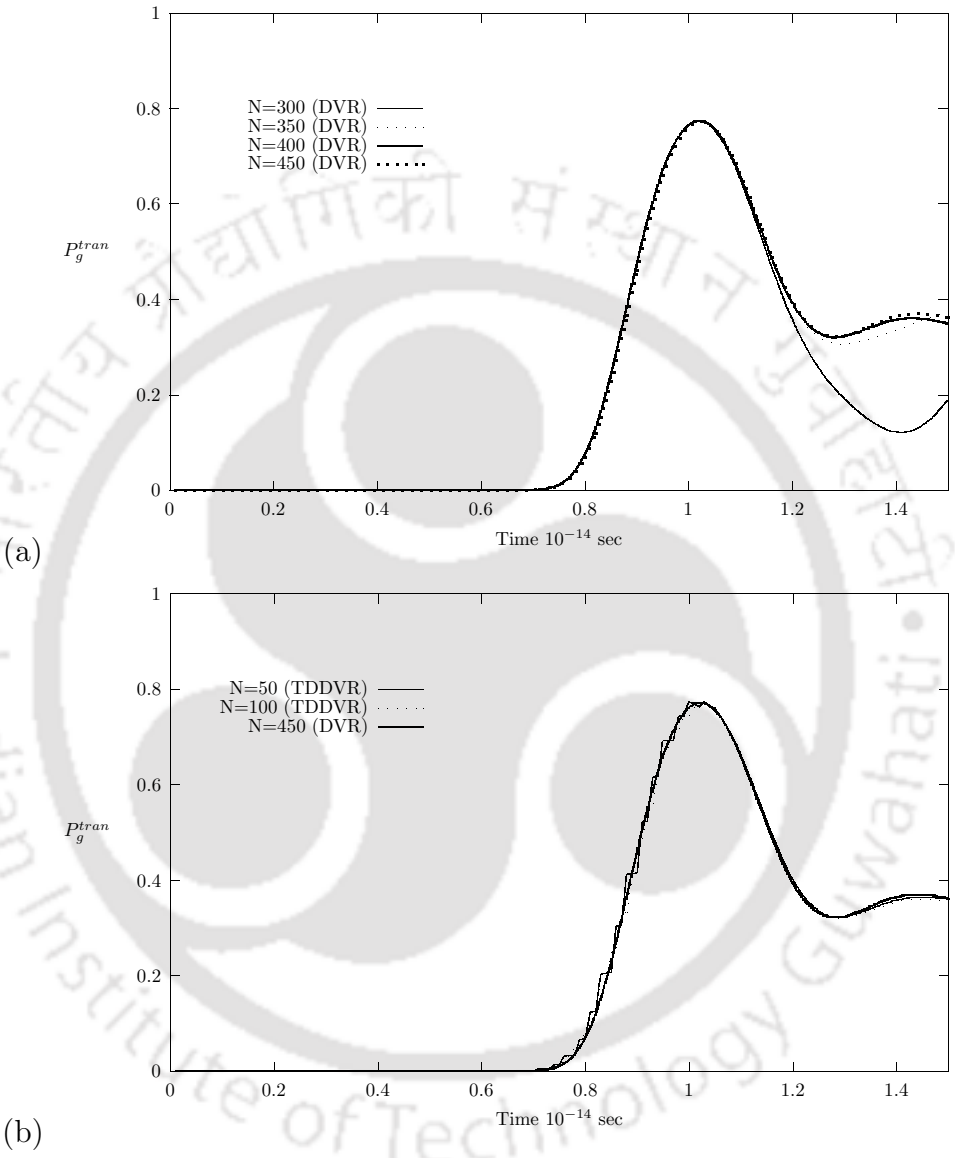

Figure 4.5: Dual avoided crossing model. Transmission probability on the ground adiabatic state as functions of time for (a) N=300, N=350, N=400 and N=450 (DVR) and (b) N=50, N=100 (TDDVR), and N=450 (DVR).

Fig. 4.5(b) displays significant reflection below $\log_e(E) < -3.5$ (a.u.) which is at par with quantum results. *At this point, we wish to specify that calculated*

TH-421_02612202

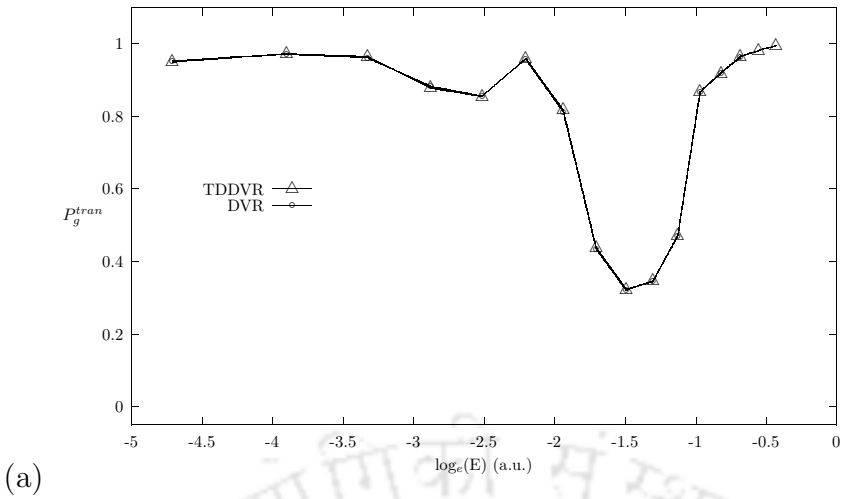

(a)

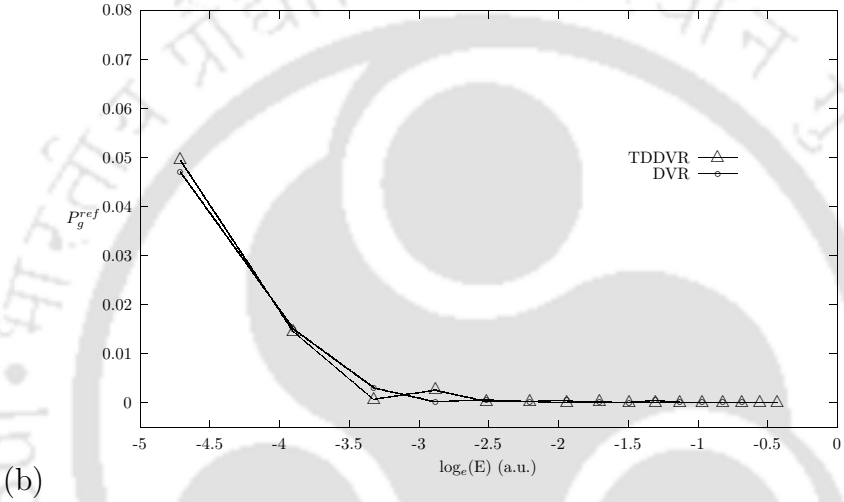

(b)

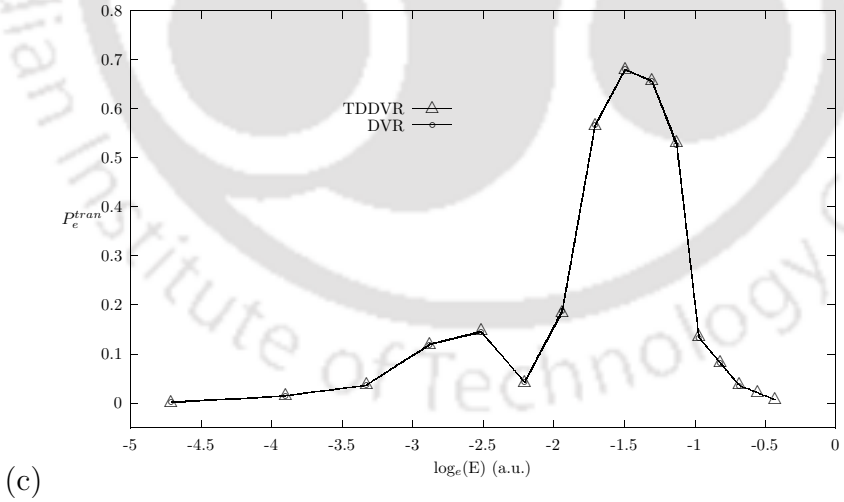

(c)

Figure 4.6: Dual avoided crossing model. Comparison of TDDVR and DVR results of (a) transmission probability on the ground adiabatic state, (b) reflection probability on the ground adiabatic state and (c)transmission probability on the excited adiabatic state as functions of initial kinetic energy ($\hbar k_0$). TDDVR and DVR calculations were performed with 50 and 450 grid - points respectively.

TH-421_02612202

transmission and reflection probabilities on the same model using different versions of trajectory surface hopping method [80, 146] have reasonably good agreement with quantum results at higher energies ($log_e(E) > -2$ (a.u.)) but at lower energies ($log_e(E) < -2$ (a.u.)) agreements are not as good. "Classical" momentum (p_{s_c}) as well as the central trajectory (s_c) are shown in Fig. 4.6 as functions of time. At k=3.0 a.u. the trajectory moves very fast between 6 -9 τ with a sudden increase in momentum.

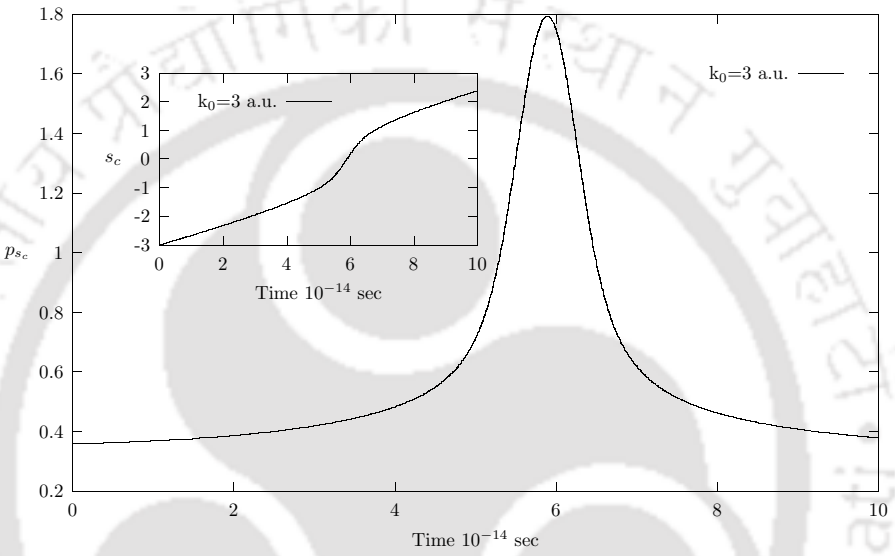

Figure 4.7: Dual avoided crossing model. The center of the wavepacket, s_c, and it's momentum, p_{s_c} as functions of time.

C. Extended coupling with reflection

Since the potential energy coupling V_{12} of this model does not vanish even at s$\rightarrow \infty$, diabatic states are coupled asymptotically and it is difficult to perform traditional quantum calculations (DVR/FFT) in this situation. Of course as the ∇V_{12} vanishes as s $\rightarrow \infty$, with a large grid and only at high energies ($k_0 > 10$ a.u.) one can obtain converged results by propagating wavepackets by fast fourier transformation (FFT) based technique. The present method, however can perform diabatic calculations with this kind of interactions even at very low energies. When the central trajectory

TH-421_02612202

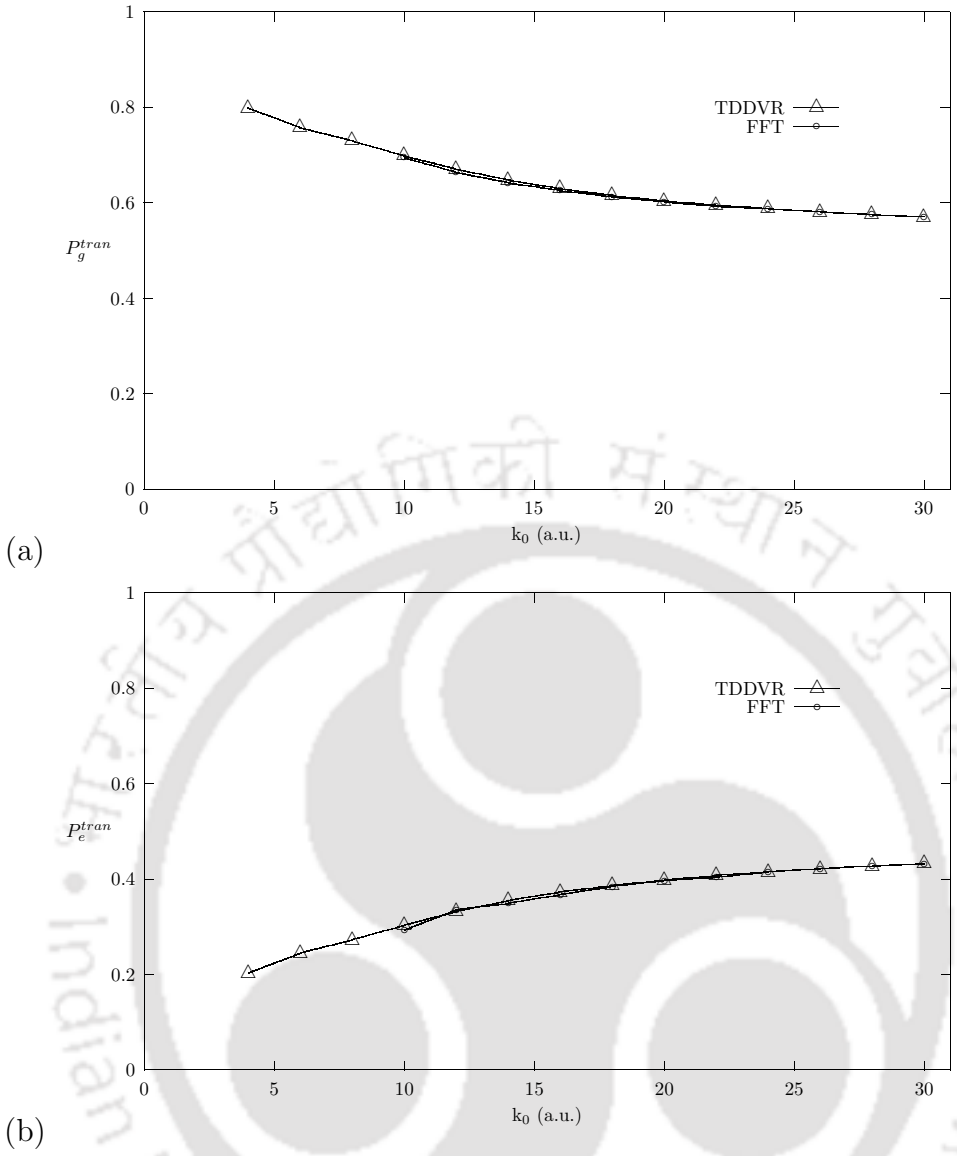

Figure 4.8: Extended coupling with reflection model. Comparison of TDDVR and FFT-Lanczos results of (a) transmission probability on the ground adiabatic state, (b) transmission probability on the excited adiabatic state as functions of initial kinetic energy ($\hbar k_0$). TDDVR and FFT calculations were performed with 50 and 1024 grid - points respectively.

(s_c) of TDDVR is sufficiently away from the point where $\nabla V_{12} = 0$, we switch from diabatic to adiabatic TDSE to avoid numerical artifact. It means outside the interaction region we have performed adiabatic calculations whereas in the interaction region diabatic calculations were done to include important quantum features. Figures 4.7(a) and (b) present transmission probabilities on ground and excited state, respectively.

TH-421_02612202

Our TDDVR results were obtained for the entire energy range and quantum results were calculated only for higher energies ($k_0 \geq 10$ a.u.). If we compare our TDDVR results with the fully quantum ones, the agreement is quantitatively excellent and impressive showing that our method is potentially exact.

4.3 The Born - Oppenheimer treatment, multi - dimensional models and TDDVR equations of motion

4.3.1 The Born - Oppenheimer Treatment

The Schroedinger equation in the adiabatic representation that describes the motion of the electrons and nuclei, can be integrated over electronic co-ordinates and expressed as,

$$-\frac{\hbar^2}{2\mu}\sum_{l'}^{M}\Big[\Big\{\nabla^2\delta_{ll'} + 2\tau^{(1)}_{ll'}.\nabla + \tau^{(2)}_{ll'}\Big\}\Psi_{l'}(\{s^k\})\Big] + \Big[U_l(\{s^k\}) - E\Big]\Psi_l(\{s^k\}) = 0 \qquad (4.3.1)$$

$$\tau^{(1)}_{ll'} = \langle\zeta_l|\nabla\zeta_{l'}\rangle; \qquad \tau^{(2)}_{ll'} = \langle\zeta_l|\nabla^2\zeta_{l'}\rangle \qquad (4.3.2)$$

$$T_{\{s^k\}} = -\frac{\hbar^2}{2\mu}\nabla^2 = -\frac{\hbar^2}{2\mu}\Big(\frac{\partial^2}{\partial {s^1}^2} + \frac{\partial^2}{\partial {s^2}^2} + \cdots + \frac{\partial^2}{\partial {s^p}^2}\Big) \qquad (4.3.3)$$

where $\Psi_l(\{s^k\})$s are considered to be the nuclear wavefunctions associated with different electronic states and ζ_ls form a complete set of electronic eigenfunctions which depend on the nuclear coordinates parametrically.

When we concentrate on a two dimensional two surface system, Eq. (4.3.1) becomes,

$$\Big[-\frac{\hbar^2}{2\mu}\nabla^2 + \bar{U}_1 - E\Big]\Psi_1(s^1,s^2) - \frac{\hbar^2}{\mu}\tau^{(1)}.\nabla\Psi_2(s^1,s^2) - \frac{\hbar^2}{2\mu}\nabla\tau^{(1)}\Psi_2(s^1,s^2) = 0 \qquad (4.3.4)$$

$$\Big[-\frac{\hbar^2}{2\mu}\nabla^2 + \bar{U}_2 - E\Big]\Psi_2(s^1,s^2) - \frac{\hbar^2}{\mu}\tau^{(1)}.\nabla\Psi_1(s^1,s^2) - \frac{\hbar^2}{2\mu}\nabla\tau^{(1)}\Psi_1(s^1,s^2) = 0 \qquad (4.3.5)$$

TH-421_02612202

where $\bar{U}_l$s are defined as, $\bar{U}_l = U_l + (\hbar^2/2\mu)(\tau^{(1)})^2$; $l = 1, 2$ and we have made use of the fact that $\tau^{(2)} = \nabla.\tau^{(1)} + (\tau^{(1)})^2$.

It turns out that Born - Oppenheimer (BO) treatment leads to a nuclear Hamiltonian that contains non-diagonal kinetic energy operators. This fact guarantees that the nuclear wavefunctions will be of the right symmetry to ensure an overall electronic - nuclear single - valued solution. The operators which govern the symmetry features of the solution, are the non-adiabatic coupling terms and therefore it is always important to incorporate them. When we ignore the non - adiabatic coupling terms, the ordinary BO approximation will yield the equation,

$$\Big[-\frac{\hbar^2}{2\mu}\nabla^2 + U_l - E\Big]\Psi_l(s^1, s^2) = 0, \qquad l = 1, 2. \tag{4.3.6}$$

The general form of electronic eigenfunctions in the adiabatic representation for a two dimensional two surface system can be expressed with the following orthogonal basis functions,

$$\zeta_1 = \begin{pmatrix} \cos\theta \\ -\sin\theta \end{pmatrix} \qquad and \qquad \zeta_2 = \begin{pmatrix} \sin\theta \\ \cos\theta \end{pmatrix} \tag{4.3.7}$$

where the angle θ depends on the nuclear coordinates as $s^1 = q\sin\theta$ and $s^2 = q\cos\theta$. Substituting ζ_1 and ζ_2 in Eqs. (4.3.4) - (4.3.5), we can rewrite these two coupled equations as,

$$\Big[T_{q,\theta} + \bar{U}_1 - E\Big]\Psi_1 - \frac{\hbar^2}{2\mu q^2}\frac{\partial}{\partial\theta}\Psi_2 = 0, \tag{4.3.8}$$

$$\Big[T_{q,\theta} + \bar{U}_2 - E\Big]\Psi_2 + \frac{\hbar^2}{2\mu q^2}\frac{\partial}{\partial\theta}\Psi_1 = 0, \tag{4.3.9}$$

where

$$T_{q,\theta} = -\frac{\hbar^2}{2\mu}\Big[\frac{\partial^2}{\partial q^2} + \frac{1}{q}\frac{\partial}{\partial q} + \frac{1}{q^2}\frac{\partial^2}{\partial\theta^2}\Big] \quad \text{and} \quad \bar{U}_l = U_l + \frac{\hbar^2}{8\mu q^2}, l = 1, 2$$

TH-421_02612202

We can solve Eqs. (4.3.8) - (4.3.9) as such but we may prefer to do it by transforming to the diabatic representation:

$$\begin{pmatrix} \Psi_1^{ad} \\ \Psi_2^{ad} \end{pmatrix} = \begin{pmatrix} \cos\frac{\theta}{2} & -\sin\frac{\theta}{2} \\ \sin\frac{\theta}{2} & \cos\frac{\theta}{2} \end{pmatrix} \begin{pmatrix} \Psi_1^{dia} \\ \Psi_2^{dia} \end{pmatrix} \tag{4.3.10}$$

In the diabatic representation, kinetic coupling vanishes and potential energy takes the following matrix form: [69]

$$\begin{aligned} W_{11} &= \frac{1}{2}\Big[U_1 + U_2 + (U_1 - U_2)\cos\theta\Big], \\ W_{22} &= \frac{1}{2}\Big[U_1 + U_2 - (U_1 - U_2)\cos\theta\Big], \\ W_{12} &= \frac{1}{2}\Big[(U_1 - U_2)\sin\theta\Big]. \end{aligned} \tag{4.3.11}$$

Similar transformation can be introduced for the adiabatic Schroedinger Eq. (4.3.1) with three electronic states. Without losing generality, following vectors are considered as the orthogonal basis functions for three electronic states: [75]

$$\begin{aligned} \eta_1 &= \begin{pmatrix} \cos\alpha\cos\beta \\ \sin\alpha\cos\beta \\ \sin\beta \end{pmatrix} \quad \eta_2 = \begin{pmatrix} \cos\alpha\sin\beta\sin\gamma + \sin\alpha\cos\gamma \\ \sin\alpha\sin\beta\sin\gamma - \cos\alpha\cos\gamma \\ -\cos\beta\sin\gamma \end{pmatrix} \\ \eta_3 &= \begin{pmatrix} -\cos\alpha\sin\beta\cos\gamma + \sin\alpha\sin\gamma \\ -\sin\alpha\sin\beta\cos\gamma - \cos\alpha\sin\gamma \\ \cos\beta\cos\gamma \end{pmatrix} \end{aligned} \tag{4.3.12}$$

where angles α, β and γ depend on nuclear coordinates and can be evaluated numerically by solving the differential equation given below,

$$\nabla\mathbf{A} + \tau\mathbf{A} = 0 \tag{4.3.13}$$

with $\mathbf{A}$ and τ are adiabatic - diabatic transformation (ADT) matrix and non - adiabatic coupling matrix, respectively. The Adiabatic - Diabatic Transformation (ADT)

TH-421_02612202

matrix [75] for three state system has the following form,

$$\mathbf{T} = \begin{pmatrix} \cos\alpha\cos\beta & \sin\alpha\cos\beta & \sin\beta \\ -\sin\alpha\cos\gamma & \cos\alpha\cos\gamma & \cos\beta\sin\gamma \\ -\cos\alpha\sin\beta\sin\gamma & -\sin\alpha\sin\beta\sin\gamma & \\ \sin\alpha\sin\gamma & -\cos\alpha\sin\gamma & \cos\beta\cos\gamma \\ -\cos\alpha\sin\beta\cos\gamma & -\sin\alpha\sin\beta\cos\gamma & \end{pmatrix} \tag{4.3.14}$$

4.3.2 Multi - dimensional models: The quasi - Jahn - Teller "scattering" model

We have studied a two coordinate quasi -"JT scattering" model in which the harmonic oscillator potential and linear coupling term are replaced by more general potentials. The adiabatic PESs U_l, $l = 1, 2, 3$ are given below,

$$\begin{aligned} U_1(s^1, s^2) &= \frac{1}{2}\mu(\omega_0 - \tilde{\omega}_1(s^1))^2(s^2)^2 + AA \times f(s^1, s^2) \\ U_2(s^1, s^2) &= \frac{1}{2}\mu\omega_0^2(s^2)^2 - (DD - AA) \times f(s^1, s^2) + DD \\ U_3(s^1, s^2) &= \frac{1}{2}\mu\omega_0^2(s^2)^2 - (DD1 - AA) \times f(s^1, s^2) + DD1 \end{aligned} \tag{4.3.15}$$

where s^1 and s^2 are the Cartesian coordinates (define in the intervals: $-\infty \leq s^1 \leq \infty$ and $-\infty \leq s^2 \leq \infty$) related to the polar coordinate q and θ. In this model, s^1 is the reaction coordinate (translational) and s^2 is the internal (vibrational) coordinate. The function $\tilde{\omega}_1(s^1)$ is an s^1 dependent function of the following form,

$$\tilde{\omega}_1(s^1) = \omega_1 \exp((-\frac{s^1}{\sigma_1})^2) \tag{4.3.16}$$

and $f(s^1, s^2)$ is chosen to be a Gaussian which peaks at (0,0),

$$f(s^1, s^2) = \exp\Big(-\frac{(s^1)^2 + (s^2)^2}{\sigma^2}\Big) \tag{4.3.17}$$

TH-421_02612202

With this choice, the three adiabatic PESs are well separated from each other and touch only at the origin (transition state). We have considered that $s^1 \to \infty$ is the reagents asymptote and $s^1 \to -\infty$ is the products asymptote.

The parameters used in Eqs. (4.3.15) - (4.3.17) are given in Table 4.2.

Table 4.2: Potential energy parameters used for the quasi - Jahn - Teller "scattering" model.

Parameter	value	unit
μ	0.58	amu
AA	3.0	eV
DD	5.0	eV
$DD1$	10.0	eV
σ	0.30	Å
σ_1	0.75	Å
ω_0	39.14×10^{13}	s^{-1}
ω_1	7.83×10^{13}	s^{-1}

4.3.3 TDDVR equations of motion

The evolution equation for quantum motion on the lth surface in a compact matrix form,

$$i\hbar \mathbf{A}\dot{\mathbf{C}}_\mathbf{l} = \mathbf{H}^\mathbf{t}_\mathbf{ll}\mathbf{C}_\mathbf{l} + \mathbf{A}\sum_{\mathbf{l'}\neq\mathbf{l}} \mathbf{V}_\mathbf{ll'}\mathbf{C}_\mathbf{l'} \tag{4.3.18}$$

which can be reorganized into a more convenient form by a similarity transformation,

$$i\hbar\dot{\mathbf{D}}_\mathbf{l}(\mathbf{t}) = \mathbf{A^{-1/2}}\mathbf{H}^\mathbf{t}_\mathbf{ll}\mathbf{A^{-1/2}}\mathbf{D}_\mathbf{l} + \sum_{\mathbf{l'}\neq\mathbf{l}} \mathbf{V}_\mathbf{ll'}\mathbf{D}_\mathbf{l'} \tag{4.3.19}$$

where $\mathbf{D}_\mathbf{l} = \mathbf{A^{1/2}}\mathbf{C}_\mathbf{l}$.

The explicit expression of an element of the TDDVR coefficients, $d_{i_1 i_2 \ldots i_p, l}$ is,

$$\begin{aligned} i\hbar\dot{d}_{i_1 i_2 \ldots i_p, l} &= \frac{1}{2}\Big\{\sum_k \dot{p}_{s_c^k}\sqrt{\frac{\hbar}{ImA^k}}\bar{X}^k_{i_k i_k}\Big\} d_{i_1 i_2 \ldots i_p, l} + \Big\{\sum_k \frac{\mu(\dot{s}_c^k)^2}{2}\Big\} d_{i_1 i_2 \ldots i_p, l} \\ &+ V_{ll}(i_1 i_2 \ldots i_p) d_{i_1 i_2 \ldots i_p, l} + \sum_{l' \neq l} V_{ll'}(i_1 i_1 \ldots i_p) d_{i_1 i_2 \ldots i_p, l'} \\ &+ \sum_k \Big\{\frac{\hbar ImA^k}{2\mu} \sum_{i'_1 i'_2 \ldots i'_p} \{2\bar{Y}^k_{i_k i'_k} - \bar{Z}^k_{i_k i'_k}\} d_{i'_1 i'_2 \ldots i'_p, l} \prod_{k' \neq k}^{p} \delta_{i_{k'} i'_{k'}}\Big\}, \end{aligned} \tag{4.3.20}$$

TH-421_02612202

and the classical path equations for the kth mode is

$$\dot{s_c^k}(t) = \frac{p_{s_c^k}(t)}{\mu} \tag{4.3.21}$$

$$\dot{p}_{s_c^k}(t) = -\Big\langle \Xi(\{s^k\},t)\Big|\frac{d\hat{V}(\{s^k\})}{ds^k}\Big|_{s^k=s_c^k(t)}\Big|\Xi(\{s^k\},t)\Big\rangle \tag{4.3.22}$$

where the classical force is evaluated by substituting the matrices, $\Xi(\{s^k\},t)$ and $\hat{V}(\{s^k\})$ (Eqs. (2.3.3) and (2.3.4)), respectively.

Using Dirac-Frenkel variational principle [37], we now arrive at a rigorous expression of $\dot{p}_{s_c^k}$ for multi-dimensional multi-surface systems by minimizing the following integral,

$$\begin{aligned} I &= \int \Big(-i\hbar\frac{\partial\Xi^\star(\{s^k\},t)}{\partial t} - H(\{p_s^k\},\{s^k\})\Xi^\star(\{s^k\},t)\Big) \\ &\times \Big(i\hbar\frac{\partial\Xi(\{s^k\},t)}{\partial t} - H(\{p_s^k\},\{s^k\})\Xi(\{s^k\},t)\Big)\prod_{k=1}^{p} ds^k, \end{aligned} \tag{4.3.23}$$

with respect to $\{\dot{p}_{s_c^k}\}$. When this derivation (!!!) is done, $\{\dot{p}_{s_c^k}\}$ takes the following form,

$$\begin{aligned} \dot{p}_{s_c^k}(t) &= \sum_l\sum_{i_k i_k'} c^\star_{i_i i_2..i_k..i_p,l}(t)c_{i_1 i_2..i_k'..i_p,l}(t) \\ &\times \Big\{\frac{2(ImA^k)^2}{\mu}\Big[S^{(2)}_{i_k i_k'}\frac{S^{(1)\star}_{i_k i_k}}{A_{i_k i_k}} - S^{(3)}_{i_k i_k'}\Big] - \frac{\hbar ImA^k}{\mu}\Big[R_{i_k i_k'}\frac{S^{(1)\star}_{i_k i_k}}{A_{i_k i_k}} - T^\star_{i_k i_k'}\Big]\Big\} \\ &/ \Big[\sum_l\sum_{i_k} c^\star_{i_1 i_2..i_k..i_p,l}(t)c_{i_1 i_2..i_k..i_p,l}(t)\frac{S^{(1)\star}_{i_k i_k}S^{(1)}_{i_k i_k}}{A_{i_k i_k}} \\ &- \sum_i\sum_{i_k i_k'} c^\star_{i_1 i_2..i_k..i_p,l}(t)c_{i_1 i_2..i_k'..i_p,l}(t)S^{\star(2)}_{i_k i_k'}\Big] \end{aligned} \tag{4.3.24}$$

4.3.4 Initialization and projection

Quantum mechanical calculations have been carried out by using DVR as well as FFT based methods while quantum - classical results are obtained from the TD-DVR approach. Both in the DVR and TDDVR cases, we need to specify the initial wavefunction to initialize the **d** vector (Eq. (4.3.20)). As we wish to investigate the

TH-421_02612202

reaction dynamics on the ground electronic state, the corresponding nuclear wavefunction at t = 0 is expanded in terms of traditional basis functions as well as in the DVR basis set leading to

$$\begin{aligned}\Psi_1(s^1, s^2, t=0) &= \sum_{kl} a_{kl,1}\Phi_k(s^1)\xi_l(s^2) \\ &= \sum_{ij} c_{ij,1}\sum_{n=0}^{N_1}\xi_n(x_i^1)\Phi_n(s^1)\sum_{m=0}^{N_2}\xi_m(x_j^2)\Phi_m(s^2) \qquad (4.3.25)\end{aligned}$$

Since GWP and harmonic oscillator wavefunctions can represent translational (s^1) and vibrational (s^2) motion respectively, and both are members of Gauss - Hermite basis set, we can set the initial wavefunction as the product of GWP and *pth* eigenfunction of the harmonic oscillator,

$$a_{kl,1}(t_0) = \delta_{k,0}\delta_{l,p} \qquad (4.3.26)$$

Hence one can rewrite Eq. (4.3.25) in the following form,

$$\Phi_0(s^1)\xi_p(s^2) = \sum_{ij} c_{ij,1}\sum_{n=0}^{N_1}\xi_n(x_i^1)\Phi_n(s^1)\sum_{m=0}^{N_2}\xi_m(x_j^2)\Phi_m(s^2) \qquad (4.3.27)$$

Using the properties of DVR basis as defined in Eq. (2.3.13), we can simplify Eq. (4.3.25) as,

$$\begin{aligned}\Phi_0(s_i^1)\xi_p(s_j^2) &= c_{ij,1}\sum_{n=0}^{N_1}\xi_n(x_i^1)\Phi_n(s_i^1)\sum_{m=0}^{N_2}\xi_m(x_j^2)\Phi_m(s_j^2) \\ &= c_{ij,1}A_{ii}^1A_{jj}^2 \qquad (4.3.28)\end{aligned}$$

Alternatively, Eq. (4.3.28) can be rearranged to define the vector **d**,

$$d_{ij,1} = c_{ij,1}\sqrt{A_{ii}^1A_{jj}^2} = \frac{\Phi_0(s_i^1)\xi_p(s_j^2)}{\sqrt{A_{ii}^1A_{jj}^2}} \qquad (4.3.29)$$

The initial amplitudes of the DVR/TDDVR wavefunction are calculated at those grid - points ($s_{i_k}^k$, $k = 1, 2$) defined in Eq. (2.3.12). In the case of quantum (DVR)

TH-421_02612202

propagations, the amplitudes of GWP are calculated by including the momentum vector k_0 in its' exponent,

$$\Phi_0(s_i^1, t_0) = \Big[\frac{2(ImA^1)^2}{\pi\hbar}\Big]^{1/4} \times \exp\Big[ik_0(s_i^1 - s_0^1) - \frac{ImA^1}{\hbar}(s_i^1 - s_0^1)^2\Big], \quad (4.3.30)$$

and only Eq. (4.3.20) is solved to monitor the dynamics and all the terms containing classical variable(s) are dropped while propagating the packet.

On the other hand, in the case of quantum - classical propagations, contribution of the GWP on the initial amplitudes are calculated from,

$$\Phi_0(s_i^1, t_0) = \Big[\frac{2(ImA^1)^2}{\pi\hbar}\Big]^{1/4} \times \exp\Big[-\frac{ImA^1}{\hbar}(s_i^1 - s_c^1)^2\Big], \quad (4.3.31)$$

where the momentum vector k_0 in the exponent of GWP is set to zero but it enters as a classical variable ($p_{s_c}^1 = \hbar k_0$) through Eqs. (4.3.21) and (4.3.20). In the TDDVR propagation, Eqs. (4.3.20) - (4.3.22) or Eq. (4.3.24) are solved simultaneously.

In order to calculate energy resolved state - to - state (vibrational) reactive and non - reactive transition probabilities on the ground electronic state, we need to project on a different basis as for example the product of plane waves and vibrational wavefunctions of harmonic oscillator,

$$\begin{aligned}\Psi_1(s^1, s^2, t) &= \sum_{nl} a_{nl,1}^{\pm}(t) \exp(\pm i k_0^n s^1)\xi_l(s^2) \\ &= \sum_{ij} c_{ij,1}(t) \sum_{n=0}^{N_1} \xi_n(x_i^1)\Phi_n(s^1) \sum_{m=0}^{N_2} \xi_m(x_j^2)\Phi_m(s^2) \quad (4.3.32)\end{aligned}$$

Hence the expansion coefficients ($a_{nl,1}$) can be written as,

$$\begin{aligned}a_{nl,1}^{\pm} &= \frac{1}{\sqrt{2\pi}}\Big(\frac{\hbar}{2ImA^1}\Big)^{\frac{1}{2}}\Big(\frac{\hbar}{2ImA^2}\Big)^{\frac{1}{2}} \sum_{ij} c_{ij,1}(t) \sum_{nm} \xi_n(x_i^1)\xi_m(x_j^2) \\ &\times \int \Phi_n(s^1) \exp(\mp i k_0^n s^1) dx^1 \int \Phi_m(s^2)\xi_l(s^2) dx^2 \quad (4.3.33)\end{aligned}$$

Since $\int dx^k (\xi_m(x^k))^2 = 1$, and approximately we have $\int dx^k \to \sum_i 1/A_{ii}^{(k)}$ at the roots

TH-421_02612202

$(x_{i_k}^k)$ of the Hermite polynomial, we can further simplify Eq. (4.3.33) as,

$$\begin{aligned} a_{nl,1}^{\pm} &= \frac{1}{\sqrt{2\pi}}\Big(\frac{\hbar}{2ImA^1}\Big)^{\frac{1}{2}}\Big(\frac{\hbar}{2ImA^2}\Big)^{\frac{1}{2}}\sum_{ij}\frac{d_{ij}(t)}{\sqrt{A_{ii}^1 A_{jj}^2}} \\ &\times \exp\{\frac{i}{\hbar}(p_{s_c}^1(s_i^2 - s_c^1)\}\exp\{\frac{i}{\hbar}(p_{s_c}^2(s_j^2 - s_c^2)\} \\ &\times \exp(\mp ik_0^n s_i^1)\xi_l(s_j^2) \end{aligned} \tag{4.3.34}$$

From these expansion coefficients we obtain the energy resolved state - to - state reactive (P_{nl}^+) and non - reactive (P_{nl}^-) transition probabilities on the ground electronic state as,

$$P_{nl\leftarrow I0}^{\pm}(E) = \frac{k_n}{k_I}\frac{|a_{nl,1}^{\pm}|^2}{P(k_I,k_0)} \tag{4.3.35}$$

where

$$\begin{aligned} P &= P^+ + P^- = \sum_{nl}(P_{nl}^+ + P_{nl}^-) \\ P(k_I,k_0) &= \Delta x\sqrt{\frac{2}{\pi}}\exp(-2(\Delta x(k_I - k_0))^2) \\ E^{tot} &= \frac{(\hbar k_n)^2}{2\mu} + E_l^{vib} = \frac{(\hbar k_I)^2}{2\mu} + E_0^{vib} \end{aligned} \tag{4.3.36}$$

4.3.5 Results and disscusion

We have solved the time - dependent Schroedinger equation in the diabatic representation with two or three coupled PESs by using the DVR as well as the TDDVR approach. Calculations are performed at four selected total energies 1.25, 1.75, 2.25 and 2.75 eV, respectively where the ground and the first excited diabatic states are 5.0 eV apart at the asymptotic region but intersect at 3 eV in the interaction region. Similarly, second excited diabatic state intersects at 3 eV with the ground and first excited states.

In Tables 4.3 and 4.4 we demonstrate various non - reactive and reactive state - to - state transition probabilities, respectively on the ground adiabatic state at the same four selected energies when calculations are performed with two diabatic PESs.

TH-421_02612202

Table 4.3: Non - reactive state - to - state transition probabilities when calculations are performed on two diabatic surfaces.

E (eV)	$0 \rightarrow 0$	$0 \rightarrow 1$	$0 \rightarrow 2$	$0 \rightarrow 3$	$0 \rightarrow 4$	$0 \rightarrow 5$	$0 \rightarrow 6$	$0 \rightarrow 7$	$0 \rightarrow 8$
1.25	0.6855[a]	0.0000	0.2167						
	0.6851[b]	0.0000	0.2172						
1.75	0.4370	0.0000	0.1942	0.0000	0.1234				
	0.4368	0.0000	0.1950	0.0000	0.1246				
2.25	0.2881	0.0000	0.1336	0.0000	0.0991	0.0000	0.0524		
	0.2862	0.0000	0.1320	0.0000	0.0983	0.0000	0.0531		
2.75	0.1641	0.0000	0.0796	0.0000	0.0607	0.0000	0.0501	0.0000	0.0196
	0.1652	0.0000	0.0799	0.0000	0.0607	0.0000	0.0500	0.0000	0.0196

[a] DVR
[b] TDDVR

Table 4.4: Reactive state - to - state transition probabilities when calculations are performed on two diabatic surfaces.

E (eV)	$0 \rightarrow 0$	$0 \rightarrow 1$	$0 \rightarrow 2$	$0 \rightarrow 3$	$0 \rightarrow 4$	$0 \rightarrow 5$	$0 \rightarrow 6$	$0 \rightarrow 7$	$0 \rightarrow 8$
1.25	0.0000	0.0815[a]	0.0000	0.0164					
	0.0000	0.0813[b]	0.0000	0.0166					
1.75	0.0000	0.0526	0.0000	0.0598	0.0000	0.1287			
	0.0000	0.0538	0.0000	0.0575	0.0000	0.1295			
2.25	0.0000	0.0112	0.0000	0.0560	0.0000	0.2326	0.0000	0.1275	
	0.0000	0.0116	0.0000	0.0540	0.0000	0.2299	0.0000	0.1323	
2.75	0.0000	0.0016	0.0000	0.0401	0.0000	0.1669	0.0000	0.3164	0.0000
	0.0000	0.0010	0.0000	0.0404	0.0000	0.1686	0.0000	0.3145	0.0000

[a] DVR
[b] TDDVR

In both these Tables, DVR results are shown in the first row whereas the results of second row are obtained from the TDDVR approach. Table 4.3 indicates that non - reactive transition probabilities apparently maintain same parity (even → even and odd → odd) like Table 5.6 (see Chapter V) but magnitudes of transition probabilities at high energies (2.25 and 2.75 eV) are affected due to non - adiabatic processes. On

TH-421_02612202

the other hand, non - adiabatic effect is so strong in case of reactive transition that not only transitions occur in different parity (i.e. even → odd and odd → even) but also the magnitudes of transition probabilities change (see Tables 5.7 and 4.4). At this point, it is important to note that present quantum - classical treatment follows correct symmetry as well as achieves high accuracy compared to the DVR results.

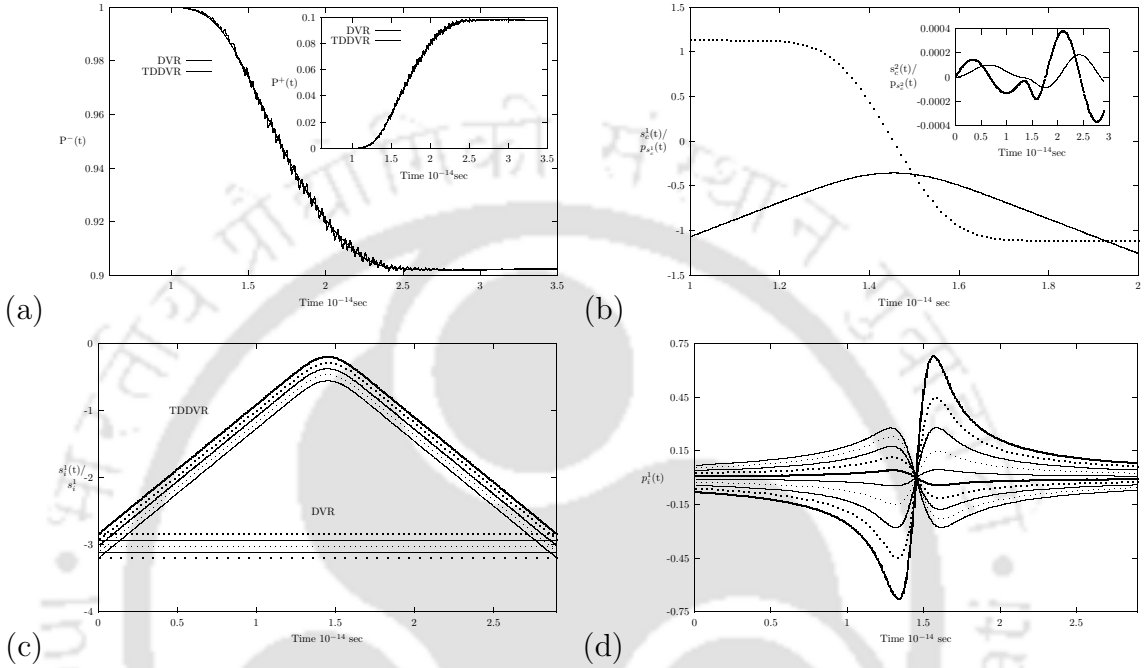

Figure 4.9: (a) Comparison of TDDVR and DVR results of total non - reactive (P^-) and reactive (P^+) transition probabilities on the ground adiabatic state as functions of time where all calculations are performed in diabatic representation with two coupled PESs. (b) Central trajectories (s_c^1 and s_c^2) and their momenta ($p_{s_c^1}$ and $p_{s_c^2}$) for both the modes as functions of time. (c) Few TDDVR grid - points (trajectories) around the central trajectory (s_c^1) of the reaction coordinate and DVR grid - points as functions of time. (d) Few momenta (p_i^1) associated with the TDDVR grid - points as functions of time.

We have obtained excellent agreement between the quantum and quantum - classical results of non - reactive (P^-) and reactive (P^+) transition probabilities as functions of time at the total energy 1.25 eV (see Fig. 4.8(a)). Time - dependent transition probabilities obtained from TDDVR approach fluctuate around DVR results during the interaction period but outside this period perfect matching is obtained. Again we wish to mention that the quantum - classical calculations require 50 grid - points

TH-421_02612202

(trajectories) on the reaction coordinate whereas in the case of fully quantum calculations, at least 200 grid - points are needed for converged results. Fig. 4.8(b) shows central trajectories (s_c^1 and s_c^2) and their associated momenta ($p_{s_c^1}$ and $p_{s_c^2}$) as functions of time.

Fig. 4.8(c) displays movements of few grid - points (trajectories) around the central trajectory (s_c^1) as functions of time. As the growth and decay of the amplitudes at the grid - points occur with the displacement of grid - points (trajectories), this quantum - classical approach attain convergence very fast. Fig. 4.8(d) presents the change of few momenta (p_i^1s)(Appendix E) associated with the corresponding grid points (s_i^1s) as functions of time. It is interesting to note that momenta of some grid - points are more effectively changing than the others. In the reaction coordinate, an initial positive momentum is given to the "classical" particle, the particle approaches the barrier until its momentum becomes zero and finally comes back with a negative momentum (see Fig. 4.8(b)). From Fig. 4.8(d), we see: (i) At t = 0, total "classical" momentum is distributed over the grid - points (trajectories) but grid - points with negative momenta accumulate higher magnitudes with time such that the overall "classical" momentum ($p_{s_c^1}$) decays; (ii) Before reaching the barrier, magnitudes of all the momenta components approach zero so that overall "classical" momentum is zero and simultaneously they change their sign; (iii) Again momenta of the grid - points with positive magnitudes increase sharply which agree with the overall increment of the momentum of the particle ($p_{s_c^1}$).

In Tables 4.5 and 4.6 we present various non - reactive and reactive state - to - state transition probabilities, respectively on the ground adiabatic state at the same four selected energies when calculations are performed with three diabatic PESs. Both Tables 4.5 and 4.6 indicate that non - reactive and reactive transition probabilities are following same parity (even → even and odd → odd) like what we found in Tables 5.6 and 5.7 (see Chapter V), but magnitudes of transition probabilities at all energies

TH-421_02612202

are substantially different from Tables 5.6 and 5.7 due to non - adiabatic effects. Again we wish to mention that the present TDDVR calculation can achieve correct symmetry as well as high accuracy with respect to DVR results.

Table 4.5: Non - reactive state - to - state transition probabilities when calculations are performed on three diabatic surfaces.

E (eV)	$0 \rightarrow 0$	$0 \rightarrow 1$	$0 \rightarrow 2$	$0 \rightarrow 3$	$0 \rightarrow 4$	$0 \rightarrow 5$	$0 \rightarrow 6$	$0 \rightarrow 7$	$0 \rightarrow 8$
1.25	0.6837[a]	0.0000	0.2178						
	0.6852[b]	0.0000	0.2169						
1.75	0.4347	0.0000	0.1915	0.0000	0.1267				
	0.4349	0.0000	0.1934	0.0000	0.1258				
2.25	0.2942	0.0000	0.1295	0.0000	0.0768	0.0000	0.0702		
	0.2940	0.0000	0.1290	0.0000	0.0777	0.0000	0.0705		
2.75	0.1665	0.0000	0.0762	0.0000	0.0522	0.0000	0.0476	0.0000	0.0250
	0.1675	0.0000	0.0764	0.0000	0.0516	0.0000	0.0469	0.0000	0.0262

[a] DVR
[b] TDDVR

Table 4.6: Reactive state - to - state transition probabilities when calculations are performed on three diabatic surfaces.

E (eV)	$0 \rightarrow 0$	$0 \rightarrow 1$	$0 \rightarrow 2$	$0 \rightarrow 3$	$0 \rightarrow 4$	$0 \rightarrow 5$	$0 \rightarrow 6$	$0 \rightarrow 7$	$0 \rightarrow 8$
1.25	0.0499[a]	0.0000	0.0482						
	0.0493[b]	0.0000	0.0485						
1.75	0.0465	0.0000	0.0097	0.0000	0.1643				
	0.0496	0.0000	0.0098	0.0000	0.1611				
2.25	0.0062	0.0000	0.0164	0.0000	0.1503	0.0000	0.2381		
	0.0069	0.0000	0.0164	0.0000	0.1510	0.0000	0.2355		
2.75	0.0102	0.0000	0.0143	0.0000	0.1155	0.0000	0.2450	0.0000	0.2348
	0.0094	0.0000	0.0135	0.0000	0.1097	0.0000	0.2447	0.0000	0.2410

[a] DVR
[b] TDDVR

In Fig. 4.9(a) we compare quantum and quantum - classical results of non -

TH-421_02612202

reactive (P^-) and reactive (P^+) transition probabilities as functions of time at the total energy 1.75 eV.

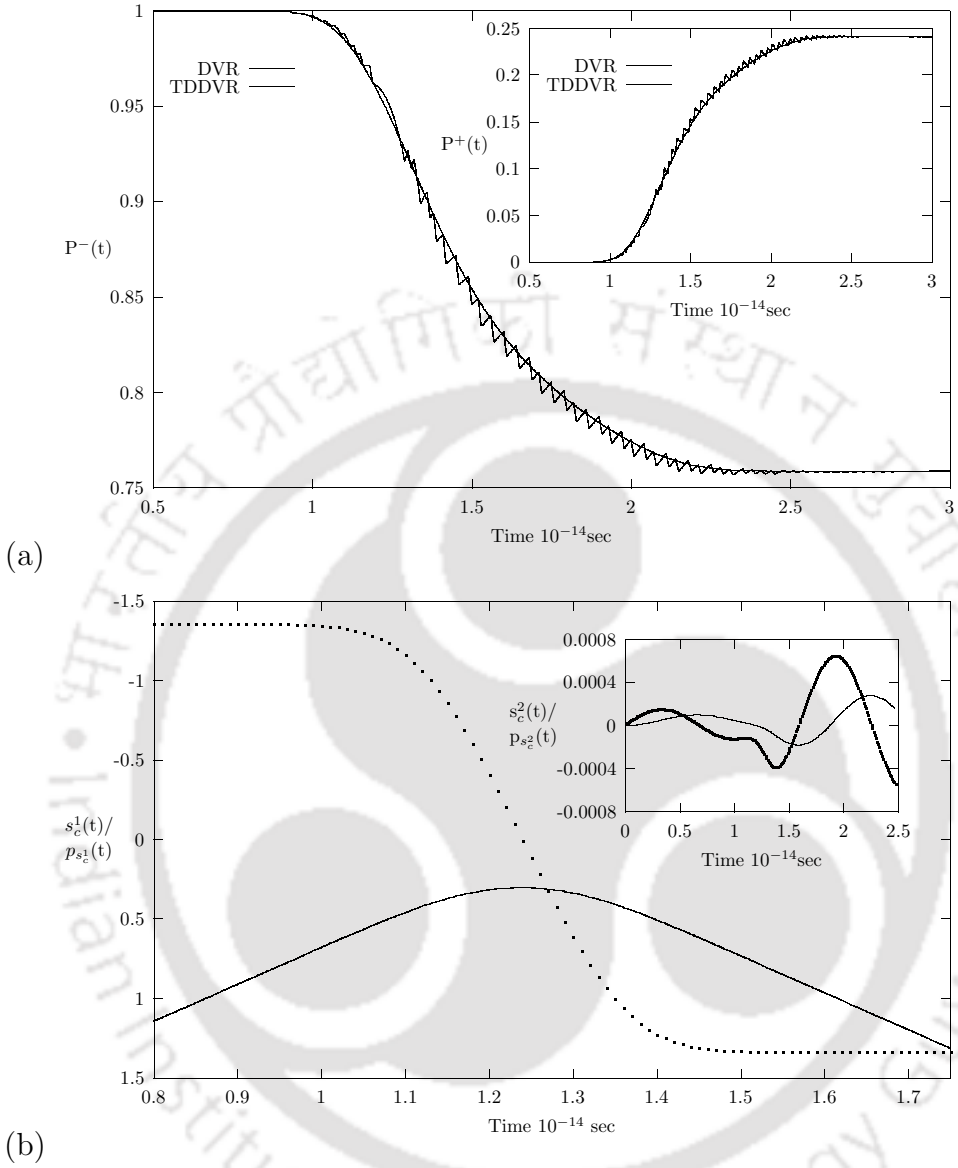

Figure 4.10: (a) Comparison of TDDVR and DVR results of total non - reactive (P^-) and reactive (P^+) transition probabilities on the ground adiabatic state as functions of time where all calculations are performed in diabatic representation with three coupled PESs. (b) Central trajectories (s_c^1 and s_c^2) and their momenta ($p_{s_c^1}$ and $p_{s_c^2}$) for both the modes as functions of time.

Even though TDDVR profiles have some fluctuations in the interaction region, asymptotically excellent agreement is obtained. All the quantum - classical calculations are

TH-421_02612202

performed with 50 grid - points (trajectories) on the reaction coordinate but more than 200 grid - points in the same coordinate are used to obtain converged quantum results. Fig. 4.9(b) displays central trajectories (s_c^1 and s_c^2) and their associated momenta ($p_{s_c^1}$ and $p_{s_c^2}$) as functions of time.

4.4 The effective Hamiltonian and TDDVR theory for the EBO equation

4.4.1 The model system and it's effective KE operator for single surface EBO equations

The three adiabatic PESs of two - coordinate quasi - "JT scattering" model [70, 75] are given below:

$$\begin{aligned} u_1(r,R) &= \frac{1}{2}\mu(\omega_0 - \tilde{\omega}_1(r))^2 R^2 + A_1 \times f(r,R) \\ u_2(r,R) &= \frac{1}{2}\mu\omega_0^2 R^2 - (D_1 - A_1) \times f(r,R) + D_1 \\ u_3(r,R) &= \frac{1}{2}\mu\omega_0^2 R^2 - (D_2 - A_1) \times f(r,R) + D_2 \end{aligned} \tag{4.4.1}$$

where $\tilde{\omega}_1(r) = \omega_1 \exp\left(\left(-\frac{r}{\sigma_1}\right)^2\right)$, $f(r,R) = \exp\left(-\frac{r^2+R^2}{\sigma^2}\right)$ and R and r are the vibrational and reaction coordinates, respectively. The PES parameters are defined as $\mu = 0.58$ amu, $A_1 = 3.0$ eV, $D_1 = 5.0$ eV, $D_2 = 10.0$ eV, $\omega_0 = 39.14 \times 10^{13}$ s^{-1}, $\omega_1 = 7.83 \times 10^{13}$ s^{-1}, $\sigma = 0.3$ Å and $\sigma_1 = 0.75$ Å.

The non - adiabatic effects on the ground adiabatic state can be incorporated by including a vector potential into the kinetic energy (KE) operator of the Hamiltonian. When two or three electronic states are coupled, the effective KE operators for the corresponding single surface EBO [70, 75] equations take the following forms,

$$\hat{T}_n'(r,R) = -\frac{\hbar^2}{2m}\left[\frac{\partial^2}{\partial r^2} + \frac{\partial^2}{\partial R^2} + \left(\frac{R}{r^2+R^2}\right) i\frac{\partial}{\partial r} - \left(\frac{r}{r^2+R^2}\right) i\frac{\partial}{\partial R} - \frac{1}{4(r^2+R^2)}\right]$$

and

$$\hat{T}_n''(r,R) = -\frac{\hbar^2}{2m}\left[\frac{\partial^2}{\partial r^2} + \frac{\partial^2}{\partial R^2} + \left(2\frac{R}{r^2+R^2}\right) i\frac{\partial}{\partial r} - \left(2\frac{r}{r^2+R^2}\right) i\frac{\partial}{\partial R} - \frac{1}{(r^2+R^2)}\right],$$

respectively.

TH-421_02612202

4.4.2 TDDVR equations of motion

We present the relevant equations of motion in the simplest but general way for the current perspective. We expand the time - dependent wavefunction for the single surface EBO Hamiltonian as

$$\begin{aligned}\Psi(r,R,t) &= \sum_{ij} c_{ij}(t)\psi_i(r,t)\psi_j(R,t) \\ &= \sum_{ij} c_{ij}(t)\sum_{n=0}^{N_r}\xi_n(x_i^r)\Phi_n(r,t)\sum_{m=0}^{N_R}\xi_m(x_j^R)\Phi_m(R,t) \qquad (4.4.2)\end{aligned}$$

where $\psi_i(r,t)$ and $\psi_j(R,t)$ are the ith and jth TDDVR basis function for the modes, r and R, respectively and the basis of a particular coordinate, q ($\equiv r$ or R), is expanded in terms of DVR basis multiplied by plane wave to represent the same coordinate as a function of time, t.

We derive the TDDVR equations of motion for the ground electronic state of "JT scattering" model where the corresponding EBO Hamiltonian is constituted with the potential energy, $u_1(r,R)$ and the effective KE operator, $\hat{T}'_n(r,R)$ or $\hat{T}''_n(r,R)$. When the TDDVR wavefunction (Eq. (4.4.2)) and EBO Hamiltonian are substituted in TDSE, we arrive to the following evolution equation for quantum motion

$$i\hbar\mathbf{A}\dot{\mathbf{C}} = \mathbf{HC}. \qquad (4.4.3)$$

The similarity transform of Eq. (4.4.3) is more convenient form to handle,

$$i\hbar\dot{\mathbf{D}} = \mathbf{H^t D}, \qquad (4.4.4)$$

with $\mathbf{D} = \mathbf{A}^{\frac{1}{2}}\mathbf{C}$ and $\mathbf{H^t} = \mathbf{A}^{-\frac{1}{2}}\mathbf{H}\mathbf{A}^{-\frac{1}{2}}$. The explicit expression of an element, d_{ij}, in

TH-421_02612202

the TDDVR equations of motion is given by,

$$
\begin{aligned}
i\hbar\dot{d}_{ij} &= \Big[\frac{p_{r_c}^2(t)}{2m}+\frac{p_{R_c}^2(t)}{2m}+\frac{\hbar\big\{R_j(t)p_{r_c}(t)-r_i(t)p_{R_c}(t)\big\}}{2m(r_i^2(t)+R_j^2(t))}+\frac{\hbar^2}{8m(r_i^2(t)+R_j^2(t))}\Big]d_{ij} \\
&+ \frac{\dot{p}_r(t)}{2}\sqrt{\frac{\hbar}{ImA_r}}\sum_{i'}\bar{X}^r_{ii'}\delta_{ii'}d_{i'j}+\frac{\dot{p}_R(t)}{2}\sqrt{\frac{\hbar}{ImA_R}}\sum_{j'}\bar{X}^R_{jj'}\delta_{jj'}d_{ij'} \\
&- \frac{\hbar ImA_r}{2m}\sum_{i'}\bar{Y}^r_{ii'}d_{i'j}-\frac{\hbar ImA_R}{2m}\sum_{j'}\bar{Y}^R_{jj'}d_{ij'}+u_1(r_i(t),R_j(t))d_{ij} \\
&+ \frac{i\hbar}{2m(r_i^2(t)+R_j^2(t))}\Big\{R_j(t)\sqrt{\hbar ImA_r}\sum_{i'}\bar{Z}^r_{ii'}d_{i'j}-r_i(t)\sqrt{\hbar ImA_R}\sum_{j'}\bar{Z}^R_{jj'}d_{ij'}\Big\}
\end{aligned}
\tag{4.4.5}
$$

where $\bar{X}^q_{ij}$, $\bar{Y}^q_{ij}$, $\bar{Z}^q_{ij}$ and A^q_{ij} have the form shown by Eqs. (2.3.19) - (2.3.24).

With the above choice of TDDVR wavefunction (Eq. (4.4.2)), equations for "classical parameters" appear naturally. We derive the rigorous expression of $\dot{q}_c(t)$ and $\dot{p}_{q_c}(t)$ for present perspective using Dirac-Frenkel variational principle as describe earlier and obtained the following:

$$
\begin{aligned}
\dot{r}_c(t) &= \frac{p_{r_c}(t)}{\mu}+\Big[i\frac{2ImA_r}{\mu}\sqrt{\frac{ImA_r}{\hbar}}\Big\{\sum_j\sum_{ip}c^\star_{pj}(t)\sum_{i'}c_{i'j}(t)S^{\star 2}_{ii'}\frac{Q^\star_{ip}}{A_{ii}} \\
&- \sum_j\sum_{ip}c_{ij}(t)\sum_{i'}c^\star_{i'j}(t)S^2_{i'p}\frac{Q_{ip}}{A_{ii}}-\sum_j\sum_{ip}c^\star_{pj}(t)c_{ij}(t)Y_{ip} \\
&+ \sum_j\sum_{ip}c^\star_{pj}(t)c_{ij}(t)Y^\star_{ip}\Big\}-\frac{i\hbar}{\mu}\sqrt{\frac{ImA_r}{\hbar}}\Big\{\sum_j\sum_{ip}c^\star_{pj}(t)\sum_{i'}c_{i'j}(t)R_{ii'}\frac{Q^\star_{ip}}{A_{ii}} \\
&- \sum_j\sum_{ip}c_{ij}(t)\sum_{i'}c^\star_{i'j}(t)R^\star_{i'p}\frac{Q_{ip}}{A_{ii}}-\sum_j\sum_{ip}c^\star_{pj}(t)c_{ij}(t)W^\star_{ip} \\
&+ \sum_j\sum_{ip}c^\star_{pj}(t)c_{ij}(t)W_{ip}\Big\}+\frac{\hbar}{2\mu}\Big\{\sum_j\sum_{ip}c^\star_{pj}(t)\sum_{i'}c_{i'j}(t)\frac{R_j}{r_{i'}^2+R_j^2}Q^\star_{ii'}\frac{Q^\star_{ip}}{A_{ii}} \\
&+ \sum_j\sum_{ip}c_{ij}(t)\sum_{i'}c^\star_{i'j}(t)\frac{R_j}{r_{i'}^2+R_j^2}Q_{i'p}\frac{Q^\star_{ip}}{A_{ii}}-\sum_j\sum_{ip}c^\star_{pj}(t)c_{ij}(t)\frac{R_j}{r_i^2+R_j^2}P^\star_{ij} \\
&- \sum_j\sum_{ip}c^\star_{ij}(t)c_{pj}(t)\frac{R_j}{r_i^2+R_j^2}P^\star_{ij}\Big\}\Big]\Big/\Big[\sum_j\sum_{ip}c^\star_{pj}(t)\sum_{i'}c_{i'j}(t)Q^\star_{ii'}\frac{Q^\star_{ip}}{A_{ii}} \\
&+ \sum_j\sum_{ip}c_{ij}(t)\sum_{i'}c^\star_{i'j}(t)Q_{ip}\frac{Q^\star_{ip}}{A_{ii}}-\sum_j\sum_{ip}c^\star_{pj}(t)c_{ij}(t)P^\star_{ip}\Big],
\end{aligned}
$$

TH-421_02612202

and

$$\begin{aligned}
\dot{p}_{r_c}(t) &= -\frac{\partial U}{\partial r}\Big|_{r=r_c(t),R=R_c(t)} + \Big[\frac{2ImA_r^2}{\mu}\Big\{\sum_j\sum_{ii'} c^\star_{ij}(t)c_{i'j}(t)\frac{S^{\star(2)}_{i'i}}{A_{ii}}S^{\star(1)}_{ii} \\
&+ \sum_j\sum_{ii'} c_{ij}(t)c^\star_{i'j}(t)\frac{S^{(2)}_{i'i}}{A_{ii}}S^{\star(1)}_{ii} - 2\sum_j\sum_{ip} c^\star_{pj}(t)c_{ij}(t)S^{\star(3)}_{ip}\Big\} \\
&- \frac{\hbar ImA_r}{\mu}\Big\{\sum_j\sum_{ii'} c^\star_{ij}(t)c_{i'j}(t)R^\star_{i'i}\frac{S^{\star(1)}_{ii}}{A_{ii}} + \sum_j\sum_{ii'} c_{ij}(t)c^\star_{i'j}(t)R_{i'i}\frac{S^{\star(1)}_{ii}}{A_{ii}} \\
&- 2\sum_j\sum_{ip} c^\star_{pj}(t)c_{ij}(t)T^\star_{ip}\Big\} - \frac{i\hbar}{2\mu}\sqrt{\hbar ImA_r}\Big\{\sum_j\sum_{ii'} c^\star_{ij}(t)c_{i'j}(t)\frac{R_j}{r^2_{i'}+R^2_j}Q^\star_{i'i}\frac{S^{\star(1)}_{ii}}{A_{ii}} \\
&- \sum_j\sum_{ii'} c_{ij}(t)c^\star_{i'j}(t)\frac{R_j}{r^2_{i'}+R^2_j}Q_{i'i}\frac{S^{\star(1)}_{ii}}{A_{ii}} - \sum_j\sum_{ip} c^\star_{pj}(t)c_{ij}(t)\frac{R_j}{r^2_i+R^2_j}Z^\star_{ip} \\
&+ \sum_j\sum_{ip} c^\star_{ij}(t)c_{pj}(t)\frac{R_j}{r^2_i+R^2_j}Z_{ip}\Big\}\Big]\Big/\Big[\sum_i\sum_j c^\star_{ij}(t)c_{ij}(t)\frac{S^{\star(1)}_{ii}}{A_{ii}}S^{\star(1)}_{ii} \\
&+ \sum_i\sum_j c^\star_{ij}(t)c_{ij}(t)\frac{S^{(1)}_{ii}}{A_{ii}}S^{\star(1)}_{ii} - 2\sum_j\sum_{ip} c^\star_{pj}(t)c_{ij}(t)S^{\star(2)}_{ip}\Big],
\end{aligned}$$

where

$$\begin{aligned}
S^n_{ij} &= \sum_{km}\xi_k(x^r_i)\xi^\star_m(x^r_j)\int(r-r_c(t))^n\Phi^\star_k(r,t)\Phi_m(r,t)dr \\
R_{ij} &= \sum_k\xi_k(x^r_i)\xi^\star_k(x^r_j)2k \\
T_{ij} &= \sum_{km}\xi_k(x^r_i)\xi^\star_m(x^r_j)2k\int(r-r_c(t))\Phi^\star_k(r,t)\Phi_m(r,t)dr \\
Q_{ij} &= \sum_{km}\xi_k(x^r_i)\xi^\star_m(x^r_j)\int\{\sqrt{k+1}\Phi^\star_{k+1}(r,t)-\sqrt{k}\Phi^\star_{k-1}(r,t)\}\Phi_m(r,t)dr \\
Z_{ij} &= \sum_{km}\xi_k(x^r_i)\xi^\star_m(x^r_j)\int(r-r_c(t))\{\sqrt{k+1}\Phi^\star_{k+1}(r,t)-\sqrt{k}\Phi^\star_{k-1}(r,t)\}\Phi_m(r,t)dr \\
A_{ii} &= \sum_k\xi_k(x^r_i)\xi^\star_k(x^r_i) \\
P_{ij} &= \sum_{km}\xi_k(x^r_i)\xi^\star_m(x^r_j)\int\{\sqrt{k+1}\Phi^\star_{k+1}(r,t)-\sqrt{k}\Phi^\star_{k-1}(r,t)\} \\
&\quad \{\sqrt{m+1}\Phi_{m+1}(r,t)-\sqrt{m}\Phi_{m-1}(r,t)\}dr \\
Y_{ij} &= \sum_{km}\xi_k(x^r_i)\xi^\star_m(x^r_j)\int(r-r_c(t))^2\{\sqrt{k+1}\Phi^\star_{k+1}(r,t)-\sqrt{k}\Phi^\star_{k-1}\}\Phi_m(r,t)dr
\end{aligned}$$

TH-421_02612202

$$W_{ij} = \sum_{km} \xi_k(x_i^r)\xi_m^\star(x_j^r)2k \int \{\sqrt{k+1}\Phi_{k+1}^\star(r,t) - \sqrt{k}\Phi_{k-1}^\star(r,t)\}\Phi_m(r,t)dr.$$

It is worth mentioning that, here we have formulated an alternative fixed width approach of TDDVR where both quantum as well as "classical" equations of motions are derived from the first principles without any approximations, nor we have assumed a "classical" path ($\dot{x} = \frac{p}{m}$) around the centre of the wavepacket.

Finally, in a similar manner, we expand the time - dependent wavefunction in the DVR representation considering harmonic oscillator eigenfunctions as primitive basis,

$$\begin{aligned}\Psi(r,R,t) &= \sum_{ij} e_{ij}(t)\phi_i(r)\phi_j(R) \\ &= \sum_{ij} e_{ij}(t) \sum_{n=0}^{N_r} \xi_n(x_i^r)\xi_n(r,t) \sum_{m=0}^{N_R} \xi_m(x_j^R)\xi_m(R,t), \end{aligned} \tag{4.4.6}$$

substitute the wavefunction along with EBO Hamiltonian in the TDSE and obtain the time derivative of DVR expansion coefficient, $\dot{e}_{ij}(t)$ as,

$$\begin{aligned} i\hbar\dot{e}_{ij} &= -\frac{\hbar ImA_r}{2m}\sum_{i'} \bar{Y}_{ii'}^r e_{i'j} - \frac{\hbar ImA_R}{2m}\sum_{j'} \bar{Y}_{jj'}^R e_{ij'} + u_1(r_i,R_j)e_{ij} \\ &+ \frac{\hbar^2}{8m(r_i^2+R_j^2)}e_{ij} + \frac{i\hbar}{2m(r_i^2+R_j^2)}\Big\{R_j\sqrt{\hbar ImA_r}\sum_{i'}\bar{Z}_{ii'}^r e_{i'j} \\ &- r_i\sqrt{\hbar ImA_R}\sum_{j'}\bar{Z}_{jj'}^R e_{ij'}\Big\}. \end{aligned} \tag{4.4.7}$$

It is important to note that the last term both in Eqs. (4.4.5) and (4.4.7) is the contribution due to vector potential in the TDDVR and DVR equation of motion, respectively.

4.4.3 Initialization and projection

We calculate energy resolved state - to - state (vibrational) transition probabilities on the ground electronic state by projecting the time - dependent wavefunction (DVR/TDDVR) on the product of plane waves and vibrational wavefunctions of harmonic oscillator at the asymptote, and obtain the energy resolved state - to - state

TH-421_02612202

reactive and non - reactive ($P_{nl}^{\pm}$) transition probabilities (see Eq. (4.3.34)) on the ground electronic state as,

$$P_{nl\leftarrow I0}^{\pm}(E) = \frac{k_n}{k_I}\frac{|a_{nl,1}^{\pm}|^2}{P(k_I,k_0)} \tag{4.4.8}$$

where

$$\begin{aligned} P(k_I,k_0) &= \Delta x\sqrt{\frac{2}{\pi}}\exp(-2(\Delta x(k_I-k_0))^2) \\ E^{tot} &= \frac{(\hbar k_n)^2}{2\mu} + E_l^{vib} = \frac{(\hbar k_I)^2}{2\mu} + E_0^{vib} \end{aligned} \tag{4.4.9}$$

4.4.4 Results and discussion

We have performed the dynamics on quasi - "JT scattering" model by using the single surface EBO equations, where the corresponding EBO Hamiltonians were derived [70, 75] by considering systems with two or three coupled electronic states. In the present model, as the point of conical intersection among the adiabatic electronic states is at 3 eV, calculations are performed at four selected total energies 1.00, 1.20, 1.40 and 1.60 eV, respectively such that EBO equations are approximately valid, i.e., upper electronic state(s) are classically closed with respect to the ground.

Since the functional forms of the PESs ($\{u_i\}$) in quasi - "JT scattering" model are even in the vibrational coordinate, dynamical calculations on any electronic state using ordinary BO equation [41, 70, 75] show up state - to - state transition probabilities only between states of same parity, i.e., even → even and odd → odd transitions are allowed but even → odd and odd → even are forbidden. On the contrary, the form of EBO equation differs with the number of electronic states originally coupled and thereby, bring qualitative as well as quantitative changes in the state - to - state transition probabilities. As for example, EBO equation derived from two coupled electronic states have sharp qualitatively different results compared to the single surface EBO equation of three coupled states. We demonstrate the workability of TDDVR method whether our approach can follow the correct symmetry and obtain

TH-421_02612202

accurate transition probabilities with the change of EBO Hamiltonian. We have carried out the dynamics on a single surface EBO equation (formulated from doubly coupled adiabatic electronic states), calculated state - to - state vibrational transition probabilities for the reactive and non - reactive modes by using TDDVR and DVR equations of motion and presented those results in Tables 4.7 - 4.9. These results indicate that even $\rightarrow$ even and odd $\rightarrow$ odd state - to - state transitions are appeared as allowed one for non - reactive mode whereas in reactive mode, even $\rightarrow$ odd and odd $\rightarrow$ even transitions have non - zero contributions. Table 4.7 demonstrates the convergence profile of reactive transition probabilities ($P_{0\rightarrow 1}$) calculated by TDDVR and DVR approaches with increasing number of basis functions (N_r) on the scattering coordinate, r and a fixed number of basis functions ($N_R = 50$) on the vibrational coordinate, R. We find that TDDVR achieves excellent quantitative agreement and convincingly fast convergence of calculated transition probabilities at total energies, 1.00 and 1.20 eV. Though the CPU time to propagate the "classical" equations of motion in TDDVR is not just negligible, the propagation time in TDDVR is still much lower than DVR propagation to achieve the required level of the convergence. Moreover, matrix construction time in DVR is substancially higher than TDDVR (see Table 4.7). Table 4.8 and 4.9 present converged non - reactive and reactive state - to - state vibrational transition probabilities, respectively where in each Table, comparison between TDDVR and DVR results has been made. Transition probabilities calculated by TDDVR approach not only follow the correct symmetry but also obtain quantitative agreement with DVR. At this point, it is important to mention that in Table 4.8 and 4.9, all the TDDVR calculations are performed with 50 grid - points each on the scattering (r) and vibrational (R) coordinates, respectively whereas DVR need at least 170 grid - points on the reaction coordinate, r. We had carried out the same calculation on the said EBO equation using FFT - Lanczos technique [46] and obtained converged results with 512 grid - points [70].

TH-421_02612202

Table 4.7: Convergence(*) profile of vibrational transition probabilities from $v = 0$ to $v = 1$ for reactive scattering of "JT model" as functions of TDDVR and DVR grid - points, N_r, on the scattering coordinate, r with a fixed number of grid - point (N_R=50) on the vibrational coordinate, R. The propagation time, T_p as well as total time, T (including matrix construction) for each calculation is also presented.

	TDDVR				DVR		
N_r	$0 \rightarrow 1$	T_p	T	N_r	$0 \rightarrow 1$	T_p	T
1.00 eV							
30	0.0427	543	549	150	0.0470	783	996
50	0.0502	813*	826	170	0.0449	1253	1603
70	0.0504	1218	1248	200	0.0503	1782*	2445
100	0.0508	1425	1471	250	0.0503	2688	4300
1.20 eV							
30	0.0332	518	524	130	0.0041	592	715
50	0.0570	821*	835	150	0.0509	818	1033
70	0.0571	1239	1270	170	0.0572	1110*	1460
100	0.0567	1488	1533	200	0.0570	1427	2091

Table 4.8: Converged state - to - state vibrational transition probabilities for elastic and inelastic scattering on "JT model". TDDVR/DVR calculations are performed on single surface adiabatic equation where extended BO equation is derived [70, 75] from doubly coupled adiabatic electronic states.

E (eV)	$0 \rightarrow 0$	$0 \rightarrow 1$	$0 \rightarrow 2$	$0 \rightarrow 3$	$0 \rightarrow 4$	$0 \rightarrow 5$
1.00	0.7265[a]	0.0022	0.2118	0.0024		
	0.7254[b]	0.0013	0.2183	0.0006		
1.20	0.6239	0.0021	0.2332	0.0032	0.0458	
	0.6232	0.0037	0.2324	0.0030	0.0415	
1.40	0.5612	0.0027	0.2130	0.0069	0.0777	
	0.5659	0.0066	0.2150	0.0080	0.0712	
1.60	0.4925	0.0047	0.2140	0.0038	0.1237	0.0017
	0.4944	0.0014	0.2271	0.0040	0.1247	0.0037

[a] TDDVR

[b] DVR

We have also formulated TDDVR and DVR equations of motion for another EBO Hamiltonian of the ground electronic state (an effective Hamiltonian considering the non - adiabatic effect from two excited electronic states), performed the dynamics

TH-421_02612202

Table 4.9: Converged state - to - state vibrational transition probabilities for reactive scattering on "JT scattering model". TDDVR/DVR calculations are performed on extended BO equation derived [70, 75] from doubly coupled electronic states.

E (eV)	$0 \rightarrow 0$	$0 \rightarrow 1$	$0 \rightarrow 2$	$0 \rightarrow 3$	$0 \rightarrow 4$	$0 \rightarrow 5$
1.00	0.0007	0.0514[a]	0.0020	0.0284		
	0.0000	0.0502[b]	0.0014	0.0270		
1.20	0.0070	0.0570	0.0034	0.0351	0.0069	
	0.0024	0.0570	0.0042	0.0349	0.0030	
1.40	0.0003	0.1233	0.0048	0.0239	0.0028	
	0.0013	0.1168	0.0033	0.0278	0.0032	
1.60	0.0070	0.1712	0.0002	0.0235	0.0055	0.0234
	0.0023	0.1701	0.0030	0.0201	0.0014	0.0137

[a] TDDVR
[b] DVR

Table 4.10: Converged state - to - state vibrational transition probabilities for non - reactive scattering on "JT model" where TDDVR/DVR calculations are performed with extended adiabatic equation derived [75] from three coupled adiabatic electronic states.

E (eV)	$0 \rightarrow 0$	$0 \rightarrow 1$	$0 \rightarrow 2$	$0 \rightarrow 3$	$0 \rightarrow 4$	$0 \rightarrow 5$
1.00	0.7176[a]	0.0022	0.2036	0.0028		
	0.7179[b]	0.0028	0.2058	0.0033		
1.20	0.5981	0.0064	0.2141	0.0087	0.0262	
	0.6065	0.0072	0.2229	0.0072	0.0281	
1.40	0.4928	0.0030	0.2129	0.0059	0.1024	
	0.4963	0.0021	0.2290	0.0037	0.1194	
1.60	0.5093	0.0054	0.1749	0.0043	0.0837	0.0021
	0.5126	0.0057	0.1880	0.0025	0.0812	0.0041

[a] TDDVR
[b] DVR

TH-421_02612202

Table 4.11: Converged state - to - state vibrational transition probabilities for reactive scattering on "JT model". TDDVR/DVR calculations are performed on single surface adiabatic equation where extended BO equation is formulated [70, 75] from three coupled adiabatic electronic states.

E (eV)	$0 \rightarrow 0$	$0 \rightarrow 1$	$0 \rightarrow 2$	$0 \rightarrow 3$	$0 \rightarrow 4$	$0 \rightarrow 5$
1.00	0.0261[a]	0.0046	0.0405	0.0040		
	0.0261[b]	0.0016	0.0369	0.0023		
1.20	0.0263	0.0024	0.0511	0.0020	0.0167	
	0.0308	0.0014	0.0538	0.0018	0.0202	
1.40	0.0684	0.0057	0.0671	0.0068	0.0136	
	0.0620	0.0017	0.0694	0.0073	0.0143	
1.60	0.0519	0.0048	0.0716	0.0056	0.0849	0.0043
	0.0512	0.0047	0.0781	0.0019	0.0919	0.0027

[a] TDDVR
[b] DVR

and calculated state - to - state vibrational transition probabilities at four selected energies, 1.00, 1.20, 1.40 and 1.60 eV. Table 4.10 and 4.11 present converged transition probabilities for the non - reactive and reactive mode, respectively, where even $\rightarrow$ even and odd $\rightarrow$ odd transitions are allowed one in both the modes. In these tables, we have demonstrated TDDVR and DVR results for comparison and found excellent quantitative agreements. Again, it is worth to mention that TDDVR dynamics are being performed with 50 grid - points each on the reactive and vibrational coordinates whereas in DVR calculations, scattering coordinate (r) requires at least 170 grid - points to achieve the desired level of convergence. Similar calculations by using FFT - Lanczos technique [46] on the same EBO equation were performed with 512 grid - points [75] to achieve convergence on the reaction coordinate.

TH-421_02612202

CHAPTER V

APPLICATION TO SCATTERING PROCESSES

5.1 Introduction

We have formulated our TDDVR method for the present perspective (multi - dimensional multi - surface systems) to explore (a) vibrational transitions in the inelastic scattering models and (b) the dynamics of reactive and non - reactive scattering processes on the single surface ordinary BO quasi - Jahn - Teller model.

5.2 Quantum dynamics of inelastic scattering

5.2.1 Theoretical Aspects of TDDVR

In this TDDVR, we formulate the quantum equations of motion in adiabatic or diabatic representation depending upon the system but "classical" equations of motion are derived in adiabatic representation in order to have real valued "classical" trajectories.

The time - dependent wavefunction, $\Psi_l(\{q_k\},t)$, in the diabatic representation for the lth surface of a p - dimensional system can be expanded as

$$\Psi_l(\{q_k\},t) = \sum_{i_1 i_2 \ldots i_p} c_{i_1 i_2 \ldots i_p, l}(t) \prod_{k=1}^{p} \psi_{i_k,l}(q_k,t), \tag{5.2.1}$$

where $i_k th$ TDDVR basis function, $\psi_{i_k,l}(q_k,t)$, for the kth mode on the lth surface is being expressed in terms of DVR basis and plane wave to represent the coordinate, q_k, as a function of time, t.

In the diabatic representation, couplings among different electronic states ($l, l' \in \{1, M\}$) come through off - diagonal elements of the potential energy operator and the kinetic energy operator, $\hat{T}_{\{q_k\}} = -\frac{\hbar^2}{2\mu}[\frac{\partial^2}{\partial {q_1}^2} + \frac{\partial^2}{\partial {q_2}^2} + \cdots + \frac{\partial^2}{\partial {q_p}^2}]$, is diagonal.

TH-421_02612202

The compact form of the matrix equation for the quantum equation of motion on the lth surface can be expressed as below,

$$i\hbar\mathbf{A}\dot{\mathbf{C}}_{\mathbf{l}} = \mathbf{H}^{\mathbf{t}}_{\mathbf{ll}}\mathbf{C}_{\mathbf{l}} + \mathbf{A}\sum_{\mathbf{l}'\neq\mathbf{l}}\mathbf{V}_{\mathbf{ll}'}\mathbf{C}_{\mathbf{l}'} \tag{5.2.2}$$

which can be reorganized into a more convenient form by a similarity transformation,

$$i\hbar\dot{\mathbf{D}}_{\mathbf{l}}(\mathbf{t}) = \mathbf{A}^{-\mathbf{1/2}}\mathbf{H}^{\mathbf{t}}_{\mathbf{ll}}\mathbf{A}^{-\mathbf{1/2}}\mathbf{D}_{\mathbf{l}} + \sum_{\mathbf{l}'\neq\mathbf{l}}\mathbf{V}_{\mathbf{ll}'}\mathbf{D}_{\mathbf{l}'} \tag{5.2.3}$$

where $\mathbf{D}_{\mathbf{l}} = \mathbf{A}^{\mathbf{1/2}}\mathbf{C}_{\mathbf{l}}$ and $\mathbf{H}^{\mathbf{t}}_{\mathbf{ll}} = \mathbf{A}^{-\mathbf{1/2}}\mathbf{H}_{\mathbf{ll}}\mathbf{A}^{-\mathbf{1/2}}$.

The explicit expression of an element of the TDDVR coefficients, $d_{i_1 i_2 \ldots i_p,l}$ is,

$$\begin{aligned} i\hbar\dot{d}_{i_1 i_2 \ldots i_p,l} &= \frac{1}{2}\Big\{\sum_k \dot{p}^{\,l}_{c_k}\sqrt{\frac{\hbar}{ImA_k}}\bar{X}_{i_k i_k}\Big\}d_{i_1 i_2 \ldots i_p,l} + \Big\{\sum_k \frac{\mu(\dot{q}^{\,l}_{c_k})^2}{2}\Big\}d_{i_1 i_2 \ldots i_p,l} \\ &+ V_{ll}(i_1 i_2 \ldots i_p)d_{i_1 i_2 \ldots i_p,l} + \sum_{l'\neq l}\bar{V}_{ll'}(i_1 i_1 \ldots i_p)d_{i_1 i_2 \ldots i_p,l'} \\ &+ \sum_k\Big\{\frac{\hbar ImA_k}{2\mu}\sum_{i'_1 i'_2 \ldots i'_p}\{2\bar{Y}_{i_k i'_k} - \bar{Z}_{i_k i'_k}\}d_{i'_1 i'_2 \ldots i'_p,l}\prod_{k'\neq k}^{p}\delta_{i_{k'} i'_{k'}}\Big\} \end{aligned} \tag{5.2.4}$$

where $i_1 = 1, 2 \cdots N_1$, $i_2 = 1, 2 \cdots N_2$, $\cdots$ $i_k = 1, 2 \cdots N_k$, $\cdots$ $i_p = 1, 2 \cdots N_p$ and $l = 1, 2 \cdots M$.

The elements of the matrices ($\mathbf{X_k}$, $\mathbf{Y_k}$, $\mathbf{Z_k}$ and $\mathbf{A_k}$) are defined in Eqs. (2.3.19) - (2.3.24) and

$$\bar{V}_{ll'}(i_1 i_2 \ldots i_p) = V_{ll'}(i_1 i_2 \ldots i_p)\prod_{k=1}^{p}\phi^{\star}_{l}(i_k)\phi_{l'}(i_k) \tag{5.2.5}$$

It is clear from Eq. (5.2.5) that couplings among different electronic states are due to the off - diagonal elements of the potential energy matrix ($\mathbf{V_{ll'}}$) where kinetic energy matrices, $\mathbf{Y_k}$ and $\mathbf{Z_k}$, couple grid - points or basis functions of the kth mode only on the surface, l. Hence, computational cost reduces substantially, particularly, for multi - dimensional multi - surface systems.

While deriving the "classical" path equations, we rewrite the diabatic wavefunction in the adiabatic representation,

$$\Psi^{ad}_{l}(\{q_k\}, t) = \sum_{i_1 i_2 \ldots i_p} e_{i_1 i_2 \ldots i_p,l}(t)\prod_{k=1}^{p}\psi_{i_k,l}(q_k, t), \tag{5.2.6}$$

TH-421_02612202

where the adiabatic coefficient vector, $\mathbf{E}$, is obtained from diabatic one, $\mathbf{C}$ (Eq. (5.2.1)), under the diabatic - adiabatic transformation, $\mathbf{E} = \mathbf{TC}$. The transformation matrix, $\mathbf{T}$, is defined as, $\mathbf{U} = \mathbf{T}^{\dagger}\mathbf{VT}$ where $\mathbf{V}$ and $\mathbf{U}$ are diabatic and adiabatic potential energy matrices, respectively. At this point, it is important to note that time - dependent expansion coefficient vector, $\mathbf{C}/\mathbf{E}$ and transformation matrix, $\mathbf{T}$ are located on the time - dependent grid - points.

When we substitute Eq. (5.2.6) in the TDSE and introduce classical path picture, "classical" path equations for the kth mode on the lth surface are,

$$\dot{q}^{l}_{c_k}(t) = \frac{p^{l}_{c_k}(t)}{\mu} \tag{5.2.7}$$

$$\dot{p}^{l}_{c_k}(t) = -\Big\langle \Psi^{ad}_{l}(\{q_k\},t)\Big|\frac{d\hat{U}_l(\{q_k\})}{dq_k}\Big|_{q_k=q^{l}_{c_k}(t)}\Big|\Psi^{ad}_{l}(\{q_k\},t)\Big\rangle \tag{5.2.8}$$

where the "classical" force is evaluated by substituting adiabatic wavefunction ($\Psi^{ad}_{l}(\{q_k\},t)$) and potential energy surface ($\hat{U}_l(\{q_k\})$).

As the quantum equations of motion in the present TDDVR are formulated with a rigorous approach contrary to the earlier versions of TDDVR, we have enough scope to derive a close form of $\dot{p}^{l}_{c_k}(t)$ starting from first principle. Using Dirac - Frenkel variational principle, we have reformulated the rigorous expression of $\dot{p}^{l}_{c_k}(t)$ for multi - dimensional multi - surface systems by minimizing the following integral with respect to $\dot{p}^{l}_{c_k}(t)$,

$$I_l = \int\prod_{k=1}^{p} dq_k\Big(-i\hbar\frac{\partial\Psi^{\star ad}_{l}(\{q_k\},t)}{\partial t} - H(\{p_k\},\{q_k\})\Psi^{\star ad}_{l}(\{q_k\},t)\Big)$$
$$\times \Big(i\hbar\frac{\partial\Psi^{ad}_{l}(\{q_k\},t)}{\partial t} - H(\{p_k\},\{q_k\})\Psi^{ad}_{l}(\{q_k\},t)\Big),\ \ l=1,2,\ldots,M. \tag{5.2.9}$$

TH-421_02612202

obtain the form of $\dot{p}_{ck}^{\,l}(t)$ as,

$$\begin{aligned}
\dot{p}_{ck}^{\,l}(t) &= \sum_{i_1 i_2..i_k i'_k..i_p} e^{\star}_{i_i i_2..i_k..i_p,l}(t) e_{i_1 i_2..i'_k..i_p,l}(t) \\
&\times \Big\{ \frac{2(ImA_k)^2}{\mu} \Big[S^{(2)}_{i_k i'_k} \frac{S^{(1)^\star}_{\ i_k i_k}}{A_{i_k i_k}} - S^{(3)}_{i_k i'_k} \Big] - \frac{\hbar ImA_k}{\mu} \Big[R_{i_k i'_k} \frac{S^{(1)^\star}_{\ i_k i_k}}{A_{i_k i_k}} - T^{\star}_{i_k i'_k} \Big] \Big\} \\
&/ \Big[\sum_{i_1 i_2..i_k..i_p} e^{\star}_{i_1 i_2..i_k..i_p,l}(t) e_{i_1 i_2..i_k..i_p,l}(t) \frac{S^{(1)^\star}_{\ i_k i_k} S^{(1)}_{i_k i_k}}{A_{i_k i_k}} \\
&- \sum_{i_1 i_2..i_k i'_k..i_p} e^{\star}_{i_1 i_2..i_k..i_p,l}(t) e_{i_1 i_2..i'_k..i_p,l}(t) S^{\star(2)}_{\ i_k i'_k} \Big], \qquad (5.2.10)
\end{aligned}$$

Matrices R, $S^{(n)}$, T and A are time - independent and calculated once for all the time. It is important to note that at each time step, diabatic coefficients ($\{c_{i_1 i_2..i_k..i_p,l}(t)\}$) obtained from quantum equations of motion are transformed to adiabatic one ($\{e_{i_1 i_2..i_k..i_p,l}(t)\}$) and used to evaluate the so called "quantum correction to classical force".

5.2.2 Initialization, Projection and Propagation

We investigate the performance of our TDDVR method in inelastic scattering of an atom from a diatom. We consider two different 2-d model Hamiltonians where the first example represent the scattering process on single surface and the second one shows strong non - adiabatic effect due to first excited state on the ground. Quantum - classical (TDDVR) results are compared with those obtained from traditional quantum mechanical (DVR and FFT based approach) calculations.

Energy resolved state - to - state (vibrational) elastic and inelastic (non - reactive) transition probabilities on the ground electronic state are calculated by projecting the asymptotic ($t \to \infty$) wavefunction on the product of outgoing plane waves and vibrational wavefunctions of harmonic oscillator,

$$\begin{aligned}
\Psi_1(q_1, q_2, t) &= \sum_{nl} a^{-}_{nl,1}(t) \exp(-ik_0^n q_1) \xi_l(q_2) \\
&= \sum_{i_1 i_2} c_{i_1 i_2,1}(t) \sum_{n=0}^{N_1} \xi_n(x_{i_1}) \Phi_{n,1}(q_1) \sum_{m=0}^{N_2} \xi_m(x_{i_2}) \Phi_{m,1}(q_2) \quad (5.2.11)
\end{aligned}$$

TH-421_02612202

where the expansion coefficients ($a^{-}_{nl,1}$) can be written as,

$$\begin{aligned} a^{-}_{nl,1} &= \frac{1}{\sqrt{2\pi}}\Big(\frac{\hbar}{2ImA_1}\Big)^{\frac{1}{2}}\Big(\frac{\hbar}{2ImA_2}\Big)^{\frac{1}{2}}\sum_{i_1 i_2} c_{i_1 i_2,1}(t)\sum_{nm}\xi_n(x_{i_1})\xi_m(x_{i_2}) \\ &\times \int \Phi_{n,1}(q_1)\exp(+ik_0^n q_1)dq_1 \int \Phi_{m,1}(q_2)\xi_l(q_2)dq_2 \end{aligned} \tag{5.2.12}$$

From the expansion coefficients we obtain the energy resolved state - to - state non - reactive (P^{-}_{nl}) transition probabilities on the ground electronic state as,

$$P^{-}_{nl\leftarrow I0}(E) = \frac{k_n}{k_I}\frac{|a^{-}_{nl,1}|^2}{P(k_I,k_0)} \tag{5.2.13}$$

where

$$\begin{aligned} P(k_I,k_0) &= \Delta x\sqrt{\frac{2}{\pi}}\exp(-2(\Delta x(k_I-k_0))^2) \\ E^{tot} &= \frac{(\hbar k_n)^2}{2\mu} + E^{vib}_l = \frac{(\hbar k_I)^2}{2\mu} + E^{vib}_0 \end{aligned} \tag{5.2.14}$$

5.2.3 Model systems, results and discussion

We assume that the following Hamiltonian with single adiabatic PES mimics inelastic scattering of an atom from a diatom,

$$H(q_1,q_2) = \frac{p_1^2}{2m_1} + C\exp(-\alpha(q_1-\gamma q_2)) + \frac{p_2^2}{2m_2} + v(q_2), \tag{5.2.15}$$

where $v(q_2)$ is the harmonic potential. Potential and dynamical parameters used in this model are given in Table 5.1.

The initial wavefunction is the product of translational wavepacket (GWP) and vibrational wavefunction centered around q_{c1} (1.5 Å) and q_{c2} (0.7418 Å), respectively. Dynamical calculations are performed with different initial kinetic energies of the atom but only from ground vibrational state of the diatom.

Table 5.2 demonstrates kinetic energy resolved transition probabilities ($P^{-}_{1\leftarrow 0}$) at $t\rightarrow\infty$ as functions of increasing number of grid - points, N_{q_1}, on the scattering coordinate, q_1. At each energy, the results of first three columns are obtained from

TH-421_02612202

moving grid approach and the last three columns stand for traditional DVR results. In general, Table 5.2 indicates transition probabilities calculated by TDDVR approach achieve convergence only with 30 grid - points whereas in DVR, at least 200 grid - points are required for the same mode. Fig. 5.1(a) displays inelastic ($P^{-}_{1\leftarrow 0}$) transition probabilities at kinetic energy 4.0 eV as functions of time with increasing number of TDDVR grid - points (N_{q_1}) on the reaction coordinate. Time - dependent profile of transition probabilities with 50 TDDVR grid - points has excellent agreement with DVR ($N_{q_1} = 250$) results. Table 5.2 and Fig. 5.1(a) clearly show that convergence of $P^{-}_{1\leftarrow 0}$ with increasing number of grid - points either at $t \rightarrow \infty$ or as functions of time is remarkably fast in TDDVR compared to DVR. Since the growth and decay of the amplitudes at the grid - points occur with the displacement of grid - points (trajectories), TDDVR achieves convergence in such faster rates.

Table 5.1: Potential energy and dynamical parameters used in the calculations.

Model I:			Model II:		
parameter	value	unit	parameter	value	unit
α	4.5167	$Å^{-1}$	μ	0.58	amu
m_1	1.875	amu	A	3.0	eV
m_2	0.666667	amu	D	5.0	eV
ω	9.7715×10^{14}	s^{-1}	σ	0.30	Å
q_{c2}	0.7416	Å	σ_1	0.75	Å
γ	0.666667		ω_0	39.14×10^{13}	s^{-1}
C	0.01	eV	ω_1	7.83×10^{13}	s^{-1}
			ρ	0.333	Å
			q_f	-2.403	Å
ImA_1	2×10^{14}	amu s^{-1}	ImA_1	0.3969×10^{14}	amu s^{-1}
$q_{c1}(t_0)$	1.5	Å	$q_{c1}(t_0)$	5.0	Å

Table 5.3 presents kinetic energy resolved converged transition probabilities to all accessible vibrational states where at each energy, first row results are calculated by using TDDVR approach and second row from DVR. We find that in all energies, TDDVR needs only 50 grid - points to achieve the same level of accuracy as DVR

TH-421_02612202

Table 5.2: Convergence profile of vibrational transition probabilities from $v = 0$ to $v = 1$ for atom - diatom collision as functions of TDDVR and DVR grid - points, N_{q_1}, on the scattering coordinate, q_1.

	TDDVR			DVR		
KE(eV)/N_{q_1}	10	30	50	150	200	250
3.00	0.0277	0.0308	0.0308	0.0887	0.0305	0.0305
4.00	0.0033	0.1030	0.1030	0.0775	0.1030	0.1030
5.00	0.0005	0.1919	0.1918	0.0411	0.1916	0.1921
6.00	-	0.2783	0.2785	0.0221	0.0721	0.2789

with 250 grid - points. Fig. 5.1(b) displays elastic ($P^-_{0\leftarrow 0}$) and inelastic ($P^-_{1\leftarrow 0}$) transition probabilities (converged) at kinetic energy 3.00 eV as functions of time. The figure indicates that transition probabilities calculated by using moving grid approach ($N_{q_1} = 50$) have quantitative agreement with DVR ($N_{q_1} = 250$) results.

Table 5.3: Converged state - to - state vibrational transition probabilities for atom - diatom elastic and inelastic scattering.

KE (eV)	$0 \rightarrow 0$	$0 \rightarrow 1$	$0 \rightarrow 2$	$0 \rightarrow 3$
3.00	0.9691[a]	0.0308		
	0.9694[b]	0.0305		
4.00	0.8938	0.1030	0.0032	
	0.8938	0.1030	0.0031	
5.00	0.7923	0.1918	0.0154	
	0.7920	0.1921	0.0154	
6.00	0.6746	0.2785	0.0436	0.0032
	0.6740	0.2789	0.0438	0.0032

[a] TDDVR ($N_{q_1} = 50$)
[b] DVR ($N_{q_1} = 250$)

Fig. 5.1(c) and Fig. 5.1(d) show the change of few TDDVR grid - points ($\{q_{i_1}\}$) around the "classical" trajectory on the reaction coordinate and their associated momenta ($\{p_{i_1}\}$) (Appendix E), respectively as functions of time where the momentum (p_{c1}) of the central trajectory on the same coordinate is in-set in Fig. 5.1(d). In the

TH-421_02612202

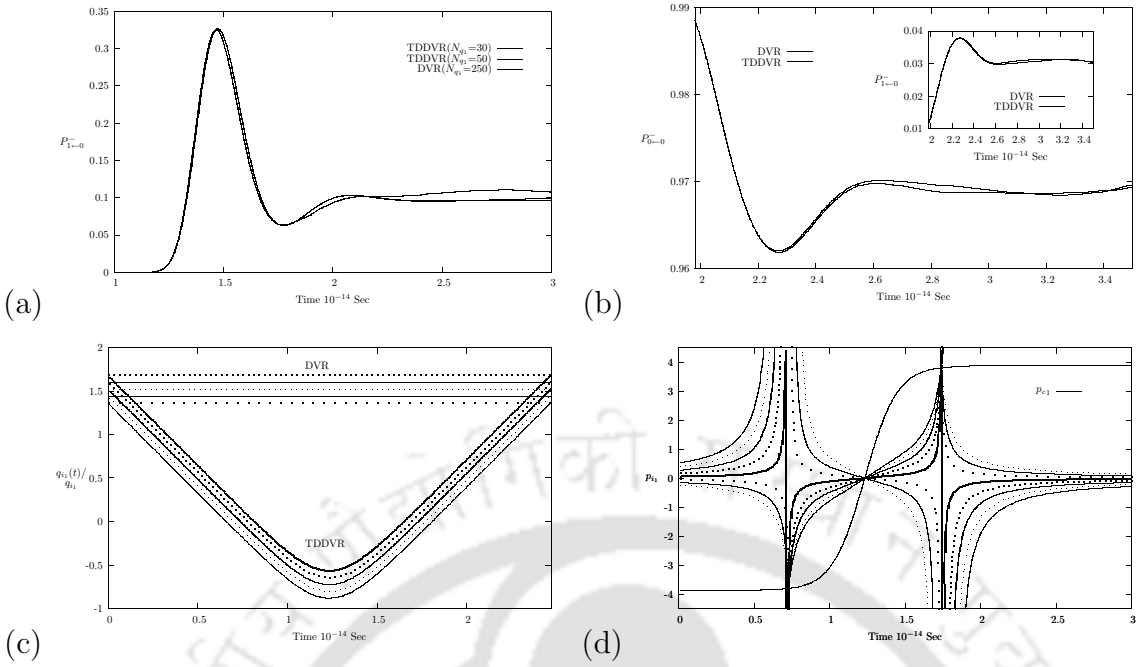

Figure 5.1: (a) Convergence of TDDVR results for non - reactive state - to - state transition probabilities ($P^-_{1\leftarrow 0}$) at KE 4.0 eV as functions of time with increasing number of grid - points (N_{q_1}) on the reaction coordinate, q_1. (b) TDDVR ($N_{q_1} = 50$) and DVR ($N_{q_1} = 250$) results (converged) of non - reactive state - to - state transition probabilities ($P^-_{0\leftarrow 0}$ and $P^-_{1\leftarrow 0}$) at KE 3.0 eV as functions of time. (c) Few TDDVR and DVR grid - points ($q_{i_1}(t)/q_{i_1}$) around the central trajectory of the reaction coordinate as functions of time. (d) Few momenta (p_{i_1}) associated with the TDDVR grid - points (q_{i_1}) and "classical" momentum (p_{c1}) of the translational coordinate as functions of time.

translational coordinate, a negative momentum is given to the "classical" particle, the particle approaches the classical turning point until its momentum is zero and returns back with a positive momentum (see Fig. 5.1(d)). It is interesting to note that: (i) At the beginning of propagation, associated momenta of the grid - points with positive magnitudes accumulate higher values compared to negative components such that overall momentum of the "classical" particle increases; (ii) Before reaching the classical turning point, magnitudes of all the component momenta approach to zero so that overall "classical" momentum is zero and consequently they change their sign; (iii) Again magnitudes of the negative components change sharply with respect to positive momenta and finally all the components along with the overall "classical"

TH-421_02612202

momentum approach to the constant magnitudes at $t \to \infty$.

We have also investigated the "non - reactive quasi -JT scattering model" in which the harmonic oscillator potential and the coupling term are replaced by more general potentials. The adiabatic PESs U_l, l = 1,2 are as below,

$$\begin{aligned} U_1(q_1,q_2) &= \frac{1}{2}\mu(\omega_0 - \tilde{\omega}_1(q_1))^2 q_2^2 + A \times f(q_1,q_2) + g(q_1) \\ U_2(q_1,q_2) &= \frac{1}{2}\mu\omega_0^2(q_2)^2 - (D-A) \times f(q_1,q_2) + D \end{aligned} \tag{5.2.16}$$

where q_1 and q_2 are the Cartesian coordinates (define in the intervals: $-\infty \leq q_1 \leq \infty$ and $-\infty \leq q_2 \leq \infty$) related to the polar coordinate r and θ as $q_1 = r\cos\theta$ and $q_2 = r\sin\theta$. In this model, q_1 is the reaction coordinate (translational) and q_2 is the internal (vibrational) coordinate. The function $\tilde{\omega}_1(q_1)$ is an q_1 dependent function of the following form,

$$\tilde{\omega}_1(q_1) = \omega_1 \exp(-\frac{q_1^2}{\sigma_1^2}) \tag{5.2.17}$$

and $f(q_1,q_2)$ is chosen to be a Gaussian which peaks at (0,0),

$$f(q_1,q_2) = \exp\Big(-\frac{q_1^2+q_2^2}{\sigma^2}\Big) \tag{5.2.18}$$

These adiabatic PESs are well separated from each other but touch only at the origin (transition state). This non - reactive double slit model is constructed by introducing the following form of the function, $g(q_1)$,

$$g(q_1) = \exp(-[(q_1 - q_f)/\rho]) \tag{5.2.19}$$

In the diabatic representation, PESs take the following matrix form,

$$\begin{aligned} V_{11} &= \frac{1}{2}\Big[U_1 + U_2 + (U_1 - U_2)\cos\theta\Big], \\ V_{22} &= \frac{1}{2}\Big[U_1 + U_2 - (U_1 - U_2)\cos\theta\Big], \\ V_{12} &= \frac{1}{2}\Big[(U_1 - U_2)\sin\theta\Big]. \end{aligned} \tag{5.2.20}$$

Potential and dynamical parameters are given in Table 5.1.

TH-421_02612202

It is well known that this Hamiltonian models atom - diatom non - reactive collision and exhibits strong non - adiabatic effect on the ground due to the excited state. Table 5.4 presents convergence of vibrational transition probabilities ($P^{-}_{2\leftarrow 0}$) at $t \rightarrow \infty$ as functions of increasing number of TDDVR and DVR grid - points at four selected total energies 1.25, 1.75, 2.25 and 2.75 eV when calculations are performed with two diabatic PESs. At all energies, we obtain the converged $P^{-}_{2\leftarrow 0}$ only with 30 - 50 TDDVR grid - points whereas in order to achieve convergence with DVR, 260 - 290 grid points are needed.

Table 5.4: Convergence profile of vibrational transition probabilities from $v = 0$ to $v = 2$ for inelastic scattering of "non - reactive JT model" as functions of TDDVR and DVR grid - points, N_{q_1}, on the scattering coordinate, q_1.

	TDDVR				DVR			
E(eV)/N_{q_1}	10	30	50	170	200	230	260	290
1.25	0.2959	0.2149	0.2177	0.1965	0.2404	0.2183	0.2180	0.2179
1.75	0.0807	0.2520	0.2555	0.2215	0.2726	0.2519	0.2546	0.2525
2.25	0.1886	0.2282	0.2282	-	0.1359	0.1560	0.2203	0.2290
2.75	-	0.2029	0.2024	-	-	0.1332	0.2148	0.2047

Table 5.5 demonstrates various non - reactive state - to - state converged transition probabilities on the ground adiabatic state at different energies. At each energy, TDDVR results are shown in the first row of Table 5.5 where the results of second row are obtained from DVR approach. Quantitative agreement between TDDVR and DVR results imply that TDDVR can achieve very high level of accuracy with small number of grid - points.

Figure 5.2 exhibits non - reactive transition probabilities (converged) ($P^{-}_{0\leftarrow 0}$ and $P^{-}_{2\leftarrow 0}$) at total energies (a) 1.25 and (b) 1.75 eV as functions of time. It is important to note that transition probabilities calculated by using moving grid approach follow correct symmetry as well as achieve high accuracy compared to DVR results. Even though time - dependent profiles of transition probabilities calculated by TDDVR

TH-421_02612202

Table 5.5: Converged state - to - state vibrational transition probabilities for elastic and inelastic scattering of "non - reactive JT model" when calculations are performed on two diabatic surfaces.

E (eV)	$0 \rightarrow 0$	$0 \rightarrow 1$	$0 \rightarrow 2$	$0 \rightarrow 3$	$0 \rightarrow 4$	$0 \rightarrow 5$	$0 \rightarrow 6$	$0 \rightarrow 7$	$0 \rightarrow 8$
1.25	0.7557[a]	0.0000	0.2177	0.0001	0.0265				
	0.7550[b]	0.0000	0.2179	0.0004	0.0266				
1.75	0.6076	0.0000	0.2555	0.0000	0.1189	0.0001	0.0178		
	0.6082	0.0001	0.2525	0.0002	0.1195	0.0000	0.0195		
2.25	0.4902	0.0000	0.2282	0.0000	0.1625	0.0001	0.1035	0.0001	0.0154
	0.4806	0.0006	0.2290	0.0032	0.1603	0.0053	0.1021	0.0029	0.0160
2.75	0.4024	0.0000	0.2024	0.0000	0.1539	0.0000	0.1308	0.0005	0.0960
	0.3982	0.0005	0.2047	0.0110	0.1454	0.0248	0.1053	0.0118	0.0860

[a] TDDVR ($N_{q_1} = 50$)
[b] DVR ($N_{q_1} = 290$)

approach have some fluctuation around DVR results during the interaction period, asymptotically ($t \rightarrow \infty$) perfect matching is obtained. At this point, it is worth mentioning that all the quantum - classical calculations require even less than 50 grid - points on the reaction coordinate for convergence whereas for the same coordinate, at least 260 grid - points are needed in the DVR calculations. Moreover, when the dynamical calculations on "reactive JT model" were performed [46] by using FFT-Lanczos technique, convergence of state - to - state transition probabilities appear with 512 grid - points on the scattering coordinate. Finally, Fig. 5.2(c) displays the change of few momenta ($p^1_{i_1}$) associated with corresponding grid - points ($q^1_{i_1}$) and momentum ($p^1_{c_1}$) of the "classical" particle as functions of time. This figure carries similar interpretations as we have discussed in case of Fig. 5.1(d).

One may note that in case of TDDVR, as the quantum propagation is approximated by "classical" mechanics, some fluctuations may appear in the transition probability profiles (See Fig. 5.2(a) - (b)). More specifically, at each time step (Δt), quantum equation of motion face the potential energy surface calculated at the time

TH-421_02612202

- dependent grid - points and theoretically, only when $\Delta t \rightarrow 0$, perfect adiabatic switching of the amplitudes of wavefunction can be achieved.

We have solved the time - dependent Schroedinger equation in the adiabatic representation with ordinary BO approximation by using the DVR as well as the TDDVR approach. Calculations are performed at four selected total energies 1.25, 1.75, 2.25 and 2.75 eV, respectively where the ground and the first excited adiabatic states are 5.0 eV apart at the asymptotic region but meet at 3 eV in the interaction region.

It is expected that in the case of single - surface adiabatic calculation with ordinary BO approximation, non - adiabatic effects due to excited state(s) on the ground will be absent. At the same time, as the PES is even in the vibrational coordinate, transitions will occur only between states of the same parity. Hence, even $\rightarrow$ even and odd $\rightarrow$ odd transitions will differ from zero but even $\rightarrow$ odd and odd $\rightarrow$ even transitions will be forbidden. This selection of transition will be applicable both for the reactive and non - reactive cases.

Table 5.6: Non - reactive state - to - state transition probabilities when calculations are performed on the single adiabatic surface with BO approximation (Eq. (4.3.6)).

E (eV)	$0 \rightarrow 0$	$0 \rightarrow 1$	$0 \rightarrow 2$	$0 \rightarrow 3$	$0 \rightarrow 4$	$0 \rightarrow 5$	$0 \rightarrow 6$	$0 \rightarrow 7$	$0 \rightarrow 8$
1.25	0.6815[a]	0.0000	0.2177						
	0.6812[b]	0.0000	0.2183						
1.75	0.4294	0.0000	0.1901	0.0000	0.1250				
	0.4282	0.0000	0.1886	0.0000	0.1272				
2.25	0.2767	0.0000	0.1211	0.0000	0.0738	0.0000	0.0688		
	0.2775	0.0000	0.1214	0.0000	0.0742	0.0000	0.0693		
2.75	0.1350	0.0000	0.0646	0.0000	0.0482	0.0000	0.0283	0.0000	0.0341
	0.1417	0.0000	0.0672	0.0000	0.0489	0.0000	0.0289	0.0000	0.0348

[a] DVR
[b] TDDVR

In Tables 5.6 and 5.7 we present various non - reactive and reactive state - to - state transition probabilities, respectively at four selected energies. The first row stands

TH-421_02612202

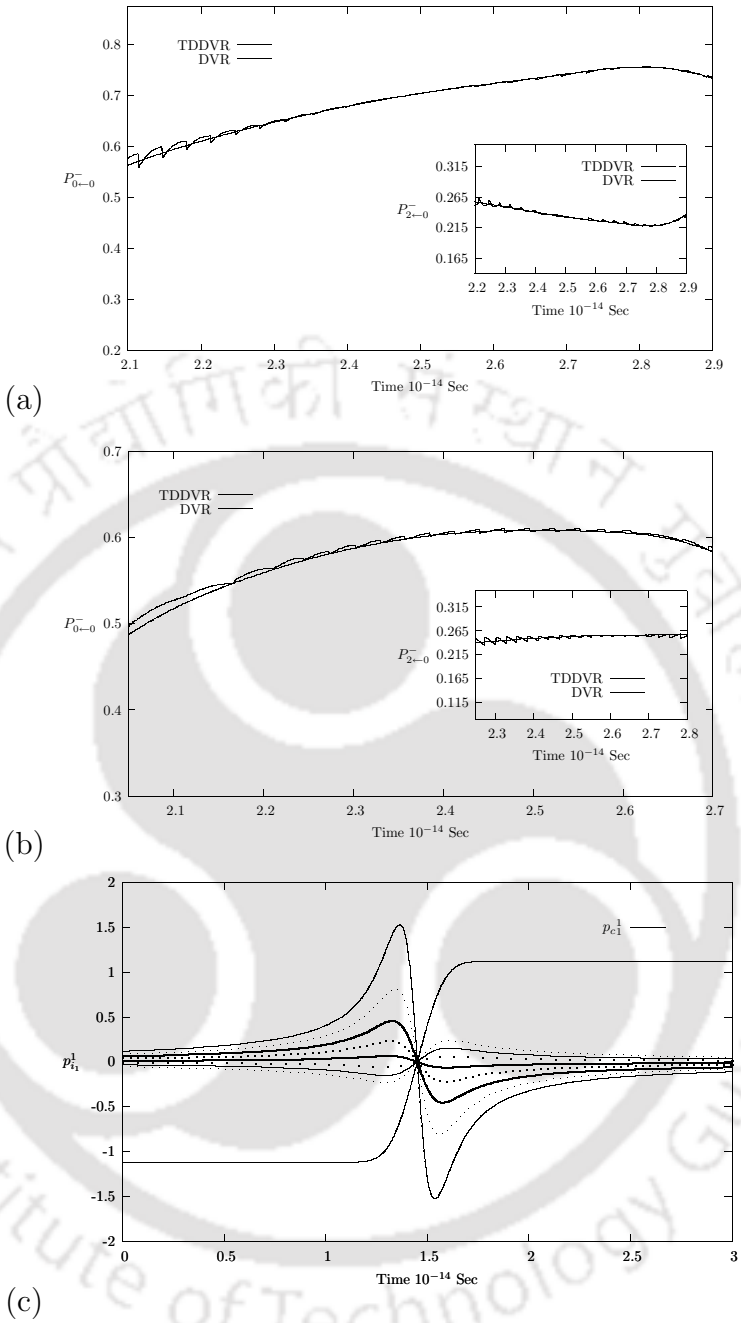

Figure 5.2: TDDVR ($N_{q_1} = 50$) and DVR ($N_{q_1} = 290$) profiles (converged) of non - reactive vibrational transition probabilities ($P^-_{0\leftarrow 0}$ and $P^-_{2\leftarrow 0}$) on the ground adiabatic state as functions of time when calculations are performed on two diabatic states at total energy (a) 1.25 eV and (b) 1.75 eV, respectively. (c) Few momenta ($p^1_{i_1}$) associated with the TDDVR grid points ($q^1_{i_1}$) and "classical" momentum ($p^1_{c_1}$) of the reaction coordinate on the ground adiabatic state as functions of time.

TH-421_02612202

Table 5.7: Reactive state - to - state transition probabilities when calculations are performed on the single adiabatic surface with BO approximation (Eq. (4.3.6)).

E (eV)	$0 \rightarrow 0$	$0 \rightarrow 1$	$0 \rightarrow 2$	$0 \rightarrow 3$	$0 \rightarrow 4$	$0 \rightarrow 5$	$0 \rightarrow 6$	$0 \rightarrow 7$	$0 \rightarrow 8$
1.25	0.0390[a]	0.0000	0.0619						
	0.0386[b]	0.0000	0.0616						
1.75	0.0450	0.0000	0.0190	0.0000	0.1691				
	0.0452	0.0000	0.0163	0.0000	0.1685				
2.25	0.0290	0.0000	0.0109	0.0000	0.1547	0.0000	0.2541		
	0.0282	0.0000	0.0103	0.0000	0.1495	0.0000	0.2494		
2.75	0.0470	0.0000	0.0010	0.0000	0.0974	0.0000	0.2146	0.0000	0.3172
	0.0469	0.0000	0.0017	0.0000	0.0950	0.0000	0.2116	0.0000	0.3083

[a] DVR
[b] TDDVR

for results obtained from the DVR and only even $\rightarrow$ even and odd $\rightarrow$ odd transitions appear as allowed ones. The results reported on the second row are calculated by using the present TDDVR approach. Transition probabilities obtained from the quantum - classical approach are seen not only to follow the correct symmetry but also achieve the accuracy at the level of DVR. Fig. 5.3(a) demonstrates the non - reactive (P^-) and reactive (P^+) transition probabilities as functions of time at a total energy 2.25 eV and shows excellent agreement between results of DVR and TDDVR. Even though quantum - classical profiles have some fluctuations around quantum results during the interaction period, these fluctuations vanish asymptotically ($t \rightarrow \infty$). It is important to note that all the TDDVR calculations have been performed with 50 grid - points (trajectories) on the reaction coordinate and 50 grid - points (trajectories) on the harmonic mode. On the other hand, DVR requires at least 200 grid - points on the reaction coordinate and calculations on the same model were carried out [70] by using FFT - Lanczos approach with 512 grid - points. TDDVR takes the advantage of both the DVR representation as well as time - dependent basis set. The movement of grid - points (trajectories) and the changes of amplitudes at these grid - points

TH-421_02612202

help to achieve fast convergence. Fig. 5.3(b) displays central trajectories (s_c^1 and s_c^2) and their associated momenta ($p_{s_c^1}$ and $p_{s_c^2}$) as functions of time. For the harmonic mode, initial values of both s_c^2 and $p_{s_c^2}$ are set equal to zero and these parameters vary around zero as functions of time. The reaction coordinate mimic the interaction between atom and diatom where the initial position and momentum (s_c^1 and $p_{s_c^1}$) of the atom enter through GWP and their change as functions of time are quite expected as shown in Fig. 5.3(b).

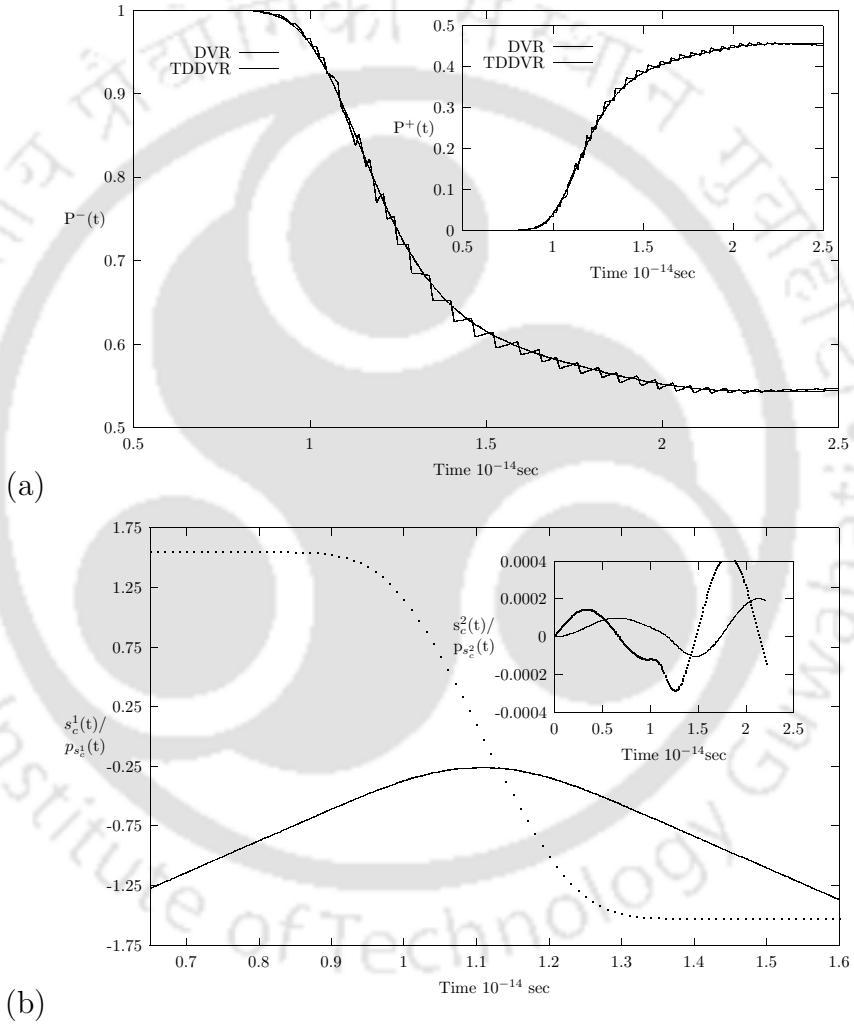

Figure 5.3: (a) Comparison of TDDVR and DVR results of total non - reactive (P^-) and reactive (P^+) transition probabilities on the ground adiabatic state as functions of time where all calculations are performed in adiabatic representation. (b) Central trajectories (s_c^1 and s_c^2) and their momenta ($p_{s_c^1}$ and $p_{s_c^2}$) for both the modes as functions of time.

TH-421_02612202

TH-421_02612202

CHAPTER VI

APPLICATION TO PHOTO - ABSORPTION SPECTRUM OF PYRAZINE

6.1 Introduction

The dynamical aspects of photo - excited pyrazine molecule have been investigated over the past years [147–159]. We have used the present method to compute the photo - absorption spectrum of pyrazine by using two different model Hamiltonians [147–149]. The system has a conical intersection, and undergoes ultrafast non - radiative energy transfer after excitation to the S_2 state. Since the vibrational states of S_2 state have short lifetime, the spectrum appears with broad peaks. The experimental spectrum is well reproduced either after homogeneous broadening of the 4 - mode model spectrum or by introducing the other vibrational modes as a bath. The details of the photo - absorption spectrum are interesting both with respect to experimental and theoretical point of view. Since this system is a challenging as well as benchmark to investigate the workability of any newly formulated method, we wish to find whether TDDVR can accurately calculate and thereby, reproduce the spectrum obtained from other contemporary approaches [147–149].

6.2 Molecular dynamics with linearly coupled model Hamiltonian

6.2.1 The Model Hamiltonian

The experimental spectrum [160] of electronic transition from the ground state S_0 to the S_1 and S_2 states of pyrazine has been accurately estimated. The important aspects of the spectrum are noted as: The excitation to the S_1 state generates a set

TH-421_02612202

of discrete lines while excitation to the S_2 state yields a broad band with little structure. In the recent past, molecular dynamics of pyrazine has brought an insight into the mechanism of protophysical processes. The broad band resulting from S_2 state indicates fast intramolecular vibrational energy transfer mainly due to the presence of a conical intersection (CI) between the two excited electronic states. The non - adiabatic effects originating from CI, also known in many molecular systems, bring special interest on dynamical aspects. Considering the four main vibrational modes, the theoretical description can reproduce the essential features of the experimental spectrum. In order to simulate the broad experimental spectrum due to S_2 state, the Lorentzian broadening of the theoretically calculated spectrum is a necessity. This convolution of spectrum appears to be a phenomenological dephasing, not just to attribute to the resolution of spectrophotometer but arises due to a further ultrafast relaxation from four main modes to the 20 remaining vibrational modes. The detailed description of the system dynamics requires a model Hamiltonian which explicitly includes the other degrees of freedom as weakly coupled heat bath affecting the dynamics of the four main modes.

The total Hamiltonian includes the four main vibrational modes as the system, the bath modes as environment and the coupling between them as below,

$$\hat{H} = \hat{H}_s + \hat{H}_b + \hat{H}_{sb} \tag{6.2.1}$$

The model Hamiltonian has been developed based on accurate ab initio calculations considering all the 24 modes of the system, where the inter - and intra - electronic state vibronic couplings are represented only with linear terms [147, 148]. Quantum dynamical benchmark calculations using multiconfigurational time - dependent Hartree (MCTDH) method [164–166] have been performed on both forms of the model Hamiltonian [148, 149] and obtained excellent agreement with experimental findings. Indeed, such rich model is an optimal system to test the performance of semi - classical [157] as well as quantum - classical approaches [159] and to find the

TH-421_02612202

possibility of applicability of such approaches in very large and complex systems. We consider the four mode model Hamiltonian as system with linear vibronic couplings,

$$\begin{aligned}\hat{\mathbf{H}}_{\mathbf{s}} &= \sum_{i=10a,6a,1,9a} \frac{\omega_i}{2}\Big(-\frac{\partial^2}{\partial Q_i^2}+Q_i^2\Big)\begin{pmatrix}1 & 0\\ 0 & 1\end{pmatrix}+\begin{pmatrix}-\Delta & 0\\ 0 & \Delta\end{pmatrix}\\ &+ \begin{pmatrix}0 & \lambda\\ \lambda & 0\end{pmatrix}Q_{10a}+\sum_{j=6a,1,9a}\begin{pmatrix}\kappa_j^{(1)} & 0\\ 0 & \kappa_j^{(2)}\end{pmatrix}Q_j \qquad (6.2.2)\end{aligned}$$

where Q_is are the normal modes of pyrazine. The non - totally symmetric mode, Q_{10a}, couples the two diabatic electronic states with non - diagonal matrix element λ; the remaining three tuning modes (Q_{6a}, Q_1, Q_{9a}) are totally symmetric with intrastate coupling constant,κ_js and 2Δ is the energy gap between the two PESs at the equilibrium ($\mathbf{Q}=\mathbf{0}$).

Since the electronic states of the system have different electronic multipole moments, an added heat bath represented by a set of harmonic oscillators around the system polarizes the environment differently and leads to different equilibrium positions of the bath oscillators for each electronic state. The bath and system - bath coupling Hamiltonians are given by,

$$\hat{\mathbf{H}}_{\mathbf{b}} = \sum_{b=1}^{n_{bath}}\frac{\omega_b}{2}\Big(-\frac{\partial^2}{\partial Q_b^2}+Q_b^2\Big)\begin{pmatrix}1 & 0\\ 0 & 1\end{pmatrix}, \qquad (6.2.3)$$

$$\hat{\mathbf{H}}_{\mathbf{sb}} = \sum_{b=1}^{n_{bath}}\begin{pmatrix}\kappa_b^{(1)} & 0\\ 0 & \kappa_b^{(2)}\end{pmatrix}Q_b. \qquad (6.2.4)$$

The bath modes are like tuning modes but couple the system and bath with much smaller coupling constants. It is important to note that energy and population transfer from the system to the bath are expected due to non - zero interstate coupling constant, λ. Since there are no off - diagonal elements in the system - bath Hamiltonian, the bath has no direct contribution for interstate coupling but modulates the

TH-421_02612202

energy gap between the states. The parameters of this model Hamiltonian are taken from Krempl *et. al.* [147] and listed in Table 6.1.

Table 6.1: Parameters (in eV) for the linearly coupled model Hamiltonian.

	ω	$\kappa^{(1)}$	$\kappa^{(2)}$
ν_{10a}	0.0936	–	–
ν_{6a}	0.0740	-0.0964	0.1194
ν_1	0.1273	0.0470	0.2012
ν_{9a}	0.1568	0.1594	0.0484
b_1	0.1347	0.0308	-0.0308
b_2	0.3431	0.0782	-0.0782
b_3	0.1157	0.0261	-0.0261
b_4	0.3242	0.0717	-0.0780
b_5	0.3621	0.0780	-0.0780
b_6	0.2673	0.0560	-0.0560
b_7	0.3052	0.0625	-0.0625
b_8	0.0968	0.0188	-0.0188
b_9	0.0589	0.0112	-0.0112
b_{10}	0.0400	0.0069	-0.0069
b_{11}	0.1726	0.0265	-0.0265
b_{12}	0.2863	0.0433	-0.0433
b_{13}	0.2484	0.0361	-0.0361
b_{14}	0.1536	0.0210	-0.0210
b_{15}	0.2105	0.0281	-0.0281
b_{16}	0.0778	0.0102	-0.0102
b_{17}	0.2294	0.0284	-0.0284
b_{18}	0.1915	0.0196	-0.0196
b_{19}	0.4000	0.0306	-0.0306
b_{20}	0.3810	0.0269	-0.0269
$\Delta =$	0.4617	$\lambda =$	0.1825

6.2.2 Theoretical aspects of TDDVR approach

In view of the current perspective, the matrix form of TDDVR equation for quantum motion on the lth PES can be written as,

$$i\hbar\mathbf{A}\dot{\mathbf{C}}_{\mathbf{l}} = \mathbf{H}^{\mathbf{t}}_{\mathbf{ll}}\mathbf{C}_{\mathbf{l}} + \mathbf{A}\sum_{\mathbf{l}'\neq\mathbf{l}}\mathbf{V}_{\mathbf{ll}'}\mathbf{C}_{\mathbf{l}'} \tag{6.2.5}$$

TH-421_02612202

and under a similarity transformation take the following convenient form,

$$i\hbar\dot{\mathbf{D}}_{\mathbf{l}}(\mathbf{t}) = \mathbf{A^{-1/2}H^{t}_{ll}A^{-1/2}D_{l}} + \sum_{\mathbf{l'\neq l}} \mathbf{V_{ll'}D_{l'}} \tag{6.2.6}$$

where $\mathbf{D_l} = \mathbf{A^{1/2}C_l}$ and $l = 1, 2$.

The explicit expression of the differential equation for an amplitude, $d_{i_1 i_2 \ldots . i_p, l}$ on the $l th$ surface is,

$$\begin{aligned} i\hbar\dot{d}_{i_1 i_2 \ldots . i_p, l} &= \frac{1}{2}\Big\{\sum_k \dot{P}_{Q_k^c}\sqrt{\frac{\hbar}{ImA_k}}\bar{X}_{i_k i_k}\Big\}d_{i_1 i_2 \ldots . i_p, l} + \Big\{\sum_k \frac{\mu(\dot{Q}_k^c)^2}{2}\Big\}d_{i_1 i_2 \ldots . i_p, l} \\ &+ V_{ll}(i_1 i_2 \ldots . i_p)d_{i_1 i_2 \ldots . i_p, l} + \sum_{l' \neq l} V_{ll'}(i_1 i_1 \ldots . i_p)d_{i_1 i_2 \ldots . i_p, l'} \\ &+ \sum_k \Big\{\frac{\hbar ImA_k}{2\mu}\sum_{i'_1 i'_2 \ldots . i'_p}\big\{2\bar{Y}_{i_k i'_k} - \bar{Z}_{i_k i'_k}\big\}d_{i'_1 i'_2 \ldots i'_p, l}\prod_{k' \neq k}^{p}\delta_{i_{k'} i'_{k'}}\Big\} \end{aligned} \tag{6.2.7}$$

On the other hand, the classical path equations for the $k th$ mode can be written as

$$\dot{Q}_k^c(t) = \frac{P_{Q_k^c}(t)}{\mu} \tag{6.2.8}$$

$$\dot{P}_{Q_k^c}(t) = -\frac{d\hat{V}(\{Q_k\})}{dQ_k}\Big|_{Q_k(t)=Q_k^c(t)} + Q_k^F(t) \tag{6.2.9}$$

where the rigorous expression of quantum force, $Q_k^F(t)$, is derived by using Dirac - Frenkel variational principle [37]. The following integral is minimized,

$$\begin{aligned} I &= \int(-i\hbar\frac{\partial\Xi^{\star}(\{Q_k\},t)}{\partial t} - H(\{P_{Q_k}\},\{Q_k\})\Xi^{\star}(\{Q_k\},t)) \\ &\times (i\hbar\frac{\partial\Xi(\{Q_k\},t)}{\partial t} - H(\{P_{Q_k}\},\{Q_k\})\Xi(\{Q_k\},t))\prod_{k=1}^{p}dQ_k, \end{aligned} \tag{6.2.10}$$

TH-421_02612202

with respect to $\dot{P}_{Q_k^c}$ to obtain the explicit form of $Q_k^F(t)$,

$$\begin{aligned} Q_k^F(t) &= \sum_l \sum_{i_1 i_2..i_k i'_k..i_p} c^{\star}_{i_i i_2..i_k..i_p,l}(t) c_{i_1 i_2..i'_k..i_p}(t) \\ &\times \Big\{ \frac{2(ImA_k)^2}{\mu} \Big[S^{(2)}_{i_k i'_k} \frac{S^{(1)\star}_{i_k i_k}}{A_{i_k i_k}} - S^{(3)}_{i_k i'_k} \Big] - \frac{\hbar ImA_k}{\mu} \Big[R_{i_k i'_k} \frac{S^{(1)\star}_{i_k i_k}}{A_{i_k i_k}} - T^{\star}_{i_k i'_k} \Big] \Big\} \\ &/ \Big[\sum_l \sum_{i_1 i_2..i_k..i_p} c^{\star}_{i_1 i_2..i_k..i_p,l}(t) c_{i_1 i_2..i_k..i_p,l}(t) \frac{S^{(1)\star}_{i_k i_k} S^{(1)}_{i_k i_k}}{A_{i_k i_k}} \\ &- \sum_i \sum_{i_1 i_2..i_k i'_k..i_p} c^{\star}_{i_1 i_2..i_k..i_p,l}(t) c_{i_1 i_2..i'_k..i_p,l}(t) S^{\star(2)}_{i_k i'_k} \Big] \end{aligned} \tag{6.2.11}$$

6.2.3 Numerical details and absorption spectra

We have studied the dynamics of the photoexcited pyrazine molecule involving S_1 and S_2 diabatic states assuming a vertical excitation from its ground (S_0) to the excited (S_2) state at the Frank - Condon point. Thus, the initial wavefunction on the S_2 state is the wavefunction of the ground state, i.e., a product of Gaussian functions (Φ_{GWP}) centered around the equilibrium geometry ($\mathbf{Q} = \mathbf{0}$) of the S_0 state. In order to specify the initial amplitude vector ($\mathbf{d}$) (Eq. 6.2.7), multi - dimensional TDDVR wavefunction is equated with the product of Φ_{GWP} functions,

$$\begin{aligned} \prod_{k=1}^{p} \Phi_{GWP}(Q_k) &= \sum_{i_1 i_2 .... i_p} c_{i_1 i_2 .... i_p,2} \prod_{k=1}^{p} \psi_{i_k}(Q_k, t) \\ &= \sum_{i_1 i_2 .... i_p} c_{i_1 i_2 .... i_p,2} \prod_{k=1}^{p} \sum_{n=0}^{N_k} \xi_n(x_{i_k}) \Phi_n(Q_k). \end{aligned} \tag{6.2.12}$$

Using the property of the TDDVR basis,

$$\psi_{i_k}(Q_k, t) = \sum_{n=0}^{N_k} \xi^{\star}_n(x_{i_k}) \Phi_n(Q_k, t) \approx \delta(Q_k - Q_{i_k}), \tag{6.2.13}$$

Eq. (6.2.12) takes the following form,

$$\begin{aligned} \prod_{k=1}^{p} \Phi_{GWP}(Q_{i_k}) &= c_{i_1 i_2 .... i_p,2} \prod_{k=1}^{p} \sum_{n=0}^{N_k} \xi_n(x_{i_k}) \Phi_n(Q_{i_k}) \\ &= c_{i_1 i_2 .... i_p,2} \prod_{k=1}^{p} A_{i_k i_k}. \end{aligned} \tag{6.2.14}$$

TH-421_02612202

Alternatively, Eq. (6.2.14) can be rearranged to define the vector d_2 on the S_2 surface,

$$d_{i_1 i_2 \ldots . i_p,2} = c_{i_1 i_2 \ldots . i_p,2} \sqrt{\prod_{k=1}^{p} A_{i_k i_k}} = \frac{\prod_{k=1}^{p} \Phi_{GWP}(Q_{i_k})}{\sqrt{\prod_{k=1}^{p} A_{i_k i_k}}}, \tag{6.2.15}$$

whereas the initial expansion coefficient vector d_1 on the S_1 surface is,

$$d_{i_1 i_2 \ldots . i_p,1} = 0. \tag{6.2.16}$$

The width parameters of the Gaussian functions are defined by the frequencies of the respective normal modes. The dynamical evolution of the system is performed by simultaneously propagating the set of differential Eqs. (6.2.7), (6.2.8) and (6.2.9) and the time - dependent amplitudes on the two surfaces are given by,

$$\begin{pmatrix} \mathbf{d_1(t)} \\ \mathbf{d_2(t)} \end{pmatrix}. \tag{6.2.17}$$

Since **d** vectors are defined at the grid points, the probability of finding the system on a particular diabatic surface is obtained by mere grid - summation,

$$P_l(t) = \sum_{i_1 i_2 \ldots . i_p} |d_{i_1 i_2 \ldots . i_p,l}|^2, l = 1, 2. \tag{6.2.18}$$

In order to calculate adiabatic population on a particular surface, diabatic amplitude vector (**d**) is transformed to the adiabatic (**e**) one,

$$\mathbf{e} = \mathbf{T}^{\dagger}\mathbf{d} \tag{6.2.19}$$

where the **T** matrix defines the transformation of diabatic (**V**) to adiabatic (**U**) PES matrices, $\mathbf{U} = \mathbf{T}^{\dagger}\mathbf{V}\mathbf{T}$.

The optimum number of TDDVR grid - points used are: N_{6a}=13, N_1=27, N_{9a}=9 and N_{10a}=21 for the first four modes, N_{b_1} or N_{b_6} =2, N_{b_2} =3, N_{b_3} or N_{b_7} =2, N_{b_4}=3 and N_{b_5}=3 for the next five modes and one basis function for the remaining bath modes. In order to know the quality of the calculated results, we find out the magnitude

TH-421_02612202

of the error due to the use of finite TDDVR basis and estimate the change in the autocorrelation function by calculating the following quantity,

$$\Delta(t) = |\langle\Psi(0)|\Psi(t)\rangle - \langle\Psi'(0)|\Psi'(t)\rangle|^2 \tag{6.2.20}$$

where $\Psi'(t)$ is the wavefunction ignoring the least populated TDDVR basis function. In case of four mode model and the system with five bath modes, we found that the change of autocorrelation function, $\Delta(t)$, remains below 10^{-3} on addition or subtraction of a TDDVR basis in a particular mode.

When a sufficient number of grid - points are used, TDDVR formulation is such that quantum results are independent of the initial choice of "classical" momentum of the central trajectory. Indeed, the choice is important when a mode is treated at the classical limit (a single grid - point) because the dynamics is solely dictated by classical mechanics. In our calculation, we have chosen $Q_i(t_0) = 0$ and $P_i(t_0) = 0$ for those modes which are treated by a minimum of two TDDVR basis. On the other hand, the choice of classical parameters for one grid - point dynamics are $Q_i(t_0) = 0$ and $P_i(t_0) = \sqrt{\hbar m\omega_i}$.

The prime interest is to calculate the photo - absorption spectrum of pyrazine. The nuclear wavefunction propagated by TDDVR method is used to calculate the autocorrelation function ($C(t)$) and the Fourier transform of $C(t)$ gives S_1 and S_2 absorption spectrum,

$$I(\omega) \propto \omega \int_{-\infty}^{\infty} C(t) \exp(i\omega t) dt \tag{6.2.21}$$

where

$$C(t) = \langle\Psi(t)|\Psi(0)\rangle \tag{6.2.22}$$

$$= \langle\Psi^\star(\frac{t}{2})|\Psi(\frac{t}{2})\rangle \tag{6.2.23}$$

It is important to note that Eq. (6.2.23) is more accurate and faster [163] than previous Eq. (6.2.22). At the same time, Eq. (6.2.23) is valid only if the wavefunction

TH-421_02612202

is real at t=0 and the Hamiltonian is symmetric. Since the propagation of wavefunction and the calculated autocorrelation function is upto finite time, artifacts known as Gibbs phenomenon develop in the spectrum. It can be reduced by multiplying the autocorrelation with the following function,

$$g(t) = \cos(\frac{\pi t}{2T}), \tag{6.2.24}$$

where T is the length of propagation. This function convolutes the spectrum with,

$$\tilde{g}(\omega) = \frac{4\pi T}{\pi^2 - (2\omega T)^2} \cos(\omega T). \tag{6.2.25}$$

such that C(t) is smoothened to zero.

6.2.4 Results and Discussion

The TDDVR wavefunction [44] of the four mode model is propagated upto 120 fs using 21 grid - points in the coupling mode (ν_{10a}) and 13, 27 and 9 grid - points respectively for the tuning modes (ν_{6a}, ν_1 and ν_{9a}). The propagation time of 120 fs corresponds to 240 fs in the propagation of autocorrelation function (Eq. (6.2.23)). The absolute values of the autocorrelation functions for DVR and TDDVR calculations are plotted as functions of time in Fig. 6.1(a). The TDDVR profile essentially follows the peaks and resonances obtained by DVR calculation during the entire propagation except for some small differences. The figure implies that the loss of coherence throughout the whole propagation is small. Since TDDVR method with sufficient grid - points converges to the exact quantum mechanical results, we can eliminate those differences with increasing number of grid - points. On the other hand, in view of including more number of modes explicitly in the model, TDDVR calculations are performed with moderate number of grid - points considering results are sufficiently close to the quantum one.

The population of the S_2 diabatic state demonstrates the coupling between the diabatic states and the effect of conical intersection. Calculated time - dependent

TH-421_02612202

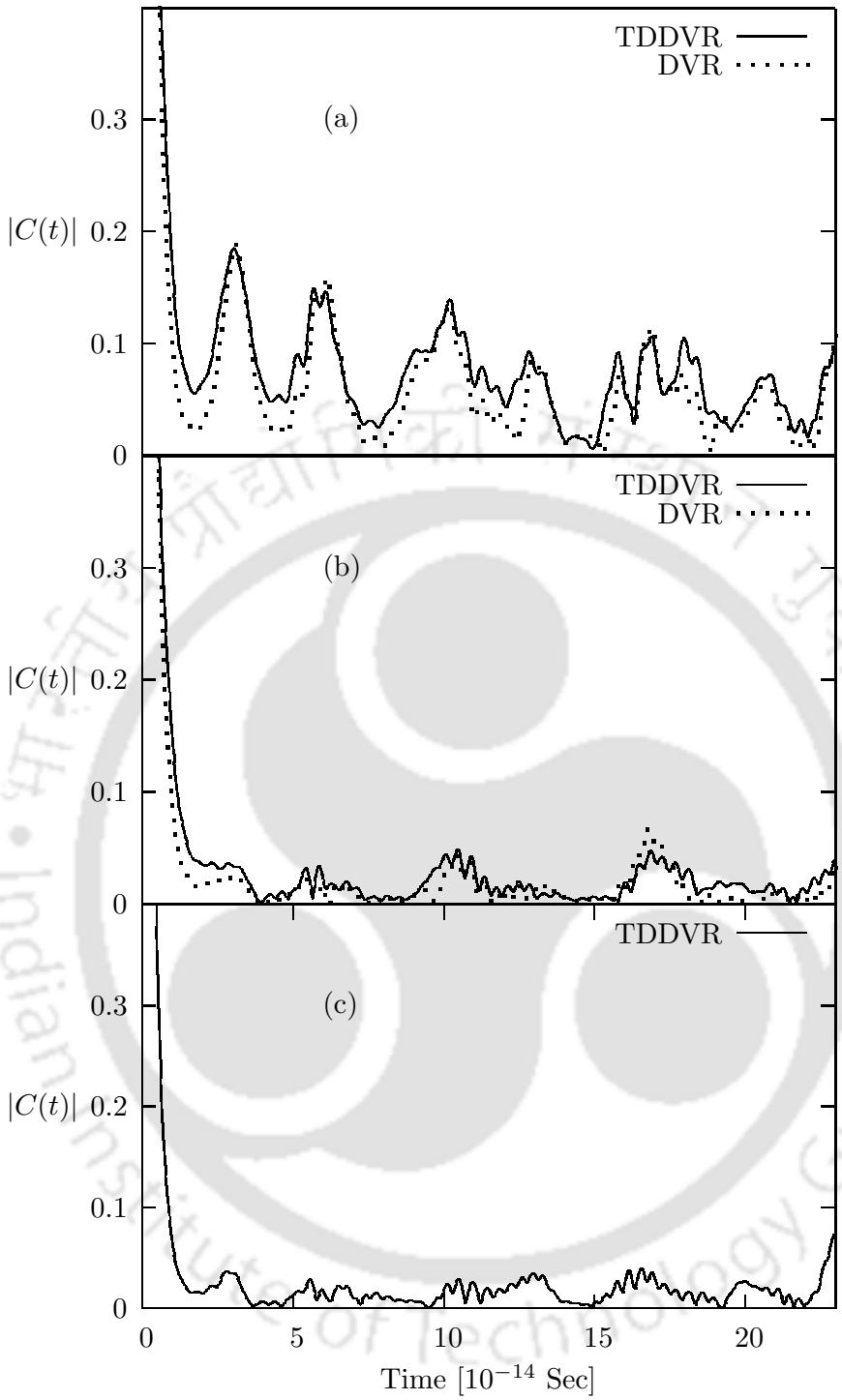

Figure 6.1: Calculated absolute values of the autocorrelation function using TDDVR approach as functions of time for the following cases: (a) Four mode model (system); (b) System coupled with five bath modes; (c) System coupled with twenty bath modes. Fig. 6.1 (a) and (b) envelopes are compared with corresponding traditional quantum mechanical results.

TH-421_02612202

probabilities of finding the isolated system on S_2 diabatic state are shown as functions of time in Fig. 6.2(a). It is remarkable to see that TDDVR and DVR profiles coincide perfectly with each other. The interstate population transfer starts almost immediately and the population drops to even below 0.2 around 45 fs. Again the population sharply arises to 0.4 after 75 fs and then quickly decays to 0.2 around 100 fs. There are some repeated patterns with smaller amplitudes at longer time.

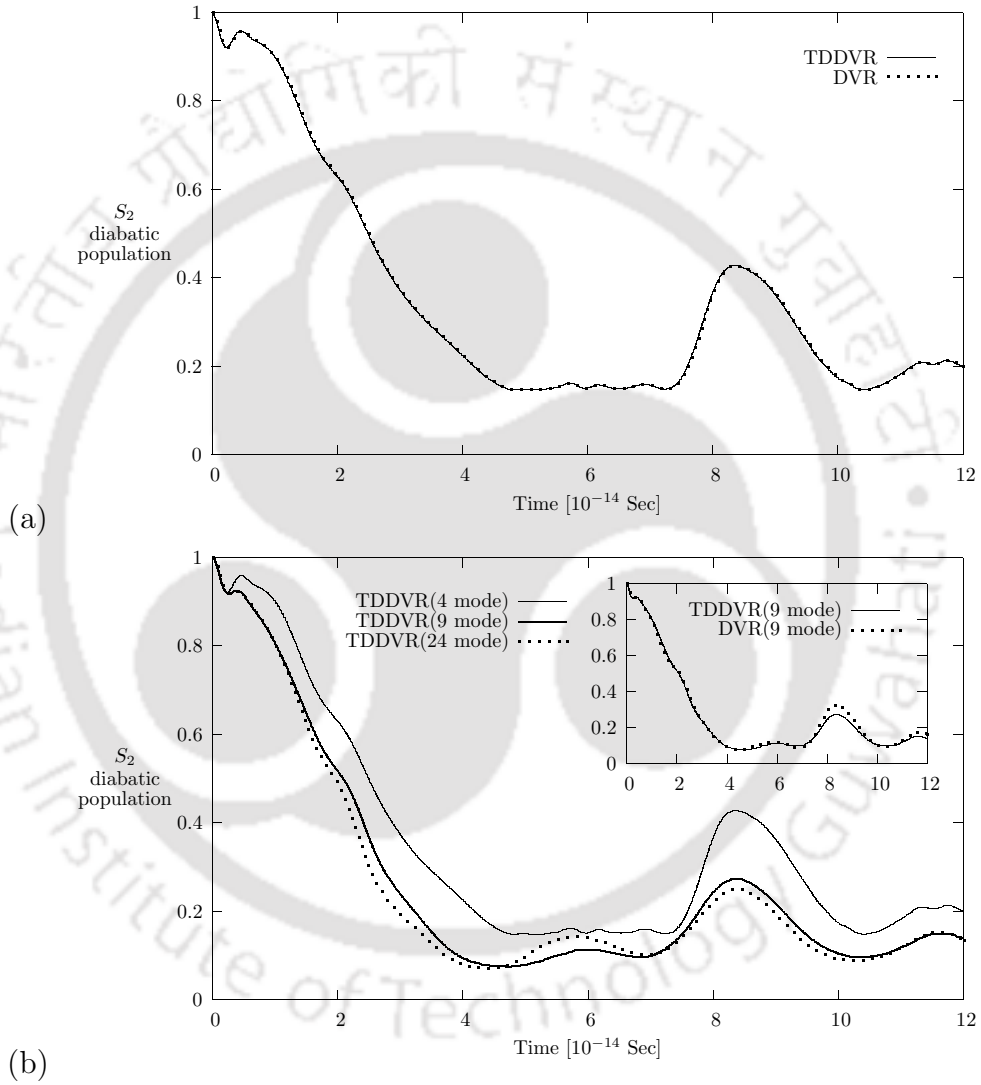

Figure 6.2: Population dynamics on the S_2 diabatic state as functions of time for the (a) four mode model and (b) four, nine and twenty four mode model. TDDVR results for the four and nine mode model are compared with corresponding DVR profiles.

TH-421_02612202

Fig. 6.3(a) presents the adiabatic S_2 population as functions of time and found excellent agreement with quantum mechanical results. The initial adiabatic S_2 population is slightly below one (1.0) since the rest contributes to the initial S_1 state population and generates S_1 spectrum. Though the initial decay of adiabatic S_2 state population is much slow upto 10 fs, after this delay, the transfer is fast and the population reduces to much lower value compared to the diabatic case. Again, around 80 fs, adiabatic population of S_2 state increases but not as much as the diabatic population at the same period of time. It is important to note that when the system is around the conical intersection, the population transfer occurs from one state (diabatic/adiabatic) to another.

The absorption spectrum of pyrazine for the four mode model is reported in Fig. 6.4(a) and we obtained good agreement with DVR envelop. Fig. 6.4(b) displays the convoluted spectrum with inclusion of phenomenological broadening and again compared with corresponding DVR results. Both the spectra have two interesting parts: (I) The discrete lines on the lower energy side represent the S_1 state spectrum; (II) The spectrum in the higher energy region is due to S_2 state. The details of the S_1 state spectrum are shown as inset in Fig. 6.4(a).

The effect of the bath modes on the system dynamics has been investigated by including more and more number of bath degrees of freedom. We have propagated the wavefunction of the nine mode model by using 21 grid - points in the coupling mode (ν_{10a}), 13, 27 and 9 grid - points respectively for the tuning modes (ν_{6a}, ν_1 and ν_{9a}), and 2, 3, 2, 3 and 3 grid - points respectively for the bath modes (b_1, b_2, b_3, b_4 and b_5). It is important to note that the bath modes effectively behave like tuning modes. The autocorrelation functions calculated by TDDVR and DVR approaches are presented as functions of time in Fig. 6.1(b). Except for some small differences, profiles have good matching with each other during the entire propagation period. We have also performed the dynamics of the total model Hamiltonian with the same

TH-421_02612202

number of grid - points in the coupling and tuning modes and with 3, 3, 3, 2 and 2 grid - points for the bath modes, b_2, b_4, b_5, b_6 and b_7, respectively but with one

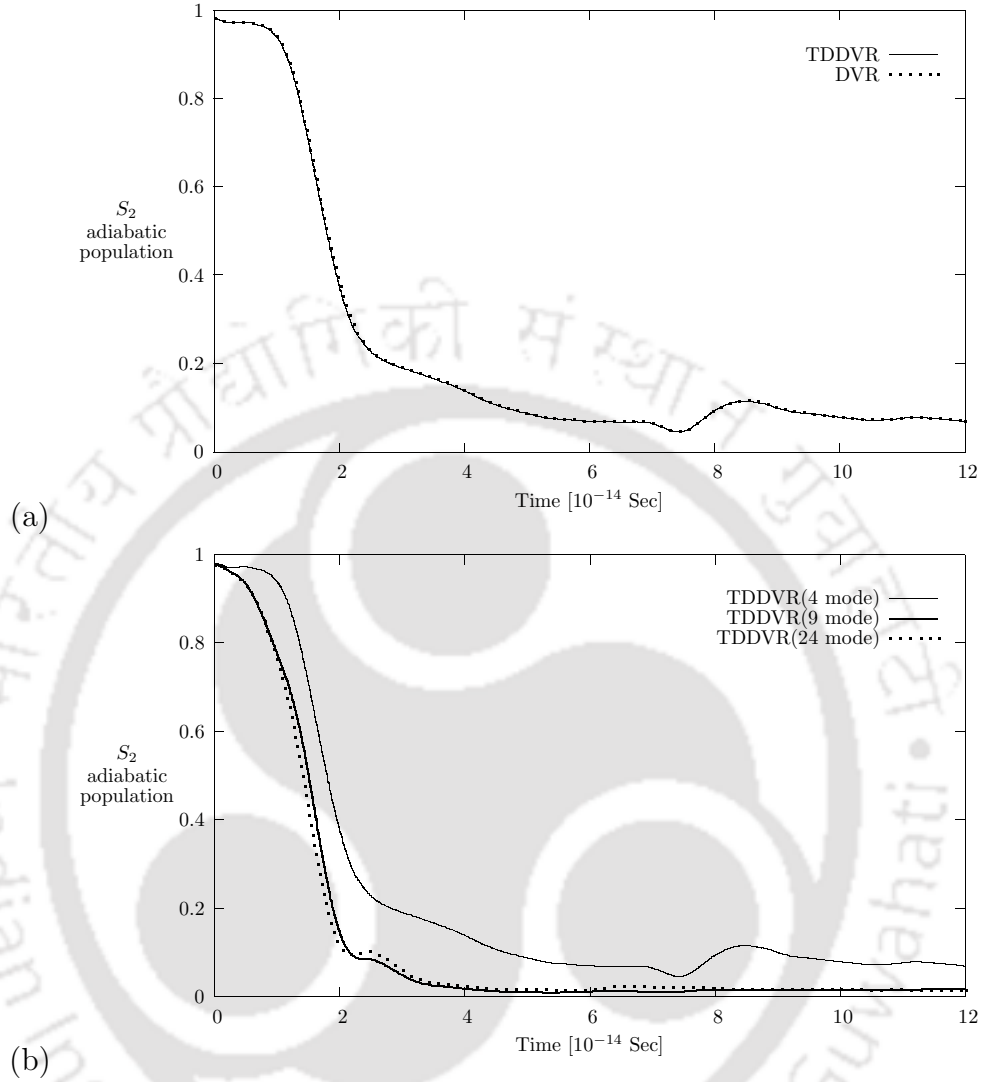

Figure 6.3: (a) TDDVR and DVR results for the adiabatic S_2 population of the four mode model as functions of time. (b) the adiabatic S_2 state population for the four, nine and twenty four mode models as functions of time.

TDDVR basis for the rest of the bath modes, b_1, b_3, b_8, b_9 ..... b_{20}. Fig. 6.1(c) displays the autocorrelation function calculated by TDDVR method for the total model Hamiltonian as a function of time. Figs. 6.1(b)-(c) indicate the sharp effect of bath modes on the system, i.e., the peaks of the autocorrelation function are not only much lower in magnitude but also they appear with more structures. These structures

TH-421_02612202

are due to the involvement of several normal mode frequencies of the Hamiltonian in the dynamics.

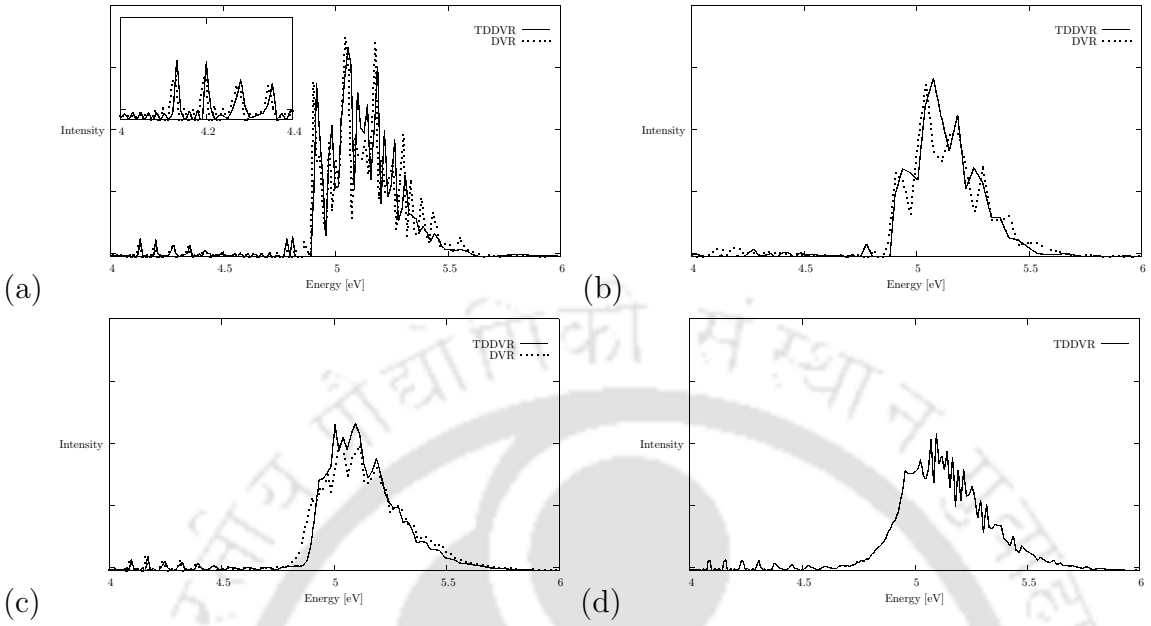

Figure 6.4: The absorption spectrum of the S_1 and S_2 states of pyrazine molecule for the four model model (a) without or (b) with phenomenological broadening where the inset in Fig. 6.4(a) is the detailed spectrum of the S_1 state. Results are compared with corresponding quantum mechanical profile. The convoluted absorption spectrum of the S_1 and S_2 states for the (c) nine and (d) twenty four mode model. The spectrum for nine mode model is compared with exact profile.

In Fig. 6.2(b), we have plotted the population of the S_2 diabatic state for the dynamics of nine mode model and total model Hamiltonian. The population dynamics of nine mode model calculated by present approach has excellent agreement with quantum dynamical results. In order to see the effect of bath modes, we have also displayed the diabatic population of S_2 state for the four mode model in the same figure. The inclusion of bath modes brings faster interstate population transfer and reduces the final population of the S_2 state. The population of the same state effectively decays to near zero after 35 fs and again rises to 0.3 around 85 fs before it decays around 100 fs. The effect is strong with the addition of first five bath modes compared to the addition of rest of the modes. Fig. 6.3(b) presents the effect of

TH-421_02612202

bath modes on the adiabatic S_2 population of the system due to the inclusion of increasing number of modes. Adiabatic population of the system also decays faster to a lower magnitude in presence of bath modes. The fast transfer of diabatic or adiabatic population is due to the lowering of conical intersection in the presence of bath modes.

Figs. 6.4(c)-(d) present the absorption spectra of pyrazine for the nine mode model and the entire model system. The effect of bath modes on the S_2 spectra is pronounced but on the form of S_1 spectra is very little. The addition of first five bath modes on the four mode model sharply reduces the structures of the S_2 spectrum appeared in the isolated system. With further inclusion of bath modes, the broad band of S_2 spectrum remains the same except for some small changes in the finer details.

It is also interesting to investigate the effect of coupling between the system and the environment by calculating the following quantities: (a) Energy flow from the system to the bath; (b) The relaxation of the system due to the bath. The instantaneous bath energy ($E_b(t)$) has been defined [148] by considering virial theorem, $2\langle\bar{T}_b\rangle_t = \langle\bar{H}_b\rangle_t + 0.5\langle\bar{H}_{sb}\rangle_t$ without including the time average as below,

$$E_b(t) = \langle H_b(t)\rangle + 0.5\langle H_{sb}(t)\rangle. \tag{6.2.26}$$

Fig. 6.5 displays the instantaneous bath energy as functions of time for the nine mode model and the total model Hamiltonian. The profiles indicate that the bath energy increases sharply upto 25 fs and then follows a plateau before the curve slowly rises from 80 fs onwards. Whenever there is energy transfer from the system to the bath, it is obvious that the system is around the conical intersection. As the number of bath modes increases, there is more and more energy flow from system to the bath. Considering the average frequency of the bath degrees of freedom and the "weak" coupling of the bath with system vis - a - vis the amount of energy transfer to the bath modes at the end of the propagation, these modes may be treated at or near

TH-421_02612202

the classical limit.

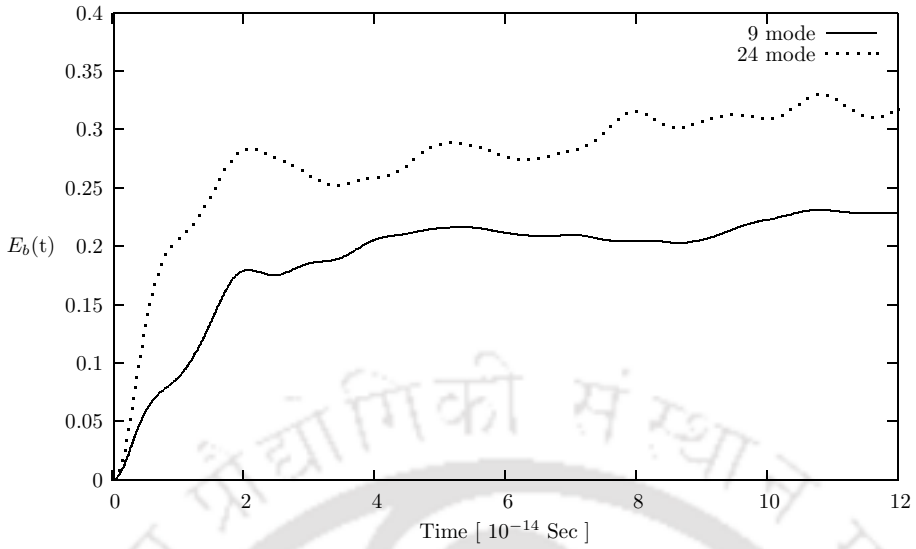

Figure 6.5: The energy transfer from the system to the bath oscillators as functions of time with increasing number of bath modes.

The effect of bath modes on the isolated system wavefunction can be followed by calculating the overlap of time - dependent wavefunctions of the model Hamiltonian with and without bath modes. Since the dimension of the wavefunction for the four mode model is different from system - bath wavefunction, we calculate the following quantity [148],

$$S(t) = tr\{\rho^{(4)}(t)\rho^{(red)}(t)\}, \tag{6.2.27}$$

where $\rho^{(4)}$ is the density matrix for the isolated system and $\rho^{(red)}$ is the reduced density matrix obtained by taking trace over bath modes.

The density overlap, $S(t)$, has been plotted as functions of time with increasing number of bath modes in Fig. 6.6. The effect of bath modes on $S(t)$ is huge and interesting. The profile decays over first 20 fs, then passes through a plateau upto 80 fs and again loses its magnitude between 80 to 100 fs. The plateau indicates that system is away from conical intersection.

All calculations are performed on a 2 CPU IBM workstation with 1 GHz processor.

TH-421_02612202

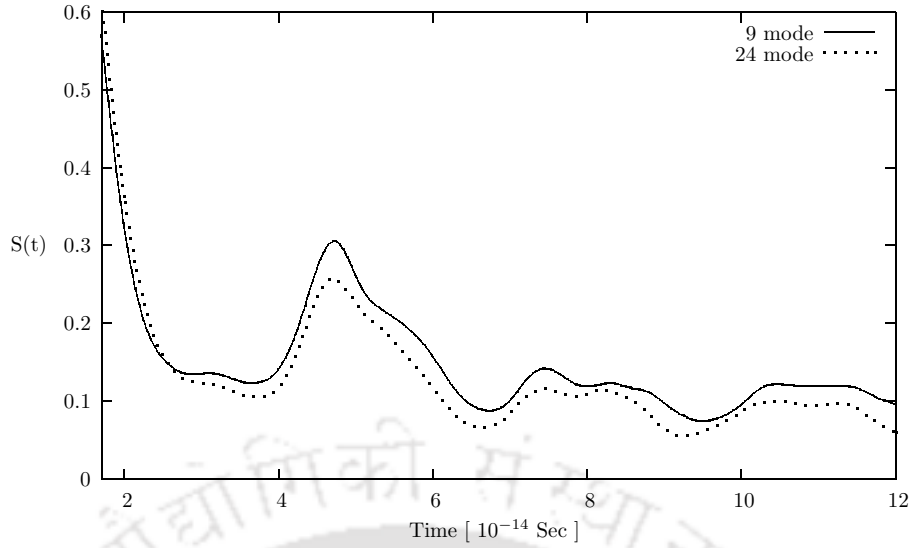

Figure 6.6: The effect of bath modes on the density overlap function (Eq. (6.2.27)) as functions of time when the system is coupled either with five or with twenty bath oscillators.

The amount of physical memory used and CPU time needed for the dynamics of four mode model are 40 MByte and 90 minutes, respectively whereas the system with five bath modes requires 3 GByte memory and 160 hour CPU time. It is important to note that the dynamics of nine mode model has been performed with more than 7 million grid - points on each surface. On the other hand, in case of total model Hamiltonian, many bath degrees of freedom are being treated with one grid - point/TDDVR basis function, where the algorithm neither requires more physical memory nor longer CPU time. TDDVR approach has enough scope to further reduce the present requirement of CPU time as well as physical memory since the contribution of different modes on the time - dependence of an amplitude of any mode can be calculated parallelly on various CPUs and the entire string of amplitudes is not needed at a time to calculate those contributions by using direct access I/O.

TH-421_02612202

6.3 Molecular dynamics with a realistic model Hamiltonian

6.3.1 The model Hamiltonian

The detail description of the system dynamics requires a suitable model Hamiltonian that incorporates the symmetry property of the molecule and should reproduce the S_1 and S_2 absorption spectra and the fast relaxation. Köppel *et al.* [161, 162] developed a model Hamiltonian consisting of four (4) vibrational modes for any such system. Though this model with *ab - initio* PE data for pyrazine molecule was found to mimic it's essential dynamics, a convolution with a broad Lorentzian was necessary to obtain good agreement between the computed [151–153] and experimental spectrum [154]. In order to eliminate this artificial inclusion of phenomenological broadening, the four mode model was extended by Krempl *et al.* [147] by including the twenty (20) remaining modes as the heat bath. The desired fast relaxation was achieved, but the model could not be expected to reproduce the S_2 absorption spectra and essential physical aspects since coupling constants among the normal modes were randomly chosen and do not retain the symmetry of the pyrazine molecule.

A further refinement of the model was made by Stock *et al.* [155], where they had introduced another seven (7) most relevant vibrational modes to the system, based on CASSCF and MRCI *ab initio* calculations. The intra - state coupling was expanded up to second order but the expansion of the inter - state coupling was restricted up to first order. This refined model obeys the proper symmetry of the pyrazine molecule but to reproduce the S_2 absorption spectra, a strong artificial broadening was included again.

Raab *et al.* [149] developed the most realistic model Hamiltonian, where both

TH-421_02612202

intra - and inter - state coupling terms were expanded up to second order as below,

$$\begin{aligned}\hat{H} &= \sum_i \frac{\omega_i}{2}(-\frac{\partial^2}{\partial Q_i^2} + Q_i^2)\mathbf{1} + \begin{pmatrix} -\triangle & 0 \\ 0 & \triangle \end{pmatrix} + \sum_{i\in G_1} \begin{pmatrix} a_i & 0 \\ 0 & b_i \end{pmatrix} Q_i \\ &+ \sum_{(i,j)\in G_2} \begin{pmatrix} a_{i,j} & 0 \\ 0 & b_{i,j} \end{pmatrix} Q_iQ_j + \sum_{i\in G_3} \begin{pmatrix} 0 & c_i \\ c_i & 0 \end{pmatrix} Q_i \\ &+ \sum_{(i,j)\in G_4} \begin{pmatrix} 0 & c_{i,j} \\ c_{i,j} & 0 \end{pmatrix} Q_iQ_j \end{aligned} \tag{6.3.1}$$

The point group of the pyrazine molecule is D_{2h}, where it's S_1 and S_2 states are B_{3u} and B_{2u} symmetry, respectively. An expansion coefficient for coupling the two electronic states is nonzero if the corresponding vibrational mode (for linear coupling) or the product of the two vibrational modes (for bilinear coupling) belongs to B_{1g} symmetry. Similarly, an expansion coefficient which leads to intra - state coupling, is nonzero if the corresponding vibrational mode (for linear coupling) or the product of the vibrational modes (for bilinear and quadratic coupling) is of symmetry A_g. The first term in the above expression represents the ground - state Hamiltonian within harmonic approximation where ω_i (Table 6.2) denotes the ground - state vibrational frequency of the ith normal mode, and Q_i is the corresponding dimensionless normal - mode coordinate $[Q_i = (x_i - x_i^{eq})(mw_i)^{-1/2}]$. The second term is the difference in energy ($2\triangle$) between the two states at Q_0. The sum G_1 denotes the linear intra - state coupling with A_g symmetry. The third sum (G_2) contains quadratic and bilinear intra - state coupling with identical symmetry (e.g., $B_{2g} \times B_{2g}$). The fourth sum (G_3) presents a single linear off - diagonal expansion term with B_{1g} symmetry for inter - state coupling between S_1 and S_2 states. The last sum (G_4) contains bilinear off - diagonal terms where the product of all pairs of modes has B_{1g} symmetry with the possible combinations like $A_g \times B_{1g}$, $B_{2g} \times B_{3g}$, $A_u \times B_{1u}$, and $B_{2u} \times B_{3u}$. Thus, there are one hundred and two (102) coupling constants a_i, b_i ,c_i, $a_{i,j}$, $b_{i,j}$ and $c_{i,j}$ which

TH-421_02612202

describe the shapes of the S_1 and S_2 potential energy surfaces (PESs) (Table 6.3 - 6.5).

Table 6.2: Experimental [160] harmonic vibrational frequencies (in eV) of the ground state of pyrazine.

Symmetry	Mode	Frequencies	Symmetry	Mode	Frequencies
A_g	ν_{6a}	0.0739	A_u	ν_{16a}	0.0423
	ν_1	0.1258		ν_{17a}	0.1190
	ν_{9a}	0.1525	B_{1u}	ν_{12}	0.1266
	ν_{8a}	0.1961		ν_{18a}	0.1408
	ν_2	0.3788		ν_{19a}	0.1840
B_{1g}	ν_{10a}	0.1139		ν_{13}	0.3734
B_{2g}	ν_4	0.0937	B_{2u}	ν_{18b}	0.1318
	ν_5	0.1219		ν_{14}	0.1425
B_{3g}	ν_{6b}	0.0873		ν_{19b}	0.1756
	ν_3	0.1669		ν_{20b}	0.3798
	ν_{8b}	0.1891	B_{3u}	ν_{16b}	0.0521
	ν_{7b}	0.3769		ν_{11}	0.0973

Table 6.3: Linear coupling constant (in eV) of the S_1 and S_2 diabatic potentials of pyrazine at the CIS level [149].

Mode	ν_{6a}	ν_1	ν_{9a}	ν_{8a}	ν_2
a_i	-0.0981	-0.0503	0.1452	-0.0445	0.0247
b_i	0.1355	-0.1710^*	0.0375	0.0168	0.0162

* The value $b_1 = -0.0171$ was taken, which lies between the MRCI and the CIS level.

6.3.2 Calculation of the spectra

The nuclear wavefunction propagated by TDDVR method is used to calculate the autocorrelation function ($C(t)$) and the Fourier transform of $C(t)$ gives S_1 and S_2 absorption spectrum,

$$I(\omega) \propto \omega \int_{-\infty}^{\infty} C(t) \exp(i\omega t) dt \tag{6.3.2}$$

TH-421_02612202

where

$$C(t) = \langle \Psi(t)|\Psi(0)\rangle \tag{6.3.3}$$

$$= \langle \Psi^{\star}(\frac{t}{2})|\Psi(\frac{t}{2})\rangle \tag{6.3.4}$$

Equation (6.3.4) is more accurate, computationally faster [163] and convenient to implement than previous Eq. (6.3.3). On the other hand, Eq. (6.3.4) is valid only if the initial wavefunction is real and the Hamiltonian is symmetric. Since the experimental spectral lines due to the resolution of the spectrometer appear broadened, one can incorporate this effect to the calculated spectra by convoluting with a suitable peaked curve. In the time - dependent picture, this phenomenological broadening is equivalent to damping the autocorrelation function by a time - dependent function as chosen below:

$$h(t) = \exp\big(-\frac{|t|}{\tau}\big) \tag{6.3.5}$$

with an appropriate parameter, τ. Though the experimental broadening alone of a spectrum requires a large value of τ ($\approx$ 150 - 250 fs), the calculated S_2 spectrum of pyrazine for the four mode model (by neglecting bath degrees of freedom) has qualitatively well agreement with the experimental one [160] with $\tau = 30$ fs.

Moreover, as the propagation of wavefunction and the calculated autocorrelation function is up to a finite time, artefacts known as Gibbs phenomenon develop in the spectrum. It can be reduced by multiplying the autocorrelation with the following function,

$$g(t) = \cos(\frac{\pi t}{2T}), \tag{6.3.6}$$

where T is the length of propagation. This function convolutes the spectrum with,

$$\tilde{g}(\omega) = \frac{4\pi T}{\pi^2 - (2\omega T)^2}\cos(\omega T). \tag{6.3.7}$$

such that C(t) is smoothened to zero.

TH-421_02612202

Table 6.4: quadratic on diagonal coupling constants (in eV) of the S_1 and S_2 diabatic potentials of pyrazine obtained at the CIS level [149]. Values specified with an asterisk are the adjusted values based on the comparison of CIS data and MRCI [151–153]/CASSCF [155] data.

A_g		ν_{6a}	ν_1	ν_{9a}	ν_{8a}	ν_2	B_{1g}		ν_{10a}
$a_{i,j}$	ν_{6a}	0.00000*	0.00108	−0.00204	−0.00135	−0.00285	$a_{i,j}$	ν_{10a}	−0.01159
	ν_1		0.00000*	0.00474	0.00154	−0.00163			
	ν_{9a}			0.00000*	0.00872	−0.00474			
	ν_{8a}				0.00000*	−0.00143			
	ν_2					0.00000*			
$b_{i,j}$	ν_{6a}	0.00000*	−0.00298	−0.00189	−0.00203	−0.00128	$b_{i,j}$	ν_{10a}	−0.01159
	ν_1		0.00000*	0.00155	0.00311	−0.00600			
	ν_{9a}			0.00000*	0.01194	−0.00334			
	ν_{8a}				0.00000*	−0.00713			
	ν_2					0.00000*			
B_{3g}		ν_{6b}	ν_3	ν_{8b}	ν_{7b}	A_u		ν_{16a}	ν_{17a}
$a_{i,j}$	ν_{6b}	−0.00741	0.01321	−0.00717	0.00515	$a_{i,j}$	ν_{16a}	0.01145*	0.00100
	ν_3		0.05183	−0.03942	0.00170		ν_{17a}		−0.02040
	ν_{8b}			−0.05733	−0.00204				
	ν_{7b}				−0.00333				
$b_{i,j}$	ν_{6b}	−0.00385	−0.00661	0.00429	−0.00246	$b_{i,j}$	ν_{16a}	−0.01459*	−0.00091
	ν_3		0.04842	−0.03034	−0.00185		ν_{17a}		−0.00618
	ν_{8b}			−0.06332	−0.00388				
	ν_{7b}				−0.00040				
B_{1u}		ν_{12}	ν_{18a}	ν_{19a}	ν_{13}	B_{2g}		ν_4	ν_5
$a_{i,j}$	ν_{12}	−0.04819	0.00525	−0.00485	−0.00326	$a_{i,j}$	ν_4	−0.02252*	−0.00049
	ν_{18a}		−0.00792	0.00852	0.00888		ν_5		−0.01825
	ν_{19a}			−0.02429	−0.00443				
	ν_{13}				−0.00492				
$b_{i,j}$	ν_{12}	−0.00840	0.00536	−0.00097	0.00034	$b_{i,j}$	ν_4	−0.03445*	0.00911
	ν_{18a}		0.00429	0.00209	−0.00049		ν_5		−0.00265
	ν_{19a}			−0.00734	0.00346				
	ν_{13}				0.00062				
B_{2u}		ν_{18b}	ν_{14}	ν_{19b}	ν_{20b}	B_{3u}		ν_{16b}	ν_{11}
$a_{i,j}$	ν_{18b}	−0.00277*	0.00016*	−0.00250	0.00357	$a_{i,j}$	ν_{16b}	−0.02176	−0.00624
	ν_{14}		0.03924*	−0.00197	−0.00355		ν_{11}		0.00315
	ν_{19b}			0.00992	0.00623				
	ν_{20b}				−0.00110				
$b_{i,j}$	ν_{18b}	−0.01179*	−0.00844*	0.07000*	−0.01249	$b_{i,j}$	ν_{16b}	−0.02214	−0.00261
	ν_{14}		0.04000*	−0.05000*	0.00265		ν_{11}		−0.00496
	ν_{19b}			0.01246	−0.00422				
	ν_{20b}				0.00069				

TH-421_02612202

Table 6.5: Quadratic off-diagonal (vibronic) coupling constants (in eV) of the S_1 and S_2 diabatic potentials of pyrazine obtained at the CIS level [149]. Values specified with an asterisk are the adjusted values based on the comparison of CIS data and MRCI [151–153] /CASSCF [155] data.

$B_{1g} \times A_g$		ν_{6a}	ν_1	ν_{9a}	ν_{8a}	ν_2
$c_{i,j}$	ν_{10a}	-0.01000^*	-0.00551	0.00127	0.00799	-0.00512
$B_{2g} \times B_{3g}$		ν_{6b}	ν_3	ν_{8b}	ν_{7b}	
$c_{i,j}$	ν_4	-0.01372	-0.00466	0.00329	-0.00031	
	ν_5	0.00598	-0.00914	0.00961	0.00500	
$A_u \times B_{1u}$		ν_{12}	ν_{18a}	ν_{19a}	ν_{13}	
$c_{i,j}$	ν_{16a}	-0.01056	0.00559	0.00401	-0.00226	
	ν_{17a}	-0.01200	-0.00213	0.00328	-0.00396	
$B_{3u} \times B_{2u}$		ν_{18b}	ν_{14}	ν_{19b}	ν_{20b}	
$c_{i,j}$	ν_{16b}	0.00118	-0.00009	-0.00285	-0.00095	
	ν_{11}	0.01281	-0.01780	0.00134	-0.00481	

6.3.3 The numerical details

The optimum number of TDDVR grid - points used are: N_{6a}=13, N_1=27, N_{9a}=9 and N_{10a}=21 for the first four modes, N_{8a}=2, N_2 =2, N_4 = 3, N_5 = 3, N_{6b}=2, N_3=1, N_{8b}=1 and N_{7b}=1 for the next eight modes and then one basis function for the remaining bath modes. We calculate the quality of the results by estimating the magnitude of the error due to the use of finite TDDVR basis in the autocorrelation function,

$$\Delta(t) = |\langle\Psi(0)|\Psi(t)\rangle - \langle\Psi'(0)|\Psi'(t)\rangle|^2 \tag{6.3.8}$$

where $\Psi'(t)$ is the wavefunction ignoring the least populated TDDVR basis function. We found that the change of autocorrelation function, $\Delta(t)$, in the four mode model and the system with eight bath modes remains below 10^{-3} on addition or subtraction of a TDDVR basis in a particular mode.

It is important to note that with a sufficient number of grid - points, TDDVR formulation is such that the calculated results appear as independent of the initial

TH-421_02612202

choice of "classical" momentum of the central trajectory and thereby, we have chosen $Q_i(t_0) = 0$ and $P_i(t_0) = 0$ for those modes. On the other hand, this choice plays a key role when a mode is treated at the classical limit (a single grid - point) or at near classical limit (few grid - points) because the dynamics is solely or essentially dictated by classical mechanics. In the present calculations, the choice of classical parameters for one grid - point dynamics are $Q_i(t_0) = 0$ and $P_i(t_0) = \sqrt{\hbar m \omega_i}$.

6.3.4 Results and discussion

The TDDVR wavefunction for the four-mode model is being propagated up to 120 fs by using 13, 27, and 9 grid - points for the tuning mode, ν_{6a}, ν_1, and ν_{9a}, respectively and 21 grid - points in the coupling mode, ν_{10a}, where a similar calculation has been performed by using relatively larger number of basis functions namely 19, 43, 13 and 29 grid - points for the mode, ν_{6a}, ν_1, ν_{9a} and ν_{10a}, respectively [45]. The Eq. (6.3.4) implies that the propagation of wavefunction up to 120 fs corresponds to 240 fs in the profile of auto - correlation function. Fig. 6.7(a) displays the absolute values of the auto - correlation functions calculated by using the above two sets of TDDVR basis functions. It shows reasonably good agreements even at the peaks, and resonances during the entire propagation, with some small exceptions at longer time. Since the loss of coherence throughout the whole propagation is small, and in principle, the TDDVR method with sufficient grid - points can reproduce the exact quantum mechanical results, we wish to perform TDDVR calculations with the smaller set of basis functions so that, the results are close enough to the exact quantum ones and more number of modes could be included explicitly in the dynamical process.

The inset in Fig. 6.8 demonstrates the calculated time - dependent probabilities of finding the four - mode subsystem on the S_2 diabatic state by using smaller and larger number of TDDVR basis functions and shows a remarkable agreement between them. The population dynamics of the S_2 diabatic state indicates the coupling between the

TH-421_02612202

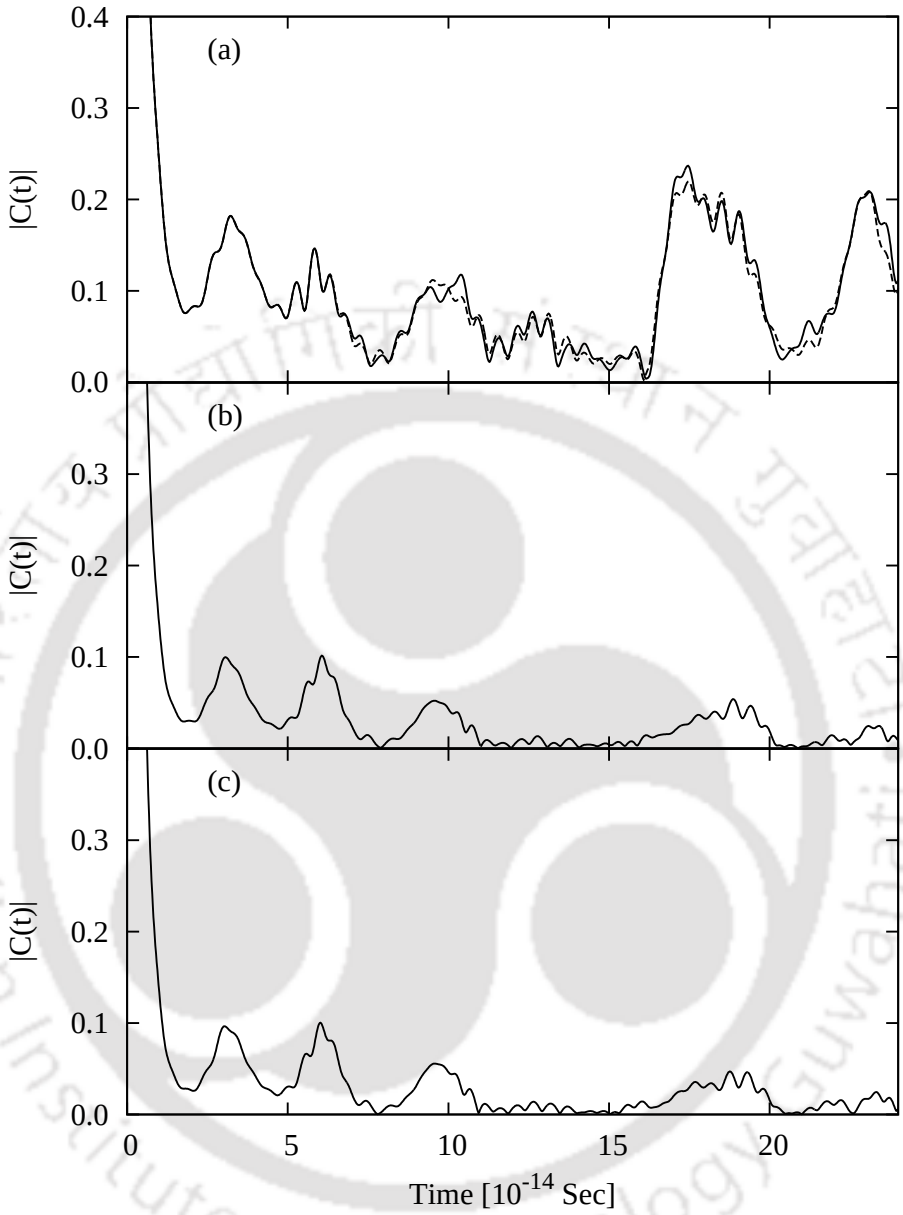

Figure 6.7: Calculated absolute values of the autocorrelation function using TD-DVR approach as functions of time for the following cases: (a) Four mode model (subsystem); (b) Subsystem coupled with eight bath modes; (c) Subsystem coupled with twenty bath modes. Fig. 6.7(a) envelope compares the results obtained by using smaller and larger sets of TDDVR basis functions.

TH-421_02612202

diabatic states in presence of conical intersection. The interstate population transfer starts almost immediately with a drop to even below 0.2 at around 45 fs and sharply arises again to 0.4 after 75 fs with a quick decay to 0.2 at around 100 fs. Though there are some repeated patterns with smaller amplitudes at longer time, but these are not much interesting to follow. In a similar manner, the inset of Fig. 6.9 displays the adiabatic S_2 state population of the four - mode subsystem as functions of time with an excellent agreement between the TDDVR profiles calculated by using two sets of basis functions. It is important to note that the initial population on the S_2 adiabatic state starts at slightly below one (1.0) since the remaining amplitude contributes to the initial adiabatic S_1 state population leading to S_1 state spectrum. Though the initial decay of the adiabatic S_2 state population is much slower compared to the diabatic one, this transfer after 10 fs in the adiabatic case is not only faster but also reduces the population to a much lower value. Finally, at around 80 fs, there is a slight increase of the adiabatic population of the S_2 state, which is negligibly small change compared to the diabatic one, but shows the effect of conical intersection at the same period of time.

Fig. 6.10(a) presents the S_2 state absorption spectrum of pyrazine calculated by using TDDVR wavefunction for the four - mode model, where the same figure includes the quantum envelope [149] indicating a reasonably good agreement. The calculated spectrum in Fig. 6.10(a) have two interesting parts namely the small discrete lines on the lower energy side show the S_1 state spectrum and the higher energy side profile originates from S_2 state. On the other hand, Fig. 6.10(b) displays convoluted S_2 state spectrum with the inclusion of a strong phenomenological broadening ($\tau = 30$ fs) and clearly demonstrates good agreement between quantum - classical (TDDVR) and quantum mechanical (MCTDH) results [149].

We have investigated the effect of bath modes on the subsystem dynamics by including different number of bath degrees of freedom. The wavefunction of the

TH-421_02612202

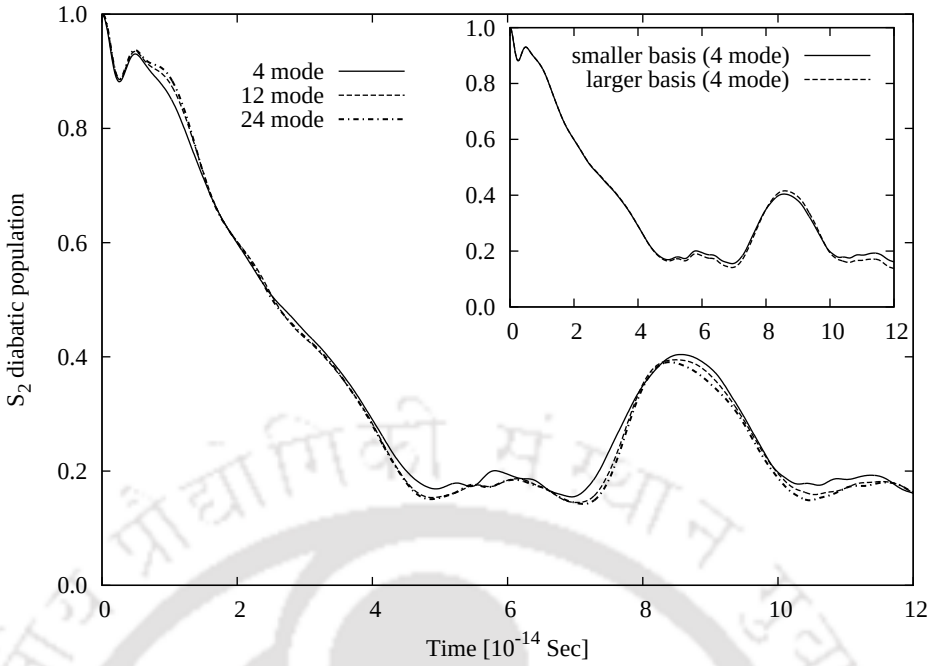

Figure 6.8: Population dynamics on the S_2 diabatic state as functions of time for the four, twelve and twenty four mode models where the inset in Fig. 2 is the result for the four mode model with smaller and larger number of TDDVR basis functions.

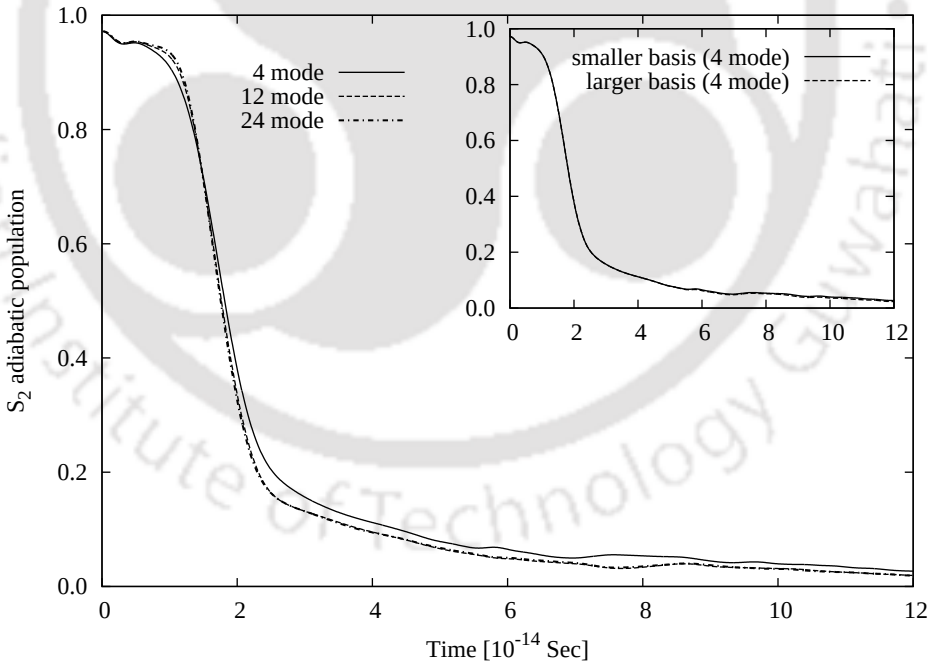

Figure 6.9: TDDVR results for the adiabatic S_2 population of the four, twelve and twenty four mode models as functions of time where the inset in Fig. 3 is the adiabatic S_2 state population for the four mode model as functions of time with two different sets of basis functions.

TH-421_02612202

twelve - mode model is being propagated by using 21 grid - points in the interstate coupling mode (ν_{10a}), 13, 27, and 9 grid - points for the tuning mode, ν_{6a}, ν_1, and ν_{9a}, respectively and 2, 2, 3, 3, 2, 1, 1, 1 grid - points for the bath mode, ν_{8a}, ν_2, ν_4, ν_5, ν_{6b}, ν_3, ν_{8b} and ν_{7b}, respectively. We have also performed the dynamics of the total model Hamiltonian with the same number of grid - points in the coupling, tuning and first eight bath modes of g symmetry as before but with one TDDVR basis for each mode of the rest bath degrees of freedom. Indeed, it is important to note that the bath modes effectively behave like tuning mode. Figures 6.7(b) and 6.7(c) display the absolute values of autocorrelation functions of the subsystem calculated by using TDDVR wavefunction for the twelve - mode and total model Hamiltonian as a functions of time. Both the figures demonstrate the sharp effect of bath modes on the subsystem. We find that the peaks of the autocorrelation functions in Figs. 6.7(b) and 6.7(c) are not only much suppressed in magnitude but also appear with more structures compared to the Fig. 6.7(a). These structures are due to the involvement of the multiple normal mode frequencies of the bath Hamiltonian in the subsystem dynamics.

Figure 6.8 displays the population dynamics of the subsystem S_2 diabatic state obtained by persuing the molecular dynamics of the twelve - mode and the total model Hamiltonian. In order to see the effect of bath modes, we have also shown the diabatic S_2 state population for the four mode model as function of time in the same figure. The inclusion of bath mode leads to a faster interstate population transfer and brings down the final population of the S_2 diabatic state. The population decays to 0.18 after 40 fs and then rises to 0.38 at around 85 fs before the final decay after 100 fs. The transfer of population with the inclusion of first eight bath modes on the four - mode model is more effective than with the addition of rest of the bath modes. In Fig. 6.9, we present the effect of increasing number of bath modes on the adiabatic S_2 state population dynamics of the subsystem. The figure clearly demonstrates that

TH-421_02612202

the adiabatic population of the subsystem in presence of bath modes decays faster to lower values than the subsystem alone. The fast transfer of the adiabatic or diabatic population and also relatively low rise of population at around 80 fs in presence of bath modes is due to the lowering of the conical intersection.

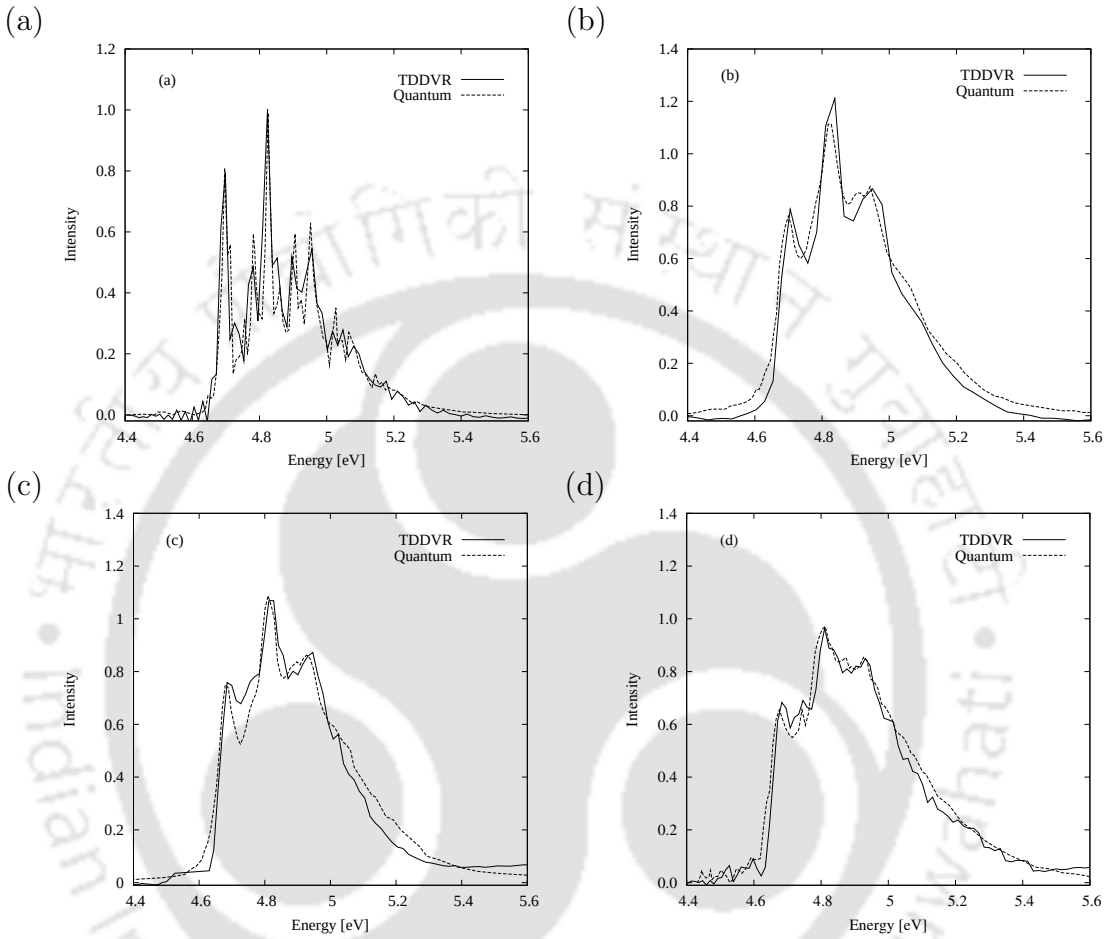

Figure 6.10: The calculated absorption spectrum of the S_2 states of pyrazine molecule for the four model model (a) without or (b) with a strong phenomenological broadening (τ=30 fs). Results are compared with corresponding quantum mechanical envelopes [149]. The convoluted absorption spectrum of the S_2 states for the (c) twelve (τ = 50 fs) and (d) twenty four (τ = 150 fs) mode model are presented and compared with quantum mechanical profile [149].

Figs. 6.10(c) and 6.10(d) show the theoretical photoabsorption spectrum of pyrazine for the twelve - mode model and the total model system along with the quantum profile. We find that the calculated spectrum have good agreement with the quantum one [149]. Moreover, it is interesting to see that the effect of bath modes on the S_2

TH-421_02612202

spectrum is very sharp in a way that only a weaker (τ = 50 fs) and the weakest (τ = 150 fs) phenomenological broadening are needed for the twelve - mode model and the total model system, respectively to reproduce quantum mechanical as well as experimental spectrum. The inclusion of first eight bath modes on the isolated subsystem reduces the structures of the four - mode S_2 spectrum and thereby, brings good matching with quantum results. On the other hand, we see that the broad band of the S_2 spectrum remain unchanged except some finer details with the addition of the rest of the bath modes.

We are also interested to investigate the effect of coupling between the subsystem and the environment and thus, have calculated the following quantities: (a) The energy flow from subsystem to the bath; (b) The relaxation of the subsystem due to the bath. The bath energy $[E_b(t)]$ as a function of time is defined by considering the virial theorem, $2\langle\bar{T}_b\rangle_t = \langle\bar{H}_b\rangle_t + 0.5\langle\bar{H}_{sb}\rangle_t$, without including the time average, $E_b(t) = \langle H_b(t)\rangle + 0.5\langle H_{sb}(t)\rangle$, where H_b and H_{sb} are the bath and subsystem - bath interaction Hamiltonian known from Eq. (6.3.1). The effect of environment on the subsystem can be monitored by calculating the overlap of time - dependent wavefunctions of the model Hamiltonian with or without including the bath modes. Since the dimension of the wavefunction for the subsystem is different from subsystem - bath wavefunction, we calculate the overlap between the density matrix ($\rho^{(4)}$) for the isolated subsystem and the reduced density matrix ($\rho^{(red)}$) by taking the trace over the bath modes as, $S(t) = tr\{\rho^{(4)}(t)\rho^{(red)}(t)\}$.

The inset in Fig. 6.11 presents the instantaneous bath energy as a function of time for the twelve - mode model. The bath energy increases up to 30 fs, then sharply decays before it steady rises around 80 fs until the end of propagation. The energy transfer from the subsystem to the bath is more effective when the system is around the conical intersection. Fig. 6.11 displays density overlap, $S(t)$, as a function of time for the twelve mode model system. The effect of the eight bath modes on $S(t)$ is huge

TH-421_02612202

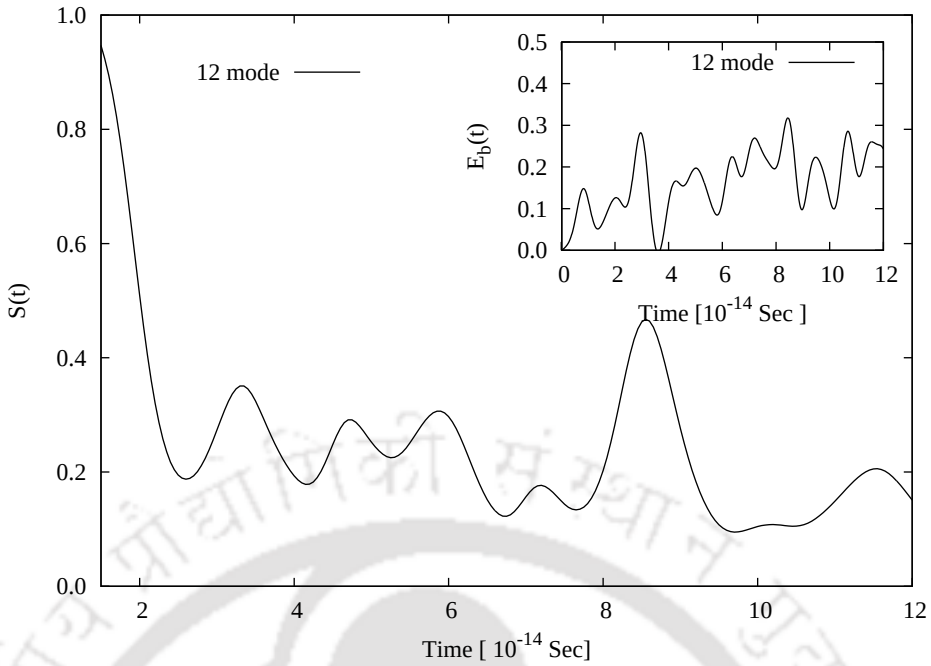

Figure 6.11: The effect of bath modes on the density overlap function as functions of time when the system is coupled with eight bath oscillators. The inset in Fig. 5 displays the energy transfer from the system to the bath oscillators as functions of time with increasing number of bath modes.

and interesting. The profile decays within first 20 fs, then passes through some small peaks before it rises sharply around 80 fs and finally decays after 100 fs. The sharp rise indicates that the system is around the conical intersection. Since the calculated profiles of $E_b(t)$ and $S(t)$ for the total model system appear as very similar to that of twelve - mode model case, those results are not being presented.

6.3.5 Computational and theoretical aspects of TDDVR and the other contemporary approaches

We have done all the calculations on a **2 CPU Sun blade 2500 work station @1.6 GHz Ultra SPARC IIIi processor with 4 GB RAM**. The amount of physical memory used and CPU time needed to perform the dynamics of four - mode model are 46 Mbytes and 45 min, respectively. The subsystem with eight bath modes requires around 3.4 Gbytes physical memory with 360 h CPU time, where the dynamics has been carried out by using 5×10^6 number of TDDVR grid - points on each surface. It is

TH-421_02612202

important to note that in case of total model Hamiltonian, since many bath degrees of freedom are being treated with one TDDVR grid - point/basis, the algorithm demands the same amount of physical memory with little more CPU time compared to the dynamics of twelve - mode Hamiltonian. On the contrary, the MCTDH [164–167] calculations were performed for the four - mode and twelve - mode model on an IBM RS/6000 power2 workstations and for the twenty - four mode model on a CRAY T90 vector computer and require [149] much less CPU time compared to the TDDVR approach. At the same time, one must note that MCTDH calculation [149] has considered the symmetry of the system or grouping of the modes due to simplicity of the Hamiltonian but at least for the time being, TDDVR method has been implemented in a robust manner leading to much higher requirement of physical memory as well as CPU time. In a similar context, we may compare the numerical efficiency of our approach with the semiclassical calculations performed on the same system. Thoss *et. al.* [157] have carried out such calculations for the 4 -, 14 - and 24 - mode linear coupling model of pyrazine on a COMPAQ XP1000 workstation with a cost of 15, 121, and 380 CPU hours and 4 Mbytes physical memory for all cases. Though such semiclassical calculations [157, 158] have clear advantage over TDDVR (even over MCTDH) at least with respect to the requirement of physical memory, the comparison between TDDVR and MCTDH approaches is more meaningful in the sense that TDDVR with sufficient grid - points on each mode tend to a quantum mechanical approach.

Though the efficiency of the MCTDH method is often significantly enhanced by grouping a number of degrees of freedom together and thereby, treating the group as a single particle known as "mode combination", MCTDH achieves further advantage by using correlation DVR (CDVR) [168] to evaluate the potential energy matrix elements very fast on the time - dependent grid with accurate correlation while employing mode combination [169]. On the other hand, since our TDDVR approach

TH-421_02612202

uses time - dependent DVR basis functions (constructed with GWP multiplied by harmonic oscillator (primitive) basis set), the calculations of potential energy matrix elements need to be performed only once for all the time. The movements of the grid - points in the TDDVR are dictated by so called "classical" mechanics and help to avoid the wastage of many grid - points to represent empty space. At this junction, we also wish to mention that the TDDVR approach has the clear scope to scale down the present necessity of physical memory and CPU time substantially since it has the possibility to parallelize the major areas of the algorithm. The contribution of different modes on a time - dependent amplitude ($\dot{d}_{i_1 i_2 \ldots . i_p, l}$) can be evaluated (Eq. (6.2.7)) independently, i.e., $\mathbf{Y_k}$ and $\mathbf{Z_k}$ matrices (Eqs. (2.3.23) and (2.3.24)) couple grid - points or basis functions of the kth mode only. This feature will allow parallelization of the algorithm, reduce computational cost remarkably and pave the possibility to pursue relatively large dimensional calculations. Moreover, we remind that the expansion of wavefunction in terms of TDDVR basis set can be such that one may also introduce the idea of mode combination either based on physical and/or symmetry consideration to reduce the present computational cost. Of course the correlation among the modes is a necessity to increase accuracy and its' implementation in our TDDVR approach is definitely possible.

TH-421_02612202

TH-421_02612202

APPENDIX A

TDDVR THEORY AND THE ABSORBING POTENTIAL

The theory is based on an expansion of the wavefunction in the Gauss - Hermite (G - H) basis set

$$\Psi(x,t) = \sum_n a_n(t)\psi_n(x,t), \tag{A1}$$

where $\psi_n(x,t)$ are the G - H basis functions

$$\psi_n(x,t) = \Phi(x,t)\phi_n(\xi,t) \tag{A2}$$

where the Gaussian wave packet ($\Phi(x,t)$) and harmonic oscillator wavefunction ($\phi_n(\xi,t)$) are

$$\Phi(x,t) = \pi^{1/4}\exp\Big(\frac{i}{\hbar}\big(\gamma(t)+p(t)(x-x(t))+ReA(x-x(t))^2\big)\Big) \tag{A3}$$

$$\phi_n(\xi,t) = \frac{1}{\sqrt{n!2^n\sqrt{\pi}}}H_n(\xi)\exp\big(-\frac{1}{2}\xi^2\big) \tag{A4}$$

with $H_n(x)$ is the Hermite polynomial and $\xi = \sqrt{2ImA(t)/\hbar}(x-x(t))$.

In order to obtain DVR representation we introduce the grid - points as zero's of the Nth basis function ($\phi_n(z)$). These zero's are the roots (z_i) of the Nth Hermite polynomial and thereby, we can introduce

$$a_n(t) = \sum_{i=1}^{N} c_i(t)\phi_n(z_i) \tag{A5}$$

Substituting Eq. (A5) in (A1), we obtain the expansion of the wavefunction in terms of time - dependent basis on a grid (DVR)

$$\Psi(x,t) = \sum_{i=1}^{N} c_i(t)\sum_n \psi_n(x,t)\phi_n(z_i). \tag{A6}$$

TH-421_02612202

Thus, the method attempts to take the best of both worlds, namely, the basis set and DVR representation. Alternatively, the basis is moving on a time - dependent grid. The amplitutes of the wavefunction are always around the center of the wave packet in the sense that the boundary grid - points hardly accumulates higher magnitudes of the amplitudes. Thus, the question of reflection from the boundary does not arise.

TH-421_02612202

APPENDIX B

FORMULATION OF TDDVR HAMILTONIAN MATRIX FOR MULTI - CURVE SYSTEMS

When the TDDVR wavefunctions (Eqs. (2.2.3) -(2.2.5)) are substituted in time - dependent Schroedinger equation (2.2.1), the general form of differential equation for any curve ($k \leq M$) is as below,

$$i\hbar\frac{\partial}{\partial t}\{\sum_i c_{ik}(t)\sum_{n=0}^{N}\xi_n^\star(x_i)\Phi'_n(s,t)\} = (\hat{T}+\hat{V}_{kk}(s))\{\sum_i c_{ik}(t)\sum_{n=0}^{N}\xi_n^\star(x_i)\Phi'_n(s,t)\}$$
$$+ \sum_{l\neq k}\hat{V}_{kl}(s))\{\sum_i c_{il}(t)\sum_{n=0}^{N}\xi_n^\star(x_i)\Phi'_n(s,t)\} \quad \text{(B1)}$$

M is the number of curves involved in the calculation, $\hat{V}_{kl}(s)$ is "diagonal" in DVR basis. Considering $x_i = \sqrt{(2ImA/\hbar)}(s_i(t) - s_c(t))$, both the operators $\frac{\partial}{\partial t}$ and $\hat{T}$ will not operate on $\xi_n^\star(x_i)$, hence Eq. (B1) can be written as,

$$i\hbar\{\sum_i \dot{c}_{ik}(t)\sum_{n=0}^{N}\xi_n^\star(x_i)\Phi'_n(s,t)\} + i\hbar\{\sum_i c_{ik}(t)\sum_{n=0}^{N}\xi_n^\star(x_i)(\frac{\partial}{\partial t}\Phi'_n(s,t))\}$$
$$= \{\sum_i c_{ik}(t)\sum_{n=0}^{N}\xi_n^\star(x_i)(\hat{T}\Phi'_n(s,t))\} + \{\sum_i c_{ik}(t)V_{kk}(s_i)\sum_{n=0}^{N}\xi_n^\star(x_i)\Phi'_n(s,t)\}$$
$$+ \sum_{l\neq k}\{\sum_i c_{ik}(t)V_{kl}(s_i)\sum_{n=0}^{N}\xi_n^\star(x_i)\Phi'_n(s,t)\} \quad \text{(B2)}$$

Evaluating the terms of $\frac{\partial}{\partial t}\Phi'_n(s,t)$ and $\hat{T}\Phi'_n(s,t)$, when we substitute back in Eq. (B2) some of them cancel each other. The terms that remain from $i\hbar\frac{\partial}{\partial t}\Phi'_n(s,t)$ are,

$$\frac{\hbar ImA}{\mu}\Phi'_n(s,t) - \dot{p}_{s_c}(t)\times(s-s_c(t))\Phi'_n(s,t) \quad \text{(B3)}$$

where

$$(s-s_c(t))\Phi'_n(s,t) = \frac{1}{2}\sqrt{\frac{\hbar}{ImA}}\{\sqrt{n+1}\Phi'_{n+1}(s,t) + \sqrt{n}\Phi'_{n-1}(s,t)\}. \quad \text{(B4)}$$

TH-421_02612202

From Eq. (B2) (after substituting Eqs. (B3) and (B4) in Eq. (B2) and projecting by a particular TDDVR basis, $\sum_{m=0}^{N} \xi_m(x_j)\Phi'^{\star}_m(s,t)\}$), we get the first term (**X**) of Eq. (2.2.17).

Similarly, the terms from $\hat{T}\Phi'_n(s,t)$ are,

$$\frac{\mu \dot{s}_c^2(t)}{2}\Phi'_n(s,t) - \frac{1}{2} \times \frac{4ImA^2}{\mu} \times (s - s_c(t))^2\Phi'_n(s,t) + \frac{\hbar ImA}{\mu} \times (2n+1)\Phi'_n(s,t) \quad \text{(B5)}$$

where

$$\begin{aligned}(s - s_c(t))^2\Phi'_n(s,t) &= \frac{\hbar}{4ImA}\{\sqrt{(n+1)(n+2)}\Phi'_{n+2}(s,t) + (2n+1)\Phi'_n(s,t) \\ &+ \sqrt{n(n-1)}\Phi'_{n-2}(s,t)\}. \end{aligned} \quad \text{(B6)}$$

Hence the terms in Eq. (B5) using Eq. (B6) can be expressed as,

$$\begin{aligned}\frac{\mu \dot{s}_c^2(t)}{2}\Phi'_n(s,t) &- \frac{\hbar ImA}{2\mu}\{\sqrt{(n+1)(n+2)}\Phi'_{n+2}(s,t) + \sqrt{n(n-1)}\Phi'_{n-2}(s,t) \\ &+ (2n+1)\Phi'_n(s,t)\} + \frac{\hbar ImA}{\mu}(2n+1)\Phi'_n(s,t) \end{aligned} \quad \text{(B7)}$$

From the first term of Eq. (B3) and the third term of Eq. (B7), we get the third term (**Y**) of Eq. (2.2.17) whereas the fourth term (**Z**) of Eq. (2.2.17) comes from the second term of (B7).

TH-421_02612202

APPENDIX C

MATRIX REPRESENTATION OF HIGHER ORDER COUPLING TERMS

Higher order coupling terms $(s - s_c)^k (k \geq 2)$, are non - diagonal in DVR (here harmonic oscillator eigenfunctions form the primitive basis) and matrix elements over $(s - s_c)^2$ are

$$
\begin{aligned}
Z'_{ij} &= \langle \sum_k \xi_k(x_i) \phi'^*_k(s,t) \Big| (s-s_c)^2 \Big| \sum_l \xi^*_l(x_j) \phi'_l(s,t) \rangle \\
&= \sum_{kl} \xi_k(x_i) \xi^*_l(x_j) \int \phi'^*_k(s,t) | (s-s_c)^2 \phi'_l(s,t) ds \\
&= \frac{\hbar}{4ImA} \Bigg[\sum_{kl} \xi_k(x_i) \xi^*_l(x_j) \Big\{ \sqrt{(l+1)(l+2)} \times \phi'^*_k(s,t) \phi'_{l+2}(s,t) ds \\
&+ \sqrt{l(l-1)} \int \phi'^*_k(s,t) \phi'_{l-2}(s,t) ds + (2l+1) \int \phi'^*_k(s,t) \phi'_l(s,t) ds \Big\} \Bigg], \\
Z_{ij} &= \sum_{k=0}^{N-2} \xi^*_{k+2}(x_j) \sqrt{(k+1)(k+2)} \xi_k(x_i) + \sum_{k=2}^{N} \xi^*_{k-2}(x_j) \sqrt{k(k-1)} \xi_k(x_i) \\
&+ \sum_{k=0}^{N} \xi^*_k(x_j)(2k+1) \xi_k(x_i), \qquad \text{(C1)}
\end{aligned}
$$

where x_i's are the roots of the Hermite polynomials. If we assume that the Z matrix is diagonal, off-diagonal elements of $\sum_{k=0}^{N} \xi^*_k(x_j)(2k+1)\xi_k(x_i)$ should compensate for the corresponding elements of the first two sum in Eq. (C1). *But that is not the case; at least numerical calculation shows Z is very much a full matrix.*

If we wish to construct a 2×2 Z matrix, we need the following three Hermite

TH-421_02612202

polynomials:

$$\begin{aligned} H_0(x) &= 1 \\ H_1(x) &= 2x, \\ H_2(x) &= 4x^2 - 2, \end{aligned} \tag{C2}$$

and the corresponding Harmonic oscillator basis functions are

$$\begin{aligned} \xi_0(x) &= (\frac{2ImA}{\pi\hbar})^{1/4} \exp(-x^2/2), \\ \xi_1(x) &= (\frac{2ImA}{\pi\hbar})^{1/4} \sqrt{2} \exp(-x^2/2)x \\ \xi_2(x) &= (\frac{2ImA}{\pi\hbar})^{1/4} \frac{1}{2\sqrt{2}} \exp(-x^2/2)(4x^2 - 2). \end{aligned} \tag{C3}$$

The roots of the highest Hermite polynomial ($H_2(x)$) will be ($4x^2 - 2 = \quad x_1 = +1/\sqrt{2}$ and $x_2 = -1/\sqrt{2}$. From Eq. (B1) we can write Z_{12} as

$$\begin{aligned} Z_{12} &= \xi_2^*(x_2)\sqrt{2}\xi_0(x_1) + \xi_0^*(x_2)\sqrt{2}\xi_2(x_1) \\ &+ \xi_0^*(x_2)\xi_0(x_1) + \xi_1^*(x_2)3\xi_1(x_1) \\ &+ \xi_2^*(x_2)5\xi_2(x_1) \end{aligned} \tag{C4}$$

The first and second terms of Z_{12} came from first and second sum of Z_{ij}, respectively, and the last three terms of Z_{12} are from the third sum of Z_{ij}. [*It is important to note that in Z_{12} a three harmonic oscillator basis and two roots of the highest Hermite polynomials, $H_2(x)$ are involved.*]

We simplify Eq. (C4) by noting that $\xi_2(x_1)$ and $\xi_2(x_2)$ (also their complex conjugate, as they are real functions) are zero as x_1 and x_2 are roots of $H_2(x)$,

$$Z_{12} = \xi_0^*(x_2)\xi_0(x_1) + \xi_1^*(x_2)3\xi_1(x_1) \tag{C5}$$

TH-421_02612202

Substituting ξ_0 and ξ_1 [from Eq. (C3)] for the roots x_1 and x_2 in Eq. (C5), we get

$$\begin{aligned} Z_{12} &= (\frac{2ImA}{\pi\hbar})^{1/2} \exp(-x_1^2/2) \exp(-x_2^2/2) \\ &+ (\frac{2ImA}{\pi\hbar})^{1/2} \exp(-x_1^2/2) \exp(-x_2^2/2) 3\sqrt{2}x_1\sqrt{2}x_2 \\ &= (\frac{2ImA}{\pi\hbar})^{1/2} \exp(-x_1^2/2) \exp(-x_2^2/2)(1+6x_1x_2) \\ &= -2(\frac{2ImA}{\pi\hbar})^{1/2} \exp(-x_1^2/2) \exp(-x_2^2/2) \neq 0 \end{aligned} \tag{C6}$$

Table 2.1 indicates that we have calculated the correct roots of the Hermite polynomial because they can form an orthogonal DVR basis. With these roots, we have calculated a Z matrix (see Table 2.4).

TH-421_02612202

TH-421_02612202

APPENDIX D

DERIVATION OF QUANTUM FORCE FOR ELECTRONIC TRANSITION

When we substitute Eq. (B2) along with Eqs. (B3) and (B5) of Appendix B in Eq. (2.3.27), we obtain

$$I = \int ds F^{\star}(s,t) F(s,t) \tag{D1}$$

where

$$F(s,t) \equiv \begin{pmatrix} f_1(s,t) \\ f_2(s,t) \\ . \\ . \\ f_k(s,t) \end{pmatrix} \tag{D2}$$

and for a particular curve (k), the functional $f_k(s,t)$ takes the following form

$$\begin{aligned} f_k(s,t) &= i\hbar \sum_i \dot{c}_{ik}(t) \sum_n \xi_n^{\star}(x_i)\Phi'_n(s,t) - \dot{p}_{s_c}(t) \sum_i c_{ik}(t) \\ &\times \sum_n \xi_n^{\star}(x_i)(s - s_c(t))\Phi'_n(s,t) - \frac{\mu \dot{s}_c^2(t)}{2} \sum_i c_{ik}(t) \sum_n \xi_n^{\star}(x_i)\Phi'_n(s,t) \\ &+ \frac{2ImA^2}{\mu} \sum_i c_{ik}(t) \sum_n \xi_n^{\star}(x_i)(s - s_c(t))^2 \Phi'_n(s,t) \\ &- \frac{\hbar ImA}{\mu} \sum_i c_{ik}(t) \sum_n \xi_n^{\star}(x_i) 2n \Phi'_n(s,t) - \sum_i c_{ik}(t) V_{kk}(s_i) \sum_n \xi_n^{\star}(x_i)\Phi'_n(s,t) \\ &- \sum_{l \neq k} \sum_i c_{il}(t) V_{kl}(s_i) \sum_{n=0}^{N} \xi_n^{\star}(x_i)\Phi'_n(s,t) \end{aligned} \tag{D3}$$

The rigorous expresion of $\dot{p}_{s_c}$ can be derived[36] by minimizing integral (C1) with

TH-421_02612202

respect to $\dot{p}_{s_c}$,

$$
\begin{aligned}
& \frac{dI}{d\dot{p}_{s_c}} = 0 \\
= \;& i\hbar \sum_k \sum_{ij} (\dot{c}^\star_{ik}(t) c_{jk}(t) - c^\star_{ik}(t)\dot{c}_{jk}(t)) \\
\times \;& \sum_{nm} \xi_n(x_i)\xi^\star_m(x_j) \int (s - s_c(t)) \Phi'^\star_n(s,t)\Phi'_m(s,t) ds \\
+ \;& 2\dot{p}_{s_c}(t) \sum_k \sum_{ij} c^\star_{ik}(t) c_{jk}(t) \sum_{nm} \xi_n(x_i)\xi^\star_m(x_j) \int (s - s_c(t))^2 \Phi'^\star_n(s,t)\Phi'_m(s,t) ds \\
+ \;& \mu \dot{s_c}^2(t) \sum_k \sum_{ij} c^\star_{ik}(t) c_{jk}(t) \sum_{nm} \xi_n(x_i)\xi^\star_m(x_j) \int (s - s_c(t)) \Phi'^\star_n(s,t)\Phi'_m(s,t) ds \\
- \;& \frac{4ImA^2}{\mu} \sum_k \sum_{ij} c^\star_{ik}(t) c_{jk}(t) \sum_{nm} \xi_n(x_i)\xi^\star_m(x_j) \int (s - s_c(t))^3 \Phi'^\star_n(s,t)\Phi'_m(s,t) ds \\
+ \;& \frac{2\hbar ImA}{\mu} \sum_k \sum_{ij} c^\star_{ik}(t) c_{jk}(t) \sum_{nm} \xi_n(x_i)\xi^\star_m(x_j) 2n \int (s - s_c(t)) \Phi'^\star_n(s,t)\Phi'_m(s,t) ds \\
+ \;& \sum_k \sum_{ij} c^\star_{ik}(t) c_{jk}(t) V_{kk}(s_j) \sum_{nm} \xi_n(x_i)\xi^\star_m(x_j) \int (s - s_c(t)) \Phi'^\star_n(s,t)\Phi'_m(s,t) ds \\
+ \;& \sum_k \sum_{ij} c^\star_{ik}(t) c_{jk}(t) V_{kk}(s_i) \sum_{nm} \xi_n(x_i)\xi^\star_m(x_j) \int (s - s_c(t)) \Phi'^\star_n(s,t)\Phi'_m(s,t) ds \\
+ \;& \sum_{kl,k\neq l} \sum_{ij} c^\star_{ik}(t) c_{jl}(t) V_{kl}(s_j) \sum_{nm} \xi_n(x_i)\xi^\star_m(x_j) \int (s - s_c(t)) \Phi'^\star_n(s,t)\Phi'_m(s,t) ds \\
+ \;& \sum_{kl,k\neq l} \sum_{ij} c^\star_{ik}(t) c_{jl}(t) V_{kl}(s_i) \sum_{nm} \xi_n(x_i)\xi^\star_m(x_j) \int (s - s_c(t)) \Phi'^\star_n(s,t)\Phi'_m(s,t) ds \qquad \text{(D4)}
\end{aligned}
$$

Projecting Eq. (B2) by a particular TDDVR basis, $\sum_{p=0}^{N} \xi_p(x_l)\Phi'^\star_p(s,t)$, we obtain

$$
\begin{aligned}
& i\hbar \dot{c}_{ik}(t) \\
= \;& \frac{\dot{p}_{s_c}(t) \sum_j c_{jk}(t) \sum_{pq} \xi^\star_p(x_j)\xi_q(x_i) \int \Phi'^\star_q(s,t)(s - s_c(t))\Phi'_p(s,t) ds}{\sum_p \xi^\star_p(x_i)\xi_p(x_i)} + \frac{\mu \dot{s}_c^2(t)}{2} c_{ik}(t) \\
- \;& \frac{2ImA^2}{\mu} \frac{\sum_j c_{jk}(t) \sum_{pq} \xi^\star_p(x_j)\xi_q(x_i) \int \Phi'^\star_q(s,t)(s - s_c(t))^2 \Phi'_p(s,t) ds}{\sum_p \xi^\star_p(x_i)\xi_p(x_i)} \\
+ \;& \frac{\hbar ImA}{\mu} \frac{\sum_j c_{jk}(t) \sum_p \xi^\star_p(x_i)\xi_p(x_j) 2p}{\sum_p \xi^\star_p(x_i)\xi_p(x_i)} + V_{kk}(s_i) c_{ik}(t) + \sum_{l\neq k} V_{kl}(s_i) c_{il}(t) \qquad \text{(D5)}
\end{aligned}
$$

Substituting (D5) in (D4) and after some algebraic simplification (!), the compact

TH-421_02612202

form of $\dot{p}_{s_c}$ can be written as

$$\begin{aligned}
\dot{p}_{s_c}(t) &= \Big[\frac{2ImA^2}{\mu}\Big\{\sum_k\sum_{ij} c^\star_{ik}(t)\frac{\sum_{i'} c_{i'k}(t)S^{(2)}_{i'j}}{A_{jj}}S^{\star(1)}_{ij} \\
&+ \sum_k\sum_{ij}\frac{\sum_{i'} c^\star_{i'k}(t)S^{\star(2)}_{i'i}}{A_{ii}}c_{jk}(t)S^{\star(1)}_{ij} - 2\sum_k\sum_{ij} c^\star_{ik}(t)c_{jk}(t)S^{\star(3)}_{ij}\Big\} \\
&- \frac{\hbar ImA}{\mu}\Big\{\sum_k\sum_{ij} c^\star_{ik}(t)\frac{\sum_{i'} c_{i'k}(t)R_{i'j}}{A_{jj}}S^{\star(1)}_{ij} \\
&+ \sum_k\sum_{ij}\frac{\sum_{i'} c^\star_{i'k}(t)R^\star_{i'i}}{A_{ii}}c_{jk}(t)S^{\star(1)}_{ij} - 2\sum_k\sum_{ij} c^\star_{ik}(t)c_{jk}(t)T^\star_{ij}\Big\}\Big] \\
&\Big/ \Big[\sum_k\sum_{ij} c^\star_{ik}(t)\frac{\sum_{i'} c_{i'k}(t)S^{(1)}_{i'j}}{A_{jj}}S^{\star(1)}_{ij} + \sum_k\sum_{ij}\frac{\sum_{i'} c^\star_{i'k}(t)S^{\star(1)}_{i'i}}{A_{ii}}c_{jk}S^{\star(1)}_{ij} \\
&- 2\sum_k\sum_{ij} c^\star_{ik}(t)c_{jk}(t)S^{\star(2)}_{ij}\Big] \qquad \text{(D6)}
\end{aligned}$$

where

$$\begin{aligned}
R_{ij} &= \sum_p \xi^\star{}_p(x_i)\xi_p(x_j)2p \\
S^{(n)}_{ij} &= \sum_{pq}\xi^\star{}_p(x_i)\xi_q(x_j)\int \Phi'^\star_q(s,t)(s-s_c(t))^n\Phi'_p(s,t)ds \\
T_{ij} &= \sum_{pq}\xi_p(x_i)\xi^\star{}_q(x_j)2p\int \Phi'^\star_p(s,t)(s-s_c(t))\Phi'_q(s,t)ds \\
A_{ij} &= \sum_p \xi^\star{}_p(x_i)\xi_p(x_j) \qquad \text{(D7)}
\end{aligned}$$

with

$$\begin{aligned}
\int \Phi'^\star_p(s,t)(s-s_c(t))\Phi'_q(s,t)ds &= \frac{1}{2}\sqrt{\frac{\hbar}{ImA}}\{\sqrt{p+1}\delta_{p+1,q}+\sqrt{p}\delta_{p-1,q}\} \\
\int \Phi'^\star_p(s,t)(s-s_c(t))^2\Phi'_q(s,t)ds &= \frac{\hbar}{4ImA}\times\{\sqrt{(p+1)(p+2)}\delta_{p+2,q}+(2p+1)\delta_{p,q} \\
&+ \sqrt{p(p-1)}\delta_{p-2,q}\} \\
\int \Phi'^\star_p(s,t)(s-s_c(t))^3\Phi'_q(s,t)ds &= \frac{1}{8}(\frac{\hbar}{ImA})^{3/2}\times\{\sqrt{(p+1)(p+2)(p+3)}\delta_{p+3,q} \\
&+ 3(p+1)\sqrt{p+1}\delta_{p+1,q}+3p\sqrt{p}\delta_{p-1,q} \\
&+ \sqrt{p(p-1)(p-2)}\delta_{p-3,q}\} \qquad \text{(D8)}
\end{aligned}$$

TH-421_02612202

Matrices (R, $S^{(n)}$, T and A) involved in Eq. (D6) are time - independent and can be calculated once for all the time while the time - dependence of $\dot{p}_{s_c}$ arises from the coefficient $\{c_{il}(t)\}$. *At this point, it is important to note that $\dot{p}_{s_c}$ does not depend explicitly on the potential of the system unlike its form in ref.[27].* Those terms which are diagonal (or considered as "diagonal") in DVR as shown in equation (D4), vanish when (D5) is substituted in (D4).

We can further simplify equation (D6) when we replace $S^{(1)}_{ij}$ by $S^{(1)}_{ij}\delta_{ij}$ as first order term $(s - s_c(t))$ is diagonal in DVR (Table 2.2),

$$\begin{aligned}
\dot{p}_{s_c}(t) &= \sum_{ijl_1l_2\ldots l_k} c^{\star}_{il_1l_2\ldots l_k}(t)c_{jl_1l_2\ldots l_k}(t)\Bigg\{\frac{2ImA^2}{\mu}\Big[S^{(2)}_{ij}\frac{S^{(1)\star}_{ii}}{A_{ii}} - S^{(3)}_{ij}\Big] \\
&- \frac{\hbar ImA}{\mu}\Big[R_{ij}\frac{S^{(1)\star}_{ii}}{A_{ii}} - T^{\star}_{ij}\Big]\Bigg\}\Bigg/\Bigg[\sum_{il_1l_2\ldots l_k} c^{\star}_{il_1l_2\ldots l_k}(t)c_{il_1l_2\ldots l_k}(t)\frac{S^{(1)\star}_{ii}S^{(1)}_{ii}}{A_{ii}} \\
&- \sum_{ijl_1l_2\ldots l_k} c^{\star}_{il_1l_2\ldots l_k}(t)c_{jl_1l_2\ldots l_k}(t)S^{\star(2)}_{ij}\Bigg]
\end{aligned} \tag{D9}$$

TH-421_02612202

APPENDIX E

TDDVR AS AN EFFECTIVELY MULTI - TRAJECTORY APPROACH

In the multi - dimensional DVR representation (Eqs. (2.3.5) -(2.3.8)), $i_k th$ basis function corresponds to the $i_k th$ grid - point ($s^k_{i_k}$) where k indicates a particular mode. Again $i_k th$ grid - point ($s^k_{i_k}$) is related with $i_k th$ root ($x^k_{i_k}$) of the Hermite polynomial,

$$x^k_{i_k} = \sqrt{\frac{2ImA^k}{\hbar}}(s^k_{i_k}(t) - s^k_c(t)). \tag{E1}$$

From the property of the TDDVR basis,

$$\psi_{i_k}(s^k, t) = \sum_{n=0}^{N} \xi^\star_n(x^k_{i_k})\Phi_n(s^k, t) \approx \delta(s^k - s^k_{i_k}), \tag{E2}$$

we can infer that the contribution of G-H ($\{\Phi_n(s^k, t)\}$) basis set to the $i_k th$ TDDVR basis comes through the amplitudes only at the point, $s^k_{i_k}$. The nth G-H at the grid - point, s^k_{ik}, is,

$$\Phi_n(s^k_i, t) = \pi^{1/4} \exp(\frac{i}{\hbar}\{p_{s^k_c}(t)[s^k_{i_k} - s^k_c(t)]\})\xi_n(x^k_{i_k}) \tag{E3}$$

We can rewrite the "classical" momentum term in the exponent of G-H as,

$$\Phi_n(s^k_{i_k}, t) = \pi^{1/4} \exp(\frac{i}{\hbar}\{p_{s^k_c}(t)[\frac{1}{1 + \frac{s^k_c(t)}{x^k_{i_k}} \times \sqrt{\frac{2ImA^k}{\hbar}}}]\} \times s^k_{i_k})\xi_n(x^k_{i_k}) \tag{E4}$$

The position, $s^k_{i_k}$(t) and momentum, $p^k_{i_k}$(t) of the $i_k th$ TDDVR function is different

TH-421_02612202

from the $i'_k th$ TDDVR function as below,

$$p^k_{i_k}(t) = p_{s^k_c}(t) \times \left[\frac{1}{1 + \frac{s^k_c(t)}{x^k_{i_k}} \times \sqrt{\frac{2ImA^k}{\hbar}}} \right] \tag{E5}$$

$$s^k_{i_k}(t) = s^k_c(t) + \sqrt{\frac{\hbar}{2ImA^k}} \times x^k_{i_k}, \tag{E6}$$

where $i_k = 1, 2.....N_k$, $k = 1, 2.....p$ and $l = 1, 2.....M$. N_k is the number of TDDVR grid - points in the kth mode where p and M are the total number of modes and surfaces, respectively involved in a system.

Time - dependence of TDDVR grid - points, $\{s^k_{i_k}(\mathrm{t})\}$ and their momenta, $\{p^k_{i_k}(\mathrm{t})\}$ are solely dictated by "classical" variables $s^k_c(t)$ and $p^k_{s_c}(t)$. Moreover, in case of TDDVR propagation, quantum calculations are performed on the potential evaluated at the time - dependent grid - points, $\{s^k_{i_k}(\mathrm{t})\}$. On the other hand, in DVR, $\{s^k_{i_k}\}$ are time - independent and $\{p^k_{i_k}\}$ are zero for all time because not only $p^k_{s_c}$ is zero at t=0 but also it does not change with time.

TH-421_02612202

LIST OF PUBLICATIONS

1. A quantum - classical treatment of non - adiabatic transitions; P. Puzari, S. A. Deshpande, and S. Adhikari, Chem. Phys. **300**, 305 (2004).

2. Semi - classical Formulation of Time Dependent Discrete Variable Representation Method; P. Puzari and S. Adhikari, Int. J. Quant. Chem. **98**, 434 (2004).

3. A Quantum - classical dynamics of scattering processes in adiabatic and diabatic representations; P. Puzari, B. Sarkar, and S. Adhikari, J. Chem. Phys. **121**, 707 (2004).

4. Quantum Dynamics of Inelastic Scattering with a Moving Grid; P. Puzari, B. Sarkar, and S. Adhikari, Int. J. Quant. Chem. **105**, 209 (2005).

5. A quantum - classical approach to the photoabsorption spectrum of pyrazine; P. Puzari, R. S. Swathi, B. Sarkar, and S. Adhikari, J. Chem. Phys. **123**, 134317 (2005).

6. Matrix representation of vector potential: DVR and TDDVR formulations and dynamics; P. Puzari, B. Sarkar, and S. Adhikari, Chem. Phys. **324**, 497 (2006).

7. A quantum - clasical approach to the molecular dynamics of pyrazine with a realistic model Hamiltonian; P. Puzari, B. Sarkar, and S. Adhikari, J. Chem. Phys. **125**, 194316 (2006).

TH-421_02612202

TH-421_02612202

Bibliography

[1] J. N. Murrell, S. Carter, S. C. Farantos, P. Huxley, and A. J. C. Varandas, *Molecular Potential Energy Functions* (John Wiley & Sons, New York, 1984).

[2] D. M. Hirst, *Potential Energy Surfaces* (Taylor & Francis, London, 1985).

[3] R. P. Feynman and A. R. Hibbs, *Quantum Mechanics and Path Integrals* (McGraw-Hill, New York, 1965).

[4] M. F. Trotter, Proc. Am. Math. Soc. **10**, 545 (1959).

[5] N. Makri and W. H. Miller, Chem. Phys. Lett. **151**, 1 (1981).

[6] N. Makri, Comput. Phys. Commun. **63**, 389 (1991).

[7] W. H. Press, B. P. Flannery, S. A. Teukolsky, and W. T. Vetterling, *Numerical Recipes* (Cambridge University Press, Cambridge, 1986).

[8] Z. Bačić and J. C. Light, J. Chem. Phys. **85**, 4594 (1986).

[9] Z. Bačić and J. C. Light, J. Chem. Phys. **87**, 4008 (1987).

[10] M. Abramowitz and I. A. Stegun, *Handbook of Mathematical Functions* (Dover Publications, New York, 1965).

[11] R. Kosloff, Ann. Rev. Phys. Chem. **45**, 145 (1994).

[12] J. K. Cullum and R. A. Willoughby, *Lanczos Algorithms for Large Symmetric Eigenvalue Computations* (Birkhaüser, Boston, 1985).

[13] G. D. Billing, Int. Revs. Phys. Chem. **13**, 309 (1994).

[14] G. D. Billing, Chem. Phys. **189**, 523 (1994).

[15] G. D. Billing, *Encyclopedia of Computational Chemistry*, edited by H. F. Schaefer III (Wiley, New York, 1998).

[16] S. Adhikari and G. D. Billing, J. Chem. Phys. **113**, 1409 (2000).

[17] G. D. Billing and S. Adhikari, Chem. Phys. Lett. **321**, 197 (2000).

[18] G. C. Schatz and M. A. Ratner, *Quantum Mechanics in Chemistry* (Prentice Hall, Englewood Cliffs, NJ, 1993).

[19] E. J. Heller, J. Chem. Phys. **62**, 1544 (1975).

[20] S. Y. Lee and E. J. Heller, J. Chem. Phys. **76**, 3035 (1982).

[21] S. Y. Lee, Chem. Phys. **108**, 451 (1986).

TH-421_02612202

[22] R. D. Coalson and M. Karplus, Chem. Phys. Lett. **90**, 301 (1982).

[23] H. -D. Meyer, Chem. Phys. **61**, 365 (1981).

[24] K. B. M⊘ller and N. E. Henriksen, J. Chem. Phys. **105**, 5037 (1996).

[25] J. Kucar and H. -D. Meyer, J. Chem. Phys. **90**, 5566 (1989).

[26] D. Hsu and D. F. Coker, J. Chem. Phys. **96**, 4266 (1992).

[27] G. D. Billing, J. Chem. Phys. **107**, 4286 (1997).

[28] S. Adhikari and G. D. Billing, Chem. Phys. Lett. **305**, 109 (1999).

[29] S. Adhikari and G. D. Billing, J. Chem. Phys. **111**, 48 (1999).

[30] S. Adhikari and G. D. Billing, Chem. Phys. Lett. **309**, 249 (1999).

[31] J. V. Lill, G. A. Parker, and J. C. Light, Chem. Phys. Lett. **89**, 483 (1982).

[32] R. W. Heather and J. C. Light, J. Chem. Phys. **79**, 147 (1983).

[33] J. V. Lill, Ph. D. thesis, University of Chicago, 1982.

[34] J. C. Light, I. P. Hamilton, and J. V. Lill, J. Chem. Phys. **82**, 1400 (1985).

[35] Z. Bačić and J. C. Light, Annu. Rev. Phys. Chem. **40**, 469 (1989).

[36] B. Barkakaty and S. Adhikari, J. Chem. Phys. **118**, 5302 (2003).

[37] P. A. M. Dirac, Proc. Cambridge Philos. Soc. **26**, 376 (1930).

[38] I. S. Gradshteyn and I. M. Ryzhik, *Table of Integrals Series and Products* (Academic Press, New York, 1965).

[39] P. Puzari, S. A. Deshpande, and S. Adhikari, Chem. Phys. **300**, 305 (2004).

[40] P. Puzari and S. Adhikari, Int. J. Quant. Chem. **98**, 434 (2004).

[41] P. Puzari, B. Sarkar, and S. Adhikari, J. Chem. Phys. **121**, 707 (2004).

[42] P. Puzari, B. Sarkar, and S. Adhikari, Int. J. Quant. Chem. **105**, 209 (2005).

[43] P. Puzari, B. Sarkar, and S. Adhikari, Chem. Phys. **324**, 497 (2006).

[44] P. Puzari, R. S. Swathi, B. Sarkar, and S. Adhikari, J. Chem. Phys **123**, 134317 (2005).

[45] P. Puzari, B. Sarkar, and S. Adhikari, J. Chem. Phys. *in press* (2006).

[46] D. Kosloff and R. Kosloff, J. Comput. Phys. **52**, 35 (1983).

TH-421_02612202

[47] D. J. Tannor, A. Besprozvannaya, and C. J. Williams, J. Chem. Phys. **96**, 2998 (1992).

[48] H. Guo, J. Chem. Phys. **96**, 6629 (1992).

[49] E. Sim and N. Makri, J. Chem. Phys. **102**, 5616 (1995).

[50] D. J. Kouri, X. Ma, W. Zhu, B. M. Petit, and D. K. Hoffman, J. Phys. Chem. **96**, 9622 (1992).

[51] Y. Huang, D. J. Kouri, M. Arnold, T. L. Marchioro II, and D. K. Hoffman, J. Chem. Phys. **99**, 1028 (1993).

[52] G. D. Billing and K. V. Mikkelsen, *Advanced Molecular Dynamics and Chemical Kinetics* (John Wiley, New York, 1997).

[53] N. Makri and W. H. Miller, J. Chem. Phys. **87**, 5781 (1987).

[54] G. D. Billing and G. Jolicard, Chem. Phys. Lett. **221**, 75 (1994).

[55] M. Gilibert and M. Baer, J. Phys. Chem. **98**, 12822 (1994).

[56] G. Schatz, J. Phys. Chem. **99**, 7522 (1995).

[57] S. L. Mielke, G. J. Tawa, D. G. Truhlar, and D. W. Schwenke, Chem. Phys. Lett. **234**, 57 (1995).

[58] S. L. Mielke, G. J. Tawa, D. G. Truhlar, and D. W. Schwenke, J. Am. Chem. Soc. **109**, 6436 (1993).

[59] M. S. Topaler, T. C. Allison, D. W. Schwenke, and D. G. Truhlar, J. Phys. Chem. **102**, 1666 (1998).

[60] M. S. Topaler, T. C. Allison, D. W. Schwenke, and D. G. Truhlar, J. Chem. Phys. **109**, 3321 (1998).

[61] G. Stock, J. Chem. Phys. **103**, 2888 (1995).

[62] G. Stock and M. Thoss, Phys. Rev. Lett. **78**, 578 (1997).

[63] X. Sun and W. H. Miller, J. Chem. Phys. **106**, 6346 (1997).

[64] S. Adhikari and G. D. Billing, J. Chem. Phys. **107**, 6313 (1997).

[65] S. Adhikari and G. D. Billing, Chem. Phys. Lett. **284**, 31 (1998).

[66] S. Adhikari and G. D. Billing, Chem. Phys. Lett. **289**, 219 (1998).

[67] M. Baer and R. Englman, Chem. Phys. Lett. **265**, 105 (1996).

[68] M. Baer, J. Chem. Phys. **107**, 10662 (1997).

TH-421_02612202

[69] R. Baer, D. M. Charutz, R. Kosloff, and M. Baer, J. Chem. Phys. **105**, 9141 (1996).

[70] S. Adhikari and G. D. Billing, J. Chem. Phys. **111**, 40 (1999).

[71] M. Baer and A. J. Beswick, Phys. Rev. A **19**, 1559 (1979).

[72] M. Baer and A. Alijah, Chem. Phys. Lett. **319**, 489 (2000).

[73] M. Baer, J. Phys. Chem. A **104**, 3181 (2000).

[74] M. Baer, S. H. Lin, A. Alijah, S. Adhikari, and G. D. Billing, Phys. Rev. A **62**, 32506:1-7 (2000).

[75] S. Adhikari, G. D. Billing, A. Alijah, S. H. Lin, and M. Baer, Phys. Rev. A **62**, 32507:1-7 (2000).

[76] S. Adhikari and G. D. Billing, Adv. Chem. Phys. **124**, 143 (2002).

[77] Y. Zeiri, G. Katz, R. Kosloff, M. S. Topaler, D. G. Truhlar, and J. C. Polanyi, Chem. Phys. Lett. **300**, 523 (1999).

[78] A. Donoso and C. C. Martens, J. Chem. Phys. **112**, 3980 (2000).

[79] M. D. Hack, A. M. Wensmann, D. G. Truhlar, M. Ben-Nun, and T. J. Martinez, J. Chem. Phys. **115**, 1172 (2001).

[80] O. V. Prezhdo and P. J. Rossky, J. Chem. Phys. **107**, 825 (1997).

[81] J. B. Delos, W. R. Thorson, and S. K. Knudson, Phys. Rev. A **6**, 709 (1972).

[82] J. B. Delos and W. R. Thorson, Phys. Rev. A **6**, 720 (1972).

[83] J. B. Delos and W. R. Thorson, Phys. Rev. A **6**, 728 (1972).

[84] J. B. Delos and W. R. Thorson, Phys. Rev. Lett. **28**, 647 (1972).

[85] G.D.Billing, Chem. Phys. Lett. **30**, 391 (1975).

[86] D. J. Diestler, J. Chem. Phys. **78**, 2240 (1983).

[87] Z. Kirson, R. B. Gerber, A. Nitzan, and M. A. Ratner, Surf. Sci. **137**, 527 (1984).

[88] Z. Kirson, R. B. Gerber, A. Nitzan, and M. A. Ratner, Surf. Sci. **151**, 531 (1985).

[89] L. J. Dunne, J. N. Murrell, and J. G. Stamper, Chem. Phys. Lett. **112**, 497 (1984).

[90] S. I. Sawada, A. Nitzan, and H. Metiu, Phys. Rev. B **32**, 851 (1985).

[91] Z. Kotler, E. Neria, and A. Nitzan, Comput. Phys. Commun. **63**, 243 (1991).

TH-421_02612202

[92] M. Amarouche, F. X. Gadea, and J. Durup, Chem. Phys. **130**, 145 (1989).

[93] D. A. Micha, J. Chem. Phys. **78**, 7138 (1983).

[94] W. H. Miller, Adv. Chem. Phys. **25**, 69 (1974).

[95] W. H. Miller, J. Chem. Phys. **70**, 3177 (1979).

[96] H. -D. Meyer and W. H. Miller, J. Chem. Phys. **70**, 3214 (1979).

[97] H. -D. Meyer and W. H. Miller, J. Chem. Phys. **71**, 2156 (1979).

[98] H. -D. Meyer and W. H. Miller, J. Chem. Phys. **72**, 2272 (1980).

[99] R. K. Preston and J. C. Tully, J. Chem. Phys. **54**, 4297 (1971).

[100] J. Stine and R. A. Marcus, Chem. Phys. Letts. **15**, 536 (1972).

[101] K. Haug, D. W. Schwenke, D. G. Truhlar, Y. Zhang, J. Z. H. Zhang, and D. J. Kouri, J. Chem. Phys. **87**, 1892 (1987).

[102] G. C. Lynch, P. Halvick, D. G. Truhlar, B. C. Garrett, D. W. Schwenke, and D. J. Kouri, Z. Naturforsch **44a**, 427 (1989).

[103] Y. -C. Sun and G. A. Voth, J. Chem. Phys. **98**, 7451 (1993).

[104] S. E. Wonchoba and D. G. Truhlar, J. Chem. Phys. **99**, 9637 (1993).

[105] D. F. Coker and L. Xiao, J. Chem. Phys. **102**, 496 (1995).

[106] D. Kohen, F. H. Stillinger, and J. C. Tully, J. Chem. Phys. **109**, 4713 (1998).

[107] J. C. Tully, *Modern Methods for Multidimensional Dynamics Computation in Chemistry* edited by D. L. Thompson (World Scientific, Singapore, 1998).

[108] F. J. Webster, J. Schnitker, M. S. Friedrichs, R. A. Friesner, and P. J. Rossky, Phys. Rev. Lett. **66**, 3172 (1991).

[109] F. Webster, P. J. Rossky, and R. A. Friesner, Comput. Phys. Commun. **63**, 494 (1991).

[110] F. Webster, E. T. Wang, P. J. Rossky, and R. A. Friesner, J. Chem. Phys. **100**, 4835 (1994).

[111] S. Sawada and H. Metiu, J. Chem. Phys. **84**, 6293 (1986).

[112] S. Sawada and H. Metiu, J. Chem. Phys. **84**, 227 (1996).

[113] R. D. Coalson, J. Chem. Phys. **86**, 6823 (1987)

[114] R. D. Coalson, J. Chem. Phys. **100**, 7896 (1987).

TH-421_02612202

[115] T. J. Martinez, M. Ben-Nun, and R. D. Levine, J. Phys. Chem. **100**, 7884 (1996).

[116] T. J. Martinez, M. Ben-Nun, and R. D. Levine, **101**, 6389 (1997).

[117] T. J. Martinez, M. Ben-Nun, and G. Ashkenazi, J. Chem. Phys. **104**, 2847 (1996).

[118] M. Ben-Nun and T. J. Martinez, J. Chem. Phys. **108**, 7244 (1998).

[119] Y. Tanimura and S. Mukamel, J. Chem. Phys. **101**, 3049 (1994).

[120] W. H. Miller and T. F. George, J. Chem. Phys. **56**, 5668 (1972).

[121] A. L. Kaledin and W. H. Miller, J. Chem. Phys. **118**, 7174 (2003).

[122] Yi Zheo and W. H. Miller, J. Chem. Phys. **117**, 9605 (2002).

[123] D. Huber, E. J. Heller, and R. G. Littlejohn, J. Chem. Phys. **89**, 2003 (1988).

[124] D. Huber and E. J. Heller, J. Chem. Phys. **89**, 4752 (1988).

[125] J. D. Doll and D. L. Freeman, Adv. Chem. Phys. **73**, 289 (1988).

[126] J. D. Doll, T. L. Beck, and D. L. Freeman, J. Chem. Phys. **89**, 5753 (1988).

[127] N. Makri and W. H. Miller, Chem. Phys. Lett. **139**, 10 (1987).

[128] N. Makri and W. H. Miller, J. Chem. Phys. **89**, 2170 (1988).

[129] R. Kosloff, J. Phys. Chem. **92**, 2087 (1988).

[130] R. Alimi, R. B. Gerber, A. D. Hammerich, R. Kosloff, and M. A. Ratner, J. Chem. Phys. **93**, 6484 (1990).

[131] S. Adhikari, P. Dutta, and S. P. Bhattacharyya, Chem. Phys. Lett. **199**, 574 (1992).

[132] S. Adhikari and S. P. Bhattacharyya, Phys. Lett. A **172**, 155 (1992).

[133] J. H. van Vleck, Proc. Natl. Acad. Sci. U.S.A. **14**, 178 (1928).

[134] C. A. Mead and D. G. Truhlar, J. Chem. Phys. **70**, 2284 (1979).

[135] A. Kuppermann and Y. M. Wu, Chem. Phys. Lett. **205**, 574 (1993).

[136] G. Herzberg and H. C. Longuet - Higgins, Discuss. Faraday Soc. **35**, 77 (1963).

[137] M. Baer, *Theory of Chemical Reaction Dynamics*, edited by M. Baer (CRC, Boca Raton, 1985), Vol. II, p. 219.

TH-421_02612202

[138] M. S. Child, *Atom - Molecule Collision Theory*, edited by R. B. Bernstein (Plenum, New York, 1979), p. 427.

[139] P. Pechukas, Phys. Rev. **181**, 174 (1969).

[140] P. Pechukas and J. P. Davis, J. Chem. Phys. **56**, 4970 (1972).

[141] T. Carrington, Discuss. Faraday Soc. **53**, 27 (1972).

[142] W. H. Miller and T. F. George, J. Chem. Phys. **56**, 5637 (1972).

[143] W. H. Miller and C. W. McCurdy, J. Chem. Phys. **69**, 5163 (1978).

[144] J. C. Tully, *Dynamics of Molecular collisions* edited by W. H. Miller (Plenum,New York, 1976), Part B, p. 217.

[145] E. R. Davidson, J. Am. Chem. Soc. **99**, 397 (1977).

[146] J. C. Tully, J. Chem. Phys. **93**, 1061 (1990).

[147] S. Krempl, M. Winterstetter, H. Plöhn, and W. Domcke, J. Chem. Phys. **100**, 926 (1994).

[148] G. A. Worth, H. -D. Meyer, and L. S. Cederbaum, J. Chem. Phys. **109**, 3518 (1998).

[149] A. Raab, G. A. Worth, H. -D. Meyer, and L. S. Cederbaum, J. Chem. Phys. **110**, 936 (1999).

[150] G. A. Worth, H. -D. Meyer, and L.S. Cederbaum, Chem. Phys. Lett. **299**, 451 (1999).

[151] C. Woywood, W. Domcke, A. L. Sobolewski, and H. -J. Werner, J. Chem. Phys. **100**, 1400 (1994).

[152] R. Schneider and W. Domcke, Chem. Phys. Lett. **150**, 235 (1988).

[153] G. Stock and W. Dumcke, J. Chem. Phys. **93**, 5496 (1990).

[154] M. Peric, S. D. Peyerimhoff, and R. J. Buenher, Z. Phys. D **24**, 177 (1992).

[155] G. Stock, C. Woywood, W. Domcke, T. Swinney, and B. S. Hudson, J. Chem. Phys. **103**, 6851 (1995).

[156] G. A. Worth, H. -D. Meyer, and L. S. Cederbaum, J. Chem. Phys. **105**, 4412 (1996).

[157] M. Thoss, W. H. Miller, and G. Stock, J. Chem. Phys. **112**, 10282 (2000).

[158] G. Stock and M. Thoss, Adv. Chem. Phys. **131**, 243 (2005).

[159] C. Coletti and G. D. Billing, Chem. Phys. Lett. **368**, 289 (2003).

TH-421_02612202

[160] I. Yamazaki, T. Murao, T. Yamanaka, and K. Yoshihara, Faraday Discuss. Chem. Soc. **75**, 395 (1983).

[161] H. Köppel, W. Domcke, and L. S. Cederbaum, Adv. Chem. Phys. **57**, 59 (1984).

[162] L. S. Cederbaum, W. Domcke, H. Koppel, and W. Von Niesen, Chem. Phys. **26**, 169 (1977).

[163] V. Engel, Chem. Phys. Lett. **189**, 76 (1992).

[164] H. -D. Meyer, U. Manthe, and L. S. Cederbaum, Chem. Phys. Lett. **165**, 73 (1990).

[165] U. Manthe, H. -D. Meyer, and L. S. Cederbaum, J. Chem. Phys. **97**, 3199 (1992).

[166] H. -D. Meyer, *The Encyclopedia of Computational Chemistry*, edited by P. v. R. Schleyer *et al* (Wiley, New York, 1998).

[167] M. H. Beck, A. Jäckle, G. A. Worth, and H. -D. Meyer, Phys. Rep. **324**, 1-105 (2000).

[168] U. Manthe, J. Chem. Phys **105**, 6989 (1996).

[169] R. v. Harrevelt and U. Manthe, J. Chem. Phys. **123**, 064106 (2005).

TH-421_02612202